Atmospheric aerosol distributions and their climatic effects over South Africa using remote sensing observations and regional climate model

Presented by

Melaku Tesfaye

A Thesis Submitted in Partial Fulfilment of the Requirements for the Degree of Doctor of Philosophy

Faculty of Natural & Agricultural Sciences

University of Pretoria

Pretoria

December 2013

© University of Pretoria

Declaration

This is to declare that the research work presented here is entirely my own work, unless or otherwise explicitly acknowledged by citation of published and unpublished sources. Furthermore, I would like to state that, even if the work presented from chapter 2 to 7 has been co-authored with my promoter and two other colleagues, the conceptualization of all these research works plus their scientific analysis and interpretations, article writings as well as the rebuttal during the peer-review processes were executed by myself. This research has not been submitted for assessment in any form to the University of Pretoria or to any other institutions for any other purposes.

Melaku Tesfaye Yigiletu (04420020)

Signature: 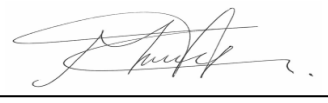

Date: 09/12/2013

Dissertation promoter

Prof. Venkataraman Sivakumar

Department of Geography, Geoinformatics and Meteorology, University of Pretoria, Lynwood Road, Pretoria 0002, South Africa

Discipline of Physics, School of Chemistry and Physics, University of KwaZulu Natal, Westville, Durban 4000, South Africa

© University of Pretoria

Abstract

Atmospheric aerosols are small solid and liquid particles suspended in the Earth's atmosphere which originate from anthropogenic and natural activities. Unlike greenhouse gases, aerosol particles are relatively short-lived in the atmosphere and exhibit multidimensional heterogeneity with respect to their composition, size, sources, mixing state and the spatio-temporal distributions. The concentration and climatic influences of atmospheric aerosols are much higher closer to their source regions. Therefore, to have a better understanding of the role of aerosols, their distribution and climatic impacts must be understood and quantified on a regional scale rather than on a global-average basis. There are multiple sources of aerosols/precursor gases in South Africa (SA) which build a complex mixture of atmospheric particulates. This contribution presents a detailed study of aerosol climatology over SA as well as examines the direct radiative and semi-direct climatic effects of individual/total aerosol particles based on their sources. The climatological study has shown that, in terms of aerosol load spatial variation, SA can be classified into three parts: the upper, central, and lower part; which corresponds to high, medium and low aerosol loads. The seasonal variation of aerosol optical signatures shows that the prevailing sources of aerosols are different in each part of SA. The lower part is dominated by particles that are induced from the air mass transport from the surrounding marine environment and other SA/neighbouring regions. The central and upper parts of SA are primarily loaded by windblown mineral dust particles and aerosols that result from anthropogenic/biomass burning activities. Following the aerosol climatological study, using the 12 year (1997 - 2008) runs of the Regional Climate Model (RegCM4), the mass distribution, radiative influences and semi-direct climatic effects of wind-eroded desert dust particles, different species of aerosols that are induced from anthropogenic and biomass burning activities over SA are examined. Investigating the influence of aerosols, based on their sources, is essential to improve the scientific understanding about the two-way interaction and feedback among various species of aerosols, radiation and different climatic variables. This is also important to distinguish the climatic signals of anthropogenic aerosols from that of natural aerosols as well as to devise climate change mitigation strategies. Before employing RegCM4 for these purposes, the model’s performance in reproducing the major observational features of aerosol optical fields over SA was evaluated. Among various semi-direct climatic influences of aerosols, this study examined their effects on: surface temperature, surface sensible heat flux, net atmospheric radiative heating rate, hydrological variables (in terms of cloud cover and cloud liquid water path), boundary layer, surface pressure and surface wind fields. The study also assessed the dependency of aerosols’ semi-direct effects on seasonal variation of meteorological parameters as well as its reliance on atmospheric aerosol distributions and properties. Overall, the semi-direct effect assessments delivered not only an important contribution towards the understanding of the interaction and feedback between different types of aerosols-radiation-climate (at a regional level), but also offered insightful information about the mutual interrelationships among different climatic feedbacks. Among different aerosol species in SA, this study critically underscores that the wind-eroded desert dust particles have a dominant climatic signal in SA. Therefore, wind-eroded desert dust particles are of high importance and need to be incorporated in climate change studies over South Africa. Additionally, the dominance of dust particle climatic signals perhaps requires some attention from governmental or non-governmental environmental organizations which are working in and around South Africa: at least in terms of making some strategic plans on how to reduce the dust production and dispersion.

© University of Pretoria

Acknowledgements

First and foremost, I am deeply indebted to my promoter Prof. Venkataraman Sivakumar for his continuous encouragement and manifold support throughout my PhD research. My sincere and special thanks also extend to Dr. Joel Botai and Dr. Gizaw Mengistu for their continual valuable cooperation. No words can express my heartfelt and immense gratitude to Teresa Faleschini. I would like to express my sincerest, immense and heartfelt gratitude to my families for their love and inspiration throughout my life journeys. Furthermore, completion of this doctoral dissertation was possible with the encouragement of several people and I do acknowledge some of them here. Thank you: Ameeth Sharma, Prof. Sisa Pityana, Dr. Ndumiso Cingo, Dr. Paul Motalane, Dr. Kittessa Roro, Tamene Mekonnen, Ezra Girma, Degol Teka, Senay, Asnake Ejigu, Tomas, Abenet, Mekdes, Prof. Fisseha Mekuria and Eleni, Donald Klopper and Micha Klopper. For the financial support and various facilities I would also like to acknowledge the African Laser Centre and CSIR National Laser Centre. Last but not least, the author is grateful to Addis Ababa University, Department of Physics, for providing computational facilities and International Centre for Theoretical Physics (ICTP) for the accessibility of RegCM.

© University of Pretoria

Abbreviations

AAs: Anthropogenic Aerosols

ACCMIP: Atmospheric Chemistry and Climate-Model Inter-comparison Project

AERONET: Aerosol Robotic Network

AGCM: Atmospheric General Circulation Model

AMS: Aerosol Mass Spectrometer

AO: Annual Oscillation

AOD: Aerosol Optical Depth

ARF: Atmospheric Radiative Forcing

ASO: August-September-October

ATM: Atmospheric

ATMRF: Atmosphere Radiative Forcing

AVHRR: Advanced Very High Resolution Radiometer

BATS: Biosphere-Atmosphere Transfer Scheme

BB: Biomass Burning

BBAs: Biomass Burning Aerosols

BC: Black Carbon

CALIOP: Cloud and Aerosol Lidar with Orthogonal Polarization

CARF: Carbonaceous aerosol Atmospheric Radiative Forcing

CC: Cloud Cover

CCN: Cloud Condensation Nuclei

CCSP: Climate Change Science Program

CDNC: Cloud Droplet Number Concentration

CDT: Convectively Driven Turbulence

CLW: Cloud Liquid Water

CLWP: Cloud Liquid Water Path

CSIR: Council for Scientific and Industrial Research

CSRF: Carbonaceous aerosol Surface Radiative Forcing

DMS: Dimethyl Sulphide

ECMWF: European Centre for Medium-Range Weather Forecasts

ER: Electromagnetic Radiation

ERA: ECMWF Re-Analysis

ERAIN: ERA-Interim

GFED3: Global Fire Emissions Database version 3

GLAS: Geoscience Laser Altimeter System

ICTP: International Centre For Theoretical Physics

IR: Infrared

JASO: July-August-September-October

LIDAR: Light Detection And Ranging

LSRF: Longwave Surface Radiative Forcing

LW: Longwave

LWARF: Longwave Atmospheric Radiative Forcing

LWC: Liquid Water Content

LW-SU-RF: Longwave Surface Radiative Forcing

LW-SUR-RF: Longwave Surface Radiative Forcing

MA: March-April

MAAP: Multi Angle Absorption Photometer

MISR: Multi-Angle Imaging Spectroradiometer

MJJ: May-June-July

MODIS: Moderate Resolution Imaging Spectroradiometer

NAHR: Net Atmospheric radiative Heating Rate

NARF: Net Atmospheric Radiative Forcing

NASA: National Aeronautics and Space Administration

NATM-RF: Net Atmosphere Radiative Forcing

NB: Negative Bias

NDJF: November-December-January-February

NIR: Near-Infrared

NLC: National Laser Centre

NOAA: National Ocean and Atmosphere Administration

NSRF: Net Surface Radiative Forcing

NSUR-RF: Net Surface Radiative Forcing

OC: Organic Carbon

OISST: Optimum Interpolated Sea Surface temperature

OMI: Ozone Monitoring Instrument

OPA: Optical Properties of Aerosols

OPC: Optical Particle Counters

© University of Pretoria

PARASOL: Polarization and Anisotropy of Reflectance for Atmospheric Science coupled with Observations from a LIDAR

PBL: Planetary Boundary Layer

POLDER: Polarization and Directionality of the Earth's Reflectance

PSAP: Particulate Soot Absorption Photometer

RADAR: Radio Detection And Ranging

RC-aerosol model: Regional Climate-aerosol model

RCM: Regional Climate Model

RegCM4: Regional Climate Model version4

RF: Radiative Forcing

RH: Relative Humidity

RT: Radiative Transfer

SA: South Africa

SAARI: Southern African Atmospheric Research Initiative

SAFARI: Southern African Regional Science Initiative

SARF: Sulfate aerosol Atmospheric Radiative Forcing

SAWS: South Africa Weather Service

SBF: Surface Buoyancy Fluxes

SBO: Sulfate-Black carbon-Organic carbon

SP: Surface Pressure

SRF: Surface Radiative Forcing

SSA: Single Scattering Albedo

SSHF: Surface Sensible Heat Flux

SSRF: Shortwave Surface Radiative Forcing

SSW: South-Southwesterly

ST: Surface Temperature

SU: Surface

SUBEX: Sub-grid Explicit Moisture Scheme

SUR-RF: Surface-Radiative Forcing

SW: Shortwave

SWARF: Shortwave Atmospheric Radiative Forcing

SW-ATM-RF: Shortwave-Atmosphere-Radiative Forcing

SW-SU-RF: Shortwave-Surface-Radiative Forcing

TARF: Total anthropogenic aerosol Atmospheric Radiative Forcing

TOA: Top of the Atmosphere

TOA-RF: TOA Radiative Forcing

TOMS: Total Ozone Mapping Spectrometer

TOTA: Total Optical Thickness of the Atmosphere

TSRF: Total anthropogenic aerosol Surface Radiative Forcing

UV: Ultraviolet

VIS: Visible

WMO: World Meteorological Organization

© University of Pretoria

Contents

© University of Pretoria

© University of Pretoria

© University of Pretoria

© University of Pretoria

Background

Based on the thermal structure, the vertical profile of the Earth's atmosphere is usually classified into four distinct regions which are named with the suffix '*spheres*'. The vertical temperature gradient in each region has a constant sign. Regions which exhibit different signs of temperature gradient are separated by a series of layers which are named with the suffix '*pauses*' (the suffix '*pauses*' mirror the region boundary). The lowest region of the atmosphere which starts at the Earth's surface and extends up to the tropopause is called the troposphere. It is much denser than the layers of the atmosphere above it and contains approximately 70% to 80% of the mass of the atmosphere (Seinfeld and Pandis, 2006). Nearly all atmospheric water vapour (~ 99%) and aerosols are found in this region. Moreover, the troposphere is relatively well mixed because of the negative temperature gradient. Most of the weather phenomena and many atmospheric reactions which influence our lives (directly/indirectly) occurred in this layer (Seinfeld and Pandis, 2006). The boundary layer which separates the troposphere and stratosphere is known as the tropopause. Depending on latitude (from equator to the poles) and seasons, the height of tropopause extends up to 10 to 15 km above the Earth's surface.

The stratosphere extends from the tropopause up to around 50 km above the Earth's surface. It is characterized by positive temperature gradient and as a result, vertical mixing (convection activity) is strongly inhibited. In this region the temperature increase is a result of the heat produced by the process of Ozone formation, via solar ultraviolet radiation absorption (e.g., WMO, 2002; Seinfeld and Pandis, 2006). The transition boundary which separates the stratosphere and mesosphere is known as the stratopause. In the mesosphere the temperature decreases with altitude, until it reaches to the coldest point in the atmosphere (i.e., mesopause). This region is separated from the thermosphere by the mesopause. Generally, the thermosphere is characterized by positive temperature gradient. The lower part of the thermosphere is usually known as the ionosphere. In this part of the thermosphere the solar energy is very strong and can break air molecules (even atoms) to form ions plus free-floating electrons. This often causes refraction of radio waves; therefore, the ionosphere is practically important for space communication and other high frequency research programs. Above the ionosphere, the thermosphere extends into its outer region and eventually merges into space of high energy solar particles and cosmic rays.

The other property of the atmosphere is the vertical pressure gradient. Since the mass density of the Earth's atmosphere decreases with height, the pressure profile declines rapidly with altitude. Broadly speaking, the thermal structure as well as various phenomena's of the Earth's atmosphere are basically determined by the composition of the Earth-atmosphere system, its interactions and feedbacks with solar and terrestrial radiations (e.g., Seinfeld and Pandis, 2006). The Earth's atmosphere is composed primarily of nitrogen (~ 78% by volume) and oxygen (~ 21% by volume). The remaining 1% of the atmosphere is a mixture of different trace gases (such as argon, water vapour, carbon dioxide, methane, ozone, etc.) and aerosols. Though these trace gases and particulate matter occur in small proportions, they are primarily accountable for some of the most significant physico-chemical characteristics of the Earth's atmosphere; in turn, they play an essential role in our climate system (e.g., Seinfeld and Pandis, 2006).

Atmospheric aerosols are small solid and liquid particles suspended in the Earth's atmosphere. Atmospheric aerosols can originate from anthropogenic and natural activities at the surface or within the atmosphere (see section 1.1.2). Wind-blown mineral dust, precursor gases from volcanic eruptions, natural wild fires, vegetation, and the oceans are the main natural sources of aerosols. While, the anthropogenic sources include agriculture practices, human-induced biomass burning, emissions from fossil/bio-fuel combustions and different industrial activities,

© University of Pretoria

photo-chemically induced smog, primarily due to vehicle emissions. A brief discussion about the sources of aerosols is given in chapter 1. It is evident that during the industrialization era (relative to the pre-industrial time) the energy consumption, traffic of vehicles, urbanisation and various human activities dramatically increased, which all, in turn, increased the emissions of atmospheric aerosols and their precursors (Gurjar and Lelieveld, 2005; Seinfeld and Pandis, 2006; IPCC, 2007). Similarly, over the past century the population growth has increased, this ensued in intensified land cover changes which gradually caused ecological changes as well as land degradation. Particularly the landscape fragmentation driven by agricultural extension and mining activities indirectly facilitates the enhancement of windblown dust particles and other aerosol-load in the atmosphere (IPCC, 2007; Finlayson-Pitts and Pitts, 2000).

The presence of aerosols in the Earth's atmosphere has a variety of important environmental and ecological influences, which can be positive or negative. Moreover, the aerosol influences can also impact human activities either directly or indirectly. Most of the studies reported in the early 1950s focused on health effects of atmospheric aerosols such as their role in causing bronchiectasis and other respiratory effects (e.g., Dautrebande and Capps, 1950). Also during the 1950s different studies started to report insightful results about the sea-salt aerosol formation processes (e.g., Woodcock et al., 1953; Kientzler et al., 1954). Aerosol particles have a capability to scatter and absorb electromagnetic radiation as well as serve as cloud condensation and ice nuclei. Based on these concepts, since the late 1960s, different studies reported the influence of aerosols on the Earth's radiation budget (direct effect) plus their role in modifying the microphysical and radiative properties of clouds by acting as cloud condensation nuclei (indirect effects) (Carslaw et al. 2010 and references therein). Following these, during the 1980s, different studies (e.g., Charlson et al., 1987) have reported about the processes of sulfate aerosol formation plus their critical role in acid rain formation during their removal. This and other aspects of aerosols initiated the clean air policy of industrial nations.

Though the influence of aerosols on the tropospheric ozone began to be reported in the 1970s (e.g. Crutzen et al., 1979); it was only after the volcanic eruption of Mt. Pinatubo in 1991 which exhibited the depletion of the stratospheric ozone layer, that the scientific society intensely realized the role of aerosols in atmospheric chemistry (e.g., WMO, 2002; Seinfeld and Pandis, 2006). In addition to these, in the late 1990s, other important influence of atmospheric aerosols on clouds (specifically by absorbing aerosols) was reported by Hansen et al. (1997) (i.e., semi-direct effect). The semi-direct effect is distinct from the indirect aerosol effect; it is generally related with the absorbing aerosol atmospheric heating influences, which may influence the ambient relative humidity and lead to changes in cloud cover. Brief discussions about the climatic role of aerosols are given in chapter 1. Due to the aforementioned relevant issues and other ecological concerns, over the past two decades, there has been increased interest in atmospheric aerosols and currently they are one of the key issues in climate research (CCSP, 2009 and references therein).

Unlike greenhouse gases, aerosol particles are relatively short-lived in the atmosphere and they are highly dynamic. Therefore, aerosols exhibit immense diversity, not only with respect to their - size, composition, sources and mixing state - but also with regards to their spatial and temporal distributions. This creates a great challenge and one of the major sources of uncertainties in studying the radiative and climatic impacts of aerosols. Moreover, Solomon et al. (2007) indicated that due to the multidimensional heterogeneity of aerosols' properties and distributions; the uncertainties associated with aerosol radiative forcing are taken to be the greatest contributor to the overall uncertainty in radiative forcing of climate change. Even though it is known that aerosols are highly mobile

© University of Pretoria

(they can cross oceans and mountain ranges), they are highly populated close to their source regions. As a result their influences are much higher in and around their source regions. Therefore, to reduce uncertainties and to have a better understanding of the role of aerosols; their distribution and climatic impacts must be understood and quantified on a regional scale (in and around their source regions) rather than on a global-average basis (Pal et al., 2007). Regional scale studies are especially important for countries like South Africa which are influenced by almost all types of major atmospheric aerosols: mineral dust, sea-salt particles as well as primary/secondary aerosols, that are emitted from different anthropogenic and biomass burning activities (see chapter 2 and chapter 4 to chapter 6).

Atmospheric aerosols which are produced from different sources typically display a large variation in their physico-chemical (and in turn, optical) properties as well as influences. Moreover, the source strength, burden level and properties (in turn the radiative/climatic impacts) of similar particles usually exhibit a large seasonal variation depending on the ambient meteorological conditions. Therefore it is crucial to examine the regional distribution of aerosols and their properties via correlating them with the ambient meteorological parameters which have a significant role in modifying the aerosol loading and properties. Such studies may advance our understanding about the regional scale aerosol source spatio-temporal distribution, as well as it is important to characterise the effects of meteorological conditions on the aerosol microphysical (in turn optical) properties plus their local dynamics (load, dispersion, and removal: see chapter 2).

Moreover, to comprehend the relative impact of aerosols which are produced from different activities, it is quite significant to examine separately the radiative and climatic effects of individual/total aerosol particles based on their sources. Such studies are essential to improve the scientific understanding about the interactions and feedbacks among various species of aerosols-radiation-climate (i.e., to distinguish the climatic signals of anthropogenic aerosols from that of natural aerosols). Furthermore, such studies are also important to develop short/long-term environmental policies, for climate change mitigation and to initiate further studies (IPCC, 2007). Based on the aforementioned details, the present thesis investigates the climatology of aerosols in South Africa. Thereafter, it examines the mass distribution, direct radiative effects and several semi-direct climatic influences of different types of aerosols that are produced from different sources (individually as well as collectively) in South Africa. Furthermore, this study also assesses the dependency of aerosols' semi-direct effects on seasonal variation of meteorological fields as well as its reliance on atmospheric aerosol distribution and properties. Overall, these semi-direct effect assessments deliver not only important contribution towards the understanding of the interaction and feedback between different types of aerosols-radiation-climate, but additionally offer insightful regional level information about the mutual interrelationships among different climatic feedbacks.

In this respect, the thesis is structured as follows: in chapter 1 an overview of atmospheric aerosols, their main sources and removal processes as well as microphysical and optical properties are provided. The discussion of aerosol optical parameters also includes a general overview of Mie theory. Thereafter, a brief discussion on the climatic implications of aerosols and a short overview of different aerosol measurement techniques (i.e., *in-situ* and remote-sensing) and modelling are described. Lastly chapter 1 provides a conceptual overview of this study and its importance together with outlined contents of the subsequent chapters. The main result parts of this thesis consist of six published/submitted journal articles (one published, one in press and the others are currently under review in different accredited journals). Chapter 2 (Tesfaye et al., 2011) offers detailed aerosol climatology over South Africa. As a first step of aerosol-climate modelling study, chapter 3 (Tesfaye et al., 2013a; in press) evaluates the performance of RegCM4-aerosol model in computing the optical properties of aerosols in South Africa, by

© University of Pretoria

comparing with ground-based and satellite observations. In addition, the need of aerosol/chemistry-climate model, a brief description about interactively coupled RegCM4-aerosol model (which is utilized in this study), its limitations and other crucial issues are given in chapter three. This information is used as the basic framework for studies that follows this chapter. The mass distribution, radiative influences and semi-direct climatic effects of wind-eroded desert dust particles, different species of aerosols which are induced from anthropogenic and biomass burning activities over South Africa are respectively provided in chapter 4 (Tesfaye et al., 2013b; in review), chapter 5 (Tesfaye et al., 2013c; in review) and chapter 6 (Tesfaye et al., 2013d; in review). It is also important to examine the bulk aerosol (i.e., bulk aerosol: mixture of different aerosols that are contributed from various sources) direct and semi-direct effects in South Africa, which is presented in chapter 7 (Tesfaye et al., 2013e; in review). Finally, the summary and the main conclusions of this study plus future perspectives are outlined in chapter 8.

© University of Pretoria

Chapter 1: Introduction

1.1 Atmospheric Aerosols

1.1.1 What are atmospheric Aerosols?

Atmospheric aerosols (often referred to as atmospheric particulate matter) are a mixture of small solid and liquid particles suspended in the Earth's atmosphere (Seinfeld and Pandis, 2006). This excludes cloud droplets, ice particles, rain drops and other forms of atmospheric hydrometeors. This definition of atmospheric aerosols encompasses a broad array of different substances with widely varying physico-chemical properties such as shape, size, number/mass density and chemical composition. The routes through which aerosols are generated and their atmospheric processes, determines the physico-chemical properties and mixing state of particles (Seinfeld and Pandis, 2006). Overall, the size of aerosol particles ranges from a diameter (assuming a spherical shape) range of ~ 3 nanometres (nm) to tens of micrometers (μm). The smallest aerosols can be defined as thermodynamic stable clusters of gas molecules, while the largest are called droplets - however, in general they are smaller than cloud droplets. The number density of tropospheric aerosols typically ranges from a few hundred (in remote locations) to more than 10^6 particles per cm^3 (in polluted zones or after strong nucleation events) (Zhu et al., 2002). When clouds of aerosols (especially smoke or small dust particles) grow to large sizes by water vapour condensation on them, they form a haze. The combination of haze and fog (small liquid water droplets) is known as smog. Smog can induce a great reduction in visibility; this is one of the several manifestations of atmospheric aerosols in our daily lives.

1.1.2 Sources

Aerosol particles that are introduced directly into the atmosphere are known as primary aerosols (e.g., sea-salt, mineral aerosols, volcanic dust, smoke and soot). Whereas, particles that are formed in the atmosphere by the chemical reactions of aerosol precursor gases (e.g. through gas-to-particle conversion processes) are referred to as secondary aerosols (e.g., sulfate, nitrate and some organics) (Finlayson-Pitts and Pitts, 1997; Seinfeld and Pandis, 2006). Gaseous precursors of secondary aerosols include sulphur dioxide (SO2), dimethyl sulphide (DMS), Hydrogen sulfide (H2S), oxides of nitrogen (NOx), ammonia (NH3) and Volatile Organic Compounds (VOCs). Mostly the diameter range of primary and secondary particles are > 1μm and < 1μm, respectively (e.g., Jayne et al., 2000; Seinfeld and Pandis, 2006).

Generally, atmospheric aerosols reside mainly in the two lowest layers of the atmosphere: the troposphere, and the stratosphere. Most aerosols are highly populated in the troposphere and their distribution decreases with altitude. Apart from extra-terrestrial sources (which have a lower contribution), strong volcanic eruptions are the main sources of stratospheric aerosols (Rampino and Self, 1984; Robock, 2000; Thomason and Pitts, 2008). In the troposphere, both primary aerosols and precursor gases of secondary particles originate from various natural processes and anthropogenic activities (e.g., Seinfeld and Pandis, 2006). The actions of wind on bare, dry and loose soil surfaces as well as over the oceans are the main natural processes which generate mineral dust and sea spray particles, respectively. Volcanic eruptions, natural wildfires and vegetation are the other natural processes which emit large quantities of primary aerosols and trace gases into the atmosphere. Whereas, emissions from fossil/bio-fuel combustions, industrial processes, vehicles, nonindustrial fugitive sources (e.g. construction work and

© University of Pretoria

agriculture practices) as well as human-induced biomass burning events are the major anthropogenic sources that are accountable for production of a variety of primary and secondary aerosols.

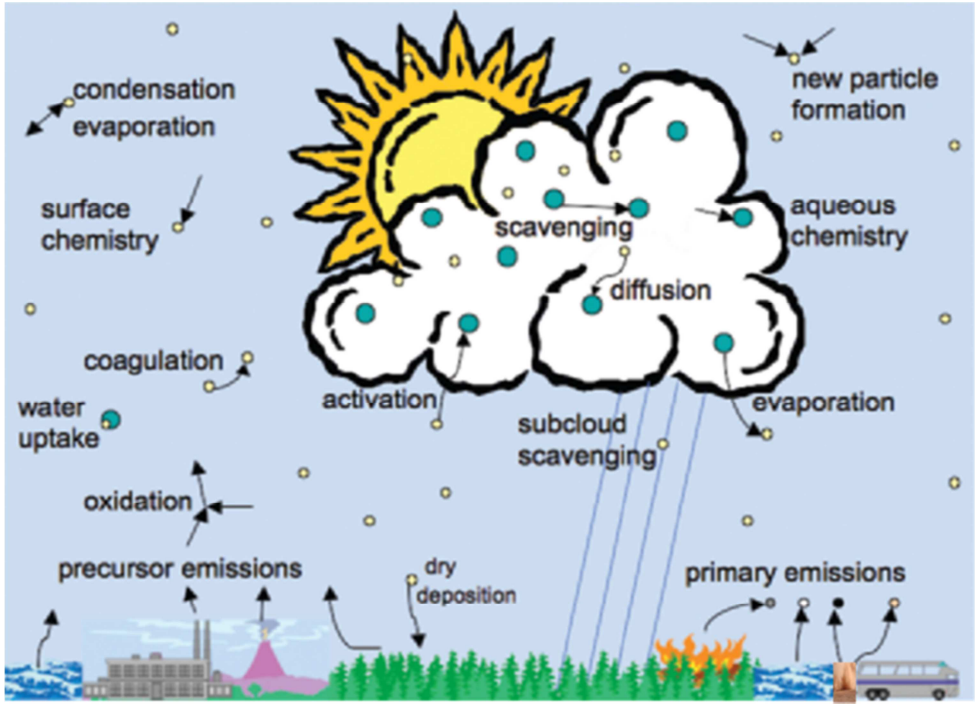

Fig. 1: Schematic diagram representing the major sources of primary aerosol emissions/secondary aerosol formation, atmospheric particulate processes (different particle aging processes) and removal mechanisms (adopted from Ghan and Schwartz, 2007).

Combining different information from ground based measurements, satellite observations, aerosol models and other information on natural events/human activities, in the recent years progress has been made in estimating emissions from different natural and anthropogenic activities (Kaufman et al., 2002). Several studies have regarded that on a global scale, the emissions of natural aerosols are higher than anthropogenic ones (Hinds, 1999; Seinfeld and Pandis, 2006). However, in certain industrialised areas - aerosols which are induced from human activities may significantly surpass the contribution of natural sources (Seinfeld and Pandis, 2006). An overview of the main natural and anthropogenic sources of aerosols and their emission strengths in terms of aerosol mass fluxes on a global scale are given in table 1 below.

Table 1: Globally averaged atmospheric aerosol emission estimates from the main natural and anthropogenic sources (adopted from Hinds, 1999).

Source	**Amount, Tg/yr (10^6 metric tons/yr)**	
	Range	**Best Estimate**
Natural		
Soil dust	1000 - 3000	1500
Sea-salt	1000 - 10000	1300
Botanical debris	26 - 80	50
Volcanic dust	4 - 10000	30
Forest fires	3 - 150	20
Gas-to-particle conversion	100 - 260	180
Photochemical	40 - 200	60
Total for natural sources	2200 - 24000	3100

© University of Pretoria

Anthropogenic		
Direct emissions	50 - 160	120
Gas-to-particle conversion	260 - 460	330
Photochemical	5 - 25	10
Total for anthropogenic sources	320 – 640	460

Compared to atmospheric gases, aerosols are characterized by extensive variations in composition, size, physical characteristics and distribution (both in space and time) (IPCC, 2001). This is due to the heterogeneity of aerosol sources/formation mechanisms; their atmospheric physico-chemical transformations as well as short lifetimes of particles (Seinfeld and Pandis, 2006). Generally, total aerosol loading comprises a complex mixture of different aerosol species with different mixing states and ratios. However, different factors such as source placements and environmental conditions, establish one or a group of aerosol species as a dominant types in the total aerosol loading. The physico-chemical properties of the dominant species influentially determine the overall effects of the total aerosol loading. Various studies showed that sulfates, black carbon, particulate organic matter, sea-salt and mineral dust particles are the major aerosol components that constitutes the total tropospheric aerosol burden (e.g., Chin et al., 2002 and references therein).

In remote areas (areas which are minimally perturbed by anthropogenic aerosol sources), windblown sea-salt and mineral dust aerosols, and naturally occurring sulfates and organic compounds are taken as a baseline aerosol for the background atmosphere. Nonetheless, in various parts of the globe, industrial and biomass burning activities are the culprits for the enhanced load of sulfates and carbonaceous aerosols. These industrial activities include fossil fuel combustion, coal refining, automobiles, chemical manufacturing as well as others. The biomass burnings are induced by natural events (for instance savannah and forest fires) as well as different anthropogenic activities, such as for the purpose of energy production (burning of charcoal), agricultural activities related cultivation shifting, land clearing due to population expansion and others. Unlike biomass burning or other aerosol sources, the emission from industrial activities shows a minimal seasonal variation (Kuenen et al., 2011). Usually changes in aerosol burden that are induced from industrial activities occur as a result of seasonally variable meteorological conditions which affect the physico-chemical transformation and other atmospheric processes of these aerosols (Zunckel et al., 2000).

Sulfate-containing compounds in the stratosphere mainly originate from photo-oxidation processes of SO_2 and H_2S, which are emitted into the stratosphere by volcanic eruptions. However, sulfurous particles in the troposphere are predominantly produced through the gas-phase and aqueous phase oxidation processes of SO_2 (from industrial activities and transportation sectors) and DMS (from biogenic sources especially marine environments) (Russell et al., 1994; Penner et al., 2001; Dentener et al., 2006). Tropospheric oxidation processes of SO2 are sensitive to ambient meteorological conditions such as temperature and relative humidity (Qian and Giorgi, 1999; Qian et al., 2001). As a result, anthropogenic activities induced sulfate aerosol concentration often exhibit strong seasonal variation (see chapter 5). Usually sulfate aerosols exist in a liquid form and their diameter falls in the sub-micron size range (smaller than 1μm).

Both natural and anthropogenic processes can induce biomass burning. For instance lightning can induce fires, which is often considered as the main cause of natural biomass burning. However, its contribution is small compared to human-initiated burning activities (Bond et al., 2004). Anthropogenic biomass burning is a common practice used for land clearing, land-use change as well as for various domestic and industrial uses (Roden et al.,

© University of Pretoria

2005). Compared to different industrial activities, most carbonaceous aerosols are derived from biomass burning events. This is because, the majority of burning materials (e.g., biomass and fossil fuels) are made of carbon, hydrogen and oxygen; thus, during the combustion process oxygen and hydrogen will be consumed. As a result, the direct emission from different combustion activities (industrial or natural) primarily contain carbonaceous particles (Bond et al., 2013 and references therein).

Most carbonaceous particles are hydrophobic and their diameter falls in the sub-micron size range (Bond et al., 2013); as a result, they can travel long distances and have a longer lifetime than other aerosols such as sulfates, desert dust particles and marine aerosols. The optical and physico-chemical properties of carbonaceous particles that are induced from combustion activities are highly dependent on the nature and environmental conditions of the combustion processes plus the type of carbon compounds found in the burnt material (e.g., Andreae and Merlet, 2001). Broadly speaking, there are two major species of carbonaceous aerosols which are produced from different combustion events: Black Carbon (BC, soot) and Organic Carbon (OC) (Kanakidou et al., 2005).

The BC particles are pure carbonaceous materials that are commonly produced through incomplete combustion processes (Bond et al., 2013 and references therein). Combustions which often take place under the presence of fewer amounts of oxygen and low temperature favour the formation of BC particles. Fresh BC particles tend to be hydrophobic and spherical; however, their environmental exposure immediately results in the absorption of organic vapour elements on their surface (Decesari et al., 2002). This clusters the BC particles together to form agglomerates of small spherical particles, referred to as soot (Naydenova, 2007). In addition, these internally mixed elements also facilitate the physico-chemical transformation of soot particles; thus, aged soot particles will exhibit a change in their hygroscopic properties (e.g. Decesari et al., 2002).

Complete combustion processes such as open biomass burning, are the main sources of primary OC aerosols (Bond et al., 2004). Secondary OC aerosols are produced mainly by the atmospheric reactions of VOCs (e.g, Hallquist et al., 2009 and references therein). Similarly to sulfate aerosols, the secondary OC aerosol formations are highly influenced by the seasonal variability of the ambient meteorological conditions (Ram et al., 2012). Moreover, the characterization of secondary OC aerosols is a challenging issue because of the wide range of VOCs present within the atmosphere and their multiphase reactions (Hallquist et al., 2009 and references therein). Therefore, to simplify this issue generally both primary and secondary OC aerosols are categorized in to two classes: water-soluble and water-insoluble. For further discussion on organic aerosols the reader is referred to Monks et al. (2009) and references therein.

The other two major aerosol components of the Earth system (i.e., mineral dust and sea-salt particles) accounts for the largest fraction of atmospheric aerosol mass as well as the generation of these aerosols are driven by the windblown processes over the desert/dusty ground and ocean surfaces (Penner et al., 2001). The mineral dust and sea-salt load in the atmosphere is strongly influenced by different climate and environmental factors in their source regions. For instance, the dust particles can be detached from the surface when the shear-force of the surface wind exceeds the adhesion force that ties the dust particles to the ground (i.e., when the surface wind speed exceeds a threshold velocity). This process is dependent on several climatic features of the dust source region; such as, wind velocity, soil moisture, soil properties, vegetation cover and other topographic issues (e.g., Zakey et al., 2006).

Mineral dust emissions are the highest in arid and semi-arid regions (areas with bare-dry soils and precipitation less than 200 mm per year) such as over the Sahara desert, across the Middle East, central and eastern

© University of Pretoria

Asia and continental Australia (Goudie and Middleton, 2006). Generally, majority of desert dust source regions are located in the northern hemisphere of the globe (Tanaka and Chiba, 2005). However, even though in a global scale the greatest contribution of dust comes from the northern hemisphere, the southern hemisphere dust source regions also donate significant amounts of dust particles which have important influences in and around their source regions (Bryant et al., 2007; Bhattachan et al., 2012). Moreover - construction, transportation, cement and metallurgy manufacturing, human-induced deforestation and soil degradation due to agricultural practices and mining activities - are among the various anthropogenic activities that produce primary dust particles or facilitate its production (e.g. Tegen et al., 2004).

Once dust particles are injected into the atmosphere, their transport and deposition are mainly driven by meso- and synoptic-scale atmospheric processes. The atmospheric lifetime of dust particles primarily depends on their size; large particles (especially those with diameters > 10μm) are quickly removed from the atmosphere by gravitational settling and other dry deposition processes, while sub-micron sized particles have a longer atmospheric lifetime. Therefore, large size dust particles are significantly abundant only around their source regions. However, as the large size dust particles fall back onto the surface, they may pass some of their impulse to other soil particles and detach finer dust particles from the ground via impaction and other processes (e.g., Lu and Shao et al., 1999). Due to all the aforementioned dust production mechanisms, usually, the dust particle range in size from 0.05 to 100 μm, with a bimodal size distribution structure and dominant influence of coarse particle mode (Dubovik et al., 2002; Chou et al., 2008).

The physico-chemical and optical properties of freshly emitted dust particles are dependent on the surface properties of dust source regions. They are usually aggregates of different irregularly shaped mineral particles such as silicon (e.g., quartz sand), aluminium (e.g., aluminium silicates from clay minerals and gibbsite), iron oxide and carbonates (e.g., hydroxide dusts, calcite, magnesite) (Chou et al., 2008). Furthermore, initially most of the airborne soil particles are not water-soluble; however, atmospheric aging processes (such as the reaction of SO2, gaseous nitric acid and VOCs on the surface of dust aerosols) may change the state of their hygroscopicity. This causes the dust particles to serve as cloud condensation nuclei as well as changes the physico-chemical (and in turn optical) properties of dust aerosols as a function of Relative Humidity (RH).

Generally, sea-spray aerosols are mechanically produced by the interaction of surface wind with deep-water surface wave fields. When the sea surface wind speed increases beyond a critical value, the waves break to disperse the excess energy; these incidences result in the formation of bubble plume (oceanic whitecaps). When spume drops under the wave/when the bubbles collapse by the wind stress they spray droplets which are the sources of marine aerosols (e.g., Zakey et al., 2008 and references therein). Basically the primary marine aerosol production is directly related to the whitecap fraction. Once the sea spray droplets get into the atmosphere they start to evaporate and eventually equilibrate themself with the atmosphere RH; and as a result, they become smaller, stable and most of them will transform into different types of aerosols (e.g., Andreas, 1995; 2005). Marine aerosols are composed of soluble inorganic salts such as sodium, potassium and magnesium chlorides, calcium sulfate as well as other particulates like ammonium sulfate, nitrates and different organic materials (e.g., O'Dowd and Leeuw, 2007 and references therein). Among various sea-spray aerosols, the sea-salt particles are one of the most widely distributed natural tropospheric aerosols, particularly in and around the marine atmosphere (e.g., Vignati et al., 2010).

© University of Pretoria

Sea-salt aerosols, which are left behind by the sea-spray droplets after evaporation, will stay in the atmosphere as liquid drops, deliquescent drops, or dry sea-salt particles depending on the ambient RH (Tang et al., 1997; Keene and Savoie, 1998). Frequently, if the ambient RH is > 95 % sea-spray droplets remain liquid and they will almost retain their sizes. When the RH is in between 95 % to 75 %, most of the sea-salt aerosols reside in the atmosphere as deliquescent particles, with radii about half of the parent sea-spray droplets (Monahan, 1986). However, when the RH is less than 75 %, the sea-spray droplets start to crystallize and will eventually develop into dry sea-salt particles when the ambient RH is < 50 %. Usually the dry sea-salt particles have a radius which is almost one fourth of the parent droplets (Zhang et al., 2006). In most coastal zones the RH ranges from 75% to 100%; therefore, the deliquescent state becomes the common state of sea-salt aerosols (Warneck, 1999).

Sea-salt particles are highly soluble; therefore, can serve as effective cloud condensation nuclei. Furthermore, due to their hydrophilic nature - their size and shape vary with RH; sequentially their optical properties become highly dependent on ambient atmosphere RH (e.g., Hess et al., 1998). The physico-chemical and optical properties of aged sea-salt aerosols are different from that of fresh sea-salt particles as well as due to their hygroscopic nature, the aging processes in sea-salt aerosols are faster than other non-hygroscopic aerosol species (e.g., Song and Carmichael, 2001). Wind speed is the main factor that determines the sea spray droplet production (in turn the sea-salt aerosol production rate); therefore, due to the seasonal variations of the wind speed, the sea-salt aerosol mass concentration and climatic impacts exhibit substantial seasonal dependence. The size distribution of sea-salt particles usually exhibit a bimodal structure (which covers a wide size range, of about 0.01 to 40 µm in diameter), with the highest number concentration in the sub-micron range and most of the masses concentrated in the super-micron range (Hess et al., 1998). Though the mass concentration of sea-salt aerosols varies substantially with time and space, different studies have estimated that oceans deliver about 10^{15} to 10^{16} g of sea-salt aerosols per year (Gong et al., 1997; Winter and Chylek, 1997; Hinds, 1999).

The wavelength (λ) dependent changes of whitecap reflectivity (r_{efl}) and emissivity (ϵ) make them detectable by remote sensors in different portions of the electromagnetic spectrum (e.g. Monahan and O'Muircheartaigh, 1986). In the visible (VIS) and near-infrared (NIR) spectral range, the whitecap r_{efl} is much higher than the surrounding water (Koepke, 1986). On the other hand, when the wavelength of the electromagnetic spectrum increases the whitecap r_{efl} gradually decreases; whereas, their ϵ progressively increases and eventually in the microwave region it reaches close to 1 (e.g., Koepke, 1986). Therefore, for satellite-borne sensors which measure the VIS radiation reflected by the ocean surface or brightness temperature in the microwave region, the spectral signatures of whitecaps (the signals of a foam-covered ocean) can be detected with a high signal-to-noise ratio (e.g., Koepke, 1986; Esaias et al., 1998). However, estimating the whitecap coverage of the ocean based on their spectral signatures is not sufficient to quantify the amount of sea-spray droplets (sea-spray aerosols) which get into the atmosphere (e.g., Monahan, 1986). Therefore, modelling the sea-salt aerosols from their emission to their re-deposition is necessary. For further information on modelling the generation function of sea-spray droplets and other atmospheric processes of sea-salt aerosols the readers may refer to Zakey et al., 2008 and references therein.

1.1.3 Aerosol size distribution

Generally, aerosols reside in the atmosphere as a mixture of species from a number of sources. There are two extreme mixing states of aerosols which are referred to as external and internal mixtures (Seinfeld and Pandis, 2006;

© University of Pretoria

Lesins et al., 2002). In an internal mixture, different species of particles from a number of sources are aggregated with one another and exist in the air as chemically homogeneous mixture of particles. In an external mixture, aerosols with a heterogeneous chemical composition are mixed in the atmosphere as physically separated particles (i.e., different aerosol species exists independently from one another) (Lesins et al., 2002). Mostly it is assumed that for a certain period, aerosols from primary emissions and secondary particle formation will reside near their sources in an externally mixed state. However, during the aerosol transportation and aging through coagulation, coalescence of particles in clouds or by chemical reactions on particle surfaces they gradually tend towards an internal mixture. The change in mixing state of particles affects both the physical and optical properties of the aerosols. Since aerosol lifetimes are short and their sources are heterogeneous, it is challenging to standardize the representation of the aerosol mixing state in models (Jacobson, 2001; Lesins et al., 2002; Stier et al., 2005). Still the treatment of aerosol mixing state and their chemistry vary among models (Lu and Bowman, 2010; Han et al., 2013). Overall, the variation in aerosol size, chemical composition and mixing state are important in governing their effects on climate and human health.

Characterizing different properties of atmospheric aerosols is a multidisciplinary topic. It is important to note that various disciplines, according to their interest, use different properties of aerosols as well as techniques for the characterization of atmospheric particulates. Size is normally used to classify aerosols because it is an easily measured property as well as many other important properties of the particles such as volume, mass, velocity and optical characteristics of aerosols are dependent on their sizes (Hinds, 1999). Moreover, the size of atmospheric particulates inferences about aerosol sources (or formation processes), their transformations and removal processes (Seinfeld and Pandis, 2006). Therefore, if the particle size and its concentration in a certain size range are known, it will be easy to estimate other physical properties of aerosols plus the source strengths. Particles in the atmosphere have widely variable shapes; therefore, different types of equivalent diameters have been used to characterize the aerosol geometrical diameters. Mostly aerodynamic diameters were used to standardize particles of various shapes and densities to spheres having the same aerodynamic property and settling velocity.

It is common to subdivide the atmospheric aerosol particles into two major size classes, so called modes (Whitby, 1978; Seinfeld and Pandis, 2006). Particles with diameters larger than 1.0 μm are identified as the coarse mode (super-micron particles), whilst those smaller than 1μm are usually referred to as fine mode (sub-micron particles). Fine mode particles can be further divided into three modes: a) an accumulation mode contains particles with diameters between 0.1-1.0 μm; b) Aitken mode refers to particles with sizes ranging from 0.01 to 0.1 μm and, c) nucleation mode (also known as ultrafine particles) are those with diameters < 0.01 μm. It is important to remark that the definition of size ranges of these modes (even sometimes the equivalent diameters used) in different disciplines, such as in climatic studies, the air quality and health issues were different. Generally, particles that are assigned in distinct size mode categories exhibit fundamental distinctions in their sources (formation), transformation processes and removal mechanisms (see Fig. 2).

The smallest aerosols (nucleation mode) are produced through gas-to-particle conversion processes which occur in the atmosphere. The formation of ultrafine particles may occur through homogeneous or heterogeneous nucleation processes (Kulmala et al., 2004). Usually under the influence of sunlight, the precursor gases get oxidized in the atmosphere and produce a compound with a lower vapour pressure. The oxidized compound can then condense together with other molecules (such as water) to form new particles (typically 1 to 2 nm size-clusters), this process is known as homogeneous nucleation. High super-saturation, strong solar radiation intensity, abundance of

© University of Pretoria

condensable vapour and typical atmospheric temperature are some of the favourable conditions for homogeneous nucleation to occur (e.g., Zhang et al., 2011). Freshly nucleated particles will grow larger through condensation of precursor gases (organic/inorganic vapours) on their surfaces; this is referred to as heterogeneous nucleation. Overall, the majority of ultrafine and Aitken mode particles (with diameters less than 0.1 μm) are created in the atmosphere by nucleation processes. In addition, the nucleation and Aitken mode particles normally dominate the particle number concentration; however, due to their small size, they represent only a small mass fraction of the total aerosol load.

After a nucleation event, due to the Brownian motion, aerosol particles will collide and then coalesce together to form one larger particle, a process called coagulation (Williams 1988). The rate of coagulation is mainly controlled by the diffusion coefficient of particles as well as the sizes and concentration of smaller particles. Overall, this transformation process plus the condensation of vapours onto Aitken mode aerosols will migrate smaller aerosols (diameters < 0.1 μm) to the accumulation mode. As nucleated particles grow to larger sizes, the concentration of the smallest particles may reduce rapidly; which in turn decrease the rate of collision-coalescence processes (coagulation) as well (Pöschl et al., 2007). Due to this, the growth of aerosol particles from the transient mode of accumulation into coarse mode will be constrained and particles will be accumulated (agglomerated) in this mode for a longer time, which is the reason it is termed the accumulation mode. Particles in the accumulation size range can also be introduced directly into the atmosphere (as primary aerosols); mainly from incomplete combustions (e.g., Dubovik et al., 2002) and occasionally from natural sources such as windborne dust and sea-spray (e.g. Todd et al., 2007). This reflects that both aerosol formation mechanisms (secondary and primary) are strongly overlapping in accumulation mode.

Most of the coarse mode particles consist of mechanically produced natural and anthropogenic primary aerosols. Sea-salt aerosols, biological particles, dust aerosols from volcanic eruptions and surface wind erosion are the main examples of naturally induced coarse particles. Mostly anthropogenic coarse particles are introduced into the atmosphere through construction work, industrial and agricultural activities. The most important mixing state for particles (especially the hydrophilic aerosols) is the mixing with water, which causes the growth of the particle size with humidity (RH) and shrinking as the RH decreases. These processes (condensation and evaporation) are not totally reversible: the rate of aerosol size growth in response to increase in RH is higher than the rate of shrinking in response to a decrease in RH. Therefore, in most urban areas and coastal regions, a small fraction of coarse mode particles ultimately result from the condensation of atmospheric water vapour on hydrophilic accumulation mode aerosols. Overall, various field studies showed that in terms of mass loadings the coarse mode particles are more dominant; however, due to their large size, they generally have relatively short atmospheric residence times compared to those of the fine mode aerosols. Observations and modelling studies also revealed that accumulation mode aerosols can be easily transported over long distances. However, the long-range transportation of coarse mode particles usually takes place when they are lifted above the boundary layer in which they are subsequently transported by free tropospheric winds.

To describe the size distribution of aerosol particles in models, it is appropriate to formulate a mathematical expression with some flexible parameters. The mass or number concentration of aerosols as a function of particle size is referred to as size distribution (dN/dr). Generally, the size distribution can be represented by a differential radius density distribution: $n(r) = dN(r)/dr$, where $N(r)$ is the number distribution function of aerosol particles. Here, $n(r)$ represent the number of particles with radii between r and $r + dr$ per unit volume (i.e., the number

© University of Pretoria

concentration of aerosols as a function of their size) and the total number of particles per unit volume, N_o, is given by $N_o = \int_0^\infty n(r)dr$. Aerosol size distribution does not always display bell shaped symmetrical curves (e.g., Maring et al., 2003). Therefore, different parametric size distribution functions were used in different models such as the Junge power law, the lognormal distribution and a modified gamma distribution (Hinds, 1999).

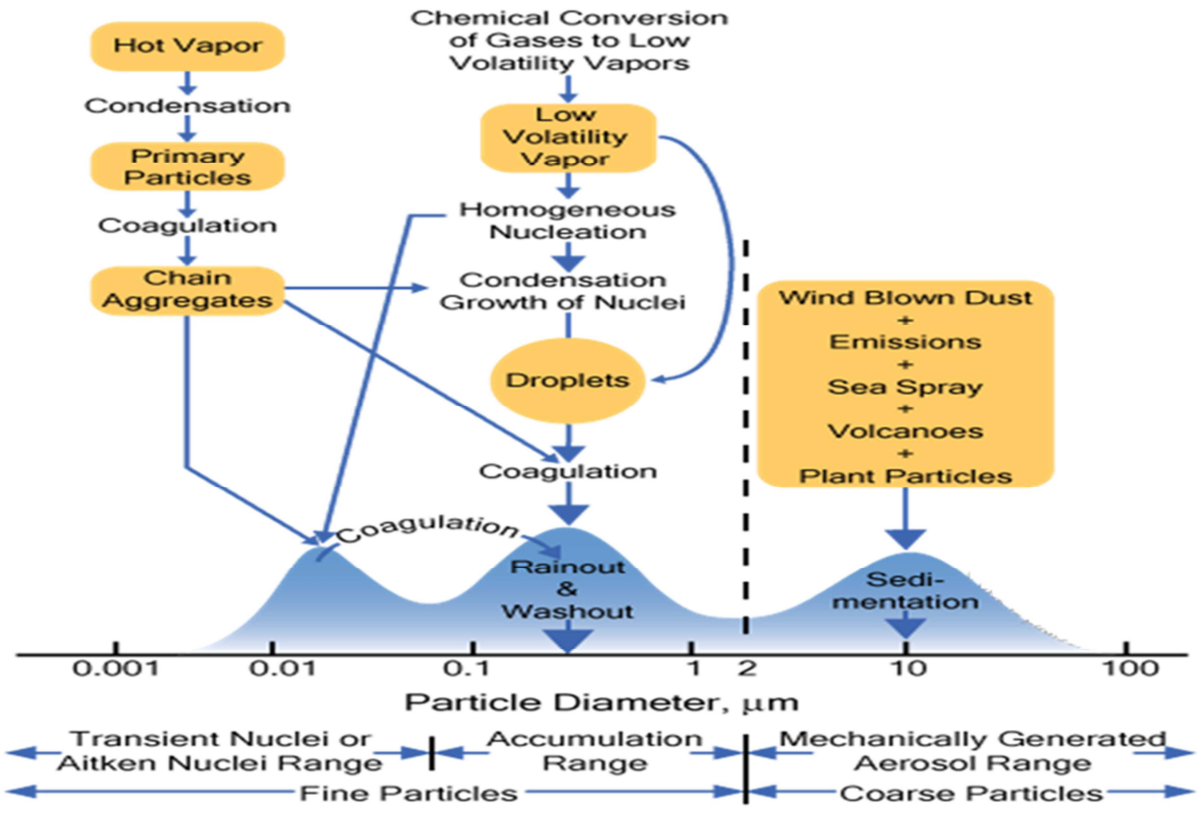

Fig. 2: Sketch of atmospheric aerosol surface area-weighted size distribution. The schematic diagram shows the three modes of aerosols, their major sources and removal mechanisms (originally from Whitby, 1978).

A lognormal distribution is one of the most widely used functions to approximate the actual number or mass distribution of aerosols which cover a wide range of sizes (Hess et.al., 1998; Seinfeld and Pandis, 2006). The occurrence of mono-disperse aerosols (i.e., particles which have narrow size distributions and lower geometric standard deviation) is very occasional (e.g., Schuster et al., 2006). It might occur during the studies of aerosols in laboratories (e.g., using particle generators) and rarely from biological sources. However, mono-disperse aerosols have symmetrical size distribution that can be approximated to be normal distribution:

$$n(r) = \frac{N_o}{\sqrt{2\pi}} \frac{1}{\delta} \, exp\left[-\frac{(r-\mu)^2}{2\delta^2}\right] \tag{1.1}$$

Where the mean, μ, and the standard deviation, δ, are defined as:

$$\mu = \frac{\int_0^\infty r\, n(r)dr}{\int_0^\infty n(r)dr} = \frac{1}{N_o}\int_0^\infty r\, n(r)dr \tag{1.2}$$

$$\delta = \frac{1}{N_o}\int_0^\infty (r - \mu)^2\, n(r)dr \tag{1.3}$$

The observations of particle size distribution using higher resolution aerosol sizing instruments showed that the size and concentration of aerosol particles generally covers several orders of magnitude - additionally, their distributions are asymmetric exhibiting a long tail at large particle sizes. Therefore, the normal distribution fit is not frequently suitable to express measured size distributions of poly-disperse aerosols (i.e., particles which have wider size distributions and higher geometric standard deviation). In addition, the normal distribution has a shortcoming of

© University of Pretoria

allowing negative radii. Therefore, to accommodate the orders of magnitude variations of poly-dispersed particle radii and number densities, usually the normal size distribution is represented on a logarithmic scale [$n(lnr) = dN(r)/dlnr$] (e.g., Jaenicke, 1988):

$$n(lnr) = \frac{dN}{dlnr} = \sum_{i=1}^{m} \frac{N_i}{\sqrt{2\pi}\, ln\, \delta_{g,i}}\ exp\left[-\frac{ln^2\left(\frac{r}{\vec{r_i}}\right)}{2\, ln^2\, \delta_{g,i}}\right] \tag{1.4}$$

where N_i denotes the aerosol number concentration in mode i and m is the total number of modes. $\delta_{g,i}$ is the geometric standard deviation representing the width of the particle size distribution of the i^{th} mode and $\vec{r_i}$ is the count median radius.

In statistical description of lognormal distributions, the log of the particle size distribution is symmetrical; thus the mean and the median of the lognormal distribution are equal. Therefore, $\vec{r_i}$ is equal to geometric mean radius of normal distributions (e.g., Voutilainen et al., 2000). As shown in Eq. (1.4) it is suitable to express the observed multi-modal aerosol size distributions as the superposition of two or more lognormal modes (Seinfeld and Pandis, 2006; Stier et al., 2005). This is because the distribution in Eq. (1.3) can be quickly described by the so called mode parameters [i.e., N_i, $\vec{r_i}$ and $\delta_{g,i}$] (Seinfeld and Pandis, 2006). Similarly, the lognormal distribution function can be used also to represent the mass size distributions of aerosols. Both the number and mass distribution have the same geometric standard deviation but their count-median radius is related by: $ln\vec{r}_{m,i} = ln\vec{r_i} + 3ln^2\delta_{g,i}$, where $\vec{r}_{m,i}$ is the mass based count median radius of the i^{th} mode.

Frequently, measured or parameterised particle size distributions are characterised by a single parameter which is known as the effective radius [r_{eff}] (McFarquhar and Heymsfield, 1998; Remer et al., 2005; Schuster et al., 2006). The r_{eff} is an important depiction of particle size distribution for describing their scattering properties. The computation of r_{eff} differs from the mean radius by including the particle area as a weight factor multiplying the particle size distribution: $r_{eff} = \frac{\int r^3 \frac{dN(r)}{dr} dr}{\int r^2 \frac{dN(r)}{dr} dr}$. The weighting factor is introduced because the amount of light scattered by aerosol particles is proportional to the area of the particle (see section 1.2.1). Therefore, various remote-sensing measurements are focused not only on retrieval of different optical properties of aerosols but also on r_{eff}.

1.1.4 Removal processes

Once airborne, particles will not persist in their original state for very long - rather through various atmospheric transformation processes (e.g., oxidation, polymerization, coagulation, condensation, evaporation) they may undergo changes in size, structure, number-density, mixing state and/or composition (Pöschl et al., 2005). Eventually, they will be removed from the atmosphere either through dry or wet deposition processes (Seinfeld and Pandis, 2006). Generally, tropospheric aerosols have relatively short atmospheric residence times, on the scale of minutes to weeks (Pöschl, 2005). The efficiency of aerosol removal processes is strongly dependent upon aerosol physico-chemical properties (such as size, hygroscopicity, etc.) and the ambient meteorological conditions (Ross et al., 2003; Pöschl et al., 2005; Seinfeld and Pandis, 2006). For instance, the sub-micron aerosols (particularly particles in the accumulation mode) have the longest atmospheric lifetime (~ from days to weeks); whereas, coarse mode particles in the lower-troposphere tend to have the shortest lifetimes of about ~ minutes to days (Lewis and Schwartz 2004; Stier et al. 2005).

© University of Pretoria

1.1.4.1 Wet deposition

Usually the formation of cloud droplets or ice particles is initiated around some condensation nuclei which tend to attract water vapour. In this regard atmospheric aerosols play an important role in the processes of cloud formation and precipitation (e.g., Penner et al., 2001; Ramanathan et al., 2001). When the ambient atmosphere RH increases, the condensation of water vapour on pre-existing aerosols will also be enhanced; this process persist the aerosol particles in equilibrium with the surrounding atmosphere RH - which in turn may cause the formation of cloud droplets (i.e., aerosols are acting as cloud condensation nuclei). Generally, this process is determined not only by the amount of moisture but also by the size and chemical composition (hygroscopicity) of the aerosol particle (Hegg et al. 2006; Tao et al., 2012). On the other hand, as the ambient RH decreases the cloud droplets will evaporate and the aerosol particles will be free to reside in the atmosphere; however, they might experience some physical and/or chemical changes. On the other hand, if the cloud droplets are dense enough to form precipitation that reaches the Earth's surface, aerosols which are in- and below-clouds will be scavenged on the way to the surface and removed from the atmosphere. The term rain-out (nucleation scavenging) is usually referred to as the removal of aerosols that are embedded or dissolved in cloud droplets; whereas, the term wash-out (impaction scavenging) designates below-cloud precipitation scavenging processes. The combination of these scavenging processes (i.e., rainout and washout) is known as wet deposition (Seinfeld and Pandis, 2006).

The Brownian diffusion and inertial impaction are the main forces which determine below-cloud scavenging processes of fine and coarse mode particles, respectively (Seinfeld and Pandis, 2006). Also, during impaction scavenging, the raindrop collision efficiency depends on both the raindrop size and particle size. Overall, due to the large surface area of cloud droplets, wet deposition is the most efficient removal mechanism for sub-micron particles with a diameter range of 0.1-1 μm as well as for coarse mode particles which are hygroscopic such as sea-salt aerosols (e.g. Croft et al. 2009). In contrast to particles which reside in the lower troposphere, stratospheric aerosols may remain for years (e.g., Hamill et al., 1997). This is primarily related with the lower level of stratospheric RH which caused the absence of efficient wet deposition processes.

1.1.4.2 Dry deposition

The deposition of airborne particles to the Earth's surface without precipitation is referred to as dry deposition. The particle size, atmospheric stability near the surface (i.e., convective transport and turbulent diffusion), surface wind speed and nature of the surfaces onto which the aerosols are being deposited play significant influences on the dry deposition process. Brownian diffusion and sedimentation are the two main mechanisms which cause dry deposition. Brownian diffusion is dependent on the particle size and adhesion process which varies with surface properties of the ground level. Generally, this mechanism is highly effective for fine particles which have diameters < 0.05 μm and it decreases with increasing particle size (Giorgi, 1988; Seinfeld and Pandis, 2006). Sedimentation (often referred to as gravitational sedimentation) is the settling of particles due to gravity. It is proportional with the square of the particle diameter and larger particles usually settle out quickly through this process (particularly the coarse mode particles which have a larger size and mass).

The dry deposition velocity of aerosol particles is described as the reciprocal of the aerodynamic and the quasi-laminar resistances (Hinds, 1999). Moreover, the deposition velocity of aerosols varies with surface uptake processes, for example: deposition velocities are larger over vegetated areas (especially in forests) than bare ground,

© University of Pretoria

ocean and snow surfaces (Giorgi, 1988; Seinfeld and Pandis, 2006). Due to this and other atmospheric conditions, for the same species of aerosol particles, the dry removal rate varies both spatially and temporarily. Studies reported that the deposition velocities of nuclei and coarse mode particles generally range from 0.01 to 0.2 cm/s and 1 to 5 cm/s, respectively. The lowest deposition velocities are reported for particles which are within the intermediate size range [i.e., accumulation mode aerosols] (e.g., Giorgi, 1988; Seinfeld and Pandis, 2006).

In general, the main differences among the two deposition mechanisms of aerosols (i.e., wet and dry deposition) is that wet removal can take place throughout the atmosphere where there is precipitating water, while dry deposition depends on the particles being transported near to the Earth's surface by turbulence or gravity (Zhao et al., 2003). Therefore, in both regional and global scale wet deposition is very important, but dry removal is relevant with respect to local air quality (in removing particles near their source regions) (e.g., Zhao et al., 2003; Tao et al., 2012).

1.2 Optical properties of aerosols

When a light beam passes through the atmosphere it undergoes a complicated interaction with the atmospheric constituents. The fundamental interaction processes among Electromagnetic Radiation (EMR) and air molecules/aerosol particles are scattering and absorption. Generally, during the interaction, the oscillating electric field of the incident radiation will set the electric charges of the air molecules/particles in oscillation. If the electromagnetic radiation stimulates state transitions between the electronic, vibrational, and rotational energy levels of air molecules/particles, this is referred to as absorption (e.g., Bohren and Huffman, 1983). In most cases, electronic transitions are stimulated by shorter-wavelengths; however, vibrational and rotational transitions (or the simultaneous transition of both of them) are stimulated by infrared and microwave radiations. These transitions (molecular absorptions) occur at a discrete set of wavelengths which are known as absorption lines. However, due to Doppler and pressure broadening processes the absorption lines of molecules exhibit broadened line width. Generally, depending on the wavelength (λ) of the incident radiation, the molecular species concentration and the physico-chemical properties the aerosol particles, parts of absorbed light can be used for photochemical changes or can be converted into thermal energy.

When the excited electric charges reradiates radiation over all directions, this is referred to as scattering (i.e., scattering is angular redistribution of energy). The two most common scattering processes in the atmosphere are: elastic scattering and inelastic scattering (e.g., Bohren and Huffman, 1983; Mishchenko 1993). In the course of inelastic scattering, the scattered radiation has a different λ from that of the incident radiation. Inelastic scattering processes include fluorescence and Raman scattering. When a beam of light is scattered elastically, the λ of the scattered light remains the same as that of the incident beam, only the trajectory of the scattered photon is modified (i.e., there is no appreciable energy exchange that takes place among the particle and the incident photons).

Depending on the size of the particle (relative to the λ of the incident radiation), elastic scattering can also be classified into Rayleigh scattering and Mie scattering. When the particle refractive index is closer to one and its size is much smaller than the λ of the incident radiation, radiating dipole is set up and the particle will scatter elastically with scattered irradiance proportional to λ^{-4}, this is referred to as Rayleigh scattering. During this case the scattering is symmetric because an electric dipole radiates equal amount of fluxes in both forward and backward directions (see Fig. 3). Usually Rayleigh scattering is applicable to describe the scattering properties of air molecules. Whereas,

© University of Pretoria

when the atmospheric particle size is comparable or larger than the λ of the incident radiation, this is referred to as Mie scattering. In Mie scattering the radiation is scattered in an anisotropic pattern, particularly the pattern develop a more intense forward lobe as the particle size increases (i.e., for larger particles more radiation is scattered in the forward direction than in the backward direction) (see Fig. 3).

In general, elastic scattering processes are relevant to describe the interaction of solar radiation (usually the visible and near-infrared spectrum) with gas molecules and aerosol particles. In addition, atmospheric gaseous molecules absorb solar and terrestrial radiation in discrete frequencies. For instance most of the solar radiation $\lambda < 0.3$ µm (ultraviolet light) is absorbed by atmospheric ozone (O_3) and $\lambda > 0.8$ µm is attenuated by oxygen molecules (O_2), O_3, water vapour (H_2O), carbon dioxide (CO_2), methane (CH_4) and other trace gases (Seinfeld and Pandis, 2006). Though in a different way, some aerosol particles also exhibit a smooth absorption curve across the solar and infrared spectrum; for example carbonaceous and dust particles (Hess et al., 1998). Also large particles such as dust (see chapter 4) as well as sea-salt aerosols (e.g., Li et al., 2008) have an important role in both shortwave and longwave spectral ranges.

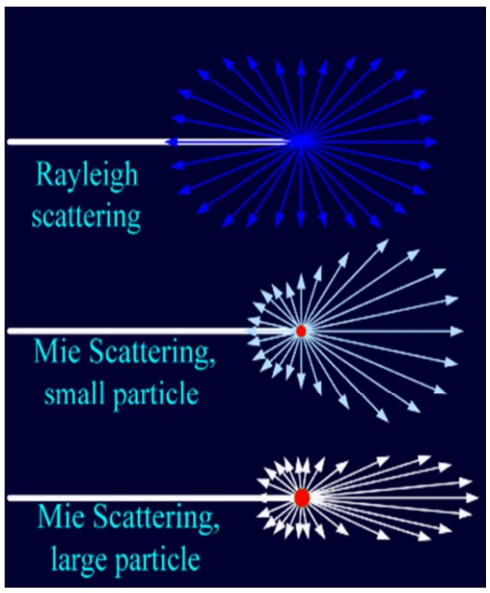

Fig. 3: The distribution of scattered radiation during Rayleigh and Mie scattering (taken from http://www.deepocean.net/deepocean/index.php?science07.php)

The interaction of aerosol particles with solar and terrestrial (usually referred to as thermal or longwave) radiation (through scattering and absorption) can considerably influence the Earth's radiation budget. Different optical phenomena such as coloured sunsets and changes in visibility are the direct manifestation of the interactions between atmospheric aerosols and the visible light. There are a number of optical properties of aerosols which describe the processes and the amount of light scattered and absorbed by aerosol particles. These optical parameters of aerosols are dependent on the λ of the incident radiation, the shape, size, chemical composition of particles, and their mixing states. In addition, the ambient atmosphere relative humidity plays an important role in determining the magnitudes of different optical parameters of aerosols, especially for these which have hydrophilic nature (e.g., Levoni et al., 1997; Hess et al., 1998). As a result, computing different optical properties of aerosols from terrestrial remote-sensing and *in-situ* measurements is relevant to retrieve the atmospheric aerosol microphysical properties as well as to assess possible impacts of aerosols on the climate system. The interpretation as well as the retrieval processes of remote-sensing observations needs a quantitative knowledge of electromagnetic interaction as a function of particle physical parameters.

© University of Pretoria

1.2.1 Mie scattering

The treatment of light scattering by atmospheric particulates is typically partitioned into three consecutive steps. The first step began by solving Maxwell equations inside the particle and in a medium where the particle is embedded (using a linear optics) and via computing the far field scattering and absorption properties of an individual particle. This approach forms the basis of the modern theory of electromagnetic scattering by small particles. The second step is, using the single-scattering approximation, solving the scattering and absorption properties of particles which are contained within a small volume element. Finally, multiple scattering by the entire atmospheric particles were group by solving the radiative transfer equation. Mie theory provides a solution for light scattering by isotropic spherical particles which reside in a homogeneous medium. The logical point of departure for Mie scattering formulation is the Maxwell equations; therefore, the electric field solution inside and outside the spherical particle are expressed in a vector spherical harmonic expansion which satisfies Maxwell's equations. Here, only a brief summary of the far field solution of Mie scattering will be given; however, for further information about the Mie theory and spherical harmonics used in its formulations, the readers are referred to (Bohren and Huffman, 1983).

For practical applications (particularly in the case of atmospheric studies), light scattering observations are normally carried out in the far-field zone (i.e., at a large distance 'r' from a spherical particle which has a radius 'a'). In the far-field ($r >> ka^2, k = 2\pi/\lambda$), by defining the two polarization states (i.e., parallel and perpendicular) the solution of the vector wave equation (in terms of electrical field) can be expressed as (Bohren and Huffman, 1983):

$$\begin{bmatrix} E_{\parallel}^{S} \\ E_{\perp}^{S} \end{bmatrix} = \frac{exp(-ikr+ikz)}{ikr} \begin{bmatrix} S_2(\chi, m, \Theta) & S_3(\chi, m, \Theta) \\ S_4(\chi, m, \Theta) & S_1(\chi, m, \Theta) \end{bmatrix} \begin{bmatrix} E_{\parallel}^{i} \\ E_{\perp}^{i} \end{bmatrix} \quad (1.5)$$

Where $exp(ikz)$ is the incident plane wave and $\frac{exp(-ikr)}{ikr}$ is the outgoing scattered wave. $E_{\parallel}^{i}$ and $E_{\perp}^{i}$ are the parallel and perpendicular components of incident electrical field. $E_{\parallel}^{S}$ and $E_{\perp}^{S}$ are the parallel and perpendicular components of scattered electrical field. $\chi = ka = \frac{2\pi a}{\lambda}$ is called the size parameter (it is one of the important parameter which relates the particle size to the wavelengths of the incident radiation) and $k = \frac{2\pi}{\lambda}$ is the circular wavenumber in the ambient medium. The matrix $\begin{bmatrix} S_2(\chi, m, \Theta) & S_3(\chi, m, \Theta) \\ S_4(\chi, m, \Theta) & S_1(\chi, m, \Theta) \end{bmatrix}$ is the scattering amplitude matrix; for spherical particles: $S_3(\chi, m, \Theta) = S_4(\chi, m, \Theta) = 0$. Thus Eq. (1.5) gives:

$$\begin{bmatrix} E_{\parallel}^{S} \\ E_{\perp}^{S} \end{bmatrix} = \frac{exp(-ikr+ikz)}{ikr} \begin{bmatrix} S_2(\chi, m, \Theta) & 0 \\ 0 & S_1(\chi, m, \Theta) \end{bmatrix} \begin{bmatrix} E_{\parallel}^{i} \\ E_{\perp}^{i} \end{bmatrix} \quad (1.6)$$

The Mie theory scattering amplitudes [$S_1(\chi, m, \Theta)$ and $S_2(\chi, m, \Theta)$] are expressed by:

$$S_1(\chi, m, \Theta) = \sum_{n=1}^{\infty} \frac{2n+1}{n(n+1)} [a_n \pi_n(\cos\Theta) + b_n \tau_n(\cos\Theta)] \quad (1.7)$$

$$S_2(\chi, m, \Theta) = \sum_{n=1}^{\infty} \frac{2n+1}{n(n+1)} [b_n \pi_n(\cos\Theta) + a_n \tau_n(\cos\Theta)] \quad (1.8)$$

Where n are positive integers. π_n and $\tau_n$are Mie angular functions which are expressed as function of associated Legender polynomials (P_n^1) with argument $\cos(\Theta)$: $\pi_n(\cos\Theta) = \frac{1}{\sin(\Theta)} P_n^1(\cos\Theta)$, $\tau_n(\cos\Theta) = \frac{d}{d\Theta} P_n^1(\cos\Theta)$. a_n and b_n are coefficients of outgoing (scattered) spherical waves which are determined from the boundary conditions at the surface of the sphere using Ricatti-Bessel functions. Both a_n and b_n are functions of the size parameter, χ and the

© University of Pretoria

complex refractive index, m. Now the far-field scattered intensity components can be written in terms of the incident intensity components:

$$I_{\parallel}^{s} = I_{\parallel}^{i} \frac{i_2(\chi,m,\Theta)}{k^2r^2}, I_{\perp}^{s} = I_{\perp}^{i} \frac{i_1(\chi,m,\Theta)}{k^2r^2} \tag{1.9}$$

Where $i_1(\chi,m,\Theta) = |S_1(\chi,m,\Theta)|^2$ and $i_2(\chi,m,\Theta) = |S_2(\chi,m,\Theta)|^2$ are the intensity functions for the perpendicular and parallel components, respectively. Consider a point located over the far-field zone at x, y, z in the forward direction (i.e. $\Theta = 0, x.y \ll z$), thus

$$r = (x^2 + y^2 + z^2)^{\frac{1}{2}} \approx z + \frac{x^2+y^2}{2z} \tag{1.10}$$

Then, to evaluate reduction of the incident energy due to absorption and scattering of light by a spherical particle over the far-field zone, we consider that the incident light is polarized linearly in the perpendicular direction - thus, the scattered electric field in Eq. (1.6) is given by

$$E_{\perp}^{s} = \frac{exp(-ikr+ikz)}{ikz} S_1(\chi,m,\Theta)E_{\perp}^{i} \tag{1.11}$$

Using Eq. (1.10) and upon superimposing the incident and scattered electric fields in the forward direction, we obtain

$\left|E_{\perp}^{s} + E_{\perp}^{i}\right| \approx \left|E_{\perp}^{i}\right|^2 \left(1 + \frac{S_1(\chi,m,0)\, exp-ik\left(\frac{x^2+y^2}{2z}\right)}{ikz}\right)$, which implies that the far field combined flux density in the forward directions is proportional to:

$$\left|E_{\perp}^{s} + E_{\perp}^{i}\right|^2 \approx \left|E_{\perp}^{i}\right|^2 \left(1 + \frac{2}{kz} Re\, \left\langle \frac{S_1(\chi,m,0)\, exp-ik\left(\frac{x^2+y^2}{2z}\right)}{i} \right\rangle\right) \tag{1.12}$$

Integrating the combined flux density over the cross section area of a spherical particle which has a radius 'a'; we obtain the total power combined:

$$\frac{\iint \left|E_{\perp}^{s} + E_{\perp}^{i}\right|^2 dx\, dy}{\left|E_{\perp}^{i}\right|^2} = \pi a^2 - \sigma_e \tag{1.13}$$

The first term on the right-hand side of Eq. (1.13) represents the cross section of area of the sphere. The physical interpretation of the second term (σ_e) is that the total amount of light reduced due to the presence of a spherical particle, or σ_e can also be interpreted as the optical shadow area of the aerosol particle (Bohren and Huffman, 1983). Overall, Eq. (1.13) shows that the total energy removed from the beam of radiation incident on the particle is proportional to the incident energy and the proportionality constant σ_e (which is referred to as extinction cross section: units of m^2). The double integral over $dxdy$ by which σ_e is defined contains two Fresnel integrals, and if the limits are assumed to extend to ∞, we get

$$\iint_{-\infty}^{\infty} exp - ik\left(\frac{x^2+y^2}{2z}\right) dxdy = \frac{2\pi z}{ik} \tag{1.14}$$

Therefore, extinction cross section can be expressed as:

$$\sigma_e = \frac{4\pi}{k^2} Re[S(\chi,m,0)] \tag{1.15}$$

© University of Pretoria

However for the forward direction (i.e., $\Theta = 0^0$) the two amplitude functions [Eq. (1.7) and Eq. (1.8)] can be reduced to:

$$S_1(\chi, m, 0) = S_2(\chi, m, 0) = S(\chi, m, 0) = \frac{1}{2}\sum_{n=1}^{\infty}(2n+1)\ (a_n + b_n) \tag{1.16}$$

The fact that there is only one $S(\chi, m, 0)$ is because of the symmetry of the forward scattering in which the extinction is independent of the state of polarization of the incident light. Overall, extinction is the total effects of scattering and absorption; thus, σ_e can be expressed as the sum of the scattering (σ_s) and absorption (σ_a) cross sections. The σ_s can also be predicted directly by Mie theory, however to satisfy energy conservation σ_a can be determined from the differences of σ_e and σ_s (i.e., $\sigma_a = \sigma_e - \sigma_s$). The dimensionless optical quantity of a particle which is known as extinction efficiency (Q_e) is defined as the ratio of σ_e to the particle geometric area projected onto the plane perpendicular to the incident beam. In the case of Mie scattering, for a spherical particle with a radius, 'a'; using Eq. (1.15) and Eq. (1.16) Q_e can be expressed as:

$$Q_e = \frac{\sigma_e}{\pi a^2} = \frac{2}{\chi^2}\sum_{n=1}^{\infty}(2n+1)\ Re(a_n + b_n) \tag{1.17}$$

where $\chi = ka = \frac{2\pi a}{\lambda}$ is the size parameter and $k = \frac{2\pi}{\lambda}$ is the wave number in the ambient medium.

The flux density of the scattered light in an arbitrary direction is given by

$$F(\theta, \varphi) = \frac{F_0}{k^2 r^2}\ [i_2(\theta)cos^2\varphi + i_1(\theta)sin^2\varphi] \tag{1.18}$$

Where F_0 represent the incident flux density. The total flux of the scattered light is, therefore,

$$f = \int_0^{2\pi}\int_0^{\pi} F(\theta, \varphi)\, r^2 \sin(\theta)\, d\theta d\varphi \tag{1.19}$$

where $\sin(\theta)\, d\theta d\varphi$ is the differential solid angle, $d\boldsymbol{\Omega}$; thus, $r^2 d\boldsymbol{\Omega}$ is the differential area. Hence, the scattering cross section may be defined as

$$\sigma_s = \frac{f}{F_0} = \frac{\pi}{k^2}\int_0^{\pi}[i_1(\theta) + i_2(\theta)]\sin(\theta)d\theta \tag{1.20}$$

Similar to Eq. (1.17), using the orthogonal and recurrence properties of the associated Legendre polynomials Bohren and Huffman, (1983), the scattering efficiency of a spherical particle can be expressed as:

$$Q_s = \frac{\sigma_s}{\pi a^2} = \frac{2}{\chi^2}\sum_{n=1}^{\infty}(2n+1)\ (|a_n|^2 + |b_n|^2) \tag{1.21}$$

Based on Eq. (1.21), the highest values of Q_s (in turn Q_e: Eq. (1.17)) can be found when the diameter of the particles is similar to the wavelength of the light Bohren and Huffman, (1983). Lastly, the absorption cross section and efficiency of a sphere particle can be expressed as:

$$\sigma_a = \sigma_e - \sigma_s = \frac{\pi}{k^2}[\sum_{n=1}^{\infty}(2n+1)(-1)^n\ (a_n - b_n)]^2 \tag{1.22}$$

$$Q_a = Q_e - Q_s = \frac{1}{\chi^2}[\sum_{n=1}^{\infty}(2n+1)(-1)^n\ (a_n - b_n)]^2 \tag{1.23}$$

As mentioned previously, the Mie coefficients (a_n, b_n) are governed by two wavelength dependent parameters: the complex refractive index of the particle, m and the dimensionless size parameter, χ. Therefore, the

© University of Pretoria

computation of particle size and their refractive index have important roles in determining other optical parameters of aerosols [Eq. (1.17), Eq. (1.21) and Eq. (1.23)]. Using the results of the single-scattering solutions, the size distribution information and different mixing state assumptions, one can approximate the scattering and absorption properties of particles which are contained within a small volume element.

When $\chi << 1$ and the imaginary part of the complex refractive index of the particle is approximated to zero (i.e., $m = m_r$), the leading terms in the expression of Mie amplitude function [Eq. (1.7) and Eq. (1.8)] will be dominated by the first term a_1: $a_1 = \frac{2\chi^3 i(m_r^2-1)^2}{3(m_r^2+2)^2}$; i.e., Mie scattering merges to Rayleigh scattering. Therefore, the Raleigh scattering cross section in terms of the molecular volume 'v' instead of radius 'a' becomes:

$$C_{scat}(\theta) = \frac{9\pi^2 v^2 (m_r^2-1)^2 (cos^2\theta+1)}{2r^2\lambda^4(m_r^2+2)^2} \tag{1.24}$$

Then the total energy scattered in all directions or the total scattering cross section obtained by the integration of Eq. (1.24) is

$$C_{scat} = \int_0^{2\pi}\int_0^{\pi} C_{scat}(\theta)\, r^2 \sin(\theta)\, d\theta d\varphi = \frac{24\pi^3 v^2 (m_r^2-1)^2}{\lambda^4(m_r^2+2)^2} = \frac{24\pi^3 (m_r^2-1)^2}{\lambda^4 N^2 (m_r^2+2)^2} \tag{1.25}$$

where N is the number of molecules that have a molecular volume 'v' per unit volume. Whereas, when $\chi >> 1$, Mie theory will merge to the geometrical optics; such as phenomena like rainbows or halos are described with geometric scattering.

1.2.2 Important optical properties of aerosols

1.2.2.1 Complex refractive index

The refractive index of aerosols is a complex dimensionless parameter which is defined as:

$$m = m_r + im_i \tag{1.26}$$

Inside a particle medium the speed of light is reduced (relative to a vacuum); therefore, the ratio of the speed of light in a vacuum (c) to the speed inside the particle (v) is defined as real part of the refractive index (m_r).

$$m_r = \frac{c}{v} = \sqrt{\frac{\mu_p \epsilon_p}{\mu_o \epsilon_o}} = \sqrt{\epsilon\mu} \tag{1.27}$$

where ϵ is the particle relative permittivity and μ is its relative permeability.

As shown in Eq. (1.27) m is an intrinsic property which is linked to the dielectric constant of a particle. The fact that aerosols reside in the atmosphere plus most atmospheric particulates are non-magnetic mediums (i.e., $\mu_p = \mu_o$); therefore m is approximately$\sqrt{\epsilon}$. To account for the absorption effects of aerosols, ϵ (and in turn m) is defined as a complex quantity. Thus, using the classical damped harmonic oscillator model (Lorentz-Lorenz and Maxwell's relation) the spectral variation of complex refractive index can be described as function of wavenumber ($\tilde{\nu} = \frac{1}{\lambda}$) dependent complex dielectric constant (relative permittivity) (Bohren and Huffman, 1983; Thomas et al., 2004):

$$m_r(\tilde{\nu}) = \left(\frac{\sqrt{\epsilon'(\tilde{\nu})^2 + \epsilon''(\tilde{\nu})^2} + \epsilon'(\tilde{\nu})}{2}\right)^{\frac{1}{2}} \tag{1.28}$$

© University of Pretoria

$$m_i(\tilde{\nu}) = \left(\frac{\sqrt{\epsilon'(\tilde{\nu})^2 - \epsilon''(\tilde{\nu})^2} + \epsilon'(\tilde{\nu})}{2}\right)^{\frac{1}{2}} \quad (1.29)$$

where ϵ' and ϵ'' are the real and imaginary part of the dielectric constant of a particle, respectively.

The real part of m determines the scattering effects of aerosols; whereas, the imaginary part accounts for the absorption characteristics. Generally, the chemical composition of aerosols (and in turn their dielectric characteristics: Eq. (1.28) and Eq. (1.29)), their mixing state and the ambient atmosphere RH determines the magnitude of aerosol complex refractive index (Liu et al., 2002; Tegen, 2003). As previously mentioned, atmospheric aerosols are composed of multi-component particles, which are mixed internally and/or externally. Therefore, the effective refractive index of atmospheric aerosols are computed using different optical mixing rules such as Lorentz–Lorenz, Maxwell-Garnett rule, effective medium approximation and others (e.g., Chylek et al., 1981; Abo Riziq et al., 2007). Overall, particles produced from incomplete biomass combustions have high shortwave absorption properties and hence high m_i. Over the visible spectrum, partially absorbing aerosols such as mineral dust and organic carbon usually exhibit intermediate values of both m_r and m_i. Sulfates, nitrates and sea-salt aerosols are examples of atmospheric particles which have high shortwave scattering properties and hence m_r.

The Mie coefficients (a_n, b_n) are a function of m; thus, any uncertainties associated with m, in turn affect the accuracy of extinction, scattering and absorption efficiencies that are respectively calculated from Eq. (1.17), Eq. (1.21) and Eq. (1.23) (e.g., Kim and Lior, 1995). Here, *in-situ* measurements plays an important role in constraining the uncertainties that are related with m as well as χ (McMurry, 2000; Irshad et al., 2009). For instance, water uptake by hydrophilic aerosol species such as sulfates, nitrates and sea-salt particles leads to an increase in the size and a change in the chemical composition of the aerosol particle; and in turn m. In this case, empirical relations derived from humidograph (humidified nephelometer) measurements are important in expressing the hygroscopic growth factor of aerosol particles and their RH dependent effective refractive index (e.g., ten Brink et al., 2000; Magi and Hobbs, 2003). Also, the knowledge of the RH dependence of m from *in-situ* measurements are important to improve the accuracies of aerosol optical property retrievals from remote-sensing measurements (e.g., Remer et al., 2005) plus to reduce the uncertainties that exist in aerosol radiative forcing computations (e.g., Ghan and Schwartz, 2007).

1.2.2.2 Aerosol optical depth

Eq. (1.17), Eq. (1.21) and Eq. (1.23) respectively represent the extinction, scattering and absorption efficiencies of single-particles. The total extinction effects of poly-dispersed particles on incident radiation can be described by another extensive optical parameter known as the extinction coefficient (α_{ext}: unit m^{-1}). For population of particles with total number concentration N_o(m^{-3}), size distribution $n(r) = dN(r)/dr$ which span from r_{min} (minimum radius) to r_{max} (maximum radius), α_{ext} can be defined as:

$$\alpha_{ext} = \int_{r_{min}}^{r_{max}} \pi r^2 Q_e \left(\frac{dN(r)}{dr}\right) dr \quad (1.30)$$

Using Eq. (1.21) (Q_s) and Eq. (1.23) (Q_a) the scattering and absorption coefficients of poly-dispersed particles can be defined similarly as Eq. (1.30); therefore, the extinction coefficient can be written as the sum of the scattering coefficient and absorption coefficient. Vertically integrated spectral extinction coefficient of aerosol particles is known as column extinction optical depth (AOD: τ_λ) and is defined as:

$$\tau_\lambda = \int_0^\infty \alpha_{ext,\lambda} dz \quad (1.31)$$

© University of Pretoria

where z is the altitude in the atmospheric column with units of length such that τ_λ is a dimensionless parameter. The τ_λ depends on the vertical profile of α_{ext} [Eq. (1.30)]; in turn, it is a complex function of m, χ and the aerosol number concentration. The AOD is one of the key optical parameter of aerosols which can be derived from ground-based and space-borne atmospheric remote-sensing measurements. The spectral dependence of α_{ext} and τ_λ can be described by an empirical expression which is known as Angstrom exponent (α). The α and its spectral derivative (α′) are important parameters to illustrate the dominant mode of aerosol size distribution. For further discussion on τ_λ, α and α′ as well as their significance the reader is requested to refer the next chapter.

Another useful optical parameter of aerosols which is determined from the extinction (scattering or absorption) coefficient is the mass specific extinction [γ_{ext}] (scattering [γ_{scat}] or absorption [γ_{abs}]) efficiency. γ_{ext} (γ_{scat} or γ_{abs}) are defined as the amount of extinction (scattering or absorption) per unit mass of aerosol (usually it is expressed with a unit of m^2/g):

$$\gamma_{x_i}^{\lambda} = \frac{3Q_x^{\lambda}}{4r_i\rho_i} \tag{1.32}$$

where the subscript x_i stands for *'ext', 'scat' or 'abs'* which represent the processes of extinction scattering, and absorption for specific particulate component, respectively. ρ_i and r_i are correspond to the density and radius of specific aerosol particles. Overall, $\gamma_{x_i}^{\lambda}$ specifies the efficiencies of a unit mass of single aerosol component in attenuating radiation. In aerosol modelling studies, $\gamma_{x_i}^{\lambda}$ is often used to determine the extinction (scattering or absorption) optical depths of individual/groups of atmospheric aerosols (see chapter 3).

1.2.2.3 Phase function

The phase function [$P_\lambda(\chi, m, \theta_s)$] of a particle describes the angular distribution of the light scattered by a particle; it is highly sensitive to the particle shape (e.g., Mishchenko 1993; Borrmann et al., 2000). Theoretically P_λ can be expressed as the scattered intensity at a specific scattering angle (θ_s) normalised by the integral of the scattered intensity over all scattering directions. Therefore, P_λ can be taken as the probability distribution function which expresses the probability of scattering within a certain differential scattering angle ($d\theta_s$) relative to the direction of the incident radiation:

$$1 = \frac{1}{2}\int_0^{\pi} P_\lambda(\theta)\sin(\theta)d\theta \tag{1.33}$$

The radiation scattered by a particle in forward and backward hemispheres are important to assess the radiative influences of aerosols. Therefore, P_λ is parameterized analytically with asymmetry parameter: g_λ, which is defined as the cosine-weighted mean of the angular scattering phase function [Eq. (1.34)]. Accordingly, g_λ is usually applicable in radiative transfer calculations which are implemented in climate models.

$$g_\lambda = \frac{1}{2}\int_0^{\pi} P_\lambda(\theta)\cos(\theta)\sin(\theta)d\theta \tag{1.34}$$

Theoretically g_λ varies between -1 (for complete back scattering; θ_s = 180°) and +1 (scattering is entirely in the forward direction: θ_s = 0°). When g_λ = 0 the scattering is isotropic (i.e., the scattering is symmetric with respect to the forward and backward directions).

© University of Pretoria

1.2.2.4 Single scattering albedo

Spectral single scattering albedo (ω_λ) is an aerosol composition dependent dimensionless quantity which represents the fraction of extinction due to scattering (i.e., it mirror the relative effects of scattering and absorption). For single particles, ω_λ can be quantified as the ratio of the scattering efficiency to extinction efficiency (i.e., for spherical particle ω_λ is the ratio of Eq. (1.21) to Eq. (1.17)):

$$\omega_\lambda = \frac{Q^\lambda_{scat}}{Q^\lambda_{ext}} \tag{1.35}$$

For poly-dispersed atmospheric aerosols, the columnar average ω_λ can be quantified as the ratio of scattering optical depth to extinction optical depth. The value of ω_λ ranges from 0 (for purely-absorbing aerosols) to 1 (for non-absorbing aerosols). Atmospheric aerosols contain a complex mixture of absorbing and scattering constituents; thus the columnar average ω_λ is in between its two extreme values. ω_λ is an important parameter in determining the amount of atmospheric heating due to the aerosol. For instance, in the visible spectral range, ω_λ of sulfate and sea-salt aerosols are close to 1 (their m_i is almost zero); therefore, their atmospheric heating effects is nearly zero. Whereas, BC and dust have lower values of ω_λ (they have higher values of m_i), thus they have atmospheric heating influences (e.g. Hess et al., 1998; see also chapter 4 and chapter 5).

Overall, ω_λ determines the sign of atmospheric aerosol direct radiative forcing: negative (cooling) or positive (warming) in the atmosphere (e.g. Hansen et al., 1997; Liao and Seinfeld, 1998). In order to retrieve different microphysical parameters of aerosols as well as to examine their radiative influences using radiative transfer theory, the quantification of τ_λ, ω_λ, and g_λ is crucial (Liao and Seinfeld, 1998). Therefore, to determine these important optical parameters of aerosols with better accuracy and to reduce uncertainties in model estimated aerosol forcing, various measurement techniques and modelling approaches need to be synchronized together. This particular topic as well as additional information about the importance of aerosol optical properties will be discussed later in this study (see chapter 3).

1.3 Climatic implications of aerosols

Atmospheric aerosols have several environmental effects (which range from local to global scale). The health effects of aerosols are typically important on a local scale, such as in highly populated regions, industrialized urban zones as well as in some sectors such as in mining areas (e.g., Forsberg et al., 2005). Depending on the concentrations, chemical composition and duration of exposure, inhalation of fine particles may cause certain health hazards which range from small cardiovascular and respiratory system irritations to serious infections (Harrison and Yin, 2000). From regional to a global scale, aerosols have a potential to influence heterogeneous chemistry processes of the atmosphere (Ravishankara, 1997; Finlayson-Pitts and Pitts, 2000) as well as the Earth's climate (Penner et al., 2001; Ramanathan et al., 2001).

Contingent on manifold environmental situations as well as the aerosol physico-chemical properties, atmospheric particulates can act as sites for heterogeneous chemical reactions to take place (e.g., Ravishankara, 1997). For instance, depending on environmental conditions of the region, the photochemical reactions of inorganic halogens (which are primarily induced from sea-salt sprays) have a dual role in promoting surface O_3 production or destruction (Finlayson-Pitts and Pitts, 1997; Keene et al., 1999; WMO, 2002). Furthermore, it has been hypothesised

© University of Pretoria

that during the polar stratospheric cloud formation, aerosol reactions lead to the formation of reactive chlorine, which eventually increases ozone destruction (e.g., WMO, 2002). Overall, the chemical reactions within sea-spray aerosols, dust and other atmospheric constituents, sulfur cycle as well as other chemical processes of particulates have a diverse influence in atmospheric chemistry and environmental processes (e.g., Dentener et al., 1996; Seinfeld and Pandis, 2006).

The deposition processes of atmospheric aerosols have also an important role in natural ecosystems, e.g., via inducing acidic rain formation and changes in biogeochemical cycling (e.g., Mahowald et al., 2011 and references therein). Even though atmospheric aerosols have been implicated in various issues, the focal point of this study is on their role in the climate system. Aerosols influence both regional and global climate through different mechanisms that are broadly classified into three basic groups: direct, semi-direct and indirect effects; which will be briefly discussed below.

1.3.1 Direct Radiative Effect

The primary source of energy that drives the Earth's climate system is radiation from the Sun (Houghton et al. 2001). The extra-terrestrial solar spectrum (spectral distribution of solar radiation at the top of the Earth's atmosphere) approximately lies within the wavelength range $0.2 < \lambda < 4.0\mu m$, with a maximum of energy at $\lambda \sim 0.475\mu m$. The total amount of solar radiation falling at the top of the Earth's atmosphere varies with different factors such as the Earth-Sun distance and tilt of the Earth's axis (Liou, 2002).

While the solar radiation passes through the Earth's atmosphere, various attenuation processes will reduce its energy such as absorption, scattering, refraction, reflection and diffraction. Mostly in the ultraviolet (UV) region selective absorption takes place due to the ozone, while water vapour and other greenhouse gases primarily absorb in the infrared (IR) region (Seinfeld and Pandis, 2006). Over the lower parts of the visible spectrum, attenuation usually takes place through scattering by gaseous constituents and fine particles (occasionally some molecules and particles also absorb in this region). Generally, the scattering and absorption by atmospheric aerosols takes place in the visible (VIS) and near-infrared (NIR) region. As the size of atmospheric particles becomes larger ($> 35\ \mu m$) the process of refraction and diffraction become dominant in attenuation, such as rain and cloud droplets as well as occasionally occurring dust and biogenic aerosols belong to this category. Attenuation through reflection (as well as multiple scattering) mostly occurred by clouds. Eventually, the solar radiation reaches the Earth's surface as two components: direct (i.e., part of extra-terrestrial solar radiation which reaches the Earth's surface without being scattered) and diffuse (part of extra-terrestrial solar radiation which arrives at the Earth's surface as a result of scattering, reflection and other dispersion). The sum of direct and diffuse components of solar radiation gives the total surface solar radiation.

Depending on the surface type (and in turn the surface albedo) as well as angle of the sun, the solar radiation falling on the Earth's surface will be absorbed or reflected (as well as diffused through multiple scattering). For example: fresh snow reflects 80-90% of the VIS-spectrum, whereas fresh asphalt reflects only 4-8%. The physical process of energy transfer in the form of electromagnetic radiation within the Earth-atmosphere system can be described mathematically using the Radiative Transfer (RT) theory. Considering various physical phenomena, the energy redistribution due to different scattering processes and various forms of energy loss - by absorption, as well as gains due to emission are comprised in three-dimensional (3D) atmospheric RT equation. Thus, the radiation budget of the Earth-atmosphere system can be computed from the solution of RT equation (e.g., Liou, 2002). Moreover,

© University of Pretoria

advanced RT theory is very important for the retrieval of atmospheric constituents plus different state parameters of the atmosphere from measured spectra (such as from passive remote-sensing measurements). For detailed information on radiation processes in planetary atmosphere, the mathematical description of RT theory and essential conditions/approximations that are necessary for RT model implementation, the readers are referred to Kiehl et al. (1996) and Liou (2002).

Generally, the absorption of solar radiation (primarily by the underlying surface and to some extent by the atmosphere) is approximately balanced by the outgoing long-wave radiation. Radiative forcing refers to a change in the radiation budget (in both shortwave and longwave) of the Earth-atmosphere system through different radiation perturbing agents. This drives the climate system to a new thermal equilibrium state and results in several changes on our climate system. Therefore, radiative forcing is often expressed as one of the main factors which causes climatic forcing (commonly known as climate change). For instance, aerosol particles and greenhouse gases can directly scatter and absorb electromagnetic radiation (which in turn can change the planetary albedo); thereby they are taken as the major atmospheric radiative forcing (climatic forcing) agents.

The net flux (F_{net} in units of W/m^2) in a specified λ range and at any level in the atmosphere is defined as the difference in downward (F_{down}) and upward (F_{up}) fluxes that are computed using radiative transfer theory:

$$F_{net} = F_{down} - F_{up} \tag{1.36}$$

Thus, aerosol Radiative Forcing (RF) at a specific level of the atmosphere is defined as (Forster et al., 2007):

$$RF = F_{net,a} - F_{net,n} \tag{1.37}$$

where $F_{net,a}$ and $F_{net,n}$ are the net flux at the same level of the atmosphere but with and without aerosols, respectively.

The negative sign of RF (Eq. (1.37)) denotes radiative cooling tendencies of aerosols and the vice versa for a positive sign of RF. Generally, atmospheric aerosols can exert radiative forcings directly and/or indirectly. Direct radiative forcing occurs due to the aerosols ability to scatter and absorb the incoming/surface and cloud reflected solar radiation as well as through their emission of thermal radiation such as from mineral dust aerosol layer. Indirect radiative forcing occurs due to their cloud condensation nuclei role, aerosols affect the microphysical and optical properties of clouds such as its albedo (first indirect effect; e.g., Forster et al., 2007 and references therein). Often, RF of aerosols is specified at the surface or top of the atmosphere (Markowicz et al., 2003). However, the RF profiles of aerosols are also important to compute their effects on the atmospheric stability and cloud cover (Ackerman et al., 2000; Seinfeld and Pandis, 2006; Jiang and Feingold, 2006).

Usually, the change in radiative equilibrium at the surface is partly balanced by alteration in outgoing surface longwave radiation and partly by adjustments in latent and sensible heat fluxes; hence modifications of the hydrological cycle (Ramanathan et al., 2001; Feichter et al., 2004; see also chapter 4 to chapter 7 and references therein). The indirect mechanism of aerosol RF is highly dependent on their chemical composition and interaction with clouds (see section 1.3.3). However, the magnitude and the sign of direct RF of aerosols is governed by their optical properties; which are: $\alpha_{ext,\lambda}/\gamma_{x_i}^{\lambda}/\tau_{\lambda}$ [Eq. (1.30)/Eq. (1.32)/Eq. (1.31)], ω_{λ} (Eq. (1.35)), g_{λ} (Eq. (1.34)) (e.g., Liao and Seinfeld, 1998). These variables are also determined by the aerosol size distribution, the physico-chemical properties of the particles and their mixing state. The variations of aerosol microphysical properties due to RH and

© University of Pretoria

other aging processes can also lead to variations in optical properties of aerosols, and in turn in their direct RF. Besides these, the aerosols' direct RF is sensitive to the altitude where the particles reside, the cloud thickness and the spatio-temporal variation of the underlying surface albedo (e.g., Forster et al., 2007).

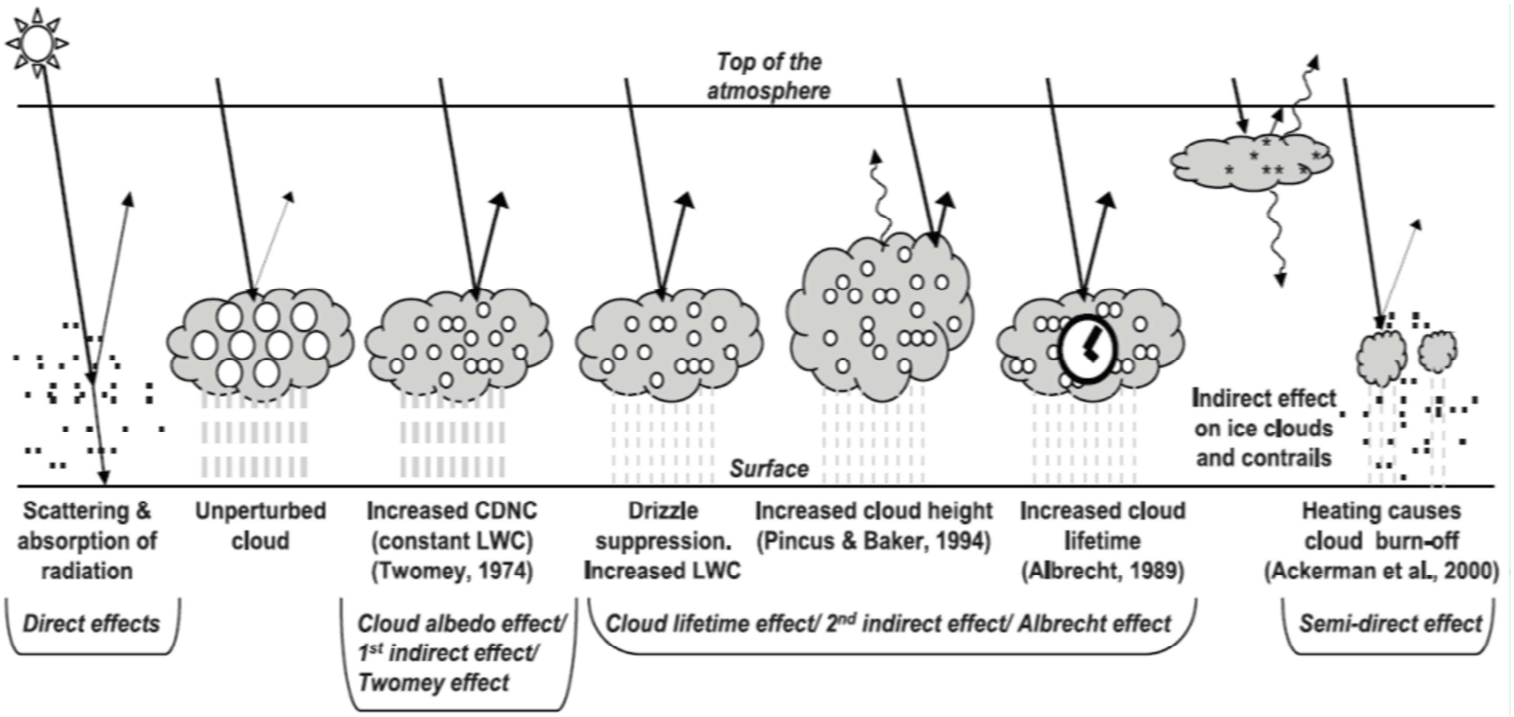

The small black dots represent aerosol particles; the larger open circles cloud droplets. Straight lines represent the incident and reflected solar radiation, and wavy lines represent terrestrial radiation. The filled white circles indicate cloud droplet number concentration (CDNC). The vertical grey dashes represent rainfall, and LWC refers to the liquid water content.

Fig. 4: Schematic diagram for direct, semi-direct and indirect effects of atmospheric aerosols. (adopted from Forster et al., 2007).

Overall, due to the aerosol scattering (see section 1.2.1) dependence on size, their direct radiative effect is dominant over the visible parts of the spectrum; except for the large size particles such as dust, sea-salt and biogenic aerosols which have an influence over the NIR region (e.g. Markowicz et al., 2003). In addition, over the longwave spectrum, the thermal emissions of dust particles also have direct radiative influence (see chapter 4 and references therein). The interactions of non-absorbing aerosols (aerosols with low m_i and high ω_λ) with shortwave radiation increase the albedo of the atmosphere and reduce the amount of radiation reaching the surface (Jacobson, 2001). Strongly or partially absorbing aerosols also directly result in radiative cooling of the underlying surface while inducing heating within the atmosphere, which is important for the semi-direct effect. Owing to the short lifetime of aerosol particles (particularly in the troposphere), their radiative effects are significant in their source regions (see chapter 4 to chapter 7). For more discussion on regional scale direct radiative effects of different aerosol species (particularly over South Africa) the reader is requested to refer chapter 4 to chapter 7.

1.3.2 Semi-direct Effect

The absorption of electromagnetic radiation by aerosols (such as the shortwave absorption by biomass burning or desert dust particles) often leads to a local heating within the atmosphere and this in turn may affect ambient relative humidity, cloud cover and its formations (e.g., Johnson et al., 2004 and reference therein). This is referred to as a semi-direct effect as it initially results from the direct interaction of aerosols with radiation as well as also influences climate indirectly by altering the clouds. Depending on the altitude where the absorbing aerosols reside relative to the clouds, the type of clouds present and its responses, aerosols' semi-direct effects may also alter

© University of Pretoria

the stability near the surface and result a change in vertical transport of moisture. As a result of these processes, semi-direct effects of aerosols induce perturbations in hydrological cycles (Ramanathan et al., 2001; Perlwitz and Miller, 2010). Overall, the change in cloud cover and convective activities by aerosols' semi-direct effects may cause modification on various climatic variables such as surface temperature, land-atmosphere energy balance, soil moisture, boundary layer height and atmospheric circulations (e.g., Zhang 2008; also see chapter 4 to chapter 7).

In addition to these, the absorbing aerosol deposition on snow/ice cover darkens the snow, thereby reducing the snow surface albedo they may promote its melting and further warming of the climate (e.g., Hansen and Nazarenko, 2004; Flanner et al., 2007). Additionally, the change in cloud cover and other possible climate feedbacks also demonstrates that the semi-direct forcing has the potential to offset the direct radiative cooling influences of aerosol particles. This presents a challenging question about the conclusive role of aerosols in climate (Lohmann and Feichter, 2001; Forster et al., 2007). Additional brief descriptions of aerosols' semi-direct effects as well as a list of important references are given in chapter 3. Furthermore, chapter 4 to chapter 7 show the regional scale semi-direct effects of aerosols (particles that are induced from different sectors) on different climatic variables as well as the correlations among them.

1.3.3 Indirect Effect

Although both semi-direct and indirect effects of aerosols influence cloud cover (cloud lifetime) and other hydrological variables, the mechanism through which they occur is quite different from one another. Indirect effects refer to the influence of atmospheric particulates on cloud optical and microphysical properties due to the role they play as Cloud Condensation Nuclei (CCN) (Lohmann and Feichter, 2005). The condensation of water vapour upon aerosol particles increases their size and eventually these particles reach a critical diameter to become active CCN. Thus, the formation of cloud droplets can be easily initiated by these CCN at much lower super-saturation points than the super-saturation threshold which is required for nucleation of homogenous water vapour (e.g., Kerminen et al., 2012). This process strongly depends on chemical properties and size distribution of aerosol particles as well as the amount of moisture available in the ambient atmosphere (e.g., Tao et al., 2012 and references therein).

Hygroscopic particles have a greater ability to attract moisture (i.e., they are effective CCN). As a result, they tend to increase cloud droplet concentrations and droplet surface area (e.g. Boucher and Lohmann, 1995). This leads to an increase in shortwave cloud albedo and alters other optical properties of cloud. This is referred to as the first indirect effect of aerosols or Twomey effect (Twomey, 1974). In addition, increasing cloud droplet number concentration and reducing the cloud droplet size below the threshold for fixed liquid water content results in a reduction in effectiveness of coalescence and precipitation efficiency (Seinfeld and Pandis, 2006; Hansen et al., 2005). Therefore, clouds will retain higher liquid water contents and have a longer lifetime (i.e., this leads to higher fractional cloud cover). This is referred to as the second indirect effect of aerosols or Albrecht effect (Lohmann and Feichter 2005 and references therein). A more detailed explanation about the mechanisms through which aerosols modify the formation of cloud droplets and ice particles can be found in Tao et al. (2012).

In most cases, both indirect effects of aerosols - by increasing cloud reflectivity (first indirect effect) and cloud lifetime (second indirect effect) - will produce negative surface radiative forcing (e.g. Charlson et al., 1992). However, it is important to note that the overall indirect radiative forcing is also highly dependent on the location where the cloud reside and time (Lohmann and Feichter, 2005). Precipitation suppression by the second indirect

© University of Pretoria

effect may also influence the processes of latent heat release, moisture convergence and other convection processes; which may lead to a change in the regional circulation patterns (e.g., Fan et al., 2012). Furthermore, the aerosol indirect effect has a positive feedback for atmospheric lifetime of particles (e.g., Lohmann and Feichter, 2005), i.e., reduced precipitation efficiency means fewer aerosols will be removed from the atmosphere by wet deposition processes (section 1.1.4.1).

1.4 Aerosol measurements and modelling

Aerosol properties and distributions as well as their climate effects are usually determined from a combination of modelling and measurement techniques. There are manifold measurement techniques which are basically categorized into two groups: *in-situ* sensing and remote-sensing. Generally, during *in-situ* observations the instruments are in contact with the medium they are sensing. Whereas, in remote-sensing observations the devices which are installed with remote sensors are located some distance away from the subject of interest. *In-situ* and remote-sensing sensors can be installed on either ground-based or airborne devices. In addition, remote-sensing sensors can also be carried on space-borne platforms. To extract different aspects of aerosol particles (either their microphysical or optical properties) from *in-situ* and/or remote-sensing observations as well as to quantify various radiative and climatic influences of aerosols, modelling is important. However, modelling techniques are complex and they span from numerical solutions of electromagnetic radiation scattering and absorption by particle to interactively coupled aerosol/chemistry-radiation-climate models.

Numerous *in-situ* sensing devices are used to measure the physical, chemical, and optical properties of aerosols (Yu et al., 2009 and references therein). Based on the information gathered from the University of Manchester Centre for Atmospheric Science and other sources, some of the aerosol sensing *in-situ* instruments and their application are summarised in table 2.

Table 2: List of *in-situ* instruments and their application

Instrument	Application
Aerodynamic Particle Sizer	Provides aerodynamic particle size distributions in the range from 0.5 to 20μm using a time-of-flight technique that measures aerodynamic diameter in real-time (Mitchell and Nagel, 1999).
Differential Mobility Particle Sizer	One of the techniques used to measure the sub-micron aerosol size distributions (particles radii in the range from 1 nm to 1μm). Compared with optical sizing instruments, these measurements are advantageous in terms of detecting a wide range of sub-micron particles and are not sensitive to the particles refractive index (Intra and Tippayawong, 2008 and reference therein).
Hygroscopic Tandem Differential Mobility Analyser	Measures size resolved aerosol hygroscopic properties (Hämeri et al., 2000; Fors et al., 2011).

© University of Pretoria

Optical Particle Counters (OPC)	This technique is based on the fact that when a particle passes through a light source (usually a laser or halogen light) some of the light is scattered. Thus detecting the scattered light in a photo-detection chamber, OPC provides the particle number, size as well as particle shape. The size detection sensitivity of OPC is usually > 0.05 μm; but it also depends on the wavelength range of the incident radiation and the photo-detector spectral resolution (Kiselev et al., 2005; Heim et al., 2008).
Integrating nephelometer	Important in providing the scattering and back scattering coefficients of atmospheric aerosols with the RH dependence as well as the size and concentration of particles. Combining the integrating nephelometer measurements with other aerosol instruments data and mathematical models it is possible to retrieve additional aerosol optical parameters. It is often used in real-time air quality controls, climate monitoring and visibility measurements (Anderson et al., 1996; Anderson and Ogren, 1998).
Aerosol Mass Spectrometer (AMS)	Used to study the chemical and physical nature of aerosol particles online (Jayne et al., 2000; Canagaratna et al., 2007).
Multi Angle Absorption Photometer (MAAP) and Particulate Soot Absorption Photometer (PSAP).	Using different operational and computational approaches both MAAP (Petzold and Schonlinner, 2004) and PSAP (Muller et al., 2011) provide the black carbon mass loading based on light absorption coefficient. MAAP are designed to reduce the PSAP scattering uncertainties. Both MAAP and PSAP external mixture assumption; however within aged air masses BC appeared as internal mixture. In accuracies in mixing state assumptions can be corrected using other instruments which measure the soot content of individual particles such as Single Particle Soot Photometer.
Photo Acoustic Soot Spectrometer	Provides the real-time optical absorption coefficient of suspended aerosol particles, absorbing angstrom exponent, black carbon mass loading and optical absorption by gases (Lack et al., 2009 and references therein).
Condensation Particle Counters	Used to measure the concentration of nano particles; which is important to study the formation of nucleation mode particles and their transformations (Sipilä et al., 2008).
Cloud Condensation Nucleus Counter	Used to determine the concentration of cloud condensation nuclei in the air at a specific super-saturation point (Lance et al., 2006).

The interaction of electromagnetic radiation with matter modifies some parameters of the incident wave (it can be amplitude, phase or spectral composition modifications). These modified parameters of the incident wave contain important signatures of the medium to which they interact. Therefore, atmospheric radiometric measurements of EM-radiation in specific spectral intervals (from ground or space based instruments) and mathematical inversions (data analysis) of these measurements - provide information about the physical and optical properties of atmospheric constituents plus other properties of the atmosphere. This is the basic principle associated

© University of Pretoria

with the art of remote-sensing of atmospheric aerosols. Moreover, related with this principle - the remote-sensing of Earth-atmosphere is classified broadly into two categories: active and passive.

In passive remote-sensing, the sensor measures the radiation which originates from natural sources; such as: direct, diffused and/or reflected components of solar radiation as well as the radiation emitted by the Earth's surface-atmosphere system. Active remote-sensing uses artificially-generated radiation sources which can be controlled by the observer e.g., lasers used for LIDAR (LIght Detection And Ranging) or microwaves used in RADAR (RAdio Detection And Ranging). Active sensors detect the radiation scattered back from the target as well as depending on the purpose of the experiment, usually active remote-sensing operates in a spectral domain spanning from the UV to the microwave region.

A multi wavelength sun-photometer is one of the most popular examples of ground based passive remote-sensing instruments. It is useful to measure the solar spectral irradiance at the surface. When it is compared with the corresponding extra-terrestrial spectral irradiance, it provides the solar spectral transmittance of the atmosphere (i.e., the Total Optical Thickness of the Atmosphere: TOTA). In cloud-free conditions, removing the molecular scattering and absorption contributions from TOTA - one may determine the column integrated spectral attenuation due to aerosols (i.e., AOD). Later, using the numerical solutions of different particulate scattering theory (such as Mie theory) and well optimized inversion based retrievals - one can determine various column-mean optical and microphysical properties of aerosols, from the measured AOD (Dubovik et al., 2000). To increase the retrieval accuracy, usually retrieved parameters are evaluated by comparison to *in-situ* measurements (e.g., Haywood et al., 2003). For instance, long-term aerosol monitoring and characterization using ground-based multiple spectral sun-photometer measurements have been achieved through worldwide network of Aerosol Robotic Network (AERONET, Holben et al., 2001; Dubovik et al., 2000). Relative to other aerosol remote-sensing measurements, AERONET observations are continuous and have a better accuracy (Dubovik et al., 2002); thus, they have also become the main data sources for the evaluation of satellite retrievals, model simulations and other aerosol remote-sensing observations (e.g., Chin et al., 2002; Torres et al., 2002; Kinne et al., 2003; Remer et al., 2005; Kahn et al., 2005). Furthermore, aerosol optical and microphysical properties which are determined from AERONET retrievals can be used in satellite retrieval algorithms (Remer et al., 2005; Levy et al., 2007).

The LIDAR is one of the practical active remote-sensing devices with multi-platforms. The choice of platforms (i.e., ground-based platform, airborne platform and space-borne platform) depends largely on the application. LIDAR uses ultraviolet, visible or near-infrared light and all of its platforms operate according to the basic principle of detecting the radiation which is scattered back to a telescope (receiver) after interacting with the target. LIDAR can be used for wide range of applications, such as in geological science, mining, survey, atmospheric research, military, astronomy and others. Atmospheric LIDARs were used to study the atmospheric composition, dynamics, structure, clouds and aerosols (e.g., Winker et al., 2013 and references therein). In atmospheric research the LIDAR systems are usually named according to the types of scattering processes used: for example, the LIDAR which uses Rayleigh scattering: Rayleigh LIDAR, Mie scattering: Mie LIDAR, Raman scattering: Raman LIDAR and so on. The Mie LIDAR and Raman LIDAR (depending on the wavelength used) are applicable in providing range-resolved vertical profiles of aerosol optical properties. Furthermore, depending on the number of transmitted wavelengths, one can also retrieve various column weighted optical and microphysical properties of aerosols from vertically resolved LIDAR measurements. Unlike the passive measurements which are constrained to column properties of aerosols, LIDAR provides both the vertical profile and column weighted aerosol optical properties,

© University of Pretoria

which are important for computation of aerosol radiative effects (e.g., Gadhavi and Jayaraman 2006; Winker et al., 2013 and references therein).

Aerosol physical and chemical properties are highly heterogeneous, both in space and time. Accordingly, due to the spatial and temporal coverage limitations of both ground/aircraft based *in-situ* and remote-sensing measurements of aerosols - they are unsuitable for the global monitoring aerosol particles. On the other hand, even if there are progressively improving accuracy confinements in satellite platforms, to this end, measurement-based long-term characterization of aerosol properties, distributions and transport on regional to global scales can only be achieved through satellite remote-sensing (King et al., 1999; Kaufman et al., 2002; Foster et al., 2007; Mishchenko et al., 2007). Passive satellite sensors measure the radiance at the top of the atmosphere (TOA) which is reflected/scattered or emitted from the Earth's surface-atmosphere system. Analysing this radiance we can extract information about aerosol properties.

Due to the combined scattering influences of air molecules and aerosols as well as reflection from clouds and the Earth's surface, the retrieval of aerosol properties from satellite measured TOA radiance is more sophisticated ill-posed problem. Therefore, satellite retrieval algorithms utilise different assumptions which are well constrained by *in-situ*/other remote-sensing measurements, such as on the surface reflectivity and physico-chemical properties of aerosol particles (Remer et al., 2005; Levy et al., 2007). After cloud-screening, retrievals from passive satellites provide column integrated (column-mean) aerosol optical properties over the ocean/land or in both surfaces. Complementary to passive satellite sensors, space-borne active remote-sensing of aerosols such as CALIPSO provide important information about the vertical structure of aerosol optical properties and clouds on a global scale (Winker et al., 2013 and references therein). Table 3 summarizes major satellites which are often applicable for the tropospheric aerosol characterization and their aerosol products (modified from Yu et al., 2009).

Table 3: Summary of the major satellites which are applicable for the tropospheric aerosol characterization and their aerosol products (modified from Yu et al., 2009).

Sensor/platform	Parameters	Spatial coverage	Temporal coverage	References
AVHRR/NOAAseries	Column-integrated: optical depth; Ångström exponent	global ocean	1981-present	Husar et al., 1997; Mishchenko et al., 1999
TOMS/Nimbus, ADEOS1, EP	Column-integrated: optical depth; absorbing aerosol index; single-scattering albedo; absorbing optical depth	global land + ocean	1979-2001	Herman et al., 1997; Torres et al., 1998; 2002
POLDER-1,-2, PARASOL	Column-integrated: optical depth; Ångström exponent; fine-mode fraction; non-spherical fraction	global land + ocean	1997-present	Deuzé et al., 2001; Bellouin et al., 2003

© University of Pretoria

MODIS/Terra, Aqua	Column-integrated: optical depth; Ångström exponent; fine-mode fraction; effective radius; asymmetry factor	global land + ocean	2000-present (Terra) 2002-present (Aqua)	Tanré et al., 1997; Remer et al., 2002; 2005; Kleidman et al., 2005
MISR/Terra	Column-integrated: optical depth; Ångström exponent; single-scatteringalbedo; Small; medium, large fractions; non-spherical fraction	global land + ocean	2000-present	Diner et al., 1998; Martonchik et al., 1998; 2002; Kahn et al., 2005
OMI/Aura	Column-integrated: optical depth; absorbing aerosol index; single-scattering albedo; absorbing optical depth	global land + ocean	2005-present	Torres et al., 2007; Ahn et al., 2008
GLAS/ICESat	Vertical-resolved: extinction/backscatter	global land + ocean	2003-present (~3months/ year)	Spinhirne et al., 2005a; 2005b
CALIOP/CALIPSO	Vertical-resolved: extinction/backscatter; color ratio; depolarization ratio	global land + ocean	2006 - present	Winker et al., 2007; 2013

Advanced Very High Resolution Radiometer (AVHRR); Total Ozone Mapping Spectrometer (TOMS); Ozone Monitoring Instrument (OMI); MODerate resolution Imaging Spectroradiometer (MODIS); Multi-angle Imaging SpectroRadiometer (MISR); Polarization and Directionality of the Earth's Reflectance (POLDER); Polarization and Anisotropy of Reflectance for Atmospheric Science coupled with Observations from a Lidar (PARASOL); Geoscience Laser Altimeter System (GLAS); Cloud and Aerosol Lidar with Orthogonal Polarization (CALIOP).

To advance the scientific understanding and quantitative assessments of aerosol atmospheric processes plus their impact on radiative budget and climate - information which have been gathered from different aerosol observation techniques needs to be synchronized with chemistry-climate models that simulate a suite of atmospheric aerosols (Forster et al., 2007 and references therein). The spatio-temporal distribution of aerosols basically depends on the emission rate of primary particles/precursor gases, their formation/transformation (aging), transport and removal processes. These processes are usually represented in climatic models by off-line or on-line coupled tracer transport equation. For different aerosol species (tracer, i) the corresponding mass-mixing ratio ξ^i can be calculated using the tracer transport equation (Solmon et al., 2006):

$$\frac{\partial \xi^i}{\partial t} = -\tilde{\nabla}.\nabla\xi^i + B_H^i + B_V^i + T_C^i + E^i - R_{W,ls}^i - R_{W,C}^i - D_d^i + \sum(\eta_p^i - \eta_l^i) \qquad (1.38)$$

where the first four terms of Eq. (1.38) represent advection, horizontal and vertical turbulent diffusion and convective transport, respectively (Solmon et al., 2006; Qian et al., 2001). ξ^i is the surface emission of primary

© University of Pretoria

particle/precursor gas. $R^i_{W,ls}$ and $R^i_{W,C}$ in Eq. (1.38) are the wet removal terms by large scale and convective rain, respectively (Giorgi, 1989; Giorgi and Chameides, 1986). D^i_d is removal by dry deposition. η^i_p and η^i_l indicate production and losses due to manifold physico-chemical transformations (Solmon et al., 2006; Qian et al., 2001).

The parameterization of each term of Eq. (1.38) is very complex and it is the major source of large uncertainties associated with the modelled aerosol forcing (Randall et al., 2007 and references therein). Basically the parameterizations of each term in Eq. (1.38) require: various input from other sources, numerical computations, assumptions, as well as measurement based prior information. The parameterization of emission, deposition and physico-chemical transformation terms varies significantly according to the type of aerosol that is considered. In this regard, *in-situ* and remote-sensing measurements - beside their significant role in providing the properties and distributions of atmospheric particulates (from local to global scale), they also deliver vital parameterizations which are important for representation of aerosol processes in climate models. For instance, *in-situ* measurements are important to develop composition dependent empirical formulations for processes involved in: formation of secondary aerosols, particles emissions, aging and removal. These measurement based parameterizations provide the fundamental basis for implementation of aerosol schemes in a climate model. For more detailed description of different aerosol modules the reader is referred to chapter 3 and references therein.

The optical properties of individual species or a group of aerosols (depending on the mixing state assumptions) are computed using simulated mass concentrations (Eq. (1.38)) and model assumed aerosol optical coefficients. Thereafter, using modelled aerosol optical properties and the radiative transfer scheme which is cooperated within the climate model - the radiative effects of aerosols and climatic feedbacks can be computed. However, the computation of the radiative feedbacks of the climate is most sophisticated as the climate system and it is highly reliant on the state of coupling among aerosol module-radiative-climate model. The magnitude of different coefficients which are essential for quantification of aerosol: atmospheric processes, optical properties (as a function of RH and other aging process) and cloud nucleating properties (CCN concentration as a function of super-saturation and kinetic limitations) - can be established from *in-situ* observations and used in place of model assumed values.

Furthermore, both *in-situ* and remote-sensing measurements can provide important data sets which can be used for the validation of model generated aerosol distributions and optical properties (see chapter 3). Such comparisons are very crucial to identify the models constraints or areas where the models need improvement. Chapter 3 of this study - other than providing the evaluation of RegCM simulated optical properties of aerosols - also briefly address the significance of studying the climatic effects of aerosols using aerosol modules which are interactively coupled with climatic models. Therefore, for additional information on the need and importance of four-dimensional aerosol-climate models (4D: models which spans with space-time grid: Eq. (1.38)), integrated approach, the advantage of RCMs, interactively coupled RegCM-aerosol model and other related issues - the reader may refer to chapter 3.

1.5 Aerosol studies in South Africa

Agricultural practices are the major source of income or simply a means of survival in most African populace. For preparation of the planting season, to control weeds or pests, to maintain crop yields and other reasons, agricultural activities involve land clearing. Open burning of crop residue, grass and bush lands as well as forest clearing (deforestation) are the major events that take place during agricultural land clearing. These anthropogenic

© University of Pretoria

biomass burning activities emit large quantities of atmospheric trace gases and aerosols as well as create smoke which may cause public health hazards. In the last decades, in order to quantify trace species that are emitted from African biomass burning activities plus to examine their transport and impacts, various observational and modelling studies have been carried out (e.g., Roelofs et al., 1997; Chatfield et al., 2002; Staudt et al., 2002; Gao et al., 2003; Johnson, 2008; Capes et al., 2008; Hand et al., 2010; Tummon, 2011 and references therein).

Additionally, one of the major components of aerosols in Africa is mineral dust particles. Basically, the majority of dust particles in Africa are induced due to wind erosions in arid and semi-arid areas - such as the Sahara in northern Africa, Kalahari in southern Africa and other locations (Engelstaedter and Washington, 2007). The other principal causes for wind-eroded dust load in Africa are deforestation and land use changes which result due to agricultural practices, well expanded mining activities and other anthropogenic practices (e.g., Tegen et al., 2004; Shao, 2008). Additionally, different studies showed that in most African nations, industrial emissions are not the major sources of aerosols; however, this excludes some countries such as South Africa (see chapter 5 and references therein). Among various nations of Africa, this study specifically will focus on examining the distribution and first degree climatic influences of aerosols in South Africa.

South Africa is located at the southernmost tip of the African continent (22° - 34° S, 16° - 32° E), surrounded by the Atlantic and Indian Oceans and borders Lesotho, Swaziland, Namibia, Botswana, Zimbabwe and Mozambique. The regional aridity index variation shows that South Africa includes all the four basic climatic features: arid, semi-arid, semi-wet and wet (e.g., Tyson and Preston-Whyte, 2000). Most of the arid areas of South Africa are located in the west and southwest parts of the country. Semi-arid regions are found on the outer edge of arid areas (i.e., the central and northern areas of South Africa). Following these, the northeast as well as the eastern and southern coastal areas of South Africa show semi-wet and wet climatic features. The vegetation coverage in South Africa is highly diverse (e.g., Thompson, 1996). Following the aforementioned climatic features, the vegetation types varies from arid and semi-arid shrubland vegetation such as Nama Karoo, succulent karoo, grasses, herbs, and geophytes - through fynbos, savanna and woodland to coastal thicket and dense alpine forest (e.g., Rutherford and Westfall, 1994; Thompson, 1996; Privette et al., 2004; Privette and Roy, 2005). For further discussions on southern Africa regional climate: such as the seasonal variation of circulation patterns, inter-annual/-decadal climate variability, temperature and precipitation trends as well as the vertical stability layers, the reader is referred to Tyson and Preston-Whyte (2000); Tummon (2011) and references therein.

The Kalahari desert/basin (annual precipitation < 200mm) - which cover almost all of Botswana, large areas of Namibia and some western parts of South Africa - is increasingly recognized to be the main source of wind-eroded desert dust particles in South Africa (e.g., Bhattachan et al., 2012 and references therein; also see chapter 4). Land cover and land use changes due to the mining operations and agricultural activities in semi-arid regions of South Africa (especially over the northern part) also cause land degradation and increase the load of windblown dust particles (e.g., Shao, 2008; Tesfaye et al., 2011).

South Africa has large reserves of different minerals such as coal, iron, vanadium, gold, silver, graphite and others. Most of these reserves are distributed over the central and northern areas (mainly over the Highveld regions of South Africa) as well as the eastern and southern parts of the country. Due to this and other reasons, most of the mining activities, power productions, metal industries, oil and sugar refineries and agricultural manufacturing centres are populated over the areas of South Africa which have a climatic future of semi-arid, semi-wet and wet. In

© University of Pretoria

addition, industrial and agricultural sectors are sources of employment and income for most South Africans. As a result, the population density of South Africa is much higher in semi-arid, semi-wet and wet areas than in the arid regions (e.g., Archer et al., 2010; Van Huyssteen et al., 2013). This reflects that most of the South African anthropogenic aerosols are emitted from these regions (see chapter 2 and chapter 5). In particular, various studies listed in chapter 5 point-out that the Highveld region of South Africa is the principal source of anthropogenic air pollutants in southern Africa.

To study the physico-chemical/optical properties, distribution, climatic influences and transport of southern Africa's aerosols, over the past decade or so, few large interdisciplinary field campaigns as well as continuous measurements have been performed using different platforms. Major regional campaigns which have studied aerosols and other pollutants in and around South Africa are listed in table 4. Also the results of these campaigns are briefly described in each of the introductory sections of each of the appropriate chapters (particularly from chapter 4 to chapter 7 as well as over some parts of chapter 2). Therefore to avoid repetition of information the reader may refer to these sections. Overall, studies which are listed in the aforementioned chapters (also for a review, see Tummon, 2011), are able to provide numerous information about the aerosols': sources/formation, atmospheric processes, distribution, transport, physico-chemical and optical properties and impacts, in and around South Africa.

Table 4: List of major field campaigns in and around South Africa (over southern Africa) that are important primarily for aerosol research as well as other atmospheric trace species.

Campaign	Region operated	Time covered	Aimed to examine	Major references
Southern African Fire-Atmosphere Research Initiative-92 (SAFARI-92)	Southern African and South Tropical Atlantic	September to October, 1992	emissions and transport of trace species from biomass burning	Diab et al., 1996; Andreae et al., 1996; Lindesay et al., 1996
Southern African Atmospheric Research Initiative (SA'ARI-1994)	southern Africa	May 1994	aerosols and trace gases which are induced from different natural and anthropogenic activities (especially outside the main biomass burning regions)	Helas et al., 1995
Southern African Regional Science Initiative (SAFARI-2000)	southern Africa	March 1999 to March 2000	emission, transport, atmospheric processes and influences of different aerosols and trace gases which are induced from different natural and anthropogenic activities	Swap et al., 2003 and references on special issue of the Journal of Geophysical Research (vol. 108, no. D13, 2003)

Chapter 2 of thesis, discuss most observational studies which have been made in South Africa, focused on characterising the physico-chemical and optical properties of aerosol particles in a particular locations/areas.

© University of Pretoria

1.6 Motivation and Outline of the Thesis

Owing to the rapid aging and short lifetimes of aerosols in the troposphere, their properties as well as their concentration are highly heterogeneous in space and time. In this regard, at least to the best of our knowledge, there has been no comprehensive study that aimed to examine the seasonal and spatial variation of aerosol optical (and in turn their microphysical) properties in correlation with the background weather parameters, over the entire South African region. Studying the long-term correlation among the regional variation of aerosol optical properties and different metrological parameters such as rainfall, RH and wind speed would contribute to further understanding of the effects of meteorological conditions on the aerosol optical, microphysical properties and their dynamics (load, dispersion, and removal processes). Associating such studies with other reports (or local information), it is possible to characterize the spatio-seasonal variation of aerosol source strengths and able to address the aerosol climatology which extends from a local to regional scale. This may offer advantageous circumstances (to some extent also guidance) for further examination of aerosol influences in various aspects.

Measurement-based long period characterization of aerosol properties and their distribution on a regional and/or global scale can be realized only through satellite remote-sensing (e.g., Foster et al., 2007 and references therein). In chapter 2, using different optical properties of aerosols which are provided by (and also derived from) MISR products, a detailed study on the spatio-seasonal aerosol climatology over South Africa is provided. This chapter also used the background weather parameters (which are obtained from the South African Weather Service) to examine the influence of local meteorological conditions on aerosol properties as well as to interpret the aerosol climatological characteristics over South Africa. Chapter 2 needs to be cited as:

> Tesfaye, M., V. Sivakumar, J. Botai, and G. Mengistu Tsidu (2011): Aerosol climatology over South Africa based on 10 years of Multiangle Imaging Spectroradiometer (MISR) data; *J. Geophys. Res., 116, D20216, doi:10.1029/2011JD016023.*

South Africa is influenced by almost all types of major atmospheric aerosols: windblown dust and sea-salt particles plus particulates that are emitted from anthropogenic/biomass burning activities (details are given in chapter 2). Tropospheric aerosols have short atmospheric residence times (Seinfeld and Pandis, 2006), which reflect that their effects are more pronounced on a regional scale (e.g. Keil and Haywood, 2003). Investigating the radiative and climatic influences of aerosol particles which are produced from specific activities/events is especially important to understand how and by how much emission from these activities influence the climate (Solomon et al., 2007). In addition, such studies are crucial to make strategic environmental management plans and climate change mitigation (IPCC, 2007). Aerosol measurements are very vital in providing numerous parameterizations which are significant to represent aerosols in climatic models. However, to closely examine the complex interactions and feedbacks among aerosols-radiation-climatic, interactively coupled aerosol-climate system models are indispensable tools (see chapter 3). Moreover, for the representation of spatio-temporarily highly variable atmospheric aerosol processes in climate models, high resolution regional aerosol-climatic models are most suitable and have better precision than the global aerosol-climate models (e.g., Simmons et al., 2004; Solmon et al., 2006; IPCC, 2007). Therefore, using the Regional Climate Model (RegCM4) of the International Centre for Theoretical Physics (ICTP) which is interactively coupled with anthropogenic-desert dust schemes – this study closely examines the distribution, direct and semi-direct effects of wind-eroded desert dust particles as well as different species of aerosols which are induced from anthropogenic

© University of Pretoria

and biomass burning sectors, in South Africa. The significance and scope of these studies, new aspects/outcomes that are realized from them and other crucial points are addressed in each chapter.

Chapter 3: provides a brief description about the need of modelling (especially RegCM), interactively coupled RegCM4-aerosol model, its limitation, the emission data sets used throughout this dissertation and other important features. Moreover, the model performance for computing the Optical Properties of Aerosols (OPA) is very vital to determine the accuracy of the model's estimated radiative forcing and related climate effects of aerosols. Therefore, chapter 3 evaluates the OPA computing performance of RegCM4-aerosol model, in South Africa. This contribution is a first step towards examining the direct and semi-direct effects of aerosols over South Africa using RegCM4. The reader may note that in this chapter an extended general introduction, as well as a brief description about the model used (i.e., RegCM4) is addressed. This is to avoid repetition of information; so parts of these sections will be used as the basic framework for other chapters that follow this contribution. Chapter 3 needs to be cited as:

> Tesfaye, M., J. Botai, V. Sivakumar, and G. Mengistu Tsidu (2013a): Evaluation of Regional Climatic Model Simulated Aerosol Optical Properties over South Africa Using Ground-Based and Satellite Observations, *ISRN Atmospheric Sciences, vol. 2013, Article ID 237483, 17 pages, 2013. doi:10.1155/2013/237483*.

Chapter 4: As stated previously, windblown desert dust particles are one of the main components of atmospheric aerosols in South Africa (e.g., Tesfaye et al., 2011; Bhattachan et al., 2012 and references therein). Generally, wind-eroded desert dust particles are highly variable in mineralogical compositions, level of occurrences, as well as are attributed with the ability to interact with both short-wave and long-wave radiation. Owing to these properties, the distribution and effects of dust particles are more complex and highly variable, both temporally and spatially. This chapter investigates the seasonal mean spatial distributions of dust loadings, along with its potential effects on surface and atmospheric radiative budget in different spectral bands [i.e., shortwave, long-wave and the net (sum of shortwave and long-wave)]. Furthermore, this study also examines the influences of desert dust particles on surface air temperature, sensible heat fluxes, columnar average net heating rate, cloud cover, cloud liquid water path and atmospheric dynamics; throughout different seasons of the year, over South Africa. Chapter 4 needs to be cited as:

> Tesfaye, M., G. Mengistu Tsidu, J. Botai, and V. Sivakumar (2013b): "Mineral dust aerosol distributions, its direct and semi-direct effects over South Africa based on regional climate model simulation", *J. Arid Environ., in review*.

Chapter 5: South Africa is one of the most industrialized countries in Africa. As a result, the climatic and air quality changes that are caused by anthropogenic emissions have progressively become one of the major concerns in and around South Africa. Based on long-term regional modelling simulations, the present study has examined the total and individual components of anthropogenic aerosols' seasonal mean column burden spatial distributions, along with their direct and semi-direct effects over South Africa. Chapter 5 needs to be cited as:

> Tesfaye, M., V. Sivakumar, J. Botai, and G. Mengistu Tsidu (2013c): "Simulation of anthropogenic aerosols mass distributions and their direct and semi-direct effects over South Africa using RegCM4", *Int. J. Climatol., in review*.

© University of Pretoria

Chapter 6: Biomass Burning (BB), resulting from both natural and anthropogenic fires, has been identified as an important source of various types of atmospheric trace gases and a mixture of aerosols. On a continental scale, many studies recognized Africa as one of the major source of BB emissions. In particular studies using MODIS products showed that BB from southern Africa contributes approximately 21% of the global active fire counts (e.g., Magi et al., 2009). Furthermore, the results from chapter 2 (Tesfaye et al., 2011) showed that South Africa experiences drastic turbidity due to high levels of biomass burning aerosol loadings during August to October. Therefore, using the aerosol-RegCM4 two-way interactively coupled regional scale simulation, the present contribution examines the interactions and feedbacks among the individual/total BB aerosol species, radiation and climatic fields, over South Africa. Chapter 6 needs to be cited as:

> Tesfaye, M., J. Botai, V. Sivakumar and G. Mengistu Tsidu (2013d): "Simulation of biomass burning aerosols mass distributions and their direct and semi-direct effects over South Africa using a regional climate model", *J. Meteorol. Atmos. Phys., in review*.

Chapter 7: The previous chapters (i.e., chapter 4 to chapter 6) examined the mass distribution, direct and semi-direct climatic effects of naturally induced desert dust particles, different species of aerosols which are induced from anthropogenic sectors and biomass burning activities, in South Africa. These studies reported separately the influences of aerosols which originate from a specific sector (activities). In reality, tropospheric aerosols never occur as individual species; but rather exist as a complex mixture (which refers to as bulk aerosol) with high variability in their spatio-temporal distributions. Therefore, the combined effects of all aerosols which originate from different natural processes and anthropogenic activities take place at the same time, but not necessarily in the same place. In this context, it becomes crucial to study the bulk aerosol climatic influences, over South Africa. Accordingly, in this study, using simulations with the Regional Climate Model-RegCM4; we have examined the seasonal mean direct and semi-direct effects of the total aerosols over South Africa. Chapter 7 needs to be cited as:

> Tesfaye, M., J. Botai, V. Sivakumar and G. Mengistu Tsidu (2013e): "Simulation of bulk aerosol direct and semi-direct effects in South Africa using RegCM4", *J. Aerosol Air Qual Res., in review*.

Chapter 8: The summary and the main conclusions drawn from this study plus the future outlooks are presented in this chapter.

Remark: chapter 2 to chapter 7 are reprints of different research articles which are published or in the pipeline to be published. As a result, there might be some format and structural differences amongst these chapters. In addition, owing to the scientific nature of this study, there might exist some unavoidable repetition of concepts, references and acknowledgements from chapter 2 to chapter 7.

© University of Pretoria

References

Abo Riziq, A. et al. (2007): Optical properties of absorbing and non-absorbing aerosols retrieved by cavity ring down (CRD) spectroscopy. Atmospheric Chemistry and Physics, 7(6), 1523-1536.

Ackerman, A.S. et al. (2000): Effects of aerosols on cloud albedo: Evaluation of Twomey's parameterization of cloud susceptibility using measurements of ship tracks. J. Atmos. Sci., 57, 2684-2695, doi:10.1175/1520-0469(2000)057<2684:EOAOCA>2.0.CO;2.

Ahn, C. et al. (2008): Comparison of Ozone Monitoring Instrument UV Aerosol Products with Aqua/Moderate Resolution Imaging Spectroradiometer and Multiangle Imaging Spectroradiometer observations in 2006, J. Geophys. Res., 113, D16S27, doi:10.1029/2007JD008832.

Anderson, T. L. and J. A. Ogren (1998): Determining aerosol radiative properties using the TSI3562 integrating nephelometer, aerosol. Sci. Technol., 29, 57-69.

Anderson, T. L. et al. (1996): Performance characteristics of a high-sensitivity, three-wavelength, total/scatter/backscatter nephelometer. J. Atmos. Oceanic. Technol., 13, 967-986.

Anderson, T. L. et al. (2000): In situ measurement of the aerosol extinction-to-backscatter ratio at a polluted continental site, J. Geophys. Res., 105(D22), 26907–26915, doi:10.1029/2000JD900400.

Andreae, M. O. et al. (1996): The Southern Tropical Atlantic Region Experiment (STARE): TRansport and Atmospheric Chemistry near the Equator – Atlantic (TRACE-15 A) and Southern African Fire/Atmosphere Research Initiative (SAFARI): An introduction, J. Geophys. Res., 101, 23 519–23 520.

Andreae, M.O. and P. Merlet (2001): Emission of trace gases and aerosols from biomass burning. Global biogeochem. Cycles. 15. 955-966.

Andreas, E. L. (1995): The temperature of evaporating sea spray droplets. Journal of the atmospheric sciences, 52(7), 852-862.

Andreas, E. L. (2005): Approximation formulas for the microphysical properties of saline droplets. Atmospheric research, 75(4), 323-345.

Archer, E. et al. (2010): South African Risk and Vulnerability Atlas; Department of Science and Technology, Pretoria, pp 62.

Bellouin, N. et al. (2003): Aerosol absorption over the clear-sky oceans deduced from POLDER-1 and AERONET observations. Geophys. Res. Lett., 30, 1748, doi:10.1029/2003GL017121.

Bhattachan, A. et al. (2012): The southern Kalahari: a potential new dust source in the southern hemisphere? Environ. Res. Lett. 7 024001, doi:10.1088/1748-9326/7/2/024001.

Bohren, C.F. and D.R. Huffman (1983): Absorption and scattering of light by small particles, Wiley and sons, New York.

Bond, T. C. et al. (2004): A technology-based global inventory of black and organic carbon emissions from combustion, J. Geophys. Res., 109, D14203, doi:10.1029/2003JD003697.

Bond, T. C., et al. (2013): Bounding the role of black carbon in the climate system: A scientific assessment, J. Geophys. Res. Atmos., 118, 5380–5552, doi:10.1002/jgrd.50171.

Borrmann, S. et al (2000): Application of the T-Matrix method to the measurement of aspherical (ellipsoidal) particles with forward scattering optical particle counters. J. Aerosol Sci., 31, 789-799.

Boucher, O. and U. Lohmann (1995): The sulfate-CCN-cloud albedo effect: A sensitivity study using two general circulation models, Tellus, 47B, 281–300.

Canagaratna, M. R. et al. (2007): Chemical and Microphysical Characterization of Ambient Aerosols with the Aerodyne Aerosol Mass Spectrometer. Mass Spectrometry Reviews 26:185–222.

Capes, G. et al. (2008): Aging of biomass burning aerosols over West Africa: Aircraft measurements of chemical composition, microphysical properties, and emission ratios, J. Geophys. Res., 113, D00C15, doi:10.1029/2008JD009845.

Carslaw, K. S. et al. (2010): A review of natural aerosol interactions and feedbacks within the Earth system, Atmos. Chem. Phys., 10, 1701–1737, doi:10.5194/acp-10-1701-2010.

CCSP 2009: Atmospheric Aerosol Properties and Climate Impacts, A Report by the U.S. Climate Change Science Program and the Subcommittee on Global Change Research. [Mian Chin, Ralph A. Kahn, and Stephen E. Schwartz (eds.)]. National Aeronautics and Space Administration, Washington, D.C., USA, 128 pp.

Charlson, R. J., et al. (1987): Oceanic phytoplankton, atmospheric sulfur, cloud albedo and climate, Nature, 326, 655–661.

Chatfield, R. B. et al. (2002): The subtropical global plume in the Pacific Exploratory Mission-Tropics A (PEM-Tropics A), PEM-Tropics B, and the Global Atmospheric Sampling Program (GASP): How tropical emissions affect the remote Pacific, J. Geophys. Res., 107(D16), doi:10.1029/2001JD000497.

Chin, M. et al. (2002): Tropospheric aerosol optical thickness from the GOCART model and comparisons with satellite and sunphotometer measurements, J. Atmos. Sci. 59, 461-483.

Chin, M., P. et al. (2002): Tropospheric aerosol optical thickness from the GOCART model and comparisons with satellite and sunphotometer measurements, J. Atmos. Sci. 59, 461-483.

Chou, C. et al. (2008): Size distribution, shape, and composition of mineral dust aerosols collected during the African Monsoon Multidisciplinary Analysis Special Observation Period 0: Dust and Biomass-Burning Experiment field campaign in Niger, January 2006, J. Geophys. Res., 113, D00C10, doi:10.1029/2008jd009897.

Chylek, P. et al. (1981): Optical properties and mass concentration of carbonaceous smokes. Applied Optics, 20(17), 2980-2985.

Croft, B. et al. (2009): Aerosol size-dependent below-cloud scavenging by rain and snow in the ECHAM5-HAM, Atmos. Chem. Phys., 9, 4653 – 4675.

Crutzen, P. J. et al. (1979): Biomass burning as a source of atmospheric gases CO, H2, N20, NO, CH3C1, and COS, Nature, 282, 253-256.

D O'Dowd, C. and De Leeuw, G. (2007): Marine aerosol production: a review of the current knowledge. Philosophical Transactions of the Royal Society A: Mathematical, Physical and Engineering Sciences, 365(1856), 1753-1774.

Dautrebande, L. and Capps, R. (1950): Studies on aerosols IX. Enhancement of irritating effects of various substances on the eye. nose, and throat by particulate matter and liquid aerosols in connection with pollution of the atmosphere. Archives internationales de pharmacodynamie et de thérapie, 82(4), 505.

Whitby, K. T. (1978), The physical characteristics of sulfur aerosols, Atmos. Env., 12, 135–159.

Decesari, S. et al. (2002): Water soluble organic compounds formed by oxidation of soot, Atmos. Environ., 36, 1827 – 1832.

Dentener, F. et al. (2006): Emissions of primary aerosol and precursor gases in the years 2000 and 1750 prescribed data-sets for AeroCom, Atmos. Chem. Phys., 6, 4321-4344.

Dentener, F.J. et al. (1996): Role of mineral aerosol as a reactive surface in the global troposphere. Journal of Geophysical Research 101: doi: 10.1029/96JD01818. issn: 0148-0227.

Deuze, J.-L. et al. (2001): Remote Sensing of aerosols over land surfaces from POLDER/ADEOS-1 polarized measurements, J. Geophys. Res., 106, 4913–4926, 2001.

Diab, R.D. et al. (1996): A comparison of anticyclone and trough influences on the vertical distribution of ozone and meteorological conditions during SAFARI-92, Journal of Geophysical Research, 101, 23809-23821.

Diner, D. J. et al. (1998): Multi-angle Imaging SpectroRadiometer (MISR) instrument description and experiment overview, IEEE Trans. Geosci. Remote Sens., 36, 1072–1087, doi:10.1109/36.700992.

Dubovik, O. et al. (2000): Accuracy assessments of aerosol optical properties retrieved from Aerosol Robotic Network (AERONET) Sun and sky radiance measurements. Journal of

© University of Pretoria

Geophysical Research: Atmospheres (1984–2012), 105(D8), 9791-9806.

Dubovik, O. et al. (2002): Variability of absorption and optical properties of key aerosol types observed in worldwide locations, J. Atmos. Sci., 59, 590–608.

Engelstaedter, S. and Washington, R. (2007): Temporal controls on global dust emissions: The role of surface gustiness, Geophys. Res. Lett., 34, L15805, doi:10.1029/2007GL029971.

Esaias, W. E. et al. (1998): An overview of MODIS capabilities for ocean science observations, IEEE Transactions on Geoscience and Remote Sensing, 36(4), 1250-1265.

Fan, J. et al. (2012): Potential aerosol indirect effects on atmospheric circulation and radiative forcing through deep convection, Geophys. Res. Lett., 39, L09806, doi:10.1029/2012GL051851.

Feichter, J. et al. (2004): Nonlinear aspects of the climate response to greenhouse gas and aerosol forcing. Journal of climate, 17(12), 2384-2398.

Finlayson-Pitts, B. J. and J. N. Pitts Jr. (1997): Tropospheric air pollution: Ozone, airborne toxics, polycyclic aromatic hydrocarbons, and particles, Science, 276, 1045–1051.

Finlayson-Pitts, B. J. and J. N. Pitts Jr. (1997): Tropospheric air pollution: Ozone, airborne toxics, polycyclic aromatic hydrocarbons, and particles, Science, 276, 1045–1051.

Finlayson-Pitts, B. J. and Pitts, J. N. (2000): Chemistry of the upper and lower atmosphere, Academic Press, 525 B Street, Suite 1900, San Diego, CA, USA, 92101–4495, 1st edn.

Flanner, M. G. et al. (2007): Present day climate forcing and response from black carbon in snow, J. Geophys. Res., 112, D11202, doi:10.1029/2006JD008003.

Formenti, P., et al. (2008): Regional variability of the composition of mineral dust from western Africa: Results from the AMMA SOP0/DABEX and DODO field campaigns, J. Geophys. Res., 113, D00C13, doi:10.1029/2008JD009903.

Fors, E. O. et al. (2011): Hygroscopic properties of the ambient aerosol in southern Sweden – a two year study, Atmos. Chem. Phys., 11, 8343–8361, doi:10.5194/acp-11-8343-2011.

Forsberg, B. et al. (2005): Comparative health impact assessment of local and regional particulate air pollutants in Scandinavia. Ambio 34, 11-19.

Forster, P. et al. (2007). Changes in Atmospheric Constituents and in Radiative Forcing. In: Climate Change 2007: The Physical Science Basis. Contribution of Working Group I to the Fourth Assessment Report of the Intergovernmental Panel on Climate Change [Solomon, S. et al. (eds.)]. Camb. Univ. Press, Camb., United Kingdom and New York, NY, USA.

Gadhavi, H. and Jayaraman, A. (2006): Airborne lidar study of the vertical distribution of aerosols over Hyderabad, an urban site in central India, and its implication for radiative forcing calculations. Annales Geophysicae, 24, pp. 2461–2470.

Gao, S. et al. (2003): Water-soluble organic components in aerosols associated with savanna fires in southern Africa: Identification, evolution, and distribution, J. Geophys. Res., 108, 8491, doi:10.1029/2002JD002324, D13.

Ghan, S. J. and Schwartz, S. E. (2007): Aerosol properties and processes: A path from field and laboratory measurements to global climate models. Bull. Amer. Meteorol. Soc. 88, 1059-1083, doi:10.1175/BAMS-88-7-1059.

Ghan, Steven J. and Stephen E. Schwartz (2007): Aerosol Properties and Processes: A Path from Field and Laboratory Measurements to Global Climate Models. Bull. Amer. Meteor. Soc., 88, 1059–1083; doi: http://dx.doi.org/10.1175/BAMS-88-7-1059.

Giorgi, F. (1988): Dry deposition velocities of atmospheric aerosols as inferred by applying a particle dry deposition parameterization to a general circulation model; Tellus B, 40B, 23-41.

Giorgi, F. (1989): Two-dimensional simulations of possible mesoscale effects of nuclear war fires. I: model description. J. Geophys. Res. 94, 1127–1144.

Giorgi, F. and Chameides, W. L. (1986): Rainout lifetimes of highly soluble aerosols and gases as inferred from simulations with a general circulation model. J. Geophys. Res. 91, 14 367–14 376.

Gong, S. L. et al. (1997): Modeling sea-salt aerosols in the atmosphere: 2. Atmospheric concentrations and fluxes, J. Geophys. Res., 102(D3), 3819–3830, doi:10.1029/96JD03401.

Goudie, A. S. and Middleton, N. J. (2006): Desert dust in the global system, Springer, Berlin, Germany.

Gurjar, B.R. and J. Lelieveld (2005): New directions: Megacities and global change. Atmos. Environ. 39, 391-393.

Hallquist M, et al. (2009): The formation, properties and impact of secondary organic aerosol: current and emerging issues. Atmos Chem Phys 9:5155–5236.

Hämeri, K. et al. (2000): Hygroscopic Growth of Ultrafine Ammonium Sulfate Aerosol Measured Using an Ultrafine Tandem Differential Mobility Analyser, J. Geophys. Res., 105, 22,231-22,242.

Hamill, P. et al. (1997): The life cycle of stratospheric aerosol particles, Bull. Am. Meteorol. Soc., 78, 1395-1410.

Han, X. et al. (2013): Model analysis of influences of aerosol mixing state upon its optical properties in East Asia. Advances in Atmospheric Sciences, 30, 1201-1212.

Hand, V. L. et al. (2010): Evidence of internal mixing of African dust and biomass burning particles by individual particle analysis using electron beam techniques, J. Geophys. Res., 115, D13301, doi:10.1029/2009JD012938.

Hansen, J. and Nazarenko, L. (2004): Soot climate forcing via snow and ice albedos. Proceedings of the National Academy of Sciences of the United States of America, 101(2), 423-428.

Hansen, J. et al. (1997): Radiative forcing and climate response. J. Geophys. Res. 102, 6831-6864.

Hansen, J. et al. (1997): Radiative forcing and climate response. J. Geophys. Res. 102, 6831-6864.

Hansen, J. et al. (2005): Efficacy of climate forcings. J. Geophys. Res., 110, D18104, doi:10.1029/2005JD005776.

Harrison, R.M. and Yin, J. (2000): Particulate matter in the atmosphere: which particle properties are important for its effects on health? The Science of the Total Environment 249, 85-101.

Haywood, J. et al. (2003): Comparison of aerosol size distributions, radiative properties, and optical depths determined by aircraft observations and Sun photometers during SAFARI 2000, J. Geophys. Res., 108(D13), 8471, doi:10.1029/2002JD002250.

Hegg, D. et al. (2006): Measurements of aerosol size-resolved hygroscopicity at sub and supermicron sizes, Geophys. Res. Lett., 33 (L21808), doi:10.1029/2006GL026,747.

Heim M. et al. (2008): Performance evaluation of three optical particle counters with an efficient “multimodal” calibration method. Journal of Aerosol Science;39:1019–1031.

Helas, G. et al. (1995): SA’ARI-94: a preliminary view on results. South African Journal of Science 91, 360–362.

Herman, J. R. et al. (1997): Global distribution of UV-absorbing aerosols from Nimbus 7/TOMS data, J. Geophys. Res., 102(D14), 16911–16922, doi:10.1029/96JD03680.

Hess, M. et al. (1998): Optical properties of aerosols and clouds: The software package OPAC. Bulletin of American Meteorological Society 79, 831–844.

Hinds, W.C. (1999): Aerosol Technology: Properties, Behaviour, and Measurement of Airborne Particles, John Willey and Sons, New York.

Holben, B. N. et al. (2001): An emerging ground-based aerosol climatology: Aerosol optical depth from AERONET, J. Geophys. Res., 106(D11), 12067–12097, doi:10.1029/2001JD900014.

Houghton, J. T. et al. Eds., (2001): Climate Change 2001: The Scientific Basis. Contribution of Working Group I to the Third Assessment Report of the Intergovernmental Panel on Climate Change. New York: Cambridge University Press.

Husar, R.B. et al. (1997): Characterization of tropospheric aerosols over the oceans with the NOAA advanced very high resolution radiometer optical thickness operational product. Journal of Geophysical Research 102, 16889-16909.

Intra, P. and Tippayawong, N. (2008): An overview of differential mobility analyzers for size classification of nanometer-sized

© University of Pretoria

aerosol particles. Songklanakarin Journal of Science and Technology, 30(2), 243-256.

IPCC (2001): Climate change 2001: The scientific basis. Third assessment of the Intergovernmental Panel on Climate Change (IPCC), edited by Houghton, J. T., Ding, Y., Griggs, D. J., Noguer, M., van der Linden, P. J., Dai, X., Maskell, K. and Johnson, C. A. Cambridge Univ. Press, New York, USA.

IPCC, (2007). Climate Change 2007: The Physical Science Basis. Contribution of Working Group I to the Fourth Assessment Report of the Intergovernmental Panel on Climate Change [Solomon, S. et al. (eds.)]. Camb. Univ. Press, Camb., UK and NY, USA, 996 pp.

Irshad, R. et al. (2009): Laboratory measurements of the optical properties of sea-salt aerosol. Atmospheric Chemistry and Physics, 9(1), 221-230.

Jacobson, M. Z. (2001): Global direct radiative forcing due to multicomponent anthropogenic and natural aerosols, J. Geophys. Res., 106(D2), 1551–1568, doi:10.1029/2000JD900514.

Jacobson, M. Z. (2001): Strong radiative heating due to the mixing state of black carbon in the atmospheric aerosols, Nature, 409, 695 – 697.

Jaenicke, R. (1988): Aerosol physics and chemistry. In: Landolt-B¨ornstein, Zahlenwerte und Funktionen aus Naturwissenschaft und Technik. Fischer, G. (ed.). Neue Serie, Band Meteorologie 4b, Springer Berlin, 391-457.

Jayne, J.T. et al. (2000): Development of an Aerosol Mass Spectrometer for Size and Composition. Analysis of Submicron Particles, Aerosol Science and Technology, 33, 49-70.

Jiang, H. and G. Feingold (2006): Effect of aerosol on warm convective clouds: Aerosol-cloud-surface flux feedbacks in a new coupled large eddy model, J. Geophys. Res., 111, D01202, doi:10.1029/2005JD006138.

Johnson, B. T. et al. (2004): The semi-direct aerosol effect: Impact of absorbing aerosols on marine stratocumulus. Quarterly Journal of the Royal Meteorological Society, 130(599), 1407-1422.

Johnson, B. T. et al. (2008): Aircraft measurements of biomass burning aerosol over West Africa during DABEX. J. Geophys. Res.-Atmos, 113, (D17).

Kahn, R. A. et al. (2005): Multiangle Imaging Spectroradiometer (MISR) global aerosol optical depth validation based on 2 years of coincident Aerosol Robotic Network (AERONET) observations, J. Geophys. Res., 110, D10S04, doi:10.1029/2004JD004706.

Kanakidou, M. et al. (2005): Organic aerosol and global climate modelling: A review. Atmos. Chem. Phys, 5, 1053-1123, doi:10.5194/acp-5-1053-2005.

Kaufman, Y. J. et al. (2002): A satellite view of aerosols in the climate system, Nature, 419, doi:10.1038/nature01091.

Kaufman, Y. J. et al. (2002): A satellite view of aerosols in the climate system. Nature, 419, 215–223.

Keene, W. C. and D. L. Savoie (1998): The pH of deliquesced sea-salt aerosol in polluted marine air. Geophys. Res. Letters, 25, 2181-2184.

Keene, W. C. et al. (1999): Composite global emissions of reactive chlorine from natural and anthropogenic sources: Reactive Chlorine Emissions Inventory, J. Geophys. Res., 104, 8429 – 8440.

Keil, A. and Haywood, J.M. (2003): Solar radiative forcing by biomass burning aerosol particles during SAFARI 2000: A case study based on measured aerosol and cloud properties. J. Geophys. Res. 108(D13,8467). Doi: 10.1029/2002JD002315.

Kerminen, V.-M. et al. (2012): Cloud condensation nuclei production associated with atmospheric nucleation: a synthesis based on existing literature and new results, Atmos. Chem. Phys., 12, 12037-12059, doi:10.5194/acp-12-12037-2012.

Kiehl, J. T. et al. (1996): Description of the NCAR Community Climate Model (CCM3), Technical Report NCAR/TN-420+STR, National Center for Atmospheric Research, Boulder, Colorado, 152 pp.

Kientzlcr C.F. et al. (1954): Photographie investigation of the projection of droplets by bubbles bursting at a water surface. Tel/us 6, 1-7.

Kim, C. and Lior, N. (1995): Easily computable good approximations for spectral radiative properties of particle—gas components and mixture in pulverized coal combustors. Fuel, 74(12), 1891-1902.

King, M. D. et al. (1999): Remote sensing of tropospheric aerosols from space: past, present and future, Bull. Am. Meteorol. Soc., 80, 2229–2259.

Kinne, S. et al. (2003): Monthly averages of aerosol properties: A global comparison among models, satellite data, and AERONET ground data, J. Geophys. Res., 108, 4634, doi:10.1029/2001JD001253, D20.

Kiselev, A. et al. (2005): White-light optical particle spectrometer for in situ measurement of condensational growth of aerosol particles, Appl. Opt., 44, 4693–4701.

Kleidman, R. et al. (2005): Comparison of Moderate Resolution Imaging Spectroradiometer (MODIS) and Aerosol Robotic Network (AERONET) remote-sensing retrievals of aerosol fine mode fraction over ocean, J. Geophys. Res., 110, doi:10.1029/2005JD005 760.

Koepke, P. (1986): Remote sensing signatures of whitecaps. In Oceanic Whitecaps (pp. 251-260), Springer Netherlands.

Kuenen, J. et al. (2011): MACC European emission inventory for the years 2003-2007 TNO report TNO-060-UT-2011-00588.

Kulmala, M. et al. (2004): Formation and growth rates of ultrafine atmospheric particles: a review of observations, J. Aerosol Sci., 35, 143–176.

Kulmala, M. et al. (2004): Formation and growth rates of ultrafine atmospheric particles: a review of observations, J. Aerosol Sci., 35, 143–176.

Lack, D. A. et al. (2009): Absorption Enhancement of Coated Absorbing Aerosols: Validation of the Photo-Acoustic Technique for Measuring the Enhancement. Aerosol Sci. Technol., 43:1006–1012.

Lance, S. et al. (2006): Mapping the operation of the DMT continuous flow CCN counter, Aerosol Sci. Tech., 40, 242–254.

Lesins, G. et al. (2002): A study of internal and external mixing scenarios and its effect on aerosol optical properties and direct radiative forcing, J. Geophys. Res., 107(D10), doi:10.1029/2001JD000973.

Levoni, C. et al. (1997): Atmospheric aerosol optical properties: a database of radiative characteristics for different components and classes; Applied optics, 36(30), 8031-8041.

Levy, R. et al. (2007): Second-generation operational algorithm: Retrieval of aerosol properties over land from inversion of Moderate Resolution Imaging Spectroradiometer spectral reflectance, J. Geophys. Res.-Atmos., 112(D13), D13211, 10.1029/2006JD007811.

Lewis, R. and Schwartz, E. (2004): Sea-salt aerosol production: mechanisms, methods, measurements and models-a critical review (Vol. 152, pp. 1-413). American Geophysical Union.

Li, J. et al. (2008): Parameterization of sea-salt optical properties and physics of the associated radiative forcing, Atmos. Chem. Phys., 8, 4787-4798, doi:10.5194/acp-8-4787-2008.

Liao, H. and J. H. Seinfeld (1998): Radiative forcing by mineral dust aerosols: Sensitivity to key variables, J. Geophys. Res., 103(D24), 31637–31645, doi:10.1029/1998JD200036.

Lindesay, J. A. et al. (1996): International Geosphere-Biosphere Programme/International Global Atmospheric Chemistry SAFARI 92 field experiment: Background and overview, d. Geophys. Res., 101, 23,521-23,530.

Liou, K.N. (2002): An Introduction to Atmospheric Radiation 2nd edition. Academic Press, 583 pp.

Lohmann, U. and Feichter, J. (2001): Can the direct and semi-direct aerosol effect compete with the indirect effect on a global scale?, Geophys. Res. Lett., 28, 159–161, 7568, 7569, 7580, 7606.

Lohmann, U. and Feichter, J. (2005): Global indirect aerosol effects: a review, Atmos. Chem. Phys., 5, 715-737, doi:10.5194/acp-5-715-2005.

© University of Pretoria

Lu, H., and Shao, Y. (1999): A new model for dust emission by saltation bombardment. Journal of Geophysical Research: Atmospheres (1984–2012), 104(D14), 16827-16842.

Lu, J. and Bowman, F. M. (2010): A detailed aerosol mixing state model for investigating interactions between mixing state, semivolatile partitioning, and coagulation; Atmospheric Chemistry and Physics, 10(8), 4033-4046.

Magi, B. I. et al. (2009): Evaluation of tropical and extratropical Southern Hemisphere African aerosol properties simulated by a climate model, J. Geophys. Res., 114, D14204, doi:10.1029/2008JD011128.

Magi, B.I. and Hobbs, P.V. (2003): Effects of humidity on aerosols in southern Africa during the biomass burning season. Journal of Geophysical Research 108: doi: 10.1029/2002JD002144. issn: 0148-0227.

Mahowald, N. et al. (2011): Aerosol impacts on climate and biogeochemistry. Annual Review of Environment and Resources, 36, 45-74.

Maring H. et al. (2003): Mineral dust aeroso size distribution change during atmospheric transport. J. Geophys. Res., 108(D19), 8592, doi: 10.0129/2002JD002536.

Markowicz, K. M. et al. (2003): Clear-sky infrared aerosol radiative forcing at the surface and the top of the atmosphere. Q.J.R. Meteorol. Soc., 129: 2927–2947. doi: 10.1256/qj.02.224.

Martonchik, J. V. et al. (1998): Techniques for the retrieval of aerosol properties over land and ocean using multi-angle imaging, IEEE Trans. Geosci. Remote Sens., 36(4), 1212–1227, doi:10.1109/36.701027.

Martonchik, J. V. et al. (2002): Regional aerosol retrieval results from MISR, IEEE Trans. Geosci. Remote Sens., 40(7), 1520–1531, doi:10.1109/TGRS.2002.801142.

McFarquhar, G. M. and Heymsfield, A. J. (1998): The Definition and Significance of an Effective Radius for Ice Clouds, J. Atmos. Sci., 55, 2039–2052.

McMurry, P. H. (2000): A review of atmospheric aerosol measurements. Atmospheric Environment, 34(12), 1959-1999.

Mishchenko, M. I. (1993): Light scattering by size-shape distributions of randomly oriented axially symmetric particles of a size comparable to a wavelength, Appl. Opt., 32, 4652–4665.

Mishchenko, M.I. et al. (1999): Aerosol retrievals over the ocean using channel 1 and 2 AVHRR data: A sensitivity analysis and preliminary results. Appl. Opt., 38, 7325-7341, doi:10.1364/AO.38.007325.

Mishchenko, M.I. et al. (2007): Accurate monitoring of terrestrial aerosols and total solar irradiance: Introducing the Glory mission. Bull. Amer. Meteorol. Soc., 88, 677-691, doi:10.1175/BAMS-88-5-677.

Mitchell, J. P. and Nagel, M. W. (1999): Time-of-flight aerodynamic particle size analyzers: their use and limitations for the evaluation of medical aerosols. Journal of aerosol medicine, 12(4), 217-240.

Monahan, E. C. et al. (1986): A model of marine aerosol generation via whitecaps and wave disruption, in Oceanic Whitecaps and Their Role in Air-Sea Exchange Processes, edited by E. C. Monahan and G. MacNiocaill, pp. 167 – 174, D. Reidel, Norwell, Mass.

Monahan, E.C. and O'Muircheartaigh, I.G. (1986): Whitecaps and the passive remote sensing of the ocean surface, International Journal of Remote Sensing, 7, pp. 627-642.

Monks et al. (2009): Atmospheric composition change – global and regional air quality, Atoms. Env., 43, 5268-5350.

Müller, T. et al. (2011): Characterization and intercomparison of aerosol absorption photometers: result of two intercomparison workshops. Atmospheric Measurements Techniques, 4: 245–268.

Naydenova, I. (2007): Soot formation modeling during hydrocarbon pyrolysis and oxidation behind shock waves. Doktorarbeit, Ruprecht-Karls-Universität Heidelberg.

Pal, J. S., et al. (2007), Regional climate modeling for the developing world: The ICTP RegCM3 and RegCNET, Bull. Am. Meteorol. Soc., 88, 1395 – 1409.

Penner, J. E. et al. (2001): Aerosols, their direct and indirect effects. Climate Change 2001: The Scientific Basis. J. T. Houghton et al., Eds., Cambridge University Press, 289–348.

Perlwitz, J. and Miller, R. L. (2010): Cloud cover increase with increasing aerosol absorptivity: A counterexample to the conventional semi-direct aerosol effect, J. Geophys. Res., 115, D08203, doi:10.1029/2009JD012637.

Petzold, A. and Schonlinner, M. (2004): Multi-angle absorption photometry - a new method for the measurement of aerosol light absorption and atmospheric black carbon, Journal of Aerosol Science, 35, 421-441.

Pöschl, U. (2005): Atmospheric aerosols: Composition, transformation, climate and health effects, Angewandte Chemie International Edition, 44, 7520–7540.

Pöschl, U. et al. (2007): Kinetic model framework for aerosol and cloud surface chemistry and gas-particle interactions; Part 1: General equations, parameters and terminology. Atmos. Chem. Phys. 7(23): 5989.

Privette, J.L. and D.P. Roy. (2005): Southern Africa as a remote sensing test bed: the SAFARI 2000 Special Issue overview. Int. J. Rem. Sens. 26. 4141-4158.

Privette, J.L. et al. (2004): Vegetation structure characteristics and relationships of Kalahari woodlands and savannas. Glob. Change. Bio. 10. 281-291.

Qian, Y. et al. (2001): Regional simulation of anthropogenic sulfur over East Asia and its sensitivity to model parameters. Tellus. 53B. 171-191.

Qian, Y., and Giorgi, F. (1999): Interactive coupling of regional climate and sulfate aerosol models over eastern Asia, J. Geophys. Res., 104(D6), 6477–6499, doi:10.1029/98JD02347.

Radke, L. F. et al. (1980): Scavenging of aerosol particles by precipitation, J. Appl. Meteor., 19, 715-722.

Ram, K. et al. (2012): Carbonaceous and secondary inorganic aerosols during wintertime fog and haze over urban sites in the Indo-Gangetic Plain. Aerosol and Air Quality Research, 12(3), 68-79.

Ramanathan, V. et al. (2001): Aerosol, climate, and hydrological cycle.Science 294, 2119-2124.

Rampino, M.R., and Self, S. (1984): Sulphur-rich volcanic eruptions and stratospheric aerosols. Nature, 310, doi:10.1038/310677a0.

Randall, D. A. et al. (2007): Climate models and their evaluation. Climate Change 2007: The Physical Science Basis. Contribution of Working Group I to the Fourth Assessment Report of the Intergovernmental Panel on Climate Change, S. Solomon, et al., Eds., Cambridge University Press, 589–662.

Ravishankara, A. R. (1997): Heterogeneous and multiphase chemistry in the troposphere. Science 276, 1058–1065.

Remer, L. A. et al. (2002): Validation of MODIS aerosol retrieval over ocean, Geophys. Res. Lett., 29(12), doi:10.1029/2001GL013204.

Remer, L. A. et al. (2005): The MODIS aerosol algorithm, products, and validation. Journal of the Atmospheric Sciences, 62(4), 947-973.

Robock, A. (2000): Volcanic eruptions and climate. Rev. Geophys. 38, 191–219. doi:10.1029/1998RG000054.

Roden, C. A. et al., (2005): Emission Factors and Realtime Optical Properties of Particles Emitted from Traditional Wood Burning Cookstoves, submitted to Env. Sci. Tech.

Roelofs, G. J. et al. (1997): Ozone production and transports in the tropical Atlantic region during the biomass burning season, J. Geophys. Res., 102, 10,637–10,651.

Ross, K. E. et al. (2003): Spatial and seasonal variation in CCN distribution and the aerosol-CCM relationship over southern Africa, J. Geophys. Res., 108(D13), 8481, doi:10.1029/2002JD002384.

Russell, L.M. et al. (1994): Aerosol production and growth in the marine boundary layer. J. Geophys. Res., 99, 20989-21003.

Rutherford, M.C. and Westfall, R.H. (1994): Biomes of southern Africa: an objective characterization. Memoirs of the Botanical Survey of South Africa 54: 1 -98.

© University of Pretoria

Schuster, G. L. et al. (2006): Angstrom exponent and bimodal aerosol size distributions. Journal of Geophysical Research: Atmospheres (1984–2012), 111(D7).

Seinfeld, J.H. and Pandis, S.N. (2006): Atmospheric chemistry and physics: from air pollution to climate. Wiley. New York.

Shao, Y. (2008): Physics and modelling of wind erosion. Springer Verlag.

Simmons, A.J. et al. (2004): Comparison of trends and low-frequency variability in CRU, ERA-40 and NCEP/NCAR analyses of surface air temperature. J. Geophys. Res. 109(D24115). Doi: 10.1029/2004JD005306.

Sipilä, M. et al. (2008): Applicability of Condensation Particle Counters to measure Atmospheric clusters, Atmos. Chem. Phys. 8, 4049-4060.

Solmon, F. et al. (2006): Aerosol modelling for regional climate studies: application to anthropogenic particles and evaluation over a European/African domain. Tellus B, 58(1), 51-72.

Solomon, S., et al. (2007): Contribution of Working Group I to the Fourth Assessment Report of the Intergovernmental Panel on Climate Change. Cambridge University Press. Cambridge, United Kingdom and New York, NY, USA.

Song, C., and Carmichael, G. (2001): A three-dimensional modeling investigation of the evolution processes of dust and sea-salt particles in east Asia, Journal of Geophysical Research-Atmospheres, 106(D16), 18131-18154.

Spinhirne, J. et al. (2005a): Cloud and Aerosol Measurements from GLAS: Overview and Initial Results. Geophysical Research Letters 32(L22S03), doi: 10.1029/2005GL023507.

Spinhirne, J. et al. (2005b): Global Aerosol Distribution from the GLAS Polar Orbiting LIDAR Instrument. Remote Sensing of Atmospheric Aerosols, 2005. IEEE Workshop 2-8.

Stier, P. (2005): The aerosol-climate model ECHAM5-HAM. Atmospheric Chemistry and Physics, 5(4), 1125-1156.

Swap, R. J. et al. (2003): Africa burning: A thematic analysis of the Southern African Regional Science Initiative (SAFARI 2000), J. Geophys. Res., 108(D13), 30 8465, doi:10.1029/2003JD003747.

Tanaka, T.Y. and Chiba, M. (2005): Global simulation of dust aerosol with a chemical transport model, MASINGAR. J. Meteorol. Soc. Jpn. 83A, 255–278.

Tang, I.N. (1997): Thermodynamic and optical properties of sea-salt aerosols. Journal of Geophysical Research 102: doi: 10.1029/97JD01806. issn: 0148-0227.

Tanre´, D. et al. (1997): Remote sensing of aerosol properties over oceans using the MODIS/EOS spectral radiances., J. Geophys. Res., 102, 16,971 – 16,988.

Tao, W.-K. et al. (2012): Impact of aerosols on convective clouds and precipitation, Rev. Geophys., 50, RG2001, 2011RG000369, 1–62.

Tegen, I. et al. (1997): Contribution of different aerosol species to the global aerosol extinction optical thickness: Estimates from model results. J. Geophys. Res., 102, 23895-23915, doi:10.1029/97JD01864.

Tegen, I. et al. (2004): Relative importance of climate and land use in determining present and future global soil dust emission. Geophys. Res. Lett., 31, L05105, doi:10.1029/2003GL019216.

ten Brink, H.M. et al. (2000): A high-flow humidograph for testing the water uptake by ambient aerosol. Atmospheric Environment 34, 4230-4291.

Thomas, G. E. et al. (2004): Retrieval of aerosol refractive index from extinction spectra using a damped oscillator band model, Appl. Optics, 44, 1332–1341.

Thomason, L. W., and Pitts, M. C. (2008): CALIPSO observations of volcanic aerosol in the stratosphere, Proc. SPIE, 7153, 71530O, doi:10.1117/ 12.804090.

Thompson M. (1996): A standard land-cover classification scheme for remote sensing in South Africa. SAJ Sci, 92, 34-42.

Todd, M. C. et al. (2007): Mineral dust emission from the Bodélé Depression, northern Chad, during BoDEx 2005, J. Geophys. Res., 112, D06207, doi:10.1029/2006JD007170.

Torres, O. et al. (1998): Derivation of aerosol properties from satellite measurements of backscattered ultraviolet radiation: Theoretical bases. J. Geophys. Res., 103, 17 009–17 110.

Torres, O. et al. (2002): A long-term record of aerosol optical depth from TOMS observations and comparison to AERONET measurements, J. Atmos. Sci., 59, 398 – 413.

Torres, O. et al. (2007): Aerosols and surface UV products from Ozone Monitoring Instrument observations: An overview, J. Geophys. Res., 112, D24S47, doi:10.1029/2007JD008809.

Tummon, F. (2011): Direct and semi-direct aerosol effects on the southern African regional climate during the austral winter season: PhD thesis. University of Cape Town, South Africa.

Twomey, S. (1974): Pollution and planetary albedo. Atmos. Environ., 8, 1251–1256.

Tyson, P.D. and Preston-Whyte, R.A. (2000): The weather and climate of southern Africa. Oxford University Press. Cape Town.

van Huyssteen, E. et al. (2013): Analysing risk and vulnerability of South African settlements: Attempts, explorations and reflections. Jàmbá: Journal of Disaster Risk Studies, 5(2), 8-pages.

Vignati, E. et al. (2010): Global scale emission and distribution of sea-spray aerosol: Sea-salt and organic enrichment. Atmospheric Environment, 44(5), 670-677.

Warneck, P. (1999): Chemistry of the natural atmosphere. Vol. 71. Access Online via Elsevier.

Whitby, K. T. (1978): The physical characteristics of sulfur aerosols, Atmos. Env., 12, 135–159.

Williams, M. (1988): A unied theory of aerosol coagulation, Appl. Phys., 21, 875-886.

Winker, D. M. et al. (2007): Initial performance assessment of CALIOP, Geophys. Res. Lett., 34, L19803, doi:10.1029/2007gl030135.

Winker, D. M. et al. (2013): The global 3-D distribution of tropospheric aerosols as characterized by CALIOP, Atmos. Chem. Phys., 13, 3345-3361, doi:10.5194/acp-13-3345-2013.

Winter, B., and Chylek, P. (1997): Contribution of sea-salt aerosol to the planetary clear-sky albedo, Tellus, Ser. B, 49, 72–79.

Woodcock, A. H. et al. (1953): Giant Condensation Nuclei from Bursting Bubbles, Nature, 172, 1144–1145.

World Meteorological Organization (WMO) Scientific Assessment of Ozone Depletion, (2002): Global Ozone Research and Monitoring Project - Report No. 47, 498pp., Geneva.

Yu, H. et al. (2009): Remote Sensing and In Situ Measurements of Aerosol Properties, Burdens, and Radiative Forcing, in Atmospheric Aerosol Properties and Climate Impacts, A Report by the U.S. Climate Change Science Program and the Subcommittee on Global Change Research. [Mian Chin, Ralph A. Kahn, and Stephen E. Schwartz (eds.)]; National Aeronautics and Space Administration, Washington, D.C., USA.

Zakey, A. S. et al. (2006): Implementation and testing of a desert dust module in a regional climate model, Atmos. Chem. Phys., 6, 4687-4704, doi:10.5194/acp-6-4687-2006.

Zakey, A. S. et al. (2008): Modeling of sea-salt in a regional climate model: Fluxes and radiative forcing, J. Geophys. Res., 113, D14221, doi:10.1029/2007JD009209.

Zhang, K. M. et al. (2005): Size distribution of sea-salt emissions as a function of relative humidity. Atmospheric Environment, 39(18), 3373-3379.

Zhang, R. et al. (2011): Nucleation and growth of nanoparticles in the atmosphere. Chemical Reviews, 112(3), 1957-2011.

Zhang, Y. (2008): The Radiative Effect Of Aerosols From Biomass Burning On The Transition From Dry To Wet Season Over The Amazon As Tested By A Regional Climate Model: PhD thesis. Georgia Institute of Technology, United State.

Zhao, T. L. et al. (2003): Modeled size segregated wet and dry deposition budgets of soil dust aerosol during ACE-Asia 2001: Implications for trans-Pacific transport. J. Geophys. Res., 108, 8665, doi:10.1029/2002JD003363.

Zhu, Y., et al. (2002): Study of ultrafine particles near a major highway with heavy-duty diesel traffic. Atmos. Environ., 36, 4323–4335.

Zunckel, M. et al. (2000): Modelled transport and deposition of sulphur over Southern Africa. Atmos. Env. 34. 2797-2808.

© University of Pretoria

Chapter 2: Aerosol climatology over South Africa based on 10 years of Multiangle-Imaging Spectroradiometer (MISR) data*

*This chapter needs to be cited as:

Tesfaye, M., V. Sivakumar, J. Botai, and G. Mengistu Tsidu (2011): Aerosol climatology over South Africa based on 10 years of Multiangle Imaging Spectroradiometer (MISR) data; J. Geophys. Res., 116, D20216, doi:10.1029/2011JD016023.

© University of Pretoria

UNIVERSITEIT VAN PRETORIA
UNIVERSITY OF PRETORIA
YUNIBESITHI YA PRETORIA

JOURNAL OF GEOPHYSICAL RESEARCH, VOL. 116, D20216, doi:10.1029/2011JD016023, 2011

Aerosol climatology over South Africa based on 10 years of Multiangle Imaging Spectroradiometer (MISR) data

M. Tesfaye,[1,2] V. Sivakumar,[1,2,3] J. Botai,[1] and G. Mengistu Tsidu[4]

Received 28 March 2011; revised 23 June 2011; accepted 12 August 2011; published 29 October 2011.

[1] In this paper, we present a detailed study of the spatial and seasonal aerosol climatology over South Africa (SA), based on Multiangle Imaging Spectroradiometer (MISR) data. We have used 10 years (2000–2009) of MISR monthly mean aerosol extinction (τ_{ext}), absorption (τ_a) optical depths at 558 nm, Angstrom exponents in visible (VIS; 446–672 nm) and near-infrared (NIR; 672–866 nm) spectral bands, and the extracted spectral curvature. The study has shown that, in terms of aerosol load level spatial variation, SA can be classified into three parts: the upper, central, and lower, which illustrate high, medium, and low aerosol loadings, respectively. The results for the three parts of SA are presented in detail. The prevailing sources of aerosols are different in each part of SA. The lower part is dominated by the air mass transport from the surrounding marine environment and other SA or neighboring regions, while the central and upper parts are loaded through wind-ablated mineral dust and local anthropogenic activities. During the biomass burning seasons (July–September), the central part of SA is more affected than the rest of SA by the biomass-burning aerosols (based on τ_a, ~20% higher than the rest of SA). In alignment with the observed higher values of τ_{ext}, aerosol size distributions were found to be highly variable in the upper part of SA, which is due to the high population and the industrial/mining/agricultural activities in this area.

Citation: Tesfaye, M., V. Sivakumar, J. Botai, and G. Mengistu Tsidu (2011), Aerosol climatology over South Africa based on 10 years of Multiangle Imaging Spectroradiometer (MISR) data, *J. Geophys. Res.*, *116*, D20216, doi:10.1029/2011JD016023.

1. Introduction

[2] Atmospheric aerosols originate from various natural and anthropogenic processes. Natural sources include wind-blown mineral dust, precursor gases from volcanic eruptions, natural wild fires, vegetation, and oceans. Anthropogenic sources include emissions from fossil fuel and biofuel combustion, industrial processes, agriculture practices, human-induced biomass burning, and photochemically induced smog, primarily due to vehicle emissions [*Charlson et al.*, 1992; *Kaufman et al.*, 1997]. Aerosols are dominant in the troposphere. The lifetime of aerosols varies from minutes to days in the troposphere, due to the prevailing precipitation and interactions with the Earth's surface, depending on aerosol size and chemistry and the height of the atmosphere. Due to unpredictable events such as large dust storms and volcanic eruptions, aerosol concentrations may vary significantly with respect to location and time (diurnal and seasonal variations). Furthermore, aerosols are highly mobile, i.e., they may even cross oceans and mountains. It is generally agreed, that due to various aging processes such as coagulation, humidification, scavenging by precipitation, and gas-to-particle conversion, aerosols often exhibit widely varying physicochemical and optical properties through time [*Mallet et al.*, 2003].

[3] It is also well known that atmospheric aerosols have direct, semidirect, and indirect impacts on the Earth's radiation budget and climate. In addition, aerosols have detrimental effects on human health such as impairment to pulmonary function [*Twomey*, 1977; *Raizenne et al.*, 1996; *Haywood and Boucher*, 2000; *James et al.*, 2000; *Jayaraman*, 2001; *Roberts et al.*, 2001; *Intergovernmental Panel on Climate Change*, 2007]. However, such effects are determined by the aerosol's optical, physical, and chemical characteristics in concert with source strength and/or advection by local to synoptic meteorological processes. Therefore, measuring and understanding changes in aerosol loading over time are essential to climate prediction. However, studying the impacts of aerosols on climate is challenging, and large uncertainties exist due to the immense diversity, not only with respect to aerosol particle size, composition, sources, and lifetime variation, but also with regard to their spatial and temporal distributions. Thus, the impacts of aerosols on climate must be understood and quantified on a regional scale rather than on a global-average basis [*Piketh et al.*, 2002]. The knowledge of aerosol characteristics at local and global scales and their temporal changes interrelated with other atmospheric parameters and

[1]Department of Geography, Geoinformatics, and Meteorology, University of Pretoria, Pretoria, South Africa.
[2]National Laser Centre, Council for Scientific and Industrial Research, Pretoria, South Africa.
[3]School of Physics, University of KwaZulu Natal, Durban, South Africa.
[4]Department of Physics, Addis Ababa University, Addis Ababa, Ethiopia.

Copyright 2011 by the American Geophysical Union.
0148-0227/11/2011JD016023

© University of Pretoria

UNIVERSITEIT VAN PRETORIA
UNIVERSITY OF PRETORIA
YUNIBESITHI YA PRETORIA

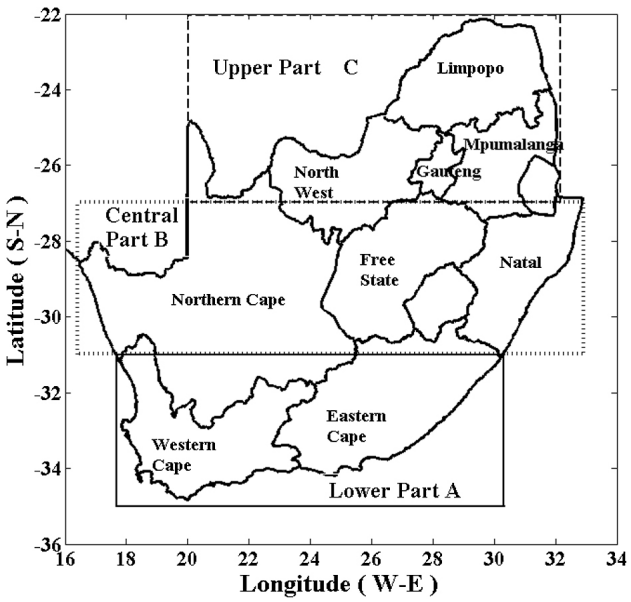

Figure 1. Geographical map of South Africa and our three regional spatial classifications in terms of aerosol load level differences.

solar radiation are of great importance for the study on the effects of aerosols in the atmosphere. Improved aerosol climatology may enable more accurate estimations of the direct and indirect aerosol forcing [*Kaufman et al.*, 1997; *Masmoudi et al.*, 2003]. Aerosol parameters can be measured in situ or remotely sensed from the ground or from aircraft or satellites [*Sivakumar et al.*, 2010]. In particular, satellite-based aerosol observation constitutes a recent and powerful tool for assessing aerosol spatial distribution and their properties. In some cases, due to its ability of providing a complete and synoptic view, large areas can be assessed in single snapshots. The data from satellite sensors can be used to improve the current understanding of climate prediction and the impacts of aerosols on climate change [*Holben et al.*, 1992; *Kaufman*, 1993; *Kaufman et al.*, 2002; *King et al.*, 1999; *Ignatov and Stowe*, 2002; *Levy et al.*, 2003, 2009; *Kahn et al.*, 2009].

[4] South Africa (SA) is located at the southernmost tip of the African continent, with geocoordinates extending from 22°S to 34°S latitude and from 16°E to 32°E longitude (see Figure 1). SA shares borders with Namibia, Botswana, Zimbabwe, and Mozambique. South Africa is famous for its brilliant orange skies at sunrise and sunset, which may also be an indicator of the presence of aerosols. Some previous studies have indicated that SA is one of the most affected countries with regard to aerosol load, due to various natural and anthropogenic activities [e.g., *Piketh et al.*, 1999, 2002; *Formenti et al.*, 2002, 2003; *Campbell et al.*, 2003; *Eck et al.*, 2003; *Freiman and Piketh*, 2003; *Ichoku et al.*, 2003; *Ross et al.*, 2003; *Liu*, 2005; *Winkler et al.*, 2008; *Queface et al.*, 2011]. Those studies focused on a limited time scale, during biomass-burning seasons, and on the northern parts of SA, where ~75% of the country's industrial infrastructure is concentrated and which is populated by coal-fired power plants.

[5] Multiangle Imaging Spectroradiometer (MISR) provides useful information for scientists studying different aspects related to the Earth's climate, such as the partitioning of energy and carbon between the land surface and the atmosphere, and the regional/global impacts of different types of atmospheric particles (aerosols) and clouds on climate [*Diner et al.*, 1998, 2001, 2005; *Kahn et al.*, 2001, 2005; *Martonchik et al.*, 2004; *Kalashnikova and Kahn*, 2008; *Dey and Di Girolamo*, 2010]. The present work aims to report the seasonal and spatial variation of aerosol optical and microphysical properties over the entire SA region, based on 10 years (2000–2009) of MISR data. In addition, by correlating the variation of aerosol optical properties and background weather parameters such as rainfall, relative humidity (RH), and wind speed (obtained from the South African Weather Service (SAWS)), the effects of local meteorological conditions on the aerosol optical, microphysical properties and their dynamics (load, dispersion, and removal processes) are evaluated. The paper is organized as follows: Section 2 provides information about MISR, as well as data and analysis, including meteorological data. Section 3 presents results obtained in terms of the spatial-seasonal variability of the observed aerosol optical parameters in association with background weather conditions, by classifying SA into three regions. Finally, section 4 provides a summary and concluding remarks.

2. Data and Methods

2.1. MISR Data and Analysis

[6] MISR was launched by National Aeronautics and Space Administration (NASA) on 18 December 1999 and has been in operation since February 2000. The device is designed to measure solar radiation reflected by the Earth's system (planetary surface and atmosphere) in various angular positions. It consists of nine push broom cameras arranged to view at nominal zenith angles relative to the surface reference ellipsoid of 0.0°, ±26.1°, ±45.6°, ±60.0° and ±70.5° and measures upwelling short wave radiance in each camera at four spectral bands, centered at 446, 558, 672, and 866 nm. This makes MISR unique among the NASA Earth-observing system Terra satellite instruments, by providing radiometrically and geometrically accurate and carefully calibrated high spatial resolution image data. The multiple angle band observations of MISR further allow us to retrieve a number of aerosol optical and microphysical properties over land (including bright desert surfaces) and ocean, as well as surface albedo and information about cloud properties [*Diner et al.*, 1998, 1999, 2001, 2005; *Martonchik et al.*, 1998, 2002, 2004; *Kahn et al.*, 2001, 2007; *Muller et al.*, 2002; *Kalashnikova et al.*, 2005; *Kalashnikova and Kahn*, 2006]. More detailed information about the instrument and the data is available at http://eosweb.larc.nasa.gov/GUIDE/campaign_documents/misr_ov2.html.

[7] Optical properties of aerosols may be described using a number of parameters. The spectral aerosol extinction optical depth (AOD; $\tau_{ext}(\lambda_i)$) is the vertical integral of fraction of incident light either scattered or absorbed by airborne particles (i.e., the sum of aerosol scattering optical depth $\tau_s(\lambda_i)$ and aerosol absorption optical depth $\tau_a(\lambda_i)$. AOD is an indicator of the aerosol load level in the vertical column of the

© University of Pretoria

UNIVERSITEIT VAN PRETORIA
UNIVERSITY OF PRETORIA
YUNIBESITHI YA PRETORIA

atmosphere and constitutes important parameters used to assess the aerosol radiative forcing and its impact on climate [*Charlson et al.*, 1992; *Hansen et al.*, 1997, and references therein; *Eck et al.*, 1999; *Cachorro et al.*, 2001; *Holben et al.*, 2001; *Christopher and Zhang*, 2002]. The MISR-AOD Level 3 data have a higher grid resolution (0.5° × 0.5°) in comparison to the Moderate Resolution Imaging Spectroradiometer (MODIS) Level 3 data which have a resolution of 1° × 1°. Further, earlier studies revealed that the MISR-retrieved AOD has better agreement with ground-based Aerosol Robotic Network (AERONET) measurements, when compared with MODIS [*Diner et al.*, 2001; *Christopher and Wang*, 2004; *Liu et al.*, 2004; *Martonchik et al.*, 2004; *Abdou et al.*, 2005; *Kahn et al.*, 2005, 2007, 2010; *Jiang et al.*, 2007; *Prasad and Singh*, 2007; *de Meij and Lelieveld*, 2011]. In the present study, we have used the latest version (version 31) of MISR Level 3 monthly averaged global 0.5° × 0.5° grid data of aerosol extinction and absorption optical depth at 558 nm.

[8] The sensitivity of the particle extinction efficiency to wavelength, i.e., $|\partial Q_{ext}(\lambda, r)/\partial\lambda|$, generally increases with decreasing particle size. This sensitivity is true for any particle composition and may easily be demonstrated using the Mie algorithm. An empirical measure of this sensitivity is obtained from spectral values of AOD at two different wavelengths, λ_1 and λ_2, expressed through Angstrom's empirical relationship [*Angstrom*, 1929]:

$$\alpha = \frac{\ln\left[\frac{\tau_{ext}(\lambda_1)}{\tau_{ext}(\lambda_2)}\right]}{\ln\left[\frac{\lambda_1}{\lambda_2}\right]}. \quad (1)$$

Using the MISR Level 3 monthly global 0.5° × 0.5° grid AOD data at 446, 672, and 866 nm in equation (1), we compute the Angstrom exponent (α) in the visible (VIS; 446–672 nm, $\alpha_{(446–672)\ nm}$) and near-infrared (NIR; 672–866 nm, $\alpha_{(672–866)\ nm}$) spectral bands. The values of both aerosol optical parameters (AOD and α) exhibit a strong dependence on the amount of aerosols of different sizes and concentrations, their chemical composition, and the wavelength of the incident radiation [*Eck et al.*, 1999, 2001, 2003; *Reid et al.*, 1999; *Cachorro et al.*, 2001; *O'Neill et al.*, 2001a, 2001b, 2002, 2003; *Adeyewa and Balogun*, 2003]. Therefore, they are widely used in atmospheric sciences dealing with optical properties of aerosol particles. The Angstrom exponent is commonly used to provide further information on particle size distribution of aerosols in the solar spectrum. Several authors have discussed how the spectral variation of α can provide information about the aerosol size distribution [e.g., *Nakajima et al.*, 1986; *Kaufman et al.*, 1992; *Eck et al.*, 1999; *Reid et al.*, 1999; *O'Neill et al.*, 2001a, 2001b, 2002, 2003; *Kaskaoutis and Kambezidis*, 2006; *Schuster et al.*, 2006]. Values of α exceeding 1.5 indicate size distributions dominated by fine-mode aerosols, radii ≤0.35 μm) that are usually associated with urban pollution (sulfate) and biomass burning (carbonaceous aerosols), whereas, α values between 1 and 1.5 indicate the presence of accumulation-mode particles (0.35 μm < radii ≤0.75 μm). Values of α < 1 indicate size distributions dominated by coarse-mode aerosols (radii >0.75 μm) (sea spray and large dust particles), especially for larger aerosol particles such as desert dust particles, α approaches zero. Generally, a very high α values at shorter wavelength intervals (UV and VIS bands), indicates the presence of submicron (fine and accumulation) particles probably resulting from various anthropogenic activities, with less influence of the supermicron (coarse) particles. In contrast, observing low values of α (<1) at longer wavelength regions implies the existence of supermicron (coarse) particles. However, the studies by *Eck et al.* [1999, 2001] and *Reid et al.* [1999] revealed high values of α (>1.4) at longer wavelength with an increase in AOD, resourced due to the presence of submicron particles which are induced by extensive biomass-burning activities. Thus, in our present study, we have also included α in the longer wavelength range (NIR) for a better understanding of biomass-burning seasons in SA.

[9] On the other hand, *King and Byrne* [1976] and *Eck et al.* [1999] inferred a large deviation in the linear fit of measured AOD and wavelength. These studies also addressed that the addition of the first derivative of α (i.e., α') into $\ln\tau_{ext}(\lambda)$ versus $\ln\lambda$ relationship provide a better result. Additionally, previous studies have indicated the inadequacies of the Angstrom exponent values in providing the relative fractional contribution of supermicron and submicron particles to the total AOD [*King et al.*, 1978; *Kaufman*, 1993; *Eck et al.*, 1999, 2001, 2003; *O'Neill et al.*, 2001a, 2001b, 2003; *Gobbi et al.*, 2007; *Basart et al.*, 2009, and references therein]. Further, the above studies have also suggested the importance of the spectral curvature of the Angstrom exponent (α') together with α for providing more information on the aerosol size distribution. Therefore, in the present study, we have determined the α in both wavelength regions (VIS and NIR) and α' for a more comprehensive understanding of the relative contribution of different modes of aerosols to the total AOD. In general, α' can be expressed as

$$\alpha' = \frac{d\alpha}{d\ln\lambda} = -\left(\frac{2}{\ln\lambda_{i+1} - \ln\lambda_{i-1}}\right)\left[\frac{\ln\tau_{i+1} - \ln\tau_i}{\ln\lambda_{i+1} - \ln\lambda_i} - \frac{\ln\tau_i - \ln\tau_{i-1}}{\ln\lambda_i - \ln\lambda_{i-1}}\right]. \quad (2)$$

In this work, equation (2) is represented as $\Delta\alpha = \alpha_{(446–672)\ nm} - \alpha_{(672–866)\ nm}$, and following the work of several authors [e.g., *Kaufman*, 1993; *Eck et al.*, 1999, 2001; *Reid et al.*, 1999; *O'Neill et al.*, 2001a, 2001b, 2003; *Gobbi et al.*, 2007; *Basart et al.*, 2009],we have used it to extract additional information about aerosol size distributions such as the relative dominant influence of coarse-mode versus submicron-mode aerosol fractions or the effect of two particle modes on the aerosol size distribution. The large positive values of α' (along with α < 1) are characteristic of coarse-mode-dominated, bimodal aerosol size distributions. While, the near zero (along with 1 < α < 1.3) or negative (along with α > 1.3) values of α' are respectively characteristic of accumulation or fine-mode-dominated aerosol size distributions.

2.2. Meteorological Data

[10] The meteorological parameters such as RH, rainfall, and wind speed have a detrimental impact in aerosol dynamics (load, dispersion, and removal processes) and various aging processes (physicochemical change) [*Mallet et al.*, 2003]. Thus, in order to assess the impacts of the background weather conditions on the spatial-seasonal variability aerosol optical and microphysical properties over SA,

© University of Pretoria

UNIVERSITEIT VAN PRETORIA
UNIVERSITY OF PRETORIA
YUNIBESITHI YA PRETORIA

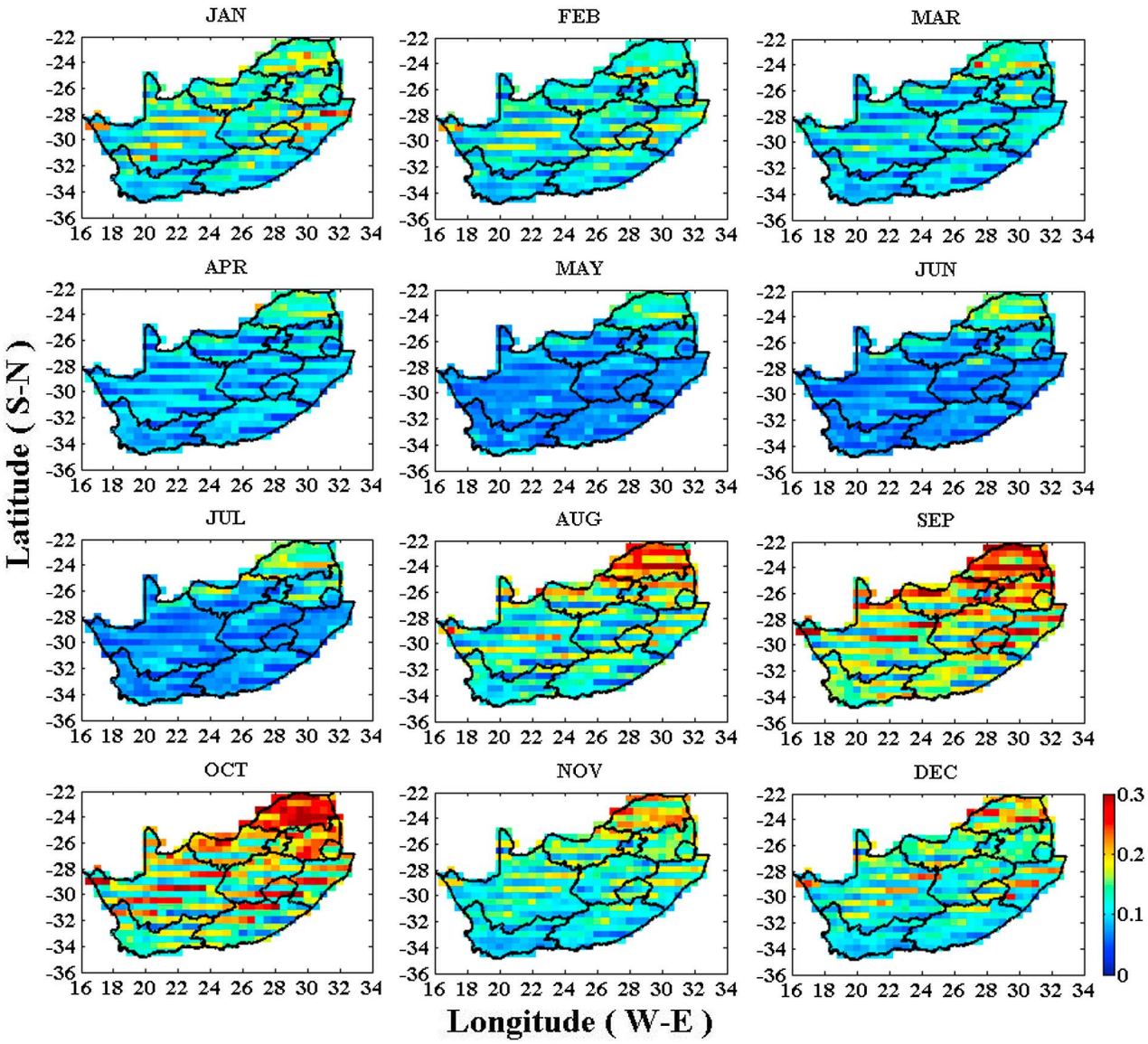

Figure 2a. Averaged aerosol extinction optical depth over South Africa obtained from 10 years of MISR data.

we have used local meteorological parameters together with the MISR data. Here, we have used the monthly mean based on 10 years (2000–2009) of archival meteorological data of RH, rainfall, wind speed, and wind direction from nine SAWS stations: Cape Town (33.9°S, 18.6°E), East London (33.0°S, 27.8°E), Durban South (29.9°S, 30.9°E), Bloemfontein (29.1°S, 26.3°E), Upington (28.4°S, 21.3°E), Johannesburg (26.2°S, 28.2°E), Ermelo (26.5°S, 29.9°E), Mafikeng (25.8°S, 25.5°E), and Polokwane (23.9°S, 29.5°E).

3. Results and Discussion

3.1. General Aerosol Seasonal Characteristics

[11] Ten years of monthly averaged aerosol optical parameters ($\tau_{ext(558\ nm)}$, $\tau_{a(558)}$, $\alpha_{(446–672)\ nm}$, $\alpha_{(672–866)\ nm}$ and α') are presented in Figures 2a–2e. Figure 2a shows the aerosol extinction optical depth at 558 nm ($\tau_{ext(558\ nm)}$). It is evident from Figure 2 that the maximum values ($\tau_{ext(558\ nm)} > 0.25$) are observed during spring (August–October) and minimum values ($\tau_{ext(558\ nm)} < 0.25$) during winter (May–July). It is also interesting to note a significant decrease in $\tau_{ext(558\ nm)}$ (~30%) during the May to July period in comparison with the other months (see Figure 2a). Such a decrease in AOD might be due to consequential results of cloud scavenging and wet removal processes of the summer months followed by low wind speed and low water vapor atmospheric weather conditions which cause respectively weak generation mechanisms and a remote chance of hygroscopic growth of aerosols. Similar seasonal variations of AOD have been reported by *Formenti et al.* [2002] and *Queface et al.* [2011], who have used measurements from the South African Astronomical Observatory at Sutherland (32.2°S, 20.5°E) and Sun photometer measurements from Skukuza (~24.6°S, 31.35°E) (an AERONET site).

© University of Pretoria

UNIVERSITEIT VAN PRETORIA
UNIVERSITY OF PRETORIA
YUNIBESITHI YA PRETORIA

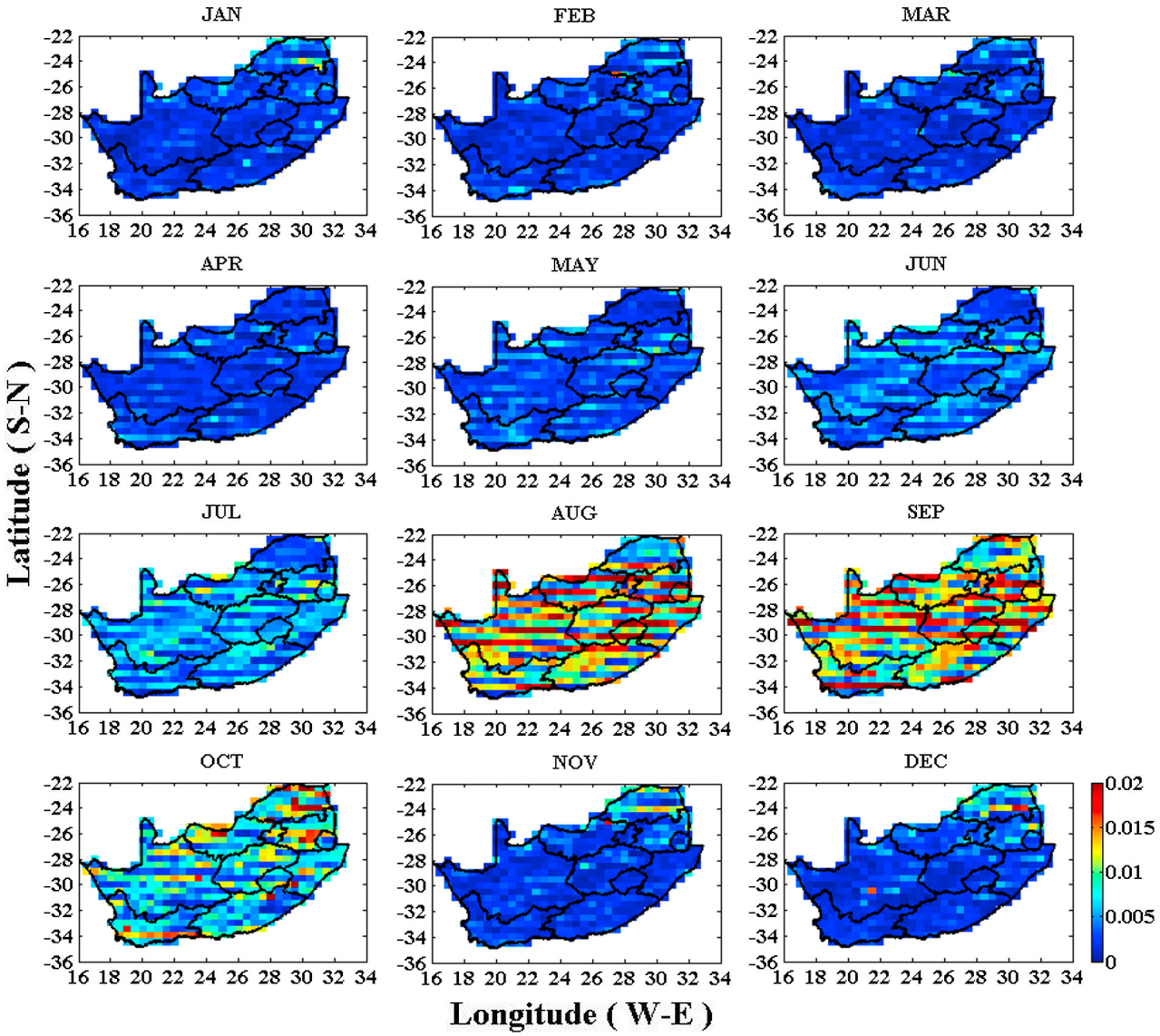

Figure 2b. Same as Figure 2a but for aerosol absorption optical depth.

[12] In order to study the seasonal and spatial variation of absorbing aerosol loads, such as aerosols from biomass burning and urban/industrial activities, the aerosol absorption optical depth ($\tau_{a(558\ nm)}$) is plotted in Figure 2b. It is evident from Figure 2 that $\tau_{a(558\ nm)}$ shows a minimum value (~0.002) during summer and early winter (November–May), except in the northern part which shows slightly higher values. Thereafter, there is a steady increase in $\tau_{a(558\ nm)}$ values from June, with a maximum value during the month of September. Overall, the maximum absorbing aerosol load is inferred during spring (August–October). The observed rise in $\tau_{a(558\ nm)}$ during June and July might be due to the air mass transport from tropical regions of southern Africa [*Freiman and Piketh*, 2003] where biomass-burning activities also happen during the same time period [*Magi et al.*, 2009]. However, the observed increase in $\tau_{a(558\ nm)}$ during spring is attributed to the local pronounced biomass-burning activities in the northeastern and eastern part of SA, in addition to a minor contribution by long-range transported biomass-burning aerosols from across the border countries, i.e., Namibia, Zimbabwe, and Botswana. Concurrently, we also observed a seasonal peak in AOD during spring (see Figure 2a).

[13] The spatial variation of $\tau_{ext(558\ nm)}$ indicates that different provinces in SA have different aerosol loading levels. The provinces, North West, Gauteng, Mpumalanga and Limpopo (see Figure 1 for locations) are highly polluted in comparison to upper part of Northern Cape, Free State, and Natal (modestly polluted) and to Western Cape, Eastern Cape, and the lower part of Northern Cape (low pollution). The above spatial variations might be due to the variations in long-range aerosol transportation, different aerosol sources and/or source strength and local meteorological parameters, such as RH, rainfall, and wind speed. Details on

© University of Pretoria

UNIVERSITEIT VAN PRETORIA
UNIVERSITY OF PRETORIA
YUNIBESITHI YA PRETORIA

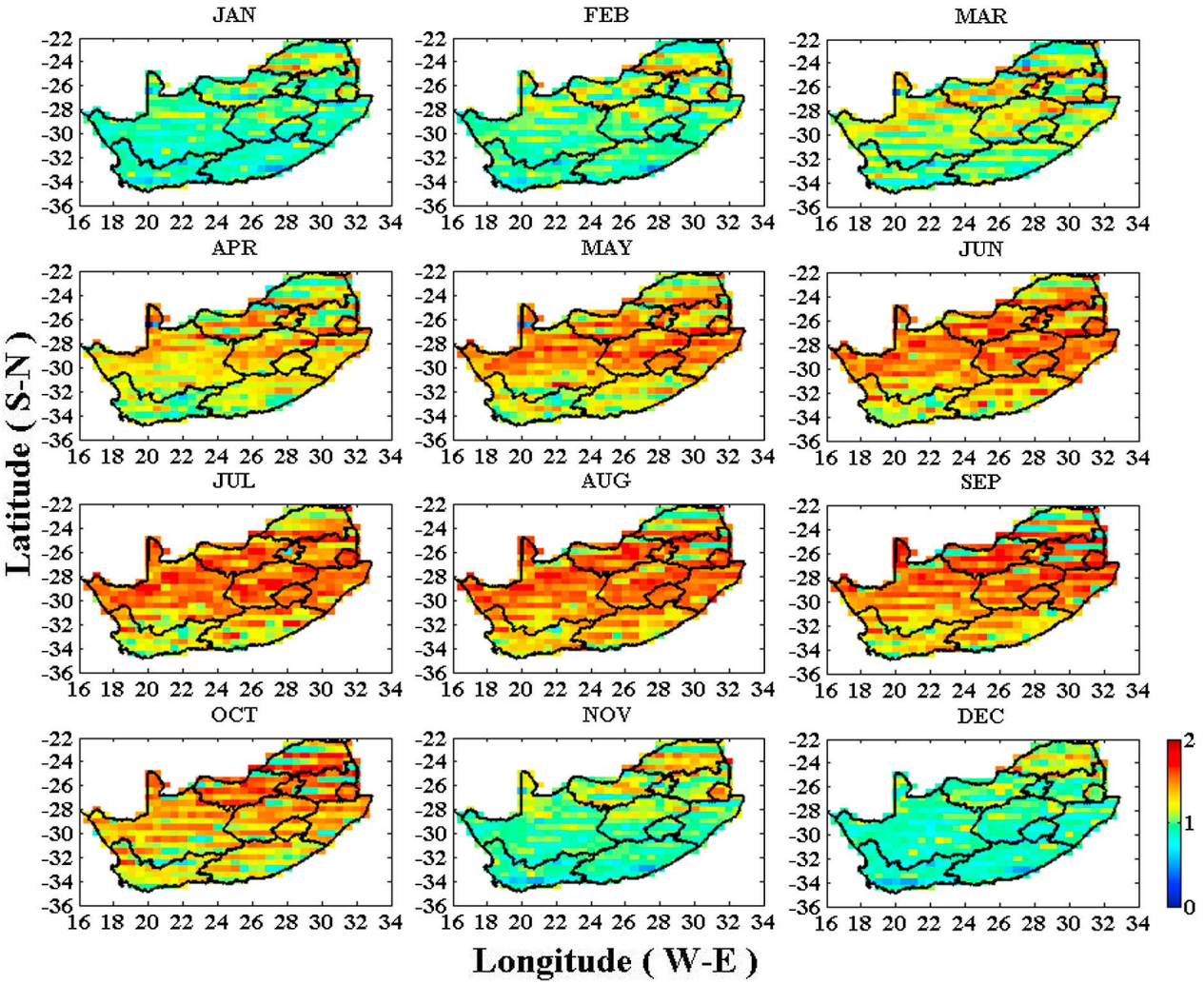

Figure 2c. Same as Figure 2a but for Angstrom exponent over visible region.

the relationship between the spatial and seasonal variability of AOD and local meteorological parameters are discussed in section 3.2.

[14] The Angstrom exponent values in the VIS ($\alpha_{(446–672)\ nm}$) and NIR ($\alpha_{(672–866)\ nm}$) bands are plotted in Figures 2c and 2d, respectively. During the dry seasons (winter to spring period, i.e., May–October) the Angstrom exponent values vary from 0.85 to 1.89 and from 0.74 to 1.95 in the VIS and NIR bands, respectively. As described in section 2, in order to extract the relative dominant particle mode in the aerosol size distribution, we have calculated α' (see Figure 2e). It is noted from Figure 2 that during this period (May–October), α' shows a lower value (from −0.25 to 0.41) with the exception of the Western Cape and Eastern Cape provinces. The above observed values of α and α' indicate that the South African atmosphere is dominantly loaded by a mixture of accumulation-mode and fine-mode particles. However, the obtained results indicate that the accumulation-mode particles in the aerosol size distribution prevail slightly (as α' indicates slightly more positive than negative). The observed higher values of $\alpha_{(672–866)\ nm}$ (from 1.25 to 1.73), especially in most areas of the Northern Cape, Free State, and Natal provinces, indicate the presence of submicron particles, which are mainly due to biomass burning and urban/industrial activities. During the summer to autumn period (November–April), the Angstrom exponent varies from 0.56 to 1.64 and from 0.41 to 1.51 in the VIS and NIR bands, respectively. In addition, over most regions of SA, the α' value varies from 0.24 to 1.06 (see Figure 2e). The above values indicate that during this period, the South African atmosphere is dominantly loaded with a mixture of accumulation-mode and coarse-mode aerosols. However, during November to January, the α value for most regions of SA varies from 0.41 to 1.20 and α' varies from 0.42 to 1.06. This indicates that the coarse-mode particles are higher than the accumulation-mode particles in the aerosol size distribution. All the above results on seasonal variation of $\tau_{ext(558\ nm)}$, $\tau_{a(558\ nm)}$, $\alpha_{(446–672)\ nm}$, $\alpha_{(672–866)\ nm}$ and α' are found to be in good agreement with earlier published reports, though their results are focused on a particular region/part of SA, based on in situ, satellite, ground based, and air mass trajectory observations [*Piketh et al.*, 1999; *Formenti et al.*, 2002, 2003; *Eck et al.*, 2003; *Freiman and Piketh*, 2003; *Ross et al.*, 2003; *Liu*, 2005; *Magi et al.*, 2009; *Queface et al.*, 2011]. Details on

© University of Pretoria

UNIVERSITEIT VAN PRETORIA
UNIVERSITY OF PRETORIA
YUNIBESITHI YA PRETORIA

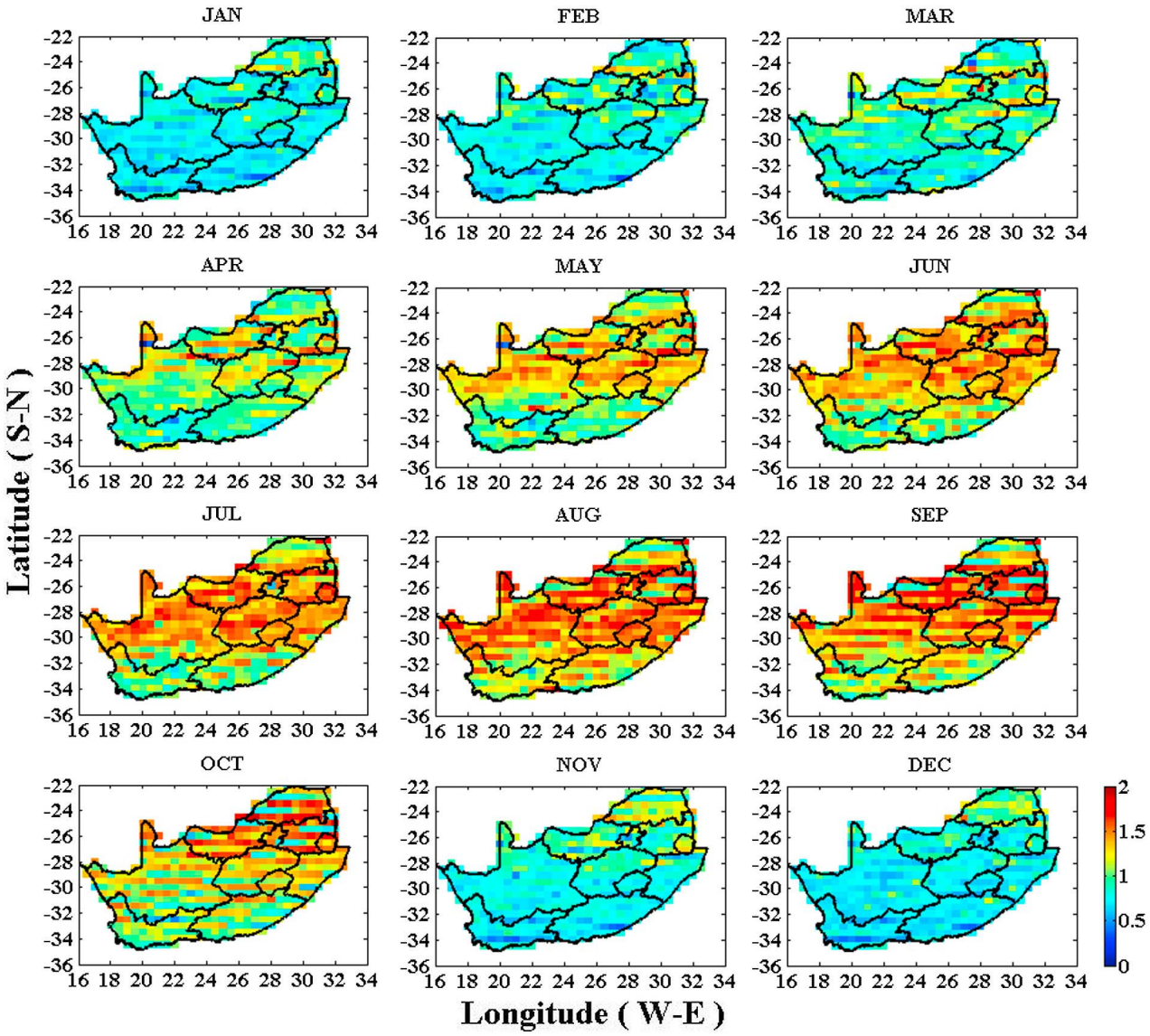

Figure 2d. Same as Figure 2a but for Angstrom exponent over NIR region.

the spatial and seasonal variability of aerosol size distribution correlated with local meteorological parameters are discussed in section 3.2.

[15] The above results confirm that different regions in SA have different aerosol loading levels and significant seasonal variations of aerosol radiative properties and their size distribution. Therefore, based on the above information, we have spatially classified SA into three broad regions: (1) lower part (35°S to 31°S; 17.5°E to 30.5°E), includes the Western Cape, Eastern Cape, and lower parts of the Northern Cape (Figure 1, box A); (2) central part (31°S to 27°S, 16.5°E to 33°E), includes the middle and upper part of the Northern Cape, Free State, and Natal provinces (Figure 1, box B); and (3) upper part (27°S to 22°S, 19.5°E to 32°E), includes North West, Gauteng, Mpumalanga, and Limpopo provinces (Figure 1, box C). This spatial classification interrelated with other local meteorological parameters allows us to handle large data sets efficiently for understanding the aerosol climatology over SA. The aerosol climatological results presented in this paper follow the above spatial classification.

3.2. The Seasonal Aerosol Climatology Over Different Parts of South Africa

[16] For each part of SA (lower, central, and upper), the monthly variations of AOD versus wind speed and α, α' versus RH, are given in Figures 4, 5, and 6. Figures 4, 5, and 6 are plotted from January to December, to represent the results in terms of different seasons: summer (November–February), early winter (March–April), winter (May–July) and early summer (August–October). The obtained results are described in detail in sections 3.2.1–3.2.3.

3.2.1. Lower Part of South Africa

[17] The lower part of SA is surrounded by the Atlantic and Indian oceans. The ocean regions are one of the major sources of natural marine aerosols. Marine aerosols are composed of (1) primary aerosols, which are generated at the sea surface

© University of Pretoria

UNIVERSITEIT VAN PRETORIA
UNIVERSITY OF PRETORIA
YUNIBESITHI YA PRETORIA

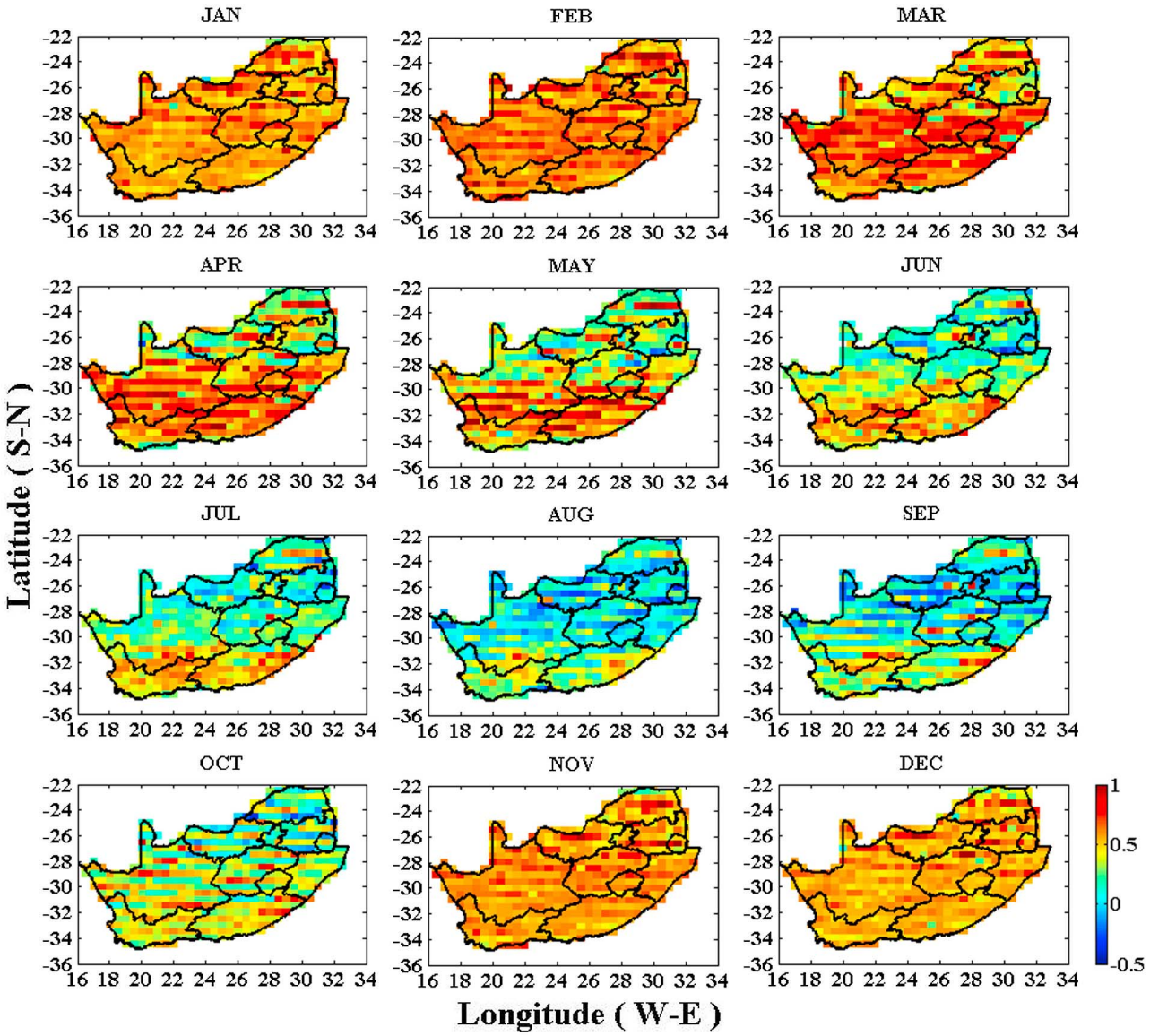

Figure 2e. Same as Figure 2a but for Angstrom exponent spectral curvature.

through wind driven processes, and (2) secondary aerosols, through gas-to-particle conversion processes [*O'Dowd and de Leeuw*, 2007]. Marine aerosols contribute to both fine-mode and coarse-mode particles, with dominant fractions of inorganic sea-salt and organic particles in the supermicron and submicron modes, respectively [*Latham and Smith*, 1990; *Kaufman et al.*, 2002; *Cavalli et al.*, 2004].

[18] Figure 4a shows the monthly mean variation of AOD and wind speed (surface) for the lower part of the SA. It is clear from Figure 4a that the AOD and wind speed follow a similar pattern of annual oscillation (AO) with a minimum during June. The maximum AOD is recorded during September and is almost twice the minimum. High wind speed is observed during December (a summer month with high rainfall; see Figure 3). We have also plotted α in the VIS and NIR, and α' and RH (see Figure 4b) for the same period, as presented in Figure 4a. The α values in both the spectral bands show a similar trend, with higher values in the VIS than the NIR band (as expected). The order of separation (α) between the VIS and NIR bands is ~0.2 and is lower during August and September (~0.1). Both the spectral bands show a minimum and maximum value recorded for December and August. The observed RH is related to the seasonal variations of α, with a maximum during winter (including August) and a minimum during summer. A more detailed discussion on the seasonal variations of AOD, α and their interrelations follows.

[19] It is evident from Figures 4a and 4b that the AOD declines together with the southeasterly wind speed during summer (November–February) and α values for VIS and NIR spectral bands vary from 0.72 to 1.06 and from 0.55 to 0.83 respectively. At the same time, the α' ranges from 0.42 to 0.92 (see Figure 4b), indicating that, during this season in the lower part of SA, the aerosol size distribution in both spectral bands are dominated by coarse-mode aerosols rather than accumulation-mode aerosols. In general, summer in the

© University of Pretoria

UNIVERSITEIT VAN PRETORIA
UNIVERSITY OF PRETORIA
YUNIBESITHI YA PRETORIA

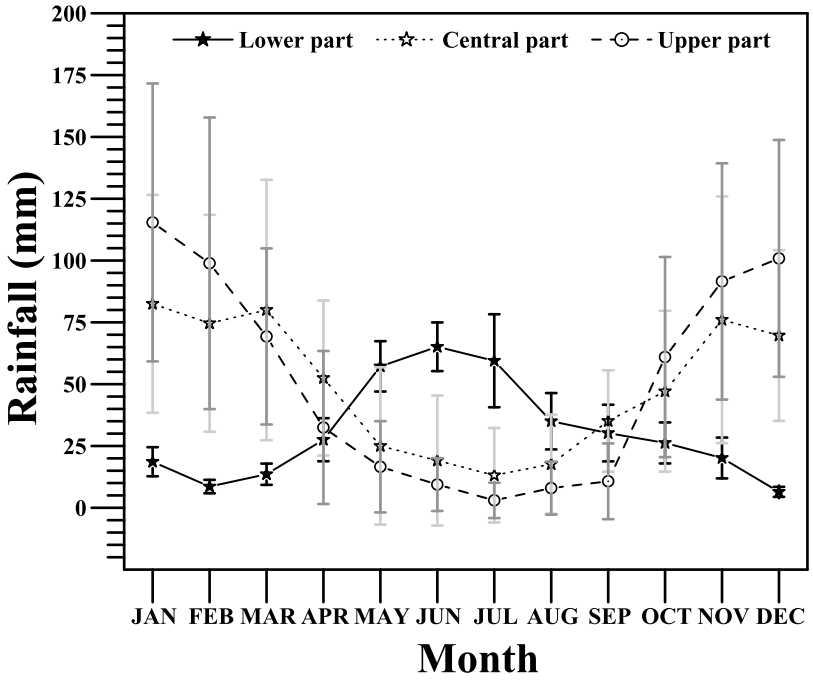

Figure 3. Monthly mean rain fall and standard deviation obtained from 10 years of data for different parts of South Africa. Lower part: Cape Town 33.9°S, 18.6°E and East London 33.0°S, 27.8°E. Central part: Durban South 29.9°S, 30.9°E, Bloemfontein 29.1°S, 26.3°E, and Upington 28.4°S 21.3°E. Upper part: Johannesburg 26.2°S, 28.2°E, Ermelo 26.5°, 29.9°E, Mafikeng 25.8°S, 25.5°E, and Polokwane 23.9°S; 29.5°E.

lower part of SA has less rain (see Figure 3), low RH, and strong southeasterly winds which bring cool air from the sea. During this period, the significant contribution of coarse-mode aerosols over this area might be explained as follows. The ground of the lower part of SA is not particularly dusty and, hence, there is only limited local aerosol generation due to wind ablation of mineral dust particles. On the other hand, a change in AOD due to a change in wind-induced, marine, coarse-mode aerosols' size distribution is well established by various researchers [e.g., *Hoppel et al.*, 1990; *O'Dowd and Smith*, 1993; *Gong et al.*, 1997; *O'Dowd et al.*, 1997; *O'Dowd and de Leeuw*, 2007; *Lehahn et al.*, 2010]. *Lehahn et al.* [2010] reported that, on average, the threshold value of surface wind speed for triggering emission of maritime aerosols is 4.1 ± 0.1 m/s. When wind speed exceeds the threshold value, the coarse-mode marine aerosols' optical depth is linearly correlated to the surface wind speed, with a consistent slope of 0.009 ± 0.002 m/s [*Lehahn et al.*, 2010]. Thus, knowledge of wind speed and direction assists in estimating the average background wind-induced marine aerosol loading in the lower part of SA. The above statements are in agreement with our observations of the increase in southeasterly wind speed (>5.5 ± 0.6 m/s) and α values in both VIS and NIR (see Figures 4a and 4b), thereby confirming that the lower part of the SA is loaded by wind-induced supermicron (marine) aerosols. It is also confirmed by earlier research done over the west coast of SA (30.5°S; 18°E) by *Piketh et al.* [1999] who mentioned that, during summer, marine aerosols contribute ~51% of total aerosol loading. Furthermore, this result along with the Mie scattering theory supports the observation of bright sunrises and sunsets during the above time period in the region.

[20] During the early winter period, the AOD further declines (12%) in comparison with summer AOD. This may be due to the decline of wave-generated supermicron maritime aerosols (wind speed <4.2 ± 0.5 m/s). Further, during this period, the α' varies from 0.24 to 0.62 and the Angstrom exponent values vary from 0.86 to 1.26 and from 0.65 to 1.07 in the VIS and NIR bands, respectively (see Figure 4b). The above values confirm that the coarse-mode aerosol contribution is diminishing with respect to accumulation-mode aerosols. This is mainly attributed to the decline in wind-induced, marine, coarse-mode aerosols and an increase in RH, which favors the growth of fine-mode particles into accumulation-mode particles through intercoagulation and humidification processes. The humidification growth of fine-mode particles may further indicate that a fraction of the wave-generated submicron organic marine aerosols (especially secondary aerosols, which are the outcome of gas-to-particle conversion processes) have a polar functional group in their nature [*Hanel*, 1976; *Horvath*, 1996; *Cavalli et al.*, 2004].

[21] The mean AOD and Angstrom exponent values in the VIS and NIR bands for winter (May–July) varies from 0.082 to 0.096, 1.07 to 1.42, and 0.91 to 1.27, respectively (see Figures 4a and 4b). These values, together with the α' (see Figure 4b), indicate that the lower part of SA is dominated by a mixture of accumulation-mode and coarse-mode aerosols during winter. Relatively, the accumulation mode is dominant in the aerosol size distribution. This part of SA, having a Mediterranean climate, gets most of its rain during winter (May–July; see Figure 3). Compared to summer and early winter, the winter AOD and wind speed are further decreased by ~27% and ~35%, respectively (see Figure 4a). The decline

© University of Pretoria

UNIVERSITEIT VAN PRETORIA
UNIVERSITY OF PRETORIA
YUNIBESITHI YA PRETORIA

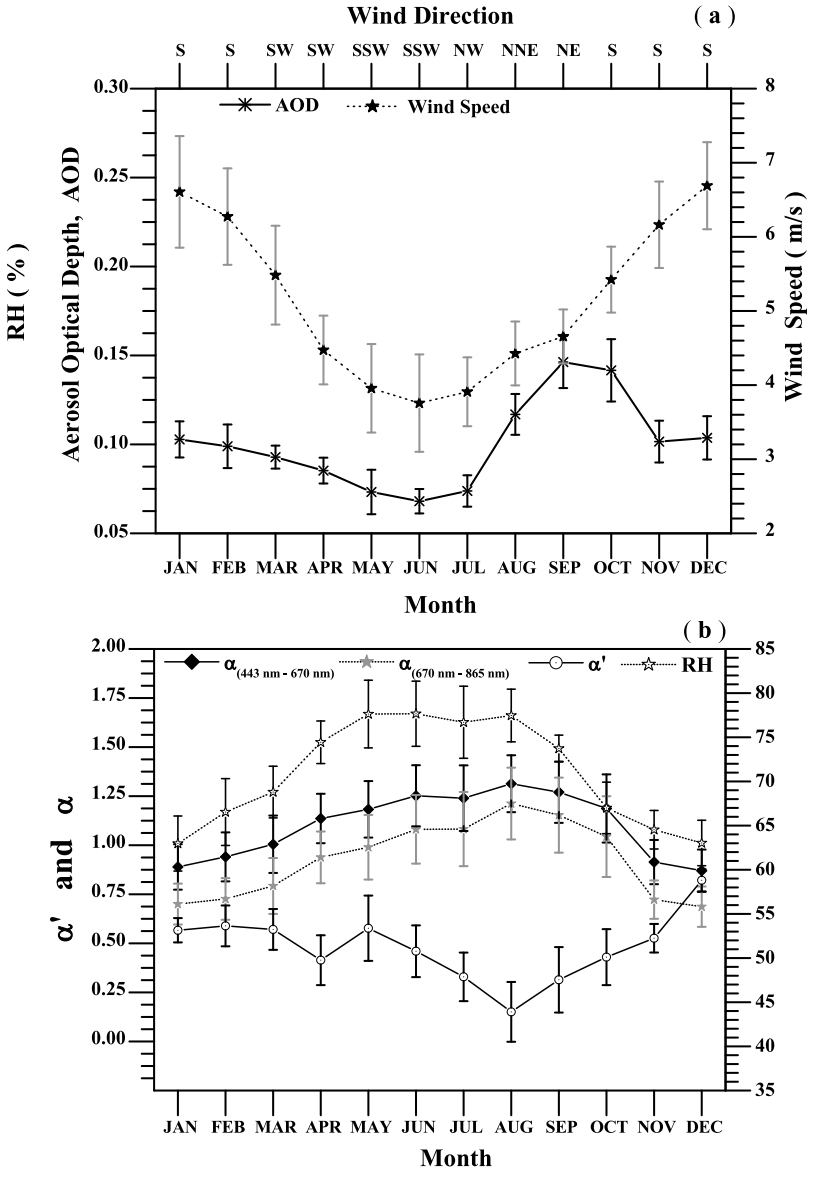

Figure 4. Monthly mean variation (a) of averaged aerosol optical depth (AOD), wind speed, and wind direction (S, southerly; SW, southwesterly; SSW, south-southwesterly; NW, northwesterly; NNE, north-northeasterly; NE, northeasterly) and (b) of Angstrom exponent in both visible and NIR regions, its spectral curvature, and relative humidity (RH) for Lower part, South Africa.

of AOD may be due to the removal of aerosols by various wet deposition processes and less wind-induced marine aerosol load. The dominance of accumulation-mode aerosols during winter can be explained by the fact that during the previous season (summer and early winter period), the atmosphere of this area is more loaded by medium and high wave-generated marine (supermicron and submicron modes) aerosols. Wave-generated inorganic fresh sea-salt spray and polar functional groups of organic particles are hygroscopic in nature. The aging process in marine aerosols results in more hygroscopic aerosols. For instance, when sulfur dioxide (SO_2) condenses into the sea-salt aerosol surface, the aerosols transform into sulfate [*Sievering et al.*, 1991; *Quinn et al.*, 2000]. Moreover, due to the more soluble mass presence, marine aerosols act as highly suitable cloud condensation nuclei [*Katoshevski et al.*, 1999; *Ross et al.*, 2003; *Matteo et al.*, 2010]. Thus, this is consistent with our results that, in a situation where the wind speed has been low for an extended period of time, the pool of hygroscopic particles are efficiently removed from the atmosphere by cloud processing and precipitation. In addition to this process, the high RH causes the enlargement of hygroscopic supermicron marine particles. Since the viscous drag is proportional to the particle surface, and the gravitational force scales with the volume, sedimentation also becomes an important removal process during this period.

[22] Early summer months (August–October) indicate that the AOD increases by ~34% in comparison to the rest of the season. During this period, the Angstrom exponent values in the VIS and NIR bands vary from 1.17 to 1.46 and from 1.03 to 1.40, respectively (see Figure 4). In addition, the observed values of α synchronized with α' values (Figure 4b) demonstrate that the optical influence of submicron particles are

© University of Pretoria

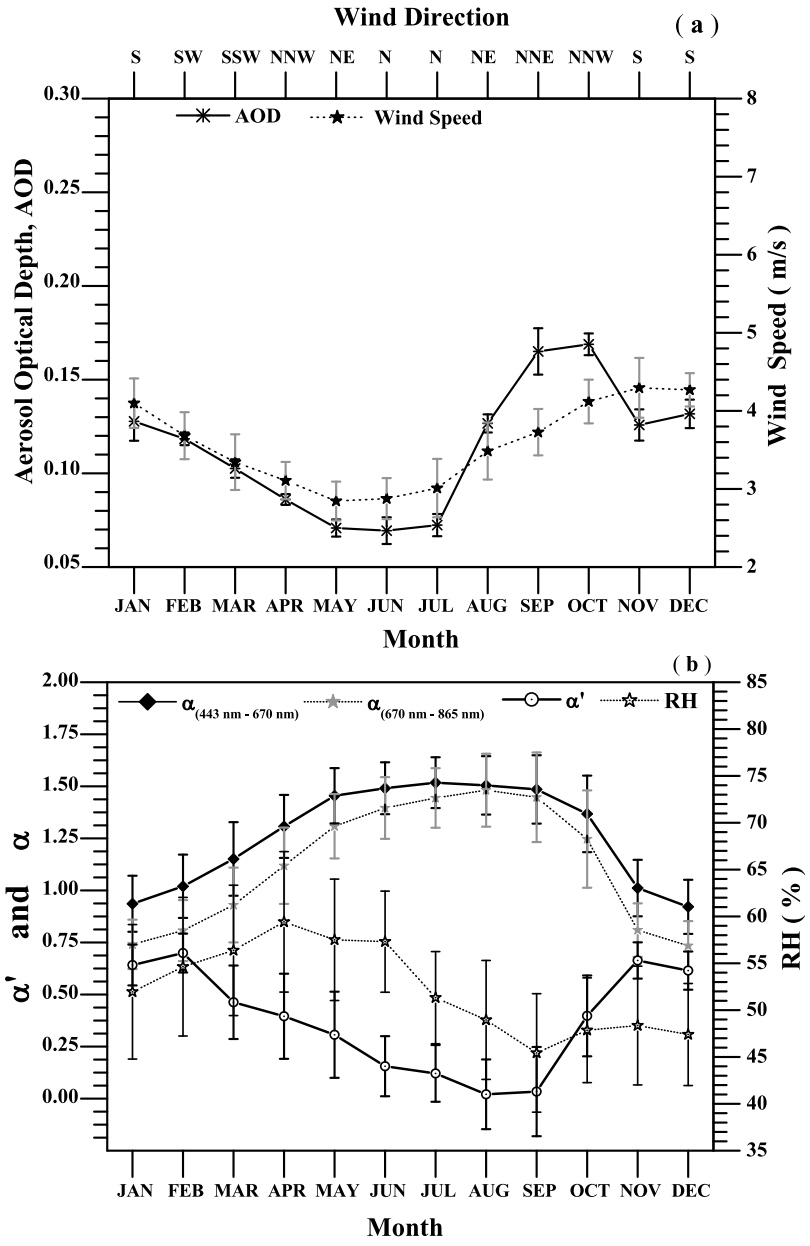

Figure 5. Same as Figure 4 but for central part, South Africa.

stronger than supermicron particles. The dominance of submicron particles can be inferred from the presence of biomass burning and urban aerosols. This is revealed by a significant increase in aerosol absorption optical depth (by about ~71% in comparison to the rest of the seasons; see Figure 2b) and increase in α_{NIR}. In addition, during this period we noticed the movement of wind from the intensive biomass-burning areas (i.e., northeastern and central parts of SA and Botswana [*Magi et al.*, 2009]) to the lower part of SA. The above results are found to be in a good agreement with earlier studies based on air mass trajectory analysis [*Garstang et al.*, 1996; *Tyson et al.*, 1996; *Tyson and D'Abreton*, 1998; *Freiman and Piketh*, 2003] and onsite measurements at particular sites of SA [*Piketh et al.*, 1999; *Formenti et al.*, 2002; *Piketh et al.*, 2002; *Winkler et al.*, 2008]. However, during the transportation processes, various coagulation and condensation processes cause both chemical and physical changes in the submicron particles.

3.2.2. Central Part of South Africa

[23] The monthly mean variation of AOD, wind speed, α, α' and RH are given in Figures 5a and 5b (similar to Figures 4a and 4b) for the central part of the SA. The AOD depicts AO similar to that in the lower part of SA, except that the maximum is observed with a month shift (October). The observed AOD values (during summer and early summer period) are found to increase (~10%–20%) while the wind speed decreases (~29%, throughout the year) in comparison to the lower part of the SA. In relation to the low wind speed, the variation (standard deviation) in AOD is also lower than that of the lower part of the SA (see Figure 5a). During August and March, the difference between observed α values (α_{vis} and α_{NIR}) shows 0.02 (minimum) and 0.22 (maximum),

© University of Pretoria

UNIVERSITEIT VAN PRETORIA
UNIVERSITY OF PRETORIA
YUNIBESITHI YA PRETORIA

respectively. This part of the country seems to be drier (low humidity) which is revealed by the observed monthly variation of RH (see Figure 5b). It is evident from Figure 5b that low RH is recorded for early summer and high RH recorded during early winter. More detailed results are discussed in terms of seasonal variations in the following paragraphs.

[24] Figure 5 shows an increase in AOD and α (both VIS and NIR) values while α', wind speed, and RH are lower in comparison to the lower parts of SA during summer. The variations of observed AOD, α_{vis}, α_{NIR} and α' from 0.12 to 0.13, 0.79 to 1.07, 0.61 to 0.93, and 0.41 to 0.77 respectively, indicate that during summer, the central part of SA is relatively dominated by coarse-mode aerosols. The significant contribution of the coarse-mode particles is probably caused by the transport of air mass by strong southerly (S) and southwesterly (SW) winds from the dry and dusty desert regions of the Northern Cape, Namibia, and Free State (an intensive agricultural places). Moreover, various growth and removal processes of submicron particles, such as scavenging by precipitation, contribute to the relative dominance of coarse-mode particles. The above finding is in relation to the high rainfall during this period (see Figure 3), which favors the growth and removal of submicron aerosols through various wet deposition processes [*Ross et al.*, 2003]. However, the observed AOD, which is higher than in the early winter and winter months, indicates the presence of insoluble particles (inorganic and/or organic mineral) which are continuously being loaded and/or transported by the strong S and SW winds. The sources of such particles are the different urban/industrial activities and aerosols transported from the arid/semiarid regions of Northern Cape together with local agricultural activities over Free State. Earlier studies by *Piketh et al.* [1999, 2002], using size-fractionated aerosol chemical analysis at Ben Macdhui Mountain (~30°S, 28°E) also revealed that the presence of higher concentration of coarse-mode, soil dust particles and agglomerated nitrate and sulfate aerosol on the surface of dust nuclei during summer.

[25] During early winter (March–April), in comparison to summer, the AOD is decreased by 25%, wind speed by 21%, and α' by 30%, with an increase in values of α_{vis} (1.23 ± 0.05) and α_{NIR} (1.02 ± 0.07). These α and α' values indicate, in both spectral bands, a relative declination of coarse-mode particles in comparison to the accumulation mode in the aerosol size distribution. Such decreases in coarse-mode particles (also AOD) are caused by weak aerosol generation and dispersion, due to the end of rainy season followed by lower wind speed conditions. During this period, the variation in RH and α values (see Figure 5b) delineate the presence of hygroscopic fine particles which are most likely sulfate and nitrate containing aerosols. The high RH values (i.e., higher moisture) and low wind speed during this period facilitates the humidification growth and different agglomeration processes of fine particles which promotes the dominance of accumulation-mode particles and favors their longer existence. Congruent with the above statement, previous studies have stated that more than 75% of the plume originate from the industrial regions (Gauteng and Mpumalanga), circulates in the central part for several days, prior to exiting SA [*Garstang et al.*, 1996; *Tyson et al.*, 1996; *Tyson and D'Abreton*, 1998; *Freiman and Piketh*, 2003]. Other studies have also observed that this plume consists mainly of submicron particles, such as industrial dust, sulfates, and nitrates [*Formenti et al.*, 1999; *Piketh et al.*, 1999, 2002; *Zunckel et al.*, 2000].

[26] It is noted from Figure 5a that the AOD shows the lowest values during winter (May–July) while it is highest during early summer (August–October), in comparison to summer and early winter. On the other hand, α and α' show almost similar variations (within ±2%) between winter and early summer (except October α' values range from 0.27 to 0.59). The low AOD during winter is in relation to the observed low and stable wind speed which decreases the number of particles generation and dispersion from local and surrounding arid/semiarid regions. It is evident from the observed α_{vis} (1.32–1.65), α_{NIR} (1.23–1.66) and α' (negative and near-zero values) during winter and early summer, that this region of SA is dominated by submicron particles. Specifically during August to September, a significant increase in $\tau_{a(558\ nm)}$ (by ~75%) is noticed in comparison to the rest of the months (see Figure 2b), as well, higher values of α_{NIR} (>1.4) are observed. This indicates that during these months, the area is more loaded by submicron particles originating from biomass burning and various anthropogenic activities. The observed high values of $\tau_{a(558\ nm)}$ and α_{NIR} are in accordance with *Formenti et al.* [2003], who noted that the contribution of submicron carbonaceous aerosol is ~80% relative to the total submicron aerosol during this period. *Magi et al.* [2009] reported that most of SA's biomass-burning activities occur in the eastern-central and north-eastern regions. These regions are dominated by sugarcane farming and refineries, where the sugarcane is burnt for preindustrial processing during August to September. In addition, the transport of particles from biomass-burning activities over Botswana and the northern industrial areas of SA also contribute to the load of submicron particles [*Tyson and D'Abreton*, 1998; *Eck et al.*, 1999, 2001, 2003; *Piketh et al.*, 1999, 2002; *Reid et al.*, 1999; *Freiman and Piketh*, 2003]. Furthermore, the presence of submicron particles during winter and early summer is favored by the dry and windy atmosphere in this region. The above findings are concurrent with the observed high AOD during early summer. However, relative to the rest of winter and early summer months, during October the declination in α_{vis} (by ~10%), and α_{NIR} (by ~13%) along with the increment in α' values were observed. This indicates the dominance of submicron particles in the aerosols size distribution being diminished. This may be due to the reduction of biomass-burning aerosols load, which is revealed by the declination of $\tau_{a(558\ nm)}$ (by ~42% in comparison to August and September; see Figure 2b) and the aging processes in submicron particles [*Formenti et al.*, 2003; *Ross et al.*, 2003]. During the Southern African Regional Science Initiative (SAFARI 2000) experiment, *Formenti et al.* [2003] stated that the range of the aging process in biomass-burning-induced submicron particles causes the depletion of their number concentration by ~41% within a few days, with respect to the young smoke.

3.2.3. Upper Part of South Africa

[27] This part of SA is considered to be highly populated, industrialized, and agricultural. As a result, there is a strong desire to study aerosol characteristics in this region. We have plotted the monthly variation of AOD, wind speed, α, α', and RH (Figures 6a and 6b). This part of SA also illustrates AO with the maximum AOD during October and the minimum during May (see Figure 6a), which is similar to the rest of SA.

© University of Pretoria

UNIVERSITEIT VAN PRETORIA
UNIVERSITY OF PRETORIA
YUNIBESITHI YA PRETORIA

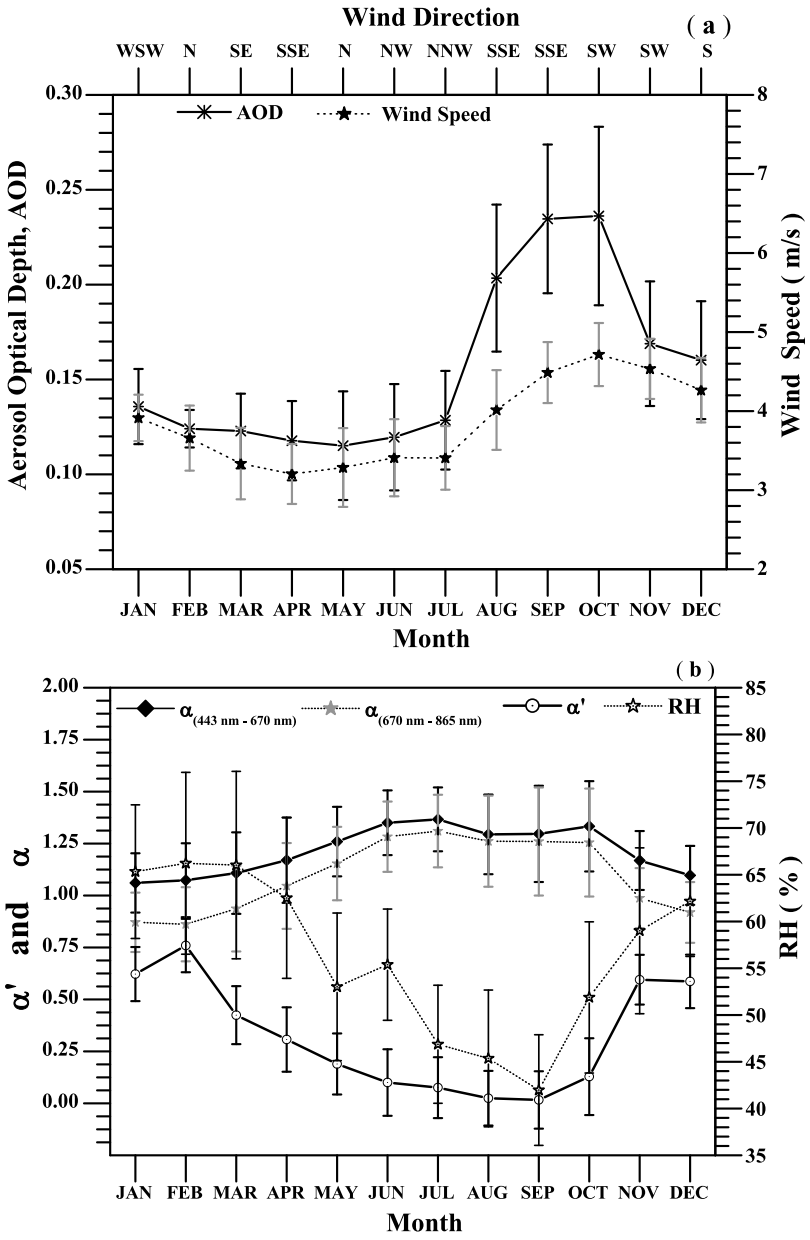

Figure 6. Same as Figure 4 but for upper part, South Africa.

The observed AOD is found to be the highest when compared to the lower (~34%) and central (~27%) parts of SA. More specifically, the value for this region is ~40% higher than that in the lower part of SA during winter and early summer, while it exceeds the central part of SA by ~37% during those periods. In comparison to the central part of SA, the observed wind speed is similar (within the standard deviation) during summer and early winter period, but the upper parts of SA differ by an increase in wind speed of ~14% during winter and early summer periods. However, the observed wind speed was found to be lower than that in the lower parts of SA, with a maximum difference during summer and early winter. Figure 6b shows that throughout the year, α values in both spectral bands are higher than the lower parts of SA while the values are relatively higher than those of the central part of SA during summer, and between the values of the lower and central parts of SA for the remaining seasons. The recorded RH indicates that the upper part of SA is driest with respect to rest of the SA, during winter and early summer. But, during the reciprocal season, the values are higher than those in the central parts of SA.

[28] During summer, AOD values vary from 0.11 to 0.20, α_{vis}, from 0.89 to 1.23, α_{NIR}, from 0.73 to 1.04 and α', from 0.21 to 1.06. This indicates the overall dominance of coarse-mode particles in the aerosol size distribution. Wind direction analysis was more complex due to easterly, westerly, north-easterly, and southerly components. The increase in AOD along with wind speed (see Figure 6a) implies that the dominance of coarse-mode aerosols is due to wind-ablated mineral particles, which are the result of local agricultural activities and the air mass transport from or through central parts of SA, Botswana, and Mozambique (arid and semiarid

© University of Pretoria

UNIVERSITEIT VAN PRETORIA
UNIVERSITY OF PRETORIA
YUNIBESITHI YA PRETORIA

regions) [*Tyson et al.*, 1996; *Freiman and Piketh*, 2003]. The observed RH and α (see Figure 6b, indirectly proportional variation) values indicate that hygroscopic growth of accumulation-mode and/or fine-mode aerosols also contribute to the dominance of coarse-mode particles. *Piketh et al.* [1999, 2002] also reported that such particles are dominantly originated and sprayed over remote regions of the subcontinent from the industrialized Highveld region (25.2°S to 27.2°S, 27.2°E to 29.2°E) of SA, which is located in our upper part. Further, continued energy dispersive analysis indicated that in moist atmosphere those fine particles will rapidly agglomerate on the surface of other particulate and increase their size [*Piketh et al.*, 1999]. In relation to the above findings (the hygroscopic nature of submicron particles); the noticed high rainfall during this period (see Figure 3) causes the degradation of submicron aerosols through various wet deposition processes.

[29] In comparison with summer, during early winter, a decrease in AOD values (~18%), α' (~25%), wind speed (~20%), and increases in values for α_{vis} (1.17 ± 0.21) and α_{NIR} (1.05 ± 0.21) are noted. The decrease in AOD is due to the observed low wind speed which causes less aerosol generation and dispersion. Also, the increase in α and decrease in α' values imply an overall dominance of accumulation-mode aerosols. It is due to the decrease in wind-induced, coarse-mode particles and the depletion of various wet deposition processes (due to the end of the rainy season; see Figure 3) [*Ross et al.*, 2003].

[30] Figure 6a shows the lowest AOD (~0.12) values during winter (May–July), when the upper part of SA is characterized by the lowest precipitation, and is driest and with lower wind conditions, relative to the central and lower parts of SA. Thus, the lowest AOD values are attributed to the extended period of lower, stable wind speed patterns which cause weak generation and dispersion of particles. Excluding the Polokwane area (24.3°S to 23.2°S, 28.5°E to 29.6°E), the α values computed for VIS and NIR spectral bands during these months vary from 1.19 to 1.53 and from 1.10 to 1.48, respectively (see Figure 6b). Further, the observed negative and near-zero values of α' (from −0.16 to 0.28; see Figure 6b) in concert with the above α values, indicate that the area is dominated by a mixture of nucleation and accumulation-mode particles during this period. This reveals that the dry and low wind speed conditions are the most advantageous for the long time existence of submicron particles. In addition, in situations where the aerosol absorption optical depth shows very low values ($\tau_{a(558\ nm)} < 0.004$), the dominance of submicron particles over most areas of the upper part of SA indicates that it is induced by large industrial and urban activities, which are highly abundant in this region.

[31] During the early summer period (August–October), the highest values of AOD (0.23 ± 0.05), wind speed (4.45 ± 0.43 m/s) and a significant increase in $\tau_{a(558\ nm)}$ (~63%) are observed, in comparison to the rest of the seasons (see Figures 2b and 6a). In addition, during this period, excluding the Polokwane area, the α_{vis} varies from 1.18 to 1.62, α_{NIR} from 1.17 to 1.55, and α' from −0.26 to 0.24, indicating the increase in the submicron particle load (in comparison to winter). These values of α, α' and $\tau_{a(558\ nm)}$ associated with the observed wind speed and directions, illustrate that the elevated loads of submicron particles might be induced by local and/or transported biomass-burning aerosols (from the northeastern and central parts of SA and neighboring countries [*Magi et al.*, 2009]) together with the contributions from the abundant industrial/urban activities within this area [*Tyson and D'Abreton*, 1998; *Eck et al.*, 1999, 2001, 2003; *Reid et al.*, 1999; *Campbell et al.*, 2003; *Formenti et al.*, 2003; *Ross et al.*, 2003; *Queface et al.*, 2011]. In general, from winter to early summer (dry seasons), the α and α' values show a dominant effect of fine-mode particles around Gauteng and Mpumalanga. These areas are highly populated and industrialized, which confirms the contribution and effect of anthropogenic activities in air pollution. However, during these dry seasons, around Polokwane (specifically, 24.3°S to 23.2°S, 28.5°E to 29.6°E), the values of α_{vis} from 0.86 to 1.10, α_{NIR} from 0.77 to 1.00, and α' from 0.31 to 0.76, are noted. The noted α and α' values indicate that there is a significant coarse-mode aerosol contribution in the aerosol size distribution around this part of SA. This is related to the intensive local agricultural activities and land cover changes around the area, including the influence of strong wind-ablated particles that originated from arid/semiarid regions of the central parts of SA, Namibia, and Botswana (evident from the observed wind speed and directions). In addition, during this period, the windy and drier meteorological conditions favor the load and dispersion of wind-ablated mineral particles and inhibit the hygroscopic growth of submicron aerosols, respectively. In addition to the above major sources, a further source of supermicron particles in Limpopo, might be due to an aged, polluted plume which is transported from intensive biomass-burning activities in the tropical region of southern Africa [*Magi et al.*, 2009] and from mining industries of Zambian copper belt [*Freiman and Piketh*, 2003; *Zunckel et al.*, 2000]. Generally, throughout the year, the exaggerated differences in AOD values (in comparison with the central (~27%) and the lower (~35%); see Figure 2a) are noted in the upper part of SA. As well as, excluding the extended biomass burning seasons in southern Africa (June–October), the absorbing aerosol load in this area is higher than the rest of SA (in terms of $\tau_{a(558\ nm)}$ by ~31%; see Figure 2b). These clearly indicate the existence of various local sources within this part of the country.

4. Summary and Concluding Remarks

[32] Here, for the first time, a thorough study of the spatial and seasonal aerosol climatological characteristics over SA, based on 10 years of MISR data is presented. The aerosol climatological characteristics were based on aerosol extinction (τ_{ext}), absorption (τ_a) optical depths at 558 nm, and an extracted Angstrom exponent (α) in two different bands (VIS and NIR) and its spectral curvature (α'). The aerosol spatial variation was studied by classifying SA into lower, central, and upper parts. The seasonal or climatological variations are described in terms of four seasons: summer (November–February), early winter (March–April), winter (May–July), and early summer (August–October). Background weather parameters, such as RH, rainfall, and wind speed are used to interpret the aerosol climatological characteristics. The major findings from this study are as follows:

[33] 1. In general, the overall aerosol extinction optical depth values at 558 nm illustrate annual trends with a maximum during early summer and minimum during winter. The observed maximum during spring corresponds with

© University of Pretoria

UNIVERSITEIT VAN PRETORIA
UNIVERSITY OF PRETORIA
YUNIBESITHI YA PRETORIA

biomass-burning activities in southern Africa. The lower, central, and upper parts of SA demonstrated lower, medium, and higher aerosol load levels, respectively. On the basis of the Angstrom exponent (α) and its spectral curvature (α'), the aerosol size (fine, accumulation/mixture, and coarse modes) distributions are found to be significantly different due to various prevailing source mechanisms.

[34] 2. The lower part of SA is dominated by coarse-mode aerosols during summer. Thereafter, the coarse-mode aerosols load recedes. There is an increase in aerosol load (~35%) during early summer in comparison with the remaining seasons. The size distribution is found to be dominated by submicron particles due to massive biomass burning and industrial/urban aerosols load (also evident from the aerosol absorption optical depth). In this part of SA, local anthropogenic aerosol sources are limited. However, the aerosol load might be due to air mass transfer from the surrounding marine environment (during summer) and polluted air mass transport from other regions of SA or from neighboring countries (for the remaining seasons) is the prevailing source of aerosols in this part of SA.

[35] 3. The central part of SA had a 10%–20% increase in aerosol load in comparison with the lower part. During summer, the area shows a dominance of coarse-mode particles in the aerosol size distribution in comparison with the other seasons. These are typically induced by the dry and dusty desert regions of Northern Cape and Namibia. Specifically, during spring a decrease in coarse-mode particles is evident due to the presence of submicron particles which are generated by the load of biomass burning aerosols (also evident from aerosol absorption optical depth) and various anthropogenic activities in and around the area.

[36] 4. The upper part of SA is found to be rich in aerosol reservoirs and the aerosol loading (based on AOD) is ~34% higher than that in the lower part and ~27% higher than that in the central part of SA. During different seasons, the aerosol size distribution is dominated by various particle modes. During summer and early winter, the area is dominated by a mixture of coarse-mode and accumulation-mode particles. During winter and early summer, it is dominated by submicron particles. Overall, this part of SA shows a high variability with respect to α, indicating numerous aerosol sources in the region. The source and generating mechanisms are found to differ with the observed aerosol mode. In general, the prevailing sources of coarse particles around the area are local agricultural activities and air mass transport from arid/semiarid regions of the central parts of SA, Botswana, and Namibia; together with various aging processes of submicron aerosols. The prevailing sources of submicron particles are industrial and urban activities (including mines and biomass burning).

[37] 5. It is found that SA experiences drastic turbidity due to high levels of biomass-burning aerosol loadings during August to October, relative to other months.

[38] 6. On the basis of simultaneous observations of monthly average aerosol optical and local meteorological parameter variations, we have noted that the rainy season, followed by a period of lower wind conditions, is the most unfavorable for aerosol generation and dispersion. In contrast, dry and high wind conditions are the most favorable for submicron aerosol loading, dispersion, and long-term existence.

[39] **Acknowledgments.** The authors are thankful to NASA Langley Atmospheric Science Data Center for providing the MISR satellite data. We are also thankful to the South Africa Weather Service for providing meteorological data. We also thank for all the anonymous reviewers for constructive comments which has improved the quality of the manuscript. The author M. Tesfaye is financially supported by the African Laser Centre, South Africa. Authors thank Ameeth Sharma for proof reading and language correction in the manuscript.

References

Abdou, W. A., et al. (2005), Comparison of coincident Multiangle Imaging Spectroradiometer and Moderate Resolution Imaging Spectroradiometer aerosol optical depths over land and ocean scenes containing Aerosol Robotic Network sites, *J. Geophys. Res.*, *110*, D10S07, doi:10.1029/2004JD004693.

Adeyewa, Z. D., and E. E. Balogun (2003), Wavelength dependence of aerosol optical depth and the fit of the Angstrom law, *Theor. Appl. Climatol.*, *74*, 105–122, doi:10.1007/s00704-002-0707-3.

Angstrom, A. K. (1929), On the atmospheric transmission of Sun radiation and on dust in the air, *Geogr. Ann.*, *12*, 130–159.

Basart, S., C. Perez, E. Cuevas, J. M. Baldasano, and G. P. Gobbi (2009), Aerosol characterization in Northern Africa, Northeastern Atlantic, Mediterranean Basin and Middle East from direct-Sun AERONET observations, *Atmos. Chem. Phys.*, *9*, 8265–8282, doi:10.5194/acp-9-8265-2009.

Cachorro, V. E., R. Vergaz, and A. M. de Frutos (2001), A quantitative comparison of α-Å turbidity parameter retrieved in different spectral ranges based on spectroradiometer solar radiation measurements, *Atmos. Environ.*, *35*, 5117–5124, doi:10.1016/S1352-2310(01)00321-1.

Campbell, J. R., E. J. Welton, J. D. Spinhirne, Q. Ji, S.-C. Tsay, S. J. Piketh, M. Barenbrug, and B. N. Holben (2003), Micropulse lidar observations of tropospheric aerosols over northeastern South Africa during the ARREX and SAFARI 2000 dry season experiments, *J. Geophys. Res.*, *108*(D13), 8497, doi:10.1029/2002JD002563.

Cavalli, F., et al. (2004), Advances in characterization of size-resolved organic matter in marine aerosol over the North Atlantic, *J. Geophys. Res.*, *109*, D24215, doi:10.1029/2004JD005137.

Charlson, R. J., S. E. Schwartz, J. M. Hales, R. D. Cess, R. D. Coakley, J. E. Hansen, and D. J. Hofmann (1992), Climate forcing by anthropogenic aerosols, *Science*, *255*, 423–430, doi:10.1126/science.255.5043.423.

Christopher, S. A., and J. Wang (2004), Intercomparison between multi-angle imaging spectroradiometer (MISR) and sunphotometer aerosol optical thickness in dust source regions over China: Implications for satellite aerosol retrievals and radiative forcing calculations, *Tellus, Ser. B*, *56*(5), 451–456, doi:10.1111/j.1600-0889.2004.00120.x.

Christopher, S. A., and J. Zhang (2002), Shortwave aerosol radiative forcing from MODIS and CERES observations over the oceans, *Geophys. Res. Lett.*, *29*(18), 1859, doi:10.1029/2002GL014803.

Dey, S., and L. Di Girolamo (2010), A climatology of aerosol optical and microphysical properties over the Indian subcontinent from 9 years (2000–2008) of Multiangle Imaging Spectroradiometer (MISR) data, *J. Geophys. Res.*, *115*, D15204, doi:10.1029/2009JD013395.

Diner, D. J., et al. (1998), Multi-angle Imaging SpectroRadiometer (MISR) instrument description and experiment overview, *IEEE Trans. Geosci. Remote Sens.*, *36*, 1072–1087, doi:10.1109/36.700992.

Diner, D. J., et al. (1999), New directions in Earth observing: Scientific applications of multi-angle remote sensing, *Bull. Am. Meteorol. Soc.*, *80*, 2209–2228, doi:10.1175/1520-0477(1999)080<2209:NDIEOS>2.0.CO;2.

Diner, D. J., et al. (2001), MISR aerosol optical depth retrievals over southern Africa during the SAFARI-2000 dry season campaign, *Geophys. Res. Lett.*, *28*(16), 3127–3130, doi:10.1029/2001GL013188.

Diner, D. J., et al. (2005), The value of multiangle measurements for retrieving structurally and radiatively consistent properties of clouds, aerosols, and surfaces, *Remote Sens. Environ.*, *97*, 495–518, doi:10.1016/j.rse.2005.06.006.

Eck, T. F., et al. (1999), Wavelength dependence of the optical depth of biomass burning, urban, and desert dust aerosols, *J. Geophys. Res.*, *104*, 31,333–31,349, doi:10.1029/1999JD900923.

Eck, T. F., et al. (2001), Characterization of the optical properties of biomass burning aerosols in Zambia during the 1997 ZIBBEE field campaign, *J. Geophys. Res.*, *106*, 3425–3448, doi:10.1029/2000JD900555.

Eck, T. F., et al. (2003), Variability of biomass burning aerosol optical characteristics in southern Africa during the SAFARI 2000 dry season campaign and a comparison of single scattering albedo estimates from radiometric measurements, *J. Geophys. Res.*, *108*(D13), 8477, doi:10.1029/2002JD002321.

Formenti, P., S. J. Piketh, and H. J. Annegarn (1999), Detection of non-sea salt sulphate aerosol at a remote coastal site in South Africa: A PIXE

© University of Pretoria

UNIVERSITEIT VAN PRETORIA
UNIVERSITY OF PRETORIA
YUNIBESITHI YA PRETORIA

study, *Nucl. Instrum. Methods Phys. Res., Sect. B*, *150*, 332–338, doi:10.1016/S0168-583X(98)01041-6.

Formenti, P., H. Winkler, P. Fourie, S. Piketh, B. Makgopa, G. Helas, and M. O. Andreae (2002), Aerosol optical depth over a remote semi-arid region of South Africa from spectral measurements of the daytime solar extinction and the nighttime stellar extinction, *Atmos. Res.*, *62*, 11–32, doi:10.1016/S0169-8095(02)00021-2.

Formenti, P., W. Elbert, W. Maenhaut, J. Haywood, S. Osborne, and M. O. Andreae (2003), Inorganic and carbonaceous aerosols during the Southern African Regional Science Initiative (SAFARI 2000) experiment: Chemical characteristics, physical properties, and emission data for smoke from African biomass burning, *J. Geophys. Res.*, *108*(D13), 8488, doi:10.1029/2002JD002408.

Freiman, M. T., and S. J. Piketh (2003), Air transport into and out of the industrial Highveld region of South Africa, *J. Appl. Meteorol.*, *42*, 994–1002, doi:10.1175/1520-0450(2003)042<0994:ATIAOO>2.0.CO;2.

Garstang, M., P. D. Tyson, R. Swap, M. Edwards, P. Kållberg, and J. A. Lindesay (1996), Horizontal and vertical transport of air over southern Africa, *J. Geophys. Res.*, *101*, 23,721–23,736, doi:10.1029/95JD00844.

Gobbi, G. P., Y. J. Kaufman, I. Koren, and T. F. Eck (2007), Classification of aerosol properties derived from AERONET direct Sun data, *Atmos. Chem. Phys.*, *7*, 453–458, doi:10.5194/acp-7-453-2007.

Gong, S., L. Barrie, and J. P. Blanchet (1997), Modeling sea-salt aerosols in the atmosphere 1. Model development, *J. Geophys. Res.*, *102*, 3805–3818, doi:10.1029/96JD02953.

Hanel, G. (1976), The properties of atmospheric aerosol particles as functions of relative humidity at thermodynamic equilibrium with surrounding moist air, *Adv. Geophys.*, *19*, 73–188, doi:10.1016/S0065-2687(08)60142-9.

Hansen, J., M. Sato, and R. Ruedy (1997), Radiative forcing and climate response, *J. Geophys. Res.*, *102*, 6831–6864, doi:10.1029/96JD03436.

Haywood, J., and O. Boucher (2000), Estimates of the direct and indirect radiative forcing due to tropospheric aerosols: A review, *Rev. Geophys.*, *38*, 513–543, doi:10.1029/1999RG000078.

Holben, B. N., E. Vermote, Y. J. Kaufman, D. Tanré, and V. Kalb (1992), Aerosol retrieval overland from AVHRR data-application for atmospheric correction, *IEEE Trans. Geosci. Remote Sens.*, *30*, 212–222, doi:10.1109/36.134072.

Holben, B. N., et al. (2001), An emerging ground-based aerosol climatology: Aerosol optical depth from AERONET, *J. Geophys. Res.*, *106*, 12,067–12,097, doi:10.1029/2001JD900014.

Hoppel, W., J. Fitzgerald, G. Frick, R. Larson, and E. Mack (1990), Aerosol size distributions and optical properties found in the marine boundary layer over the Atlantic Ocean, *J. Geophys. Res.*, *95*, 3659–3686, doi:10.1029/JD095iD04p03659.

Horvath, H. (1996), Spectral extinction coefficients of rural aerosol in southern Italy: A case study of cause and effect of variability of atmospheric aerosol, *J. Aerosol Sci.*, *27*, 437–453, doi:10.1016/0021-8502(95)00544-7.

Ichoku, C., L. A. Remer, Y. J. Kaufman, R. Levy, D. A. Chu, D. Tanré, and B. N. Holben (2003), MODIS observation of aerosols and estimation of aerosol radiative forcing over southern Africa during SAFARI 2000, *J. Geophys. Res.*, *108*(D13), 8499, doi:10.1029/2002JD002366.

Ignatov, A., and L. Stowe (2002), Aerosol retrievals from individual AVHRR channels, part I: Retrieval algorithm and transition from Dave to 6S radiative transfer model, *J. Atmos. Sci.*, *59*, 313–334, doi:10.1175/1520-0469(2002)059<0313:ARFIAC>2.0.CO;2.

Intergovernmental Panel on Climate Change (2007), *Climate Change 2007: Synthesis Report*, edited by The Core Writing Team, R. K. Pachauri, and A. Reisinger, Geneva, Switzerland. [Avaliable at http://www.ipcc.ch/pdf/assessment-report/ar4/syr/ar4_syr.pdf]

James, W., et al. (2000), Association between air pollution and lung function growth in southern California children, *Am. J. Respir. Crit. Care Med.*, *162*, 1383–1390.

Jayaraman, A. (2001), Aerosol radiation cloud interactions over the tropical Indian Ocean prior to the onset of the summer monsoon, *Curr. Sci.*, *81*, 1437–1445.

Jiang, X., Y. Liu, B. Yu, and M. Jiang (2007), Comparison of MISR aerosol optical thickness with AERONET measurements in Beijing metropolitan area, *Remote Sens. Environ.*, *107*, 45–53, doi:10.1016/j.rse.2006.06.022.

Kahn, R., P. Banerjee, and D. McDonald (2001), Sensitivity of multiangle imaging to natural mixtures of aerosols over ocean, *J. Geophys. Res.*, *106*, 18,219–18,238, doi:10.1029/2000JD900497.

Kahn, R. A., B. J. Gaitley, J. V. Martonchik, D. J. Diner, K. A. Crean, and B. Holben (2005), Multiangle Imaging Spectroradiometer (MISR) global aerosol optical depth validation based on 2 years of coincident Aerosol Robotic Network (AERONET) observations, *J. Geophys. Res.*, *110*, D10S04, doi:10.1029/2004JD004706.

Kahn, R. A., M. J. Garay, D. L. Nelson, K. K. Yau, M. A. Bull, B. J. Gaitley, J. V. Martonchik, and R. C. Levy (2007), Satellite-derived aerosol optical depth over dark water from MISR and MODIS: Comparisons with AERONET and implications for climatological studies, *J. Geophys. Res.*, *112*, D18205, doi:10.1029/2006JD008175.

Kahn, R. A., D. L. Nelson, M. J. Garay, R. C. Levy, M. A. Bull, D. J. Diner, J. V. Martonchik, S. R. Paradise, E. G. Hansen, and L. A. Remer (2009), MISR aerosol product attributes and statistical comparisons with MODIS, *IEEE Trans. Geosci. Remote Sens.*, *47*, 4095–4114, doi:10.1109/TGRS.2009.2023115.

Kahn, R. A., B. J. Gaitley, M. J. Garay, D. J. Diner, T. F. Eck, A. Smirnov, and B. N. Holben (2010), Multiangle Imaging SpectroRadiometer global aerosol product assessment by comparison with the Aerosol Robotic Network, *J. Geophys. Res.*, *115*, D23209, doi:10.1029/2010JD014601.

Kalashnikova, O. V., and R. Kahn (2006), Ability of multiangle remote sensing observations to identify and distinguish mineral dust types: 2. Sensitivity over dark water, *J. Geophys. Res.*, *111*, D11207, doi:10.1029/2005JD006756.

Kalashnikova, O. V., and R. A. Kahn (2008), Mineral dust plume evolution over the Atlantic from MISR and MODIS aerosol retrievals, *J. Geophys. Res.*, *113*, D24204, doi:10.1029/2008JD010083.

Kalashnikova, O. V., R. Kahn, I. N. Sokolik, and W.-H. Li (2005), The ability of multi-angle remote sensing observations to identify and distinguish mineral dust types: Optical models and retrievals of optically thick plumes, *J. Geophys. Res.*, *110*, D18S14, doi:10.1029/2004JD004550.

Kaskaoutis, D. G., and H. D. Kambezidis (2006), Checking the validity of the Angstrom's formula with spectral data of direct beam irradiance obtained in Athens, Greece, *Atmos. Res.*, *79*, 67–87, doi:10.1016/j.atmosres.2005.05.001.

Katoshevski, D., A. Nenes, and J. H. Seinfeld (1999), A study of processes that govern the maintenance of aerosols in the marine boundary layer, *J. Aerosol Sci.*, *30*, 503–532, doi:10.1016/S0021-8502(98)00740-X.

Kaufman, Y. J. (1993), Aerosol optical thickness and atmospheric path radiance, *J. Geophys. Res.*, *98*, 2677–2692, doi:10.1029/92JD02427.

Kaufman, Y. J., A. Setzer, D. Ward, D. Tanre, B. N. Holben, P. Menzel, M. C. Pereira, and R. Rasmussen (1992), Biomass burning airborne and space borne experiment in the Amazonas (BASE-A), *J. Geophys. Res.*, *97*, 14,581–14,599, doi:10.1029/92JD00275.

Kaufman, Y. J., D. Tanre, L. A. Remer, E. F. Vermote, A. Chu, and B. N. Holben (1997), Operational remote sensing of tropospheric aerosol over land from EOS moderate resolution imaging spectroradiometer, *J. Geophys. Res.*, *102*, 17,051–17,067, doi:10.1029/96JD03988.

Kaufman, Y., D. Tanre, and O. Boucher (2002), A satellite view of aerosols in the climate system, *Nature*, *419*, 215–223, doi:10.1038/nature01091.

King, M. D., and D. M. Byrne (1976), A method for inferring total ozone content from spectral variation of total optical depth obtained with a solar radiometer, *J. Atmos. Sci.*, *33*, 2242–2251, doi:10.1175/1520-0469(1976)033<2242:AMFITO>2.0.CO;2.

King, M., D. Byrne, B. Herman, and J. Reagan (1978), Aerosol size distributions obtained by inversion of spectral optical depth measurements, *J. Atmos. Sci.*, *35*, 2153–2167, doi:10.1175/1520-0469(1978)035<2153:ASDOBI>2.0.CO;2.

King, M. D., Y. J. Kaufman, D. Tanre, and T. Nakajima (1999), Remote sensing of tropospheric aerosols from space: Past, present, and future, *Bull. Am. Meteorol. Soc.*, *80*, 2229–2259, doi:10.1175/1520-0477(1999)080<2229:RSOTAF>2.0.CO;2.

Latham, J., and M. Smith (1990), Effect on global warming of wind-dependent aerosol generation at the ocean surface, *Nature*, *347*, 372–373, doi:10.1038/347372a0.

Lehahn, Y., I. Koren, E. Boss, Y. Ben-Ami, and O. Altaratz (2010), Estimating the maritime component of aerosol optical depth and its dependency on surface wind speed using satellite data, *Atmos. Chem. Phys.*, *10*, 6711–6720, doi:10.5194/acp-10-6711-2010.

Levy, R. C., et al. (2003), Evaluation of the Moderate-Resolution Imaging Spectroradiometer (MODIS) retrievals of dust aerosol over the ocean during PRIDE, *J. Geophys. Res.*, *108*(D19), 8594, doi:10.1029/2002JD002460.

Levy, R. C., G. G. Leptoukh, R. Kahn, V. Zubko, A. Gopalan, and L. A. Remer (2009), A critical look at deriving monthly aerosol optical depth from satellite data, *IEEE Trans. Geosci. Remote Sens.*, *47*, 2942–2956, doi:10.1109/TGRS.2009.2013842.

Liu, L. (2005), Improving GCM Aerosol Climatology using satellite and ground based measurements, paper presented at 15th ARM Science Team Meeting, Atmos. Radiat. Meas. (ARM) Program, Daytona Beach, Fla., 14–18 March.

Liu, Y., J. A. Sarnat, B. A. Coull, P. Koutrakis, and D. J. Jacob (2004), Validation of Multiangle Imaging Spectroradiometer (MISR) aerosol optical thickness measurements using Aerosol Robotic Network (AERONET)

© University of Pretoria

UNIVERSITEIT VAN PRETORIA
UNIVERSITY OF PRETORIA
YUNIBESITHI YA PRETORIA

observations over the contiguous United States, *J. Geophys. Res.*, *109*, D06205, doi:10.1029/2003JD003981.

Magi, B. I., P. Ginoux, Y. Ming, and V. Ramaswamy (2009), Evaluation of tropical and extratropical Southern Hemisphere African aerosol properties simulated by a climate model, *J. Geophys. Res.*, *114*, D14204, doi:10.1029/2008JD011128.

Mallet, M., J. C. Roger, S. Despiau, O. Dubovik, and J. P. Putaud (2003), Microphysical and optical properties of aerosol particles in urban zone during ESCOMPTE, *Atmos. Res.*, *69*, 73–97, doi:10.1016/j.atmosres.2003.07.001.

Martonchik, J. V., et al. (1998), Techniques for the retrieval of aerosol properties over land and ocean using multi-angle imaging, *IEEE Trans. Geosci. Remote Sens.*, *36*(4), 1212–1227, doi:10.1109/36.701027.

Martonchik, J. V., D. J. Diner, K. A. Crean, and M. A. Bull (2002), Regional aerosol retrieval results from MISR, *IEEE Trans. Geosci. Remote Sens.*, *40*(7), 1520–1531, doi:10.1109/TGRS.2002.801142.

Martonchik, J. V., D. J. Diner, R. Kahn, B. Gaitley, and B. N. Holben (2004), Comparison of MISR and AERONET aerosol optical depths over desert sites, *Geophys. Res. Lett.*, *31*, L16102, doi:10.1029/2004GL019807.

Masmoudi, M., M. Chaabane, D. Tanre, P. Gouloup, L. Blarel, and F. Elleuch (2003), Spatial and temporal variability of aerosol: Size distribution and optical properties, *Atmos. Res.*, *66*, 1–19, doi:10.1016/S0169-8095(02)00174-6.

Matteo, R., et al. (2010), Primary and secondary organic marine aerosol and oceanic biological activity: Recent results and new perspectives for future studies, *Adv. Meteorol.*, *310682*, doi:10.1155/2010/310682.

de Meij, A. and J. Lelieveld (2011), Evaluating aerosol optical properties observed by ground-based and satellite remote sensing over the Mediterranean and the Middle East in 2006, *Atmos. Res.*, *99*, 415–433, doi:10.1016/j.atmosres.2010.11.005.

Muller, J., A. Mandanayake, C. Moroney, R. Davies, D. J. Diner, and S. Paradise (2002), MISR stereoscopic image matchers: Techniques and results, *IEEE Trans. Geosci. Remote Sens.*, *40*(7), 1547–1559, doi:10.1109/TGRS.2002.801160.

Nakajima, T., T. Takamura, and M. Yamano (1986), Consistency of aerosol size distributions inferred from measurements of solar radiation and aerosols, *J. Meteorol. Soc. Jpn.*, *64*, 765–776.

O'Dowd, C., and G. de Leeuw (2007), Marine aerosol production: A review of the current knowledge, *Philos. Trans. R. Soc. A*, *365*, 1753–1774, doi:10.1098/rsta.2007.2043.

O'Dowd, C., and M. Smith (1993), Physicochemical properties of aerosols over the northeast Atlantic: Evidence for wind-speed-related submicron sea-salt aerosol production, *J. Geophys. Res.*, *98*, 1137–1149, doi:10.1029/92JD02302.

O'Dowd, C., M. Smith, I. Consterdine, and J. Lowe (1997), Marine aerosol, sea-salt, and the marine sulphur cycle: A short review, *Atmos. Environ.*, *31*, 73–80, doi:10.1016/S1352-2310(96)00106-9.

O'Neill, N. T., O. Dubovik, and T. F. Eck (2001a), A modified Angstrom coefficient for the characterization of sub-micron aerosols, *Appl. Opt.*, *40*, 2368–2374.

O'Neill, N. T., T. F. Eck, B. N. Holben, A. Smirnov, and O. Dubovick (2001b), Bimodal size distribution influences on the variation of Angstrom derivatives in spectral and optical depth space, *J. Geophys. Res.*, *106*, 9787–9806, doi:10.1029/2000JD900245.

O'Neill, N. T., T. F. Eck, B. N. Holben, A. Smirnov, A. Royer, and Z. Li (2002), Optical properties of boreal forest fire smoke derived from Sun photometry, *J. Geophys. Res.*, *107*(D11), 4125, doi:10.1029/2001JD000877.

O'Neill, N. T., T. F. Eck, A. Smirnov, B. N. Holben, and S. Thulasiraman (2003), Spectral discrimination of coarse and fine mode optical depth, *J. Geophys. Res.*, *108*(D17), 4559, doi:10.1029/2002JD002975.

Piketh, S. J., H. J. Annegarn, and P. D. Tyson (1999), Lower tropospheric aerosol loadings over South Africa: The relative contribution of aeolian dust, industrial emissions, and biomass burning, *J. Geophys. Res.*, *104*, 1597–1607, doi:10.1029/1998JD100014.

Piketh, S. J., R. J. Swap, W. Maenhaut, H. J. Annegarn, and P. Formenti (2002), Chemical evidence of long-range atmospheric transport over southern Africa, *J. Geophys. Res.*, *107*(D24), 4817, doi:10.1029/2002JD002056.

Prasad, A. K., and R. P. Singh (2007), Comparison of MISR-MODIS aerosol optical depth over the Indo-Gangetic basin during the winter and summer seasons (2000–2005), *Remote Sens. Environ.*, *107*, 109–119, doi:10.1016/j.rse.2006.09.026.

Queface, A. J., et al. (2011), Climatology of aerosol optical properties in southern Africa, *Atmos. Environ.*, *45*, 2910–2921, doi:10.1016/j.atmosenv.2011.01.056.

Quinn, P. K., et al. (2000), Surface submicron aerosol chemical composition: What fraction is not sulfate? *J. Geophys. Res.*, *105*, 6785–6805, doi:10.1029/1999JD901034.

Raizenne, M., et al. (1996), Health effects of acid aerosols on North American children: Pulmonary function, *Environ. Health Perspect.*, *104*, 506–514, doi:10.1289/ehp.96104506.

Reid, J. S., T. F. Eck, S. A. Christopher, P. V. Hobbs, and B. N. Holben (1999), Use of the Ångstrom exponent to estimate the variability of optical and physical properties of aging smoke particles in Brazil, *J. Geophys. Res.*, *104*, 27,473–27,489, doi:10.1029/1999JD900833.

Roberts, G. C., M. O. Andreae, J. Zhou, and P. Artaxo (2001), Cloud condensation nuclei in the Amazon Basin: "Marine" conditions over a continent? *Geophys. Res. Lett.*, *28*, 2807–2810, doi:10.1029/2000GL012585.

Ross, K. E., S. J. Piketh, R. T. Bruintjes, R. P. Burger, R. J. Swap, and H. J. Annegarn (2003), Spatial and seasonal variation in CCN distribution and the aerosol-CCM relationship over southern Africa, *J. Geophys. Res.*, *108*(D13), 8481, doi:10.1029/2002JD002384.

Schuster, G. L., O. Dubovick, and B. N. Holben (2006), Angstrom exponent and bimodal aerosol size distributions, *J. Geophys. Res.*, *111*, D07207, doi:10.1029/2005JD006328.

Sievering, H. J., G. J. Boatman, W. Keene, Y. Kim, M. Luria, and J. Ray (1991), Heterogeneous sulfur conversion in sea-salt aerosol particles: The role of aerosol water content and size distribution, *Atmos. Environ. Part A*, *25*, 1479–1487, doi:10.1016/0960-1686(91)90007-T.

Sivakumar, V., M. Tesfaye, W. Alemu, A. Sharma, C. Bollig, and G. Mengistu (2010), Aerosol measurements over South Africa using LIDAR, satellite and Sun photometer, *Adv. Geosci.*, *16*, 263–270.

Twomey, S. (1977), The influence of pollution on the shortwave albedo of clouds, *J. Atmos. Sci.*, *34*, 1149–1152, doi:10.1175/1520-0469(1977)034<1149:TIOPOT>2.0.CO;2.

Tyson, P. D., and P. C. D'Abreton (1998), Transport and recirculation of aerosols off southern Africa: Macroscale plume structure, *Atmos. Environ.*, *32*, 1511–1524, doi:10.1016/S1352-2310(97)00392-0.

Tyson, P. D., M. Garstang, R. Swap, P. Kållberg, and M. Edwards (1996), An air transport climatology for subtropical southern Africa, *Int. J. Climatol.*, *16*, 265–291, doi:10.1002/(SICI)1097-0088(199603)16:3<265::AID-JOC8>3.0.CO;2-M.

Winkler, J., P. Formenti, D. J. Esterhuyse, R. J. Swap, G. Helas, H. J. Annegarn, and M. O. Andreae (2008), Evidence for large-scale transport of biomass burning aerosols from sunphotometry at a remote South African site, *Atmos. Environ.*, *42*, 5569–5578, doi:10.1016/j.atmosenv.2008.03.031.

Zunckel, M., L. Robertson, P. D. Tyson, and H. Rodhe (2000), Modelled transport and deposition of sulphur over southern Africa, *Atmos. Environ.*, *34*, 2797–2808, doi:10.1016/S1352-2310(99)00495-1.

J. Botai, V. Sivakumar, and M. Tesfaye, Department of Geography, Geoinformatics and Meteorology, University of Pretoria, Pretoria 0002, South Africa. (mela_20062@yahoo.com; svenkataraman@csir.co.za)

G. Mengistu Tsidu, Department of Physics, Addis Ababa University, PO Box 1176, Addis Ababa, Ethiopia.

© University of Pretoria

Chapter 3: Evaluation of regional climatic model simulated aerosol optical properties over South Africa using ground-based and satellite observations*

*This chapter needs to be cited as:

Tesfaye, M., J. Botai, V. Sivakumar and G. Mengistu Tsidu (2013a): Evaluation of Regional Climatic Model Simulated Aerosol Optical Properties over South Africa Using Ground-Based and Satellite Observations, *ISRN Atmospheric Sciences, vol. 2013, Article ID 237483, 17 pages, 2013. doi:10.1155/2013/237483.*

© University of Pretoria

UNIVERSITEIT VAN PRETORIA
UNIVERSITY OF PRETORIA
YUNIBESITHI YA PRETORIA

Hindawi Publishing Corporation
ISRN Atmospheric Sciences
Volume 2013, Article ID 237483, 17 pages
http://dx.doi.org/10.1155/2013/237483

Hindawi

Research Article

Evaluation of Regional Climatic Model Simulated Aerosol Optical Properties over South Africa Using Ground-Based and Satellite Observations

M. Tesfaye,[1,2] J. Botai,[1] V. Sivakumar,[1,3] and G. Mengistu Tsidu[4]

[1] *Department of Geography, Geoinformatics and Meteorology, University of Pretoria, Lynwood Road, Pretoria 0002, South Africa*
[2] *National Laser Centre, Council for Scientific and Industrial Research, P.O. Box 395, Pretoria 0001, South Africa*
[3] *Discipline of Physics, School of Chemistry and Physics, University of KwaZulu Natal, Westville, Durban 4000, South Africa*
[4] *Department of Physics, Addis Ababa University, P.O. Box 1176, Addis Ababa, Ethiopia*

Correspondence should be addressed to M. Tesfaye; mela_20062@yahoo.com

Received 21 August 2013; Accepted 13 September 2013

Academic Editors: G. A. Gerosa and K. Schaefer

Copyright © 2013 M. Tesfaye et al. This is an open access article distributed under the Creative Commons Attribution License, which permits unrestricted use, distribution, and reproduction in any medium, provided the original work is properly cited.

The present study evaluates the aerosol optical property computing performance of the Regional Climate Model (RegCM4) which is interactively coupled with anthropogenic-desert dust schemes, in South Africa. The validation was carried out by comparing RegCM4 estimated: aerosol extinction coefficient profile, Aerosol Optical Depth (AOD), and Single Scattering Albedo (SSA) with AERONET, LIDAR, and MISR observations. The results showed that the magnitudes of simulated AOD at the Skukuza station (24°S, 31°E) are within the standard deviation of AERONET and ±25% of MISR observations. Within the latitudinal range of 26.5°S to 24.5°S, simulated AOD and SSA values are within the standard deviation of MISR retrievals. However, within the latitude range of 33.5°S to 27°S, the model exhibited enhanced AOD and SSA values when compared with MISR observations. This is primarily associated with the dry bias in simulated precipitation that leads to the overestimation of dust emission and underestimation of aerosol wet deposition. With respect to LIDAR, the model performed well in capturing the major aerosol extinction profiles. Overall, the results showed that RegCM4 has a good ability in reproducing the major observational features of aerosol optical fields over the area of interest.

1. Introduction

Atmospheric aerosols which originate from different natural events (e.g., wind-blown dust and sea salt particles) and human activities such as combustion of biomass and fossil fuels, as well as various industrial processes (e.g., sulfates, nitrates, ammonium, and carbonaceous aerosols) are ubiquitous in the Earth's atmosphere [1]. Relative to the well mixed and long-lived greenhouse gases, one of the main typical properties of atmospheric aerosols is their immense diversity, not only with respect to their physicochemical and optical properties, but also with regards to their spatial and temporal distributions (e.g., [2]). This is attributed to their diverse local source mechanisms, rapid aging, and chemical transformation processes, as well as short lifetime [3]. Though, owing to these heterogeneous properties of aerosols, the quantification of their climatic roles remains with large uncertainties; they are increasingly reported as one of the crucial components of the atmosphere for multi-climatic issues ([4] and references therein).

Primarily, atmospheric aerosols play an important role in modulating the regional radiation budget either through scattering or absorption of radiation (direct effects) (e.g., [5]). The perturbation of the radiation balance of the Earth through scattering of the incoming solar radiation back to space cools the Earth's surface as well as certain portions of the troposphere, but it induces stratospheric warming (e.g., [6]). The absorption of short and long wave radiation predominantly prompts atmospheric heating effects; nevertheless, depending on the underlying surface as well as the atmospheric situations, it might also result to surface cooling (e.g., [7, 8] and references therein). Particulates that

© University of Pretoria

UNIVERSITEIT VAN PRETORIA
UNIVERSITY OF PRETORIA
YUNIBESITHI YA PRETORIA

are highly absorbing solar radiation such as black carbon and mineral dust particles have a substantial influence in converting the solar energy into heat; this radiative heating in turn creates the semidirect effect of aerosols. The semidirect effect is the response of thermal, hydrological, and dynamical variables of the climate to atmospheric heating induced by light-absorbing aerosols (e.g., [7, 9]). For instance, the warming influence of aerosols in lower troposphere often enhances the low-level cloud evaporation and atmospheric stability, which consecutively results in the reduction of cloudiness as well as the slowing of the hydrological cycle and the suppression of convection processes (e.g., [1, 9–14]). Additionally, the strong heating effects of absorbing aerosols in the lower troposphere will produce alterations in atmospheric circulation (e.g., [14, 15]). Furthermore, as discussed by different studies, depending on the relative position of the absorbing aerosol layer with respect to clouds (e.g., [13, 16–18]) as well as the underlying surface properties [19, 20], the semidirect effect may also result in instability of the atmosphere and an increase in cloud water.

In general, attributed to the involvement of various atmospheric, surface, and other variables, the computation of semi-direct effects of aerosols is quite complicated and highly variable [19, 20]. Moreover, aerosols enhance the cloud number droplets and decrease its mean droplet size by acting as cloud condensation nuclei. This results in the change in cloud albedo and radiative properties, reducing precipitation efficiency which might influence the cloud lifetime as well as its formation processes and coverage (indirect effects) ([21–23] and references therein). Likewise, different reports point to the involvement of atmospheric aerosols in several climatic system topics: in a range of tropospheric chemistry variations [24], stratospheric ozone depletion [25], and in several ecological concerns (e.g., [26–28]).

Once aerosols are released into (formed in) the atmosphere, they will be transported to fields far away from the areas of their origin. However, during their transportation they will be subjected to numerous physicochemical transformations and removal processes such as dry and wet deposition and gravitational settling [29–31]. Thus, as aerosols travel further away from their source regions, their concentration and impact will decline drastically [3, 32]. As a result of this declination, the impact of aerosols on climate must be understood and quantified on a regional scale (i.e., in and around their source regions) rather than on a global-average basis (e.g., [1, 33, 34]). Due to the extreme heterogeneity of aerosol space-time distribution, as well as physicochemical properties, the quantitative assessments of certain puzzling climatic roles and different aspects of aerosols through observations (field experiments) are prohibitively expensive and highly constrained by various factors (e.g., [4, 35–39]).

Therefore, studying the climatic effects of aerosols using chemistry/aerosol models which are radiatively active and coupled with the meteorological models with online feedback on the radiation and climatic schemes (e.g., [40–45]) is crucial. In addition, models are also indispensable tools for estimating the past and projecting the future climatic role of aerosol forcing (e.g., [46, 47]). Since the late 1980s, interactively coupled climate-aerosol models for global scale (e.g., [48, 49] and references therein) and regional scale ([50] and references therein) simulations have been developed. Global and regional models are now becoming more complex as they incorporate new parameterizations of aerosol properties and processes. Global-scale models, due to their frequently implemented coarse grid resolution, do not accurately simulate the regional-scale spatiotemporal distributions of atmospheric aerosols, as well as meteorological processes that govern the aerosol-atmosphere-radiation-chemistry interactions (e.g., [30, 51–54]). As a result of this and other aspects, predictions of aerosol optical properties and climatic forcings employing global-scale models are exposed to remarkable uncertainties (e.g., [8, 30, 53, 55–58] and references therein).

On the other hand, the high-resolution climatic system (i.e., the surface, ocean as well as atmospheric processes) representations of Regional Climate Models (RCMs) offer enhanced advantages in assessing the downscaled meteorological processes as well as different climatic information and patterns (e.g., [59–61] and references therein). Furthermore, interactively coupled high-resolution regional climate-chemistry/aerosol models progressively turn out to be a suitable tool in assessing the regional scale distribution and complex climatic roles of aerosols with a much better computational cost, relative to global climatic models (e.g., [29, 62–69]). In addition, the results from high-resolution RCMs are well suited for comparison with measurements of individual events at selected sites/areas. Therefore, to evaluate the regional scale aerosol distributions, along with their radiative and climatic impact with improved accuracy, simulations utilizing high resolution RCMs are vital (e.g., [29, 69]).

The literature on aerosol studies employing the art of RCM over Africa is not exhaustive. Most studies which have been reported over this continent such as Solmon et al. [67], Konare et al. [70], and Malavelle et al. [71] have focused on the effect of mineral dust and biomass burning particles over the West African regions. On the other hand, South Africa, which has plenty of industries and mining sectors, is the most industrialized country in the continent. These human activities, along with the wide usage of coal for electricity generation, make South Africa one of the remarkable spots in the globe, which contributes several types of aerosols via anthropogenic activities (e.g., [72–75]). Further, many space- and ground-based observational studies (e.g., [2, 76–80] and references therein) and modeling studies ([69, 80, 81] and references therein) identify South Africa as a major source of anthropogenic aerosols in the subcontinent. Different intensive field-campaign observations such as Southern African Regional Science Initiative (SAFARI) (e.g., [82–84]) and aerosol climatology studies (e.g., [2, 85]) indicate that during the dry seasons, South Africa experiences a drastic burden of aerosols from biomass burning activities. In addition, the dust blowing from the arid/semiarid regions of South Africa and its neighboring countries [2, 76, 86], along with marine aerosols—which are induced from the surrounding oceans [2, 85]—is another main component of natural aerosols over South Africa.

In overall, due to various natural/anthropogenic events, the South African atmosphere is burdened by almost all

© University of Pretoria

major types of aerosols. As aforementioned, the impact of aerosols is considerably substantial near to their source regions; therefore, the regional scale distributions as well as climatic impact of aerosols—which are induced in and around South African regions—need to be assessed and reported separately. To date, only a single study has been reported employing interactively coupled regional climate-chemistry/aerosol model (ICTP RegCM4-aerosol model) over southern Africa [69]. This study focused on the direct and semidirect radiative effects of biomass burning and dust aerosols on southern Africa's regional climate during the dry winter season only. A study devoted to compressively examine the seasonal distributions and long-term climatic signals of individual/combined aerosol components using the above model over South Africa is still lacking. Therefore, using the ICTP RegCM4-aerosol model [50], studies that follow this paper and are reported elsewhere will compressively examine the seasonal distributions, as well as the direct and semi-direct effects of different components of aerosols over South Africa. However, before employing the model for the investigation of atmospheric aerosol radiative and climatic effects, its performance in computing the magnitudes as well as the spatiotemporal evolution of the optical properties of aerosols needs to be evaluated via comparing with a range of remote sensing/in-situ observations.

Modeling the direct influence of aerosols on the earth's radiation balance by solving the radiative transfer equation needs the following spectral aerosol optical parameters: (a) aerosol extinction optical depth (AOD), (b) asymmetry parameter, and (c) single scattering albedo (SSA) (e.g., [5, 29]). These optical parameters are significantly dependent on the aerosol's composition (complex refractive index), particle size (particle size distribution), shape, wavelength, and relative humidity [87–90]. AOD is the vertical integral of fraction of solar/terrestrial radiation either scattered or absorbed by airborne particles (i.e., the sum of aerosol scattering and absorption optical depths) (e.g., [87]). The asymmetry parameter is the intensity-weighted mean value of the cosine of the scattering angle (e.g., [91]); it determines the net angular distribution of aerosol scattered light. The SSA (i.e., the ratio of the extinction due to scattering to the total extinction due to scattering plus absorption) is an important parameter that governs the relative efficiency of particles to scatter solar/thermal radiation compared to absorption (e.g., [92]). Depending on the underlying surface albedo, these optical properties of aerosols are the key parameters driving the magnitude, as well as a sign of aerosol direct radiative forcing (i.e., in driving the aerosol radiative cooling/heating roles) (e.g., [7, 93]). Therefore, to understand and evaluate various aspects of atmospheric aerosols, a reasonable quantification of these optical parameters is crucial. Additionally, these aerosol optical properties are the most comprehensive standard quantities that link the observations with the outcomes of the model.

Concerning aerosol microphysical and optical property inquiries, field measurements provide more detailed information with better accuracies (e.g., [87, 94]); however, they are confined within temporal or spatial coverage (e.g., [95]). Satellite observations provide the requisite aerosol optical property distributions with extensive temporal and spatial coverage (e.g., [95]). Nonetheless, due to high variability of the earth's system reflectance, both in space and time, as well as aerosol physicochemical properties, satellite retrievals are exposed to some accuracy limitations and constraints to deliver some essential aerosol quantities such as aerosol compositions [37, 38, 96–100]. As a result, neither field measurements nor satellite observations, alone, would be sufficient to fully describe the total regional scale aerosol distributions as well as its physical, chemical, and optical properties. Alternatively, interactively coupled regional climate-chemistry/aerosol models (RC-aerosol models), which comprises a suite of major atmospheric aerosols, with their detailed parameterizations, are essential in delivering various parameters which are related to aerosols and their climatic roles, with high-temporal and spatial resolutions. To this end, the RC-aerosol models have a capability of providing important information about the complex aerosols-radiation-climatic interactions and the physicochemical production/transformation rate of particles as well as their concentration and optical parameters. Some of this information gained from modeling studies cannot be easily addressed from either satellite retrievals or field measurements.

Notwithstanding the contribution of RC-aerosol models, modeling the entire complex aerosol processes (i.e., emission, transportation, physicochemical transformation, and removal, as well as wavelength and climatic condition dependent aerosol optical properties) is fundamentally a challenging task [29]. Further, errors in simulated meteorological fields, insufficiently understood physico-chemical processes of aerosols, inaccurately estimated precursor-gas/particulate emissions by the inventories used (e.g., [101]), and many other factors will impose significant uncertainties in simulating optical characteristics of aerosols [30, 34, 57]. The inaccuracies in model estimated optical parameters of aerosols will also propagate a substantial uncertainty on the computation of aerosol's direct radiative forcing and its consequential semidirect influences (e.g., [4, 34]). Thus, to compensate the deficiencies of one technique via another and to reduce inaccuracies in model predicted optical properties of aerosols, an hybrid research effort that integrates observational records and numerical modeling techniques is essential (e.g., [40, 81, 95, 102–105]).

The present study will evaluate the ICTP RegCM4-aerosol model capability of simulating the magnitude as well as the spatiotemporal evolution of optical properties of aerosols via comparing with different field observations, in South Africa. Such studies would also contribute important role to pointing-out the shortcomings of the model's parameterizations (e.g., [29]). In this study, including different types of aerosols which is induced from natural processes and distinct emission sectors in and around South Africa (see our simulation domain in Figure 1), a long-term regional climate/aerosol simulation has been carried out using RegCM4-aerosol model (see Sections 2.2 and 2.4). To estimate particulates/precursor-gases which are emitted from different anthropogenic/biomass burning sectors, recently updated emission inventories have been used (see Section 2.3). Subsequent to these, the evaluation of simulated

© University of Pretoria

UNIVERSITEIT VAN PRETORIA
UNIVERSITY OF PRETORIA
YUNIBESITHI YA PRETORIA

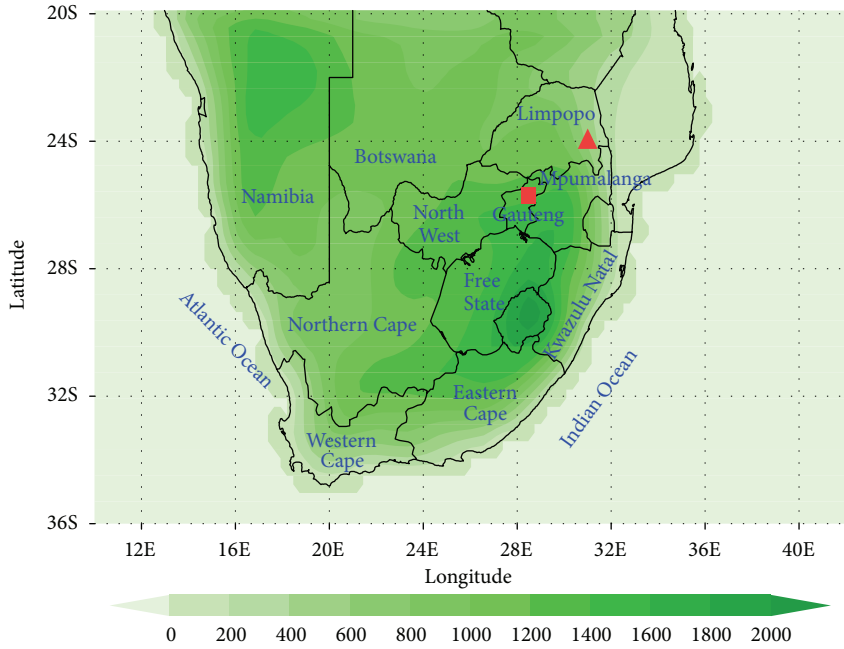

Figure 1: Model domain and topography (unit: m). The red triangle and square, respectively, indicate the geographical location of AERONET (Skukuza; 24°S, 31°E) and LIDAR (University of Pretoria; 25.7°S; 28.2°E) surface observation sites.

aerosol optical fields over South Africa (22°S to 34°S and 16°E to 32°E (see Figure 1)) has been carried out by comparing with values obtained from ground (sun-photometer and LIDAR) and spaceborne (MISR) observations. The paper is organized as follows. Section 2 will provide a brief description about the ICTP RegCM4-aerosol model along with the employed model physics parameterization, emission inventories used in the model, and the experimental design. In addition, the different surface/satellite products used for evaluating model outputs will be addressed in this section. In Section 3, comparing with different remote sensing products, we present the evaluation of the model's performance in simulating the magnitude and spatio-temporal evolution of column integrated aerosol optical properties, as well as their vertical distribution. Along with the validation, different rationale aspects which might be accountable for the biases of the simulated aerosol optical fields are discussed. A summary, concluding remarks, and future perspectives are given in Section 4.

2. Methodology

2.1. Model Description. In this study, for the regional climate/aerosol simulation, interactively coupled regional climate-aerosol model is used. The climate component of the coupled model is the Regional Climate Model (RegCM) version 4.0 (RegCM4.0), developed at the International Centre for Theoretical Physics (ICTP). RegCM4 is a hydrostatic, compressible, sigma vertical coordinate model, which is an upgraded version of RegCM3 with the similar basic model dynamics but with certain improvements in various physics representations and software code [50]. For a more detailed description of RegCM and its substantial evolution starting from the first generation (RegCM1; [106]) to the current version, the reader is referred to ([50, 61] and references therein).

Among different model physics parameterization schemes of RegCM4, this study employs the following scheme: for the radiative transfer computation—the Community Climate Model-CCM3 radiative transfer package [107] is used. This radiative transfer package takes into account the radiative effect of different greenhouse gases, atmospheric aerosols and cloud water-ice, in different spectral bands. The radiative flux calculations include 18 spectral intervals which are within a wavelength range of 0.2 to 4.5 μm. Among these 18 spectral bands, seven of them are situated in the ultraviolet spectral interval (0.2–0.35 μm), one is in the visible band (0.35–0.64 μm) and the remaining spectral bands cover the infrared/special absorption windows [107]. The ocean surface fluxes are computed according to the scheme of Zeng et al. [108], and the land surface physics, which describe the transfer of energy, mass, and momentum between the atmosphere and the biosphere, is described by the biosphere-atmosphere transfer scheme (BATS; [109, 110]). The planetary boundary layer processes are characterized according to the nonlocal parameterization of Holtslag et al. [111]. The convective precipitation is represented by the mass flux scheme of Grell [112] with the Fritsch and Chappell [113] closure assumption, while the large-scale cloud and non-convective precipitation computations follow the Sub-grid explicit moisture scheme (SUBEX) of Pal et al. [114].

2.2. RegCM4-Aerosol Model. The RegCM4-aerosol model is interactively coupled model between RegCM4 and radiatively active simplified anthropogenic and dust aerosol models, which can be used to examine the two-way

© University of Pretoria

UNIVERSITEIT VAN PRETORIA
UNIVERSITY OF PRETORIA
YUNIBESITHI YA PRETORIA

aerosol-climate feedback [50]. The RegCM4-aerosol model allows the simulation of major tropospheric aerosols, which originate from anthropogenic and biomass burning activities [29], as well as wind eroded desert dust particles [63, 67]. The anthropogenic and biomass burning aerosol schemes account for sulfur dioxide (SO_2), sulfate (SO_4^{-2}), hydrophobic and hydrophilic components of black carbon (BC), and organic carbon (OC) particles [29]. Following Qian et al. [42] the model takes into account the chemical conversion of SO_2 to SO_4^{-2} through both gaseous-phase and aqueous-phase pathways.

The atmospheric processes of these aerosols: surface emission, transportation (via advection by atmospheric winds, turbulent diffusion and deep convection), physico-chemical transformations, and removal processes (via wet and dry depositions) are described by the tracer transport equation of Solmon et al. [29]. The essential steps and mechanisms which are considered for developing and implementing the online dynamical dust production scheme, together with the parameterizations of several factors which influence the dust emission processes, are described in detail by Zakey et al. [63]. The dust scheme of RegCM4 represents the dry dust particle size distribution through size bin approach. The whole-size spectrum of dust particles covers a diameter range of 0.01 to 20.0 μm, divided into 4 size-bins, that is, the fine (0.01–1.0 μm), accumulation (1.0–2.5 μm), coarse (2.5–5.0 μm), and giant (5.0–20.0 μm) particle size modes [63]. As described in Zakey et al. [63], during the inclusion of dust module in RegCM framework, some new parameterizations of the dustatmospheric process (such as, size-dependent gravitational settling processes of dust particles) are incorporated into the tracer transport equation of Solmon et al. [29].

For each wavelength of the RegCM4 radiation scheme and for each aerosol species, the aerosol size distribution and refractive index dependent optical properties (i.e., asymmetry factor, single scattering albedo, and mass extinction coefficient) are computed using the Mie theory and employed in the model [29]. Using prognostic dust bin concentrations, long-wave refractive indices, and absorption cross sections, the dust particles long-wave emissivity/absorptivity influences are implemented based on Solmon et al. [67]. The relative humidity influences on optical properties of hydrophilic aerosols are specified according to Solmon et al. [29]. Accordingly, the model computes the shortwave radiative influences of all the above aerosol types using these optical properties, along with the long-wave effects of dust particles [50]. More information on different aspects of RegCM4-aerosol model is described in Giorgi et al. [50]. Over the years, this model has been widely used to examine the regional-scale direct radiative forcing of aerosols and their climatic effects in different parts of the globe (e.g., [43, 67, 69–71, 115–117]). In this study, also employing two recently updated emission inventories in the model (which are described in Section 2.3), a long term regional climate/aerosol simulation has been carried out.

Before we carry on to the next section, we would like to highlight some of the limitations which are associated with our simulation, as well as the aerosol schemes of RegCM4. This, further than assisting this study, it will also avoid the repetition of information in studies that follow this contribution [118–121]. Most of the earlier studies, for example, several studies reported in IPCC [4] clearly stated the importance of the indirect effects of aerosols along with its current uncertainties. Nonetheless, one of the main caveats of RegCM4-aerosol model is that it does not include this aerosol effect. The next limitation is associated with the assumption used regarding the complex mixing state of the particles. Throughout our studies, the external mixing assumption is used for the computation of the total optical parameters of aerosols. This is based on previous studies which reported that nearby the aerosol source region, the extinction cross section is slightly sensitive to the mixing hypothesis (e.g., [93, 122]). However, there are several processes in the atmosphere that will alter an external mixture of particles into an internal mixture (e.g., [123]). In fact, different studies show a high sensitivity of the bulk aerosol optical and microphysical properties as well as its radiative and climatic influences to the aerosol mixing state assumptions (e.g., [41, 124–128]). Accordingly, the effort of understanding the internal/external mixture assumptions, along with their consequential aspects (via modifying the RegCM4-aerosol model parameterizations), is currently in progress [129], while the sea salt particles contribution is primarily noted only within limited coastal areas of South Africa, following the rise of south-easterly wind speed for a short period of time (e.g., [2]). Thus, for meanwhile our simulations do not encompass marine aerosols. Additionally, the simulation does not take into account the long-wave effects of carbonaceous and sulfate particles. In fact, the particle interaction with thermal infrared radiation is significant if the aerosols are large in size such as for dust and sea salt particles. For smaller aerosols, the extinction coefficient decreases rapidly with increasing wavelength (e.g., [90, 130]). Therefore, omitting the long-wave radiation effects of carbonaceous and sulfate particles will not impose a significant error in long-wave radiation computation, as well as in assessing the direct and semi-direct effects of these particles.

2.3. Emission Datasets. In this study, the emission estimates of black carbon (BC) and organic carbon (OC) particles, and sulfur dioxide (SO_2) which are induced from anthropogenic and biomass burning activities are derived from two recently updated emission inventories: MACCity [131] and Global Fire Emissions Database, version 3 (GFED3) [132], respectively. Both inventories are provided at spatial resolution of 0.5×0.5 degree over the globe with a monthly temporal resolution. The MACCity inventory is the upgraded extension of ACCMIP (Atmospheric Chemistry and Climate-Model Intercomparison Project) emissions dataset [131]. Covering a period from 1990 to 2010, this emission database provides various gases and aerosol species, which are contributed from different anthropogenic sectors such as power plant, industrial activities, and transportations. The GFED3 inventory applies global scale satellite-derived products such as vegetation characteristics, productivity, and burned area estimates, along with a fire module of a biogeochemical model, as well as several conditions to estimate emissions

© University of Pretoria

from biomass burning activities (i.e., from grass, peat, woodland, forest, open savanna, deforestation fires, and agricultural waste burnings; see Giglio et al. [133] and van der Werf et al. [132, 134]. Further details of GFED3 approaches and spatio-temporal emission variability are compressively described in van der Werf et al. [132] and references therein. This dataset contains several trace gases and particulate matter which emitted from these open biomass burning activities, for the period from 1997 to 2009.

2.4. Experimental Design. For the purpose of evaluating the coupled model's (i.e., RegCM4-aerosol model) capability of simulating the total atmospheric aerosol optical parameters, as well as extracting the aerosol-induced climate-impact signal from the underlying noise, a long term simulation is essential. Implementing the above recently updated emission inventories we have conducted a series of simulations, which extends from January 1997 to December 2008 and analyses the recent 11 years' results. To eliminate boundary effects (e.g., [135, 136]), the simulation domain is designed to be larger than the area of interest; that is, our simulation domain (from 5.5°E to 47.1°E and from 37.5°S to 18.6°S) encompasses the entire South Africa and its surrounding land/ocean regions (Figure 1) at a horizontal grid resolution of 60 km with 18 vertical layers. Though, the finest horizontal resolution of RegCM4 can be set to 10 km; considering our domain size, the horizontal spacing used in this study is fairly adequate to make a multiyear simulation with a reasonable computational time. Taking into account the aerosol influence on radiation, as well as the two-way aerosol-climate feedbacks, all the ten tracers available in RegCM4 are included in our simulation under external mixture assumption. The European Centre for Medium-Range Weather Forecasts (ECMWF) reanalysis ERA interim (ERAIN: [137, 138]) and the weekly mean product of National Ocean and Atmosphere Administration's (NOAA) Optimum Interpolated sea surface temperature (OISST) [139] are implemented for limited-area model that required time-dependent initial and lateral boundary conditions. The simulations presented here use a time setup of 10 minutes for surface parameter files (topography, land use, vegetation, soil type, etc.), along with the dynamical model time step of 150 seconds and 6 hours updating lateral boundary conditions. Most of the model's climatic schemes, as well as meteorological lateral boundary condition selections, are based on Tummon [80] sensitivity and performance studies of RegCM schemes over Southern Africa. Since this work is the first step towards applying the RegCM4-aerosol model for the investigation of radiative and climatic effects of different types of aerosol over South Africa, we have tested and discussed the model's performance in terms of computing different optical fields of aerosols over this region only.

2.5. Observational Data

2.5.1. AERONET Surface Observation. The Aerosol Robotic Network (AERONET) is a global ground-based network of automated sun-photometer measurements [140]. AERONET provides aerosol optical depth and surface solar flux, as well as employing improved retrieval algorithms; it delivers different sets of atmospheric column aerosol optical and microphysical parameters (e.g., [141]). Even if there are different AERONET stations in South Africa, only one site has continuous AOD observations (from 1998 to 2008), that is, at Skukuza (24°S, 31°E; see Figure 1). In the present work, quality-assured dataset (Level 2.0) of AERONET aerosol optical depth (AOD at 500 nm) from this site is used for comparison with the AOD derived from the model simulations.

2.5.2. MISR Satellite Observation. Multiangle Imaging SpectroRadiometer (MISR) was launched by the National Aeronautics and Space Administration (NASA) on December 18, 1999 and has been in operation since February 2000. The device consists of nine push broom cameras arranged to view at nominal zenith angles relative to the surface reference ellipsoid of 0.0°, ±26.1°, ±45.6°, 18 ± 60.0°, and ±70.5° and measures upwelling short wave radiance in each camera at four spectral bands, centered at 446, 558, 672, and 866 nm [142]. With high spatial resolution and a better radiometrical and geometrical accuracy, the multiple angle-band observations of MISR allow the retrieval of a number of aerosol optical and microphysical properties over land (including a bright desert surfaces) and ocean [36–38, 100, 143–145]. Furthermore, MISR-AOD retrievals (level-3 data) have a higher grid resolution ($0.5^\circ \times 0.5^\circ$) in comparison to the Moderate Resolution Imaging Spectroradiometer (MODIS) of Level-3 which has the resolution of $1^\circ \times 1^\circ$. In the present study from MISR-level-3-monthly-averaged datasets (version 31, which are available from 2000 onward), the AOD and SSA at 558 nm are utilized to evaluate the simulated results.

2.5.3. LIDAR Observation. A mobile LIDAR system was developed at the Council for Scientific and Industrial Research (CSIR), National Laser Centre (NLC), Pretoria (25°5°S; 28°2°E), South Africa [146, 147]. At present, the CSIR-NLC mobile LIDAR can provide aerosol backscatter measurements at 532 nm for the altitude region from ground to 40 km with a height resolution of 10 m [148–150]. For a better understanding of the atmospheric boundary layer evolution and aerosol concentrations, during October 2008 the LIDAR experiment has been performed at the University of Pretoria (25.7°S; 28.2°E). The experiment has been made continuous for 23 hour measurement, that is, from 16 October, 16 h00 to 17 October, 15 h00. To assess the model's performance in simulating the vertical distribution of aerosols, LIDAR retrieved extinction coefficient profiles from this experiment are compared with the corresponding model-simulated results.

3. Results and Discussion

In the following subsections, we present the RegCM4-aerosol model's estimated aerosol optical field evaluation results, over South Africa. The magnitude and temporal variability of simulated columnar AOD comparison with AERONET and MISR observations at Skukuza (24S, 31E) is given in Section 3.1. The latitudinal variations of simulated AODs

© University of Pretoria

and SSAs values within South Africa, in comparison with their corresponding column-integrated MISR retrievals, are provided in Section 3.2. Further, the simulated aerosol extinction coefficient profiles with respect to ground-based CSIR-mobile LIDAR retrievals are presented in Section 3.3. The geographical location of the surface observation sites, that is, for AERONET and LIDAR, is shown in Figure 1. One of the important factors that propagate a bias in simulated aerosol concentration in model predicted aerosol optical fields is the model's insufficiency in simulating meteorological fields. In this context, even though the evaluation of model estimated meteorological parameters is beyond the scope and the aim of this study, to clarify some of the disparities between simulated and measured optical parameters, the bias in model estimated meteorological parameter, in comparison with specific meteorological sites, is presented in Appendix.

3.1. Comparisons with AERONET and MISR. The comparison of model-simulated monthly-averaged AOD (at 550 nm) with the available data from AERONET (at 500 nm) and MISR (at 558 nm) observations at Skukuza (24°S, 31°E), South Africa, is shown in Figure 2. Skukuza is situated in a region of the northeastern area of the Mpumalanga province (see Figure 1), which is relatively close to the major industrial areas of South Africa (i.e., Gauteng and western areas of Mpumalanga). This site is influenced by several aerosols, which are induced from various local activities, for instance, primary/secondary aerosols from frequently occurring local biomass burning activities (e.g., [69, 80]), a variety of agricultural practices, and natural-resource based industrial activities, such as coal production (e.g., [72, 77]). Besides, the conveyance of aerosols from the main industrial Highveld regions of South Africa and the slight contribution of long-range transported particles are the additional sources of aerosols for this site (e.g., [85, 151, 152]). In reproducing the magnitude of AERONET and MISR AOD values, the model relatively performs well. At least the magnitudes of simulated AODs are within the standard deviation of AERONET and ±25% of MISR observations. The other important aspect in studying the climatic role of aerosols is the model's performance in capturing the temporal evolution of aerosol loading. In this regard, the model shows a good performance of capturing the seasonal and interannual variability of AOD (i.e., the temporal pattern of simulated AOD exhibits a temporal correlation coefficient of ~0.6 when compared with both observations).

Under cloud-free conditions, the AERONET AOD uncertainties for wavelengths > 400 nm are quite small (< ±0.01, [94]); therefore, taking AERONET measurements as a reference in our evaluation during some years one/two month advance/late predictions of maximal/minimal values of AOD by the model has been noted. Nevertheless, similar levels of temporal pattern inconsistencies, between AERONET and MISR measurements, are also seen. Such arbitrarily occurring temporal biases on simulated AODs are most likely related (at least partially associated) to three factors: (1) since the air quality around this site is strongly influenced by biomass burning events and different

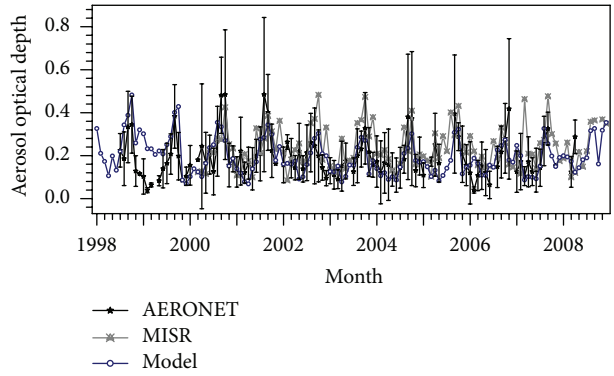

Figure 2: The comparison of RegCM4-aerosol model simulated monthly-averaged column-integrated aerosol extinction optical depth (at 550 nm—blue solid line) with its corresponding observations derived from MISR (at 558 nm—gray dotted line) and AERONET (at 500 nm—black solid line denoting the values and standard deviation), at Skukuza, South Africa.

industrial activities, uncertainties associated with biomass burning/anthropogenic/sporadic urban emissions estimates by the emission inventories used in our simulations will impose such temporal biases (e.g., [80, 101]); (2) it is also likely that the bias in simulated meteorological fields could be a contributing factor in inducing temporal evolution biases on simulated aerosol concentrations, in turn in model predicted AOD patterns (e.g., [30, 34, 57, 153]), and (3) biases that propagate from the interpolation scheme used to get model AOD at the AERONET site.

3.2. Comparison of Simulated and MISR Satellite-Observed AOD and SSA Latitudinal Variations. In order to evaluate the model performance in capturing the spatial variability of column-integrated AODs and SSAs values, the simulated results are compared with MISR observations. The 9-year (i.e., from 2000 to 2008) simulated AOD and SSA values (at 550 nm) are averaged over the longitudinal range, which encompasses only South Africa; subsequently their latitudinal variations (i.e., from the lower tip of Western Cape to the upper end of Limpopo, see Figure 1) in comparison with the corresponding MISR retrieved data (at 558 nm) are presented in Figures 3(a) and 3(b), respectively. Over most of the latitudinal locations which correspond to Gauteng, Mpumalanga, North West, and Western Cape regions, the simulated columnar AOD values are within the standard deviation of MISR observations. However, over the latitudinal locations which comprise the Northern Cape, KwaZulu Natal, Free State, and most areas of the Eastern Cape regions, the model slightly overestimates the AOD values with respect to the MISR observations. In contrast, relative to MISR retrieval, the model underestimates the AOD signal in Limpopo province (i.e., within latitudinal range of 25.5°S to 22°S). Within latitudinal ranges that extend from the southern tip of the Western Cape to central areas of Gauteng (except at 34.5°S), the model's estimated SSA values are within the standard deviation of MISR observations. However, this comparison shows a slight positive bias that varies from +0.6

© University of Pretoria

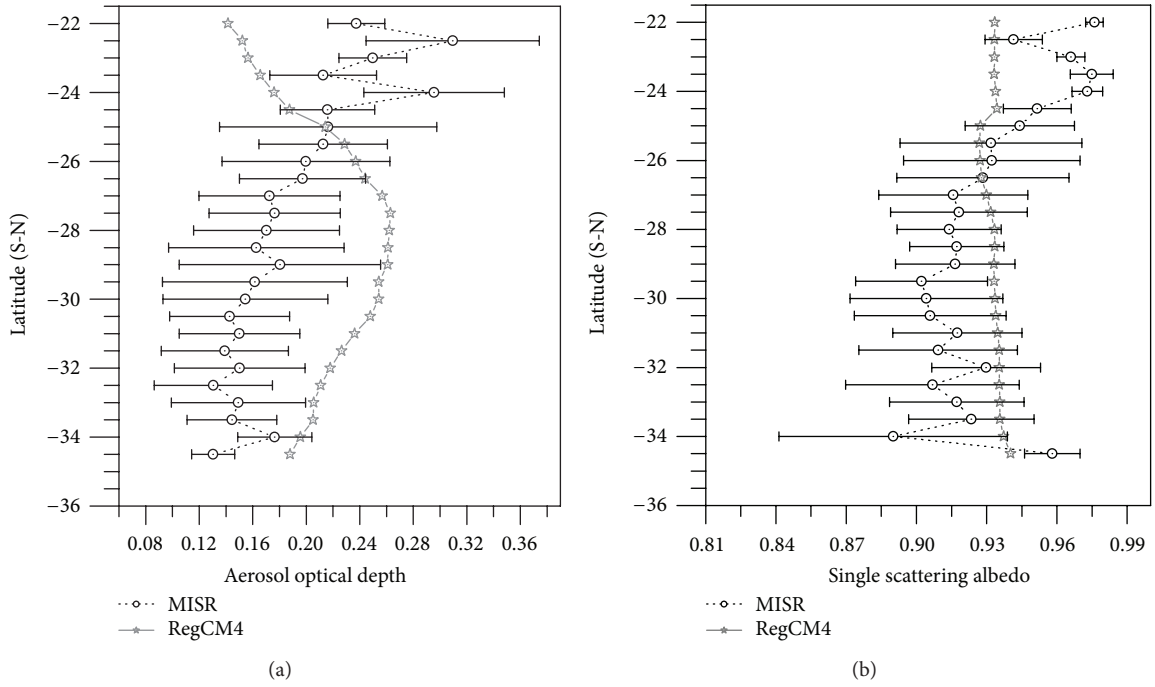

FIGURE 3: The latitudinal variation of the 9 years averaged column-integrated (a) AOD and (b) SSA values over South Africa, which are derived from MISR (at 558 nm—black dot line denoting the values and its standard deviation) and the model (at 550 nm—gray solid line).

to +4% relative to MISR mean values. For latitudinal locations which are above 25°S the model's predicted SSA values are lower than their corresponding MISR retrieved mean values.

The aerosol characteristics extracted from model simulations such as the distributions of atmospheric aerosol concentrations (in turn, their optical properties), the rate of production, and removal of particles are mostly controlled by meteorological parameters, which are highly variable both temporally and spatially (e.g., [2, 30, 31, 34, 153]). The model's performance in computing the actual precipitation values and patterns has a central role in determining the removal of aerosols from the atmosphere via wet deposition processes, as well as in regulating the soil moisture which in turn influences the dust production (e.g., [30, 31, 63]). As a result, the biases in the model's estimated precipitation values, in turn the aerosol concentrations, will significantly affect the robustness of simulated aerosol optical properties (e.g., [30, 57, 80, 154]). Even though it is not the intention of the current work to evaluate the simulated meteorological parameters, in order to decipher their contribution to the accuracy of model's estimated values of AOD and SSA, within a latitudinal range of 33.5°S to 27°S, it is valuable to assess the bias in the model's estimated precipitation values. For this purpose, a single South African weather service (SAWS) metrological station's datasets (only one representative station per Province) are used as representative of these provinces and are compared with simulated results (see Appendix, Figures 4 and 5). The comparison period covers 108 months (from 2000 to 2008; please see Appendix). From the total compared months in Bloemfontein (29.1°S, 26.3°E) which is in Free State and Upington (28.4°S, 21.3°E) which is in Northern Cape, ~80% of simulated precipitation values are in a negative bias (see Appendix, Figure 5).

The processes that control the dust emission through wind erosion are quite different to those involved in the anthropogenic/biomass burning emissions [29, 63]. The computation of naturally emitted dust production involves numerous criteria of land surface characterization. It also depends upon the model's capability of simulating different meteorological fields and land surface conditions. One of the surface parameters that determine the dust production is soil moisture (e.g., [63, 155]) The model's predicted precipitation values exhibit a dry bias, which in turn will cause the surface to become dry and favorable for excessive dust particles emission depending on the wind intensity, [63, 156, 157]. Concurrently, the dry bias in simulated precipitation values will elongate the atmospheric residence time of the particles by reducing the wet removal rate (e.g., [30, 31, 158]). Soil dust particles do not readily dissolve in water ([159] and references therein); thus the negative bias in simulated precipitation will especially extend the atmospheric life-time of hydrophilic aerosols such as sulfate aerosols [30, 80].

Within the simulation domain of the present work, the arid/semiarid regions of the Northern Cape, as well as Namibia and Botswana, are major sources of wind-induced desert dust particles over South Africa ([2, 160] and references therein). Moreover, as presented in Tesfaye et al. [121] the largest contribution of sulfate aerosols to the total AOD is found in the Free State province of South Africa. In the visible part of the spectrum, excluding the slight absorption influence of larger dust particles [161], both dust and sulfate aerosols have a prevailing role of scattering (i.e., these aerosols

© University of Pretoria

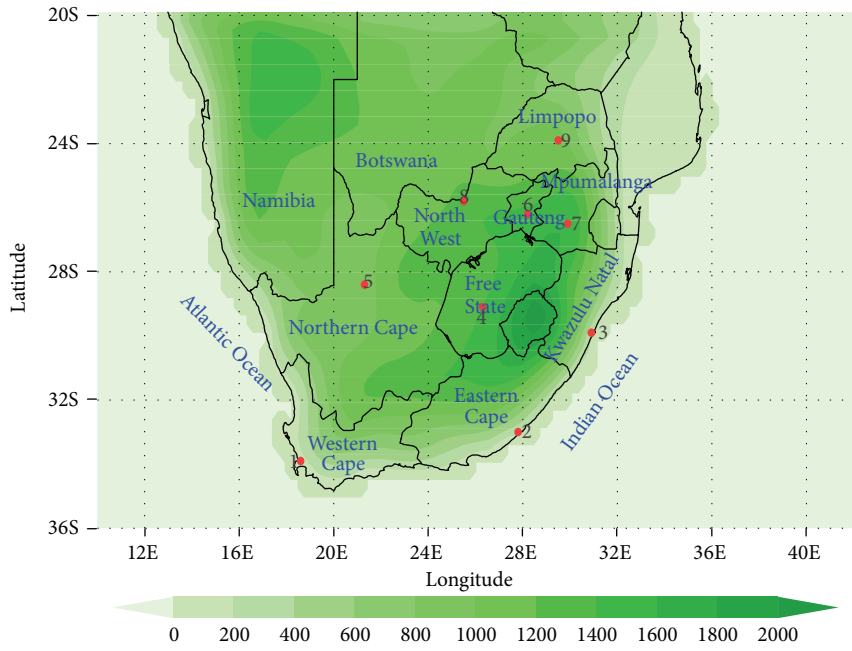

Figure 4: Model domain and topography (unit: m). The selected SAWS station locations are numbered as (1) Cape Town (33.9°S, 18.6°E), (2) East London (33.0°S, 27.8°E), (3) Durban South (29.9°S, 30.9°E), (4) Bloemfontein (29.1°S, 26.3°E), (5) Upington (28.4°S, 21.3°E), (6) Johannesburg (26.2°S, 28.2°E), (7) Ermelo (26.5°S, 29.9°E), (8) Mafikeng (25.8°S, 25.5°E), and (9) Polokwane (23.9°S, 29.5°E).

have higher values of SSA) (e.g., [88, 90, 92]). Connecting all the aforementioned interrelated actualities, it is evident that within latitudinal range of 33.5°S to 27°S (i.e., which includes the Northern Cape and Free State provinces of South Africa as well as the nearby regions; see Figure 1), the model's estimated higher values of AOD and SSA (relative to MISR retrieval, Figure 3) may have been caused by the overestimated dust and sulfate aerosol atmospheric concentrations. This is also ensued due to the prevailing dry bias incidences around the primary source region of these aerosols (see Appendix, Figure 5).

Even though the arid/semiarid surfaces are the main source areas of dust particles, anthropogenic activities induced land surface degradations that are related to agricultural use, mining activities, and many other events result in an increment in wind-generated dust production (e.g., [162]). The areas of South Africa which are bounded within a latitudinal range of 25°S to 22°S (i.e., the Limpopo province) are highly populated with different mining and agricultural practices. Consequently, these activities will raise the dust emission in local and regional scales. However, the RegCM4 dust emission parameterizations are effective for cells which are dominated by desert and semidesert land cover only [63]. Therefore, primarily owing to the lack of cooperating anthropogenic activity-related dust production in Limpopo province (i.e., 25°S to 22°S), the model underestimates the AOD, as well as SSA values with respect to MISR observations (Figure 3). Such bias, in turn, will affect the accuracy of the model's estimated direct and semi-direct radiative effects of total aerosols.

Due to the high dynamical nature of human activities, it is challenging to estimate anthropogenic events triggered by dust load. The above results notify the necessity of cooperating these particles for a better representation of bulk aerosol and its climatic roles in South Africa. Besides the above primary reason, the shortage of accounting the long-range transported particles in the model—especially from mining industries of Zambian to Limpopo areas (25°S to 22°S)—will have a slight contribution to the observed essential differences in Figure 3 (e.g., [163]). As a final point, as indicated in Section 2, our simulation did not take into account marine aerosols. In the meanwhile, at Cape Town's (33.9°S, 18.6°E) metrological site, largely positive biases in simulated precipitation values were noted (see Appendix, Figure 5), this will result in an overestimation of aerosol wet deposition (e.g., [30, 31]). Therefore, most likely related to these two factors, the model's estimated SSA values around the Cape Point (i.e., 34.5°S) are slightly underestimated with respect to MISR observations.

3.3. Comparisons with LIDAR. The aerosol extinction coefficient profiles that are retrieved from the LIDAR experiment (532 nm; see Section 2.5.3) on 16 October observation at 18:00 and 17 October at 00:00 and 06:00 were compared to their corresponding model results (550 nm) and provided in Figures 6(a)–6(c), respectively. In all comparisons, except at 18:00, both experimental and simulated profiles exhibit larger extinction coefficients below the altitude of 6 km. Above 6 km (i.e., above ~490 hPa), the simulated extinction profiles display a more rapid decline than the experimental observation. Especially on 16 October (at 18:00) and 17 October (at 06:00), considerable discrepancies between the model's and LIDAR's extinction profiles, above the height region of

© University of Pretoria

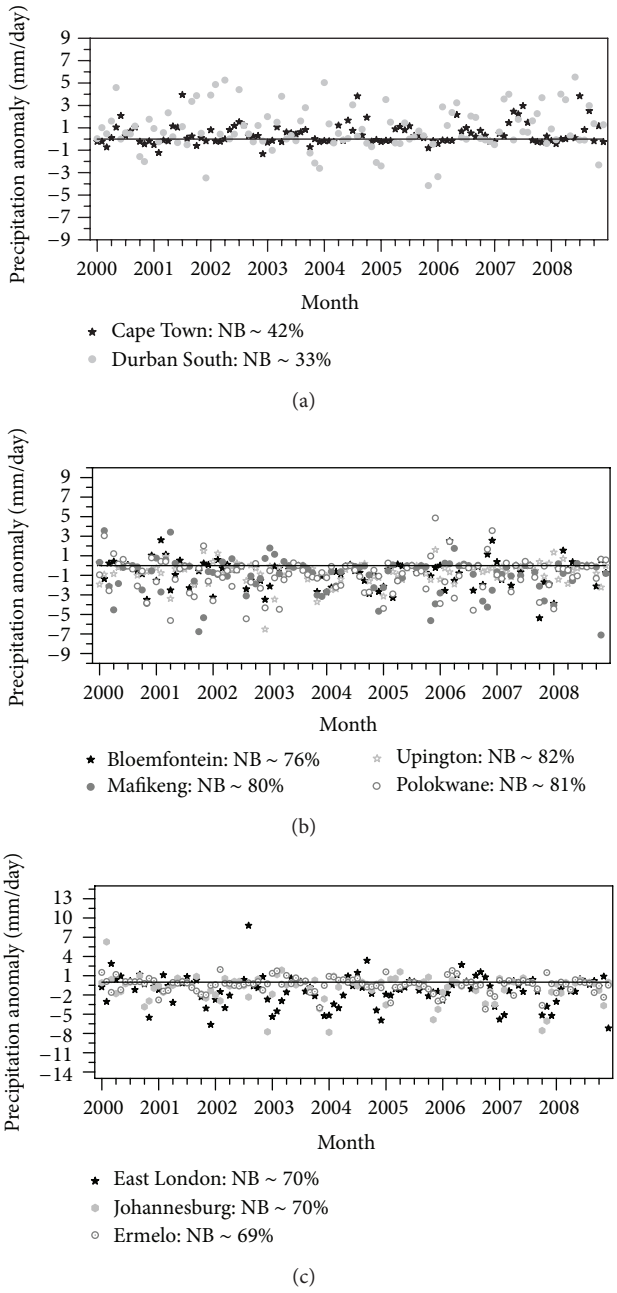

Figure 5: The bias in RegCM4 estimated total daily precipitation (mm/day) in comparison with the specific metrological station's data. From the total compared months (108 months, i.e., 2000 to 2008) the percentage of the number of points that exhibit a negative bias (NB) is given in each plot.

6 km, have been noted. Using the same LIDAR datasets and air mass trajectory analysis, Tesfaye et al. [150] showed that particles above the height region of 6 km were particularly donated from long-range transportation processes. However, related with our future concern of investigating different types of aerosol impacts on South African climate—especially those which are originated in and around South Africa, we have configured the domain (see Figure 1), as well as the inflow/outflow boundary conditions, in order to account only for the natural and anthropogenic aerosol sources in and around South Africa. These configurations neglect the contribution of aerosols from external sources (which are outside of the domain) to the regional aerosol budget. This may partially attribute for the differences between experimental and simulated extinction profiles which are noted above the altitude profile of 6 km.

In overall, to regulate the complex semidirect effect of aerosols—especially their role in cloud cover, studies have shown the importance of the relative position of the aerosol layer with respect to the cloud position (e.g., [16, 17]). Nonetheless, there are several factors that will impose substantial inaccuracies on simulated profiles of aerosol optical properties such as, the model's deficiency in representing convective processes (e.g., [57, 65, 68]), the number of aerosol components which are cooperated in the model along with their mixing state hypothesis (e.g., [5, 124]), and the various aspects which are mentioned in Section 1. Considering the presence of these all confining circumstances which will inflict discrepancies between simulated and LIDAR profiles, the model exhibits quite satisfactory performance in capturing the major aerosol extinction profiles. Although in our discussion several factors that will impose a bias on simulated aerosol optical signals are highlighted; at this scope of the study it is difficult to accurately assess the contribution of each factors in-depth and to point out which one is more responsible for enforcing these biases.

4. Summary and Concluding Remarks

Before we employ the Regional Climate Model-RegCM4 for the investigation of direct and semi-direct effects of aerosols over South Africa, in this study its performance to capture the observed aerosol optical properties has been evaluated and discussed. The evaluations were performed by comparing the simulated columnar Aerosol Optical Depth (AOD) and Single Scattering Albedo (SSA) against ground-based (AERONET) and satellite (Multiangle Imaging SpectroRadiometer: MISR) observations. Additionally, the simulated aerosol extinction profiles were compared with ground-based LIDAR retrieval. In our current contribution, the following conclusions can be drawn.

(i) At Skukuza (24°S, 31°E), the values of simulated AOD were within the standard deviation of AERONET and ±25% of MISR observations. Occasionally, the model-estimated maximum/minimum AOD values displayed a slight temporal shift with respect to AERONET observations. Nonetheless, such irregularly occurring temporal biases, as well as magnitude differences, are also noted among the MISR and AERONET platform estimates. In this frame, the model's simulated AOD climatology at Skukuza site is legitimately acceptable.

(ii) Considering the longitudinal range which includes only South Africa—the 9-year averaged values of simulated AOD and SSA latitudinal variations were also compared with the corresponding values retrieved

© University of Pretoria

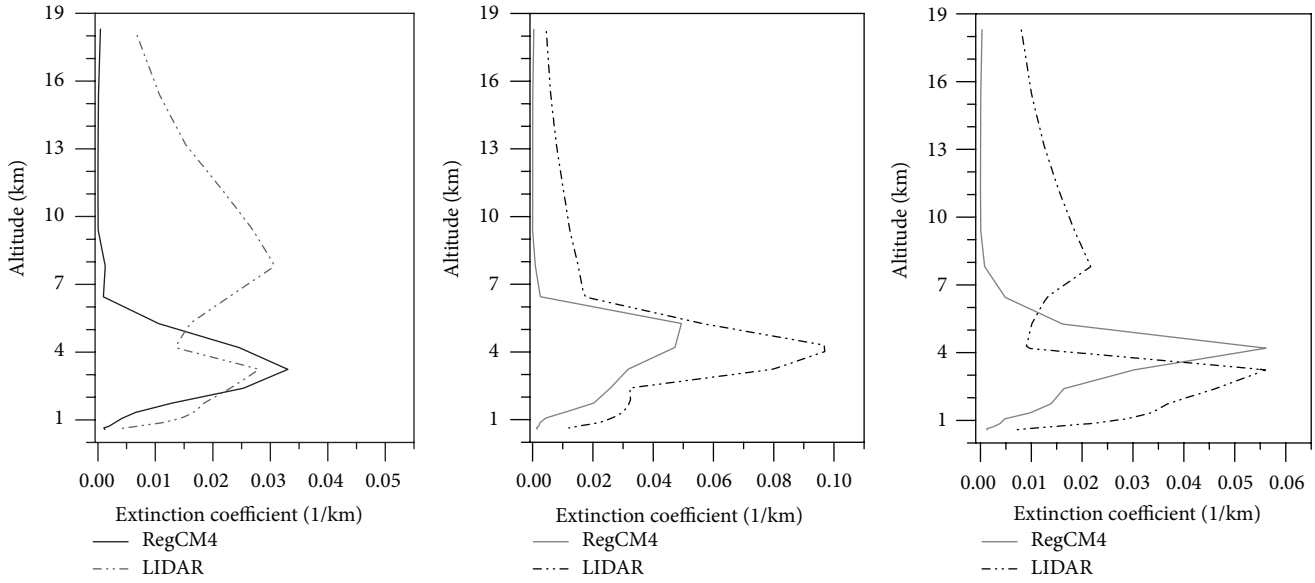

FIGURE 6: Aerosol extinction coefficient profiles, retrieved from LIDAR measurements at Pretoria (black dash-dot line) and its corresponding profiles provided by RegCM4 (gray line) (a) on 16 October at 18:00, (b) and (c) on 17 October at 00:00 and at 06:00, respectively.

from MISR observations. Within a latitudinal range of 26.5°S to 24.5°S, the simulated columnar AOD values were within the standard deviation of MISR. However, within the regions of 33.5°S to 27°S, the model tends to predict slightly higher values of AOD relative to MISR observation. This was predominantly caused by the negative (dry) bias in simulated precipitation that leads to the overestimation of dust and sulfate aerosol loads over these regions.

(iii) With respect to MISR, over the latitudinal range that corresponds to the Limpopo province (i.e., 25°S to 22°S), the model underestimates both AOD and SSA signals. This was primarily due to the model's shortage in cooperating the anthropogenic activities prompted dust loads, such as dust from agricultural and mining practices. Therefore, in our region of interest (i.e., South Africa), this is considered as the main deficiency of RegCM4. Besides, in most of the latitudinal ranges, the simulated SSA values were within standard deviations of MISR observations.

(iv) Excluding the model's underestimated extinction coefficient profiles above 6 km, RegCM4 performs very well in capturing the main aerosol extinction profiles, relative to LIDAR measurements. The aerosol extinction signals at higher altitude (>6 km) were donated by long-range transportation of particles from regions which were outside our simulation domain.

(v) Relative to observational data, the model fairly reproduced optical properties of aerosols. This affirmed that sulfate and carbonaceous aerosols from both anthropogenic and biomass burning activities and wind eroded desert dust particles were the main aerosol components in the South African atmosphere.

(vi) Overall, RegCM4 appeared to be a suitable tool for the examination of the direct and semi-direct effects of aerosols over the South African regional climate.

(vii) In the series of studies to follow, we will provide the distribution, direct and semi-direct effects of wind eroded desert dust particles, and the different species of aerosols which were induced from anthropogenic and biomass burning sectors, in South Africa [118–121]. Thus, we would like to remark here that, in the present study, a bit of an extended general introduction, as well as a brief description about RegCM4, was addressed. Parts of these sections will be used as the basic framework for those of our future studies.

Appendix

The meteorological parameters such as precipitation, relative humidity, temperature, and wind speed play a major role in determining aerosol dynamics, as well as the changes in aerosol optical and physico-chemical properties (e.g., [2, 34, 153]). The model's deficiency in representing the actual precipitation values and patterns will impose a significant bias simulated aerosol production (via influencing surface wetness), as well as their atmospheric lifetime and concentration (via influencing wet aerosol deposition) [2, 30, 31]. The biases in simulated aerosol concentrations will consequently affect the model's accuracy in computing the optical properties of aerosols. Therefore, comparing the simulated precipitation values, with respect to the South Africa Weather Service (SAWS) metrological station observations, the biases in

© University of Pretoria

UNIVERSITEIT VAN PRETORIA
UNIVERSITY OF PRETORIA
YUNIBESITHI YA PRETORIA

model's predicted precipitation values are estimated. For this purpose, from each province of South Africa, a single weather service station is designated as a representative of these areas (Figure 4).

The bias in simulated total precipitation, while being compared to the datasets of the specific metrological sites, is shown in Figure 5. Generally, excluding the stations which are nearby the coastal areas of South Africa (i.e., Cape Town and Durban South stations, Figure 5(a)), the model predominantly exhibits a negative bias (Figures 5(b) and 5(c)); that is, out of total compared months in 75% ± 5% of the points RegCM4 tends to underestimate the total daily precipitation values. The dry bias over the west (i.e., at Upington station, Figures 4 and 5(b)) and central (i.e., at Bloemfontein station, Figures 4 and 5(b)) parts of South Africa will promote the over emission of wind eroded dust particles and reduced wet deposition of hydrophilic aerosols. The precipitation bias in these comparisons has to be considered under caution; this is not a complete indicator of the overall performance of the model.

The model might actually be a demonstration of the region, but may not match exactly with the precise site observations. Further, the bias in metrological parameters can be induced by numerous complex factors such as radiation balance and energy flux inaccuracies induced through aerosol processes and surface properties (such as surface albedo), temperature advection, and cloud process representations [30, 57, 68, 164, 165]. However, determining the actual cause of these metrological parameter biases requires a further deep examination of the model's physics in representing the atmospheric dynamics, cloud, and surface processes as well as several other factors, which is beyond the scope of this study. Nevertheless, the expressive correlation between the biases in simulated AOD and precipitation values strengthens the remarkable importance of interactive coupling of aerosol-climate interactions.

Acknowledgments

The authors are grateful to Addis Ababa University, Department of Physics, for providing computational facilities. For the accessibility of RegCM model, the authors are thankful to the International Centre for Theoretical Physics (ICTP). The authors would like to acknowledge the AERONET, MISR, and SAWS for providing an easy access to the datasets used in this study. They are also indebted to Teresa Faleschini, Tamene Mekonnen, Fiona Tummon, and Addisu Gezahegn, for their valuable assistances. This work was supported by the African Laser Centre and NRF bi-lateral research grant (UID: 68688/65086), in addition to CSIR National Laser Centre.

References

[1] J. E. Penner, M. Andreae, H. Annegarn et al., "Aerosols, their direct and indirect effects," in *Climate Change 2001: The Scientific Basis. Contribution of Working Group I to the Third Assessment Report of the Intergovernmental Panel on Climate Change*, J. T. Houghton, Y. Ding, D. J. Griggs et al., Eds., pp. 289–348, Cambridge University Press, Cambridge, UK, 2001.

[2] M. Tesfaye, V. Sivakumar, J. Botai, and G. M. Tsidu, "Aerosol climatology over South Africa based on 10 years of multiangle imaging spectroradiometer (MISR) data," *Journal of Geophysical Research D*, vol. 116, no. 20, Article ID D20216, 2011.

[3] D. T. Shindell, H. Levy II, M. D. Schwarzkopf, L. W. Horowitz, J.-F. Lamarque, and G. Faluvegi, "Multi-model projections of climate change from short-lived emissions due to human activities," *Journal of Geophysical Research*, vol. 113, Article ID D11109, 2008.

[4] IPCC, "IPCC fourth assessment report (AR4)," in *Climate Change 2007: The Physical Science Basis. Contribution of Working Group I to the Fourth Assessment Report of the Intergovernmental Panel on Climate Change*, S. Solomon, D. Qin, M. Manning et al., Eds., p. 996, Cambridge University Press, Cambridge, UK, 2007.

[5] J. Haywood and O. Boucher, "Estimates of the direct and indirect radiative forcing due to tropospheric aerosols: a review," *Reviews of Geophysics*, vol. 38, no. 4, pp. 513–543, 2000.

[6] J. Hansen, M. Sato, R. Ruedy et al., "Efficacy of climate forcings," *Journal of Geophysical Research*, vol. 110, Article ID D18104, 2005.

[7] J. Hansen, M. Sato, and R. Ruedy, "Radiative forcing and climate response," *Journal of Geophysical Research*, vol. 102, no. 6, pp. 6831–6864, 1997.

[8] P. Forster, V. Ramaswamy, P. Artaxo et al., "Changes in atmospheric constituents and in radiative forcing," in *Climate Change 2007: The Physical Science Basis. Contribution of Working Group I to the Fourth Assessment Report of the Intergovernmental Panel on Climate Change*, S. Solomon, D. Qin, M. Manning et al., Eds., Cambridge University Press, Cambridge, UK, 2007.

[9] A. S. Ackerman, O. B. Toon, D. E. Stevens, A. J. Heymsfield, V. Ramanathan, and E. J. Welton, "Reduction of tropical cloudiness by soot," *Science*, vol. 288, no. 5468, pp. 1042–1047, 2000.

[10] R. L. Miller and I. Tegen, "Climate response to soil dust aerosols," *Journal of Climate*, vol. 11, no. 12, pp. 3247–3267, 1998.

[11] M. Z. Jacobson, "Control of fossil-fuel particulate black carbon and organic matter, possibly the most effective method of slowing global warming," *Journal of Geophysical Research D*, vol. 107, no. D19, p. 4410, 2005.

[12] I. Koren, Y. J. Kaufman, L. A. Remer, and J. V. Martins, "Measurement of the effect of Amazon smoke on inhibition of cloud formation," *Science*, vol. 303, no. 5662, pp. 1342–1345, 2004.

[13] J. Cook and E. J. Highwood, "Climate response to tropospheric absorbing aerosols in an intermediate general-circulation model," *Quarterly Journal of the Royal Meteorological Society*, vol. 130, no. 596, pp. 175–191, 2004.

[14] Y. Zhang, *The radiative effect of aerosols from biomass burning on the transition from dry to wet season over the Amazon as tested by a regional climate model [Ph.D. thesis]*, Georgia Institute of Technology, Atlanta, Ga, USA, 2008.

[15] C. E. Chung, V. Ramanathan, and J. T. Kiehl, "Effects of the South Asian absorbing haze on the northeast monsoon and surface-air heat exchange," *Journal of Climate*, vol. 15, no. 17, pp. 2462–2476, 2002.

[16] B. T. Johnson, K. P. Shine, and P. M. Forster, "The semi-direct aerosol effect: impact of absorbing aerosols on marine stratocumulus," *Quarterly Journal of the Royal Meteorological Society*, vol. 130, no. 599, pp. 1407–1422, 2004.

© University of Pretoria

[17] G. Feingold, H. Jiang, and J. Y. Harrington, "On smoke suppression of clouds in Amazonia," *Geophysical Research Letters*, vol. 32, no. 2, Article ID L02804, 2005.

[18] J. E. Penner, S. Y. Zhang, and C. C. Chuang, "Soot and smoke aerosol may not warm climate," *Journal of Geophysical Research D*, vol. 108, no. 21, pp. 1–9, 2003.

[19] D. Koch and A. D. Del Genio, "Black carbon semi-direct effects on cloud cover: review and synthesis," *Atmospheric Chemistry and Physics*, vol. 10, no. 16, pp. 7685–7696, 2010.

[20] R. J. Allen and S. C. Sherwood, "Aerosol-cloud semi-direct effect and land-sea temperature contrast in a GCM," *Geophysical Research Letters*, vol. 37, no. 7, Article ID L07702, 2010.

[21] S. Twomey, "The influence of pollution on the shortwave albedo of clouds," *Journal of the Atmospheric Sciences*, vol. 34, pp. 1149–1152, 1977.

[22] B. A. Albrecht, "Aerosols, cloud microphysics, and fractional cloudiness," *Science*, vol. 245, no. 4923, pp. 1227–1230, 1989.

[23] U. Lohmann and J. Feichter, "Global indirect aerosol effects: a review," *Atmospheric Chemistry and Physics*, vol. 5, no. 3, pp. 715–737, 2005.

[24] F. J. Dentener, G. R. Carmichael, Y. Zhang, J. Lelieveld, and P. J. Crutzen, "Role of mineral aerosol as a reactive surface in the global troposphere," *Journal of Geophysical Research D*, vol. 101, no. 17, pp. 22869–22889, 1996.

[25] R. R. Dickerson, S. Kondragunta, G. Stenchikov, K. L. Civerolo, B. G. Doddridge, and B. N. Holben, "The impact of aerosols on solar ultraviolet radiation and photochemical smog," *Science*, vol. 278, no. 5339, pp. 827–830, 1997.

[26] W. L. Chameides, H. Yu, S. C. Liu et al., "Case study of the effects of atmospheric aerosols and regional haze on agriculture: an opportunity to enhance crop yields in China through emission controls?" *Proceedings of the National Academy of Sciences of the United States of America*, vol. 96, no. 24, pp. 13626–13633, 1999.

[27] H. R. Anderson, "Differential epidemiology of ambient aerosols," *Philosophical Transactions of the Royal Society A*, vol. 358, no. 1775, pp. 2771–2785, 2000.

[28] G. Oberdorster, J. Finkelstein, J. Ferin et al., "Ultrafine particles as a potential environmental health hazard: studies with model particles," *Chest*, vol. 109, no. 3, 1996.

[29] F. Solmon, F. Giorgi, and C. Liousse, "Aerosol modelling for regional climate studies: application to anthropogenic particles and evaluation over a European/African domain," *Tellus, Series B*, vol. 58, no. 1, pp. 51–72, 2006.

[30] B. Croft, J. R. Pierce, R. V. Martin, C. Hoose, and U. Lohmann, "Uncertainty associated with convective wet removal of entrained aerosols in a global climate model," *Atmospheric Chemistry and Physics*, vol. 12, pp. 10725–10748, 2012.

[31] N. Oshima, Y. Kondo, N. Moteki et al., "Wet removal of black carbon in Asian outflow: Aerosol Radiative Forcing in East Asia (A-FORCE) aircraft campaign," *Journal of Geophysical Research D*, vol. 117, no. 3, Article ID D03204, 2012.

[32] D. T. Shindell, M. Chin, F. Dentener et al., "A multi-model assessment of pollution transport to the Arctic," *Atmospheric Chemistry and Physics*, vol. 8, no. 17, pp. 5353–5372, 2008.

[33] V. Ramanathan, P. J. Crutzen, J. Lelieveld et al., "Indian ocean experiment: an integrated analysis of the climate forcing and effects of the great Indo-Asian haze," *Journal of Geophysical Research D*, vol. 106, no. 22, pp. 28371–28398, 2001.

[34] D. Rind, M. Chin, G. Feingold et al., "Modeling the effects of aerosols on climate," in *Atmospheric Aerosol Properties and Impacts on Climate, A Report by the U.S. Climate Change Science Program and the Subcommittee on Global Change Research*, M. Chin, R. A. Kahn, and S. E. Schwartz, Eds., pp. 64–97, National Aeronautics and Space Administration, 2009.

[35] E. Hirst, P. H. Kaye, R. S. Greenaway, P. Field, and D. W. Johnson, "Discrimination of micrometre-sized ice and super-cooled droplets in mixed-phase cloud," *Atmospheric Environment*, vol. 35, no. 1, pp. 33–47, 2001.

[36] D. J. Diner, B. H. Braswell, R. Davies et al., "The value of multi-angle measurements for retrieving structurally and radiatively consistent properties of clouds, aerosols, and surfaces," *Remote Sensing of Environment*, vol. 97, no. 4, pp. 495–518, 2005.

[37] R. Kahn, P. Banerjee, and D. McDonald, "Sensitivity of multiangle imaging to natural mixtures of aerosols over ocean," *Journal of Geophysical Research D*, vol. 106, no. 16, pp. 18219–18238, 2001.

[38] R. A. Kahn, M. J. Garay, D. L. Nelson et al., "Satellite-derived aerosol optical depth over dark water from MISR and MODIS: comparisons with AERONET and implications for climatological studies," *Journal of Geophysical Research D*, vol. 112, no. 18, Article ID D18205, 2007.

[39] A. S. Goudie and N. J. Middleton, *Desert Dust in the Global System*, Springer, Berlin, Germany, 2006.

[40] M. Chin, P. Ginoux, S. Kinne et al., "Tropospheric aerosol optical thickness from the GOCART model and comparisons with satellite and sun photometer measurements," *Journal of the Atmospheric Sciences*, vol. 59, no. 3, pp. 461–483, 2002.

[41] S. H. Chung and J. H. Seinfeld, "Global distribution and climate forcing of carbonaceous aerosols," *Journal of Geophysical Research D*, vol. 107, no. 19, pp. 14–33, 2002.

[42] Y. Qian, F. Giorgi, Y. Huang, W. Chameides, and C. Luo, "Regional simulation of anthropogenic sulfur over East Asia and its sensitivity to model parameters," *Tellus, Series B*, vol. 53, no. 2, pp. 171–191, 2001.

[43] F. Giorgi, X. Bi, and Y. Qian, "Direct radiative forcing and regional climatic effects of anthropogenic aerosols over East Asia: a regional coupled climate-chemistry/aerosol model study," *Journal of Geophysical Research D*, vol. 107, no. 20, pp. 7–18, 2002.

[44] F. Giorgi, X. Bi, and Y. Qian, "Indirect vs. direct effects of anthropogenic sulfate on the climate of east Asia as simulated with a regional coupled climate-chemistry/aerosol model," *Climatic Change*, vol. 58, no. 3, pp. 345–376, 2003.

[45] A. M. L. Ekman and H. Rodhe, "Regional temperature response due to indirect sulfate aerosol forcing: impact of model resolution," *Climate Dynamics*, vol. 21, no. 1, pp. 1–10, 2003.

[46] T. Takemura, T. Nakajima, T. Nozawa, and K. Aoki, "Simulation of future aerosol distribution, radiative forcing, and long-range transport in East Asia," *Journal of the Meteorological Society of Japan*, vol. 79, no. 6, pp. 1139–1155, 2001.

[47] I. Tegen, M. Werner, S. P. Harrison, and K. E. Kohfeld, "Relative importance of climate and land use in determining present and future global soil dust emission," *Geophysical Research Letters*, vol. 31, no. 5, pp. L05105–4, 2004.

[48] A. Baklanov, B. Fay, G. Weather et al., "Overview of existing integrated (off-line and on-line) mesoscale systems in Europe," report of Working Group 2, 2007, http://www.cost728.org/.

[49] A. Baklanov, A. Mahura, and R. Sokhi, *Integrated Systems of Meso-Meteorological and Chemical Transport Models*, Springer, New York, NY, USA, 2011.

[50] F. Giorgi, E. Coppola, F. Solmon et al., "RegCM4: model description and preliminary tests over multiple CORDEX domains," *Climate Research*, vol. 52, pp. 7–29, 2012.

© University of Pretoria

[51] M. Kanakidou, J. H. Seinfeld, S. N. Pandis et al., "Organic aerosol and global climate modelling: a review," *Atmospheric Chemistry and Physics*, vol. 5, no. 4, pp. 1053–1123, 2005.

[52] X. Liu, J. E. Penner, B. Das et al., "Uncertainties in global aerosol simulations: assessment using three meteorological data sets," *Journal of Geophysical Research D*, vol. 112, no. 11, Article ID D11212, 2007.

[53] E. Vignati, M. Karl, M. Krol, J. Wilson, P. Stier, and F. Cavalli, "Sources of uncertainties in modelling black carbon at the global scale," *Atmospheric Chemistry and Physics*, vol. 10, no. 6, pp. 2595–2611, 2010.

[54] L. Lee, K. J. Pringle, C. L. Reddington et al., "The magnitude and causes of uncertainty in global model simulations of cloud condensation nuclei," *Atmospheric Chemistry and Physics*, vol. 13, pp. 6295–6378, 2013.

[55] G. Myhre, F. Stordal, T. F. Berglen, J. K. Sundet, and I. S. A. Isaksen, "Uncertainties in the radiative forcing due to sulphate aerosols," *Journal of the Atmospheric Sciences*, vol. 61, no. 5, pp. 485–498, 2004.

[56] M. Schulz, C. Textor, S. Kinne et al., "Radiative forcing by aerosols as derived from the AeroCom present-day and pre-industrial simulations," *Atmospheric Chemistry and Physics*, vol. 6, no. 12, pp. 5225–5246, 2006.

[57] H. Tost, M. G. Lawrence, C. Brühl, and P. Jöckel, "Uncertainties in atmospheric chemistry modelling due to convection parameterisations and subsequent scavenging," *Atmospheric Chemistry and Physics*, vol. 10, no. 4, pp. 1931–1951, 2010.

[58] P. Stier, N. A. J. Schutgens, N. Bellouin et al., "Host model uncertainties in aerosol radiative forcing estimates: results from the AeroCom prescribed inter-comparison study," *Atmospheric Chemistry and Physics*, vol. 13, pp. 3245–3270, 2013.

[59] F. Giorgi and M. R. Marinucci, "An investigation of the sensitivity of simulated precipitation to model resolution and its implications for climate studies," *Monthly Weather Review*, vol. 124, no. 1, pp. 148–166, 1996.

[60] F. Giorgi and C. Shields, "Tests of precipitation parameterizations available in latest version of NCAR regional climate model (RegCM) over continental United States," *Journal of Geophysical Research D*, vol. 104, no. 6, pp. 6353–6375, 1999.

[61] F. Giorgi and R. O. Anyah, "Evolution of regional climate modeling: the road towards RegCM4," *Climate Research*, vol. 52, pp. 3–6, 2012.

[62] M. Z. Jacobson, *Developing, coupling, and applying a gas, aerosol, transport, and radiation model to study urban and regional air pollution [Ph.D. thesis]*, Department of Atmospheric Sciences, University of California, Los Angeles, Calif, USA, 1994.

[63] A. S. Zakey, F. Solmon, and F. Giorgi, "Implementation and testing of a desert dust module in a regional climate model," *Atmospheric Chemistry and Physics*, vol. 6, no. 12, pp. 4687–4704, 2006.

[64] A. S. Zakey, F. Giorgi, and X. Bi, "Modeling of sea salt in a regional climate model: fluxes and radiative forcing," *Journal of Geophysical Research D*, vol. 113, no. 14, Article ID D14221, 2008.

[65] P. Zanis, C. Douvis, I. Kapsomenakis, I. Kioutsioukis, D. Melas, and J. S. Pal, "A sensitivity study of the Regional Climate Model (RegCM3) to the convective scheme with emphasis in central eastern and southeastern Europe," *Theoretical and Applied Climatology*, vol. 97, no. 3-4, pp. 327–337, 2009.

[66] Y. Zhang, X.-Y. Wen, and C. J. Jang, "Simulating chemistry-aerosol-cloud-radiation-climate feedbacks over the continental U.S. using the online-coupled Weather Research Forecasting Model with chemistry (WRF/Chem)," *Atmospheric Environment*, vol. 44, no. 29, pp. 3568–3582, 2010.

[67] F. Solmon, M. Mallet, N. Elguindi, F. Giorgi, A. Zakey, and A. Konaré, "Dust aerosol impact on regional precipitation over western Africa, mechanisms and sensitivity to absorption properties," *Geophysical Research Letters*, vol. 35, no. 24, Article ID L24705, 2008.

[68] F. Solmon, N. Elguindi, and M. Mallet, "Radiative and climatic effects of dust over West Africa, as simulated by a regional climate model," *Climate Research*, vol. 52, pp. 97–113, 2012.

[69] F. Tummon, F. Solmon, C. Liousse, and M. Tadross, "Simulation of the direct and semidirect aerosol effects on the southern Africa regional climate during the biomass burning season," *Journal of Geophysical Research D*, vol. 115, no. 19, Article ID D19206, 2010.

[70] A. Konare, A. S. Zakey, F. Solmon et al., "A regional climate modeling study of the effect of desert dust on the West African monsoon," *Journal of Geophysical Research D*, vol. 113, no. 12, Article ID D12206, 2008.

[71] F. Malavelle, V. Pont, M. Mallet et al., "Simulation of aerosol radiative effects over West Africa during DABEX and AMMA SOP-0," *Journal of Geophysical Research D*, vol. 116, no. 8, Article ID D08205, 2011.

[72] Eskom, "Effects of atmospheric pollution on the Mpumalanga Highveld," Power Technology No. 70, Eskom Technology Group, Cleveland, South Africa, 1996.

[73] R. Spalding-Fecher and D. K. Matibe, "Electricity and externalities in South Africa," *Energy Policy*, vol. 31, no. 8, pp. 721–734, 2003.

[74] K. E. Ross, S. J. Piketh, R. T. Bruintjes, R. P. Burger, R. J. Swap, and H. J. Annegarn, "Spatial and aerosol variations in CCN distribution and the aerosol-CCN relationship over southern Africa," *Journal of Geophysical Research D*, vol. 108, no. 13, pp. 1–18, 2003.

[75] A. J. Mills, A. V. Milewski, C. Sirami et al., "Aerosol capture by small trees in savannas marginal to treeless grassland in South Africa," *Geoderma*, vol. 189-190, pp. 124–132, 2012.

[76] H. Winkler, P. Formenti, D. J. Esterhuyse et al., "Evidence for large-scale transport of biomass burning aerosols from sunphotometry at a remote South African site," *Atmospheric Environment*, vol. 42, no. 22, pp. 5569–5578, 2008.

[77] A. J. Queface, S. J. Piketh, T. F. Eck, S.-C. Tsay, and A. F. Mavume, "Climatology of aerosol optical properties in Southern Africa," *Atmospheric Environment*, vol. 45, no. 17, pp. 2910–2921, 2011.

[78] B. I. Magi, "Chemical apportionment of southern African aerosol mass and optical depth," *Atmospheric Chemistry and Physics*, vol. 9, no. 19, pp. 7643–7655, 2009.

[79] M. Tesfaye, V. Sivakumar, J. Botai, and G. Mengistu, "Latitudinal variations of aerosol optical parameters over South Africa based on MISR satellite data," in *Proceedings of the 26th Annual Conference of South African Society for Atmosphere Science*, pp. 105–106, September 2010.

[80] F. Tummon, *Direct and semi-direct aerosol effects on the southern African regional climate during the austral winter season [Ph.D. thesis]*, University of Cape Town, Cape Town, South Africa, 2011.

[81] B. I. Magi, P. Ginoux, Y. Ming, and V. Ramaswamy, "Evaluation of tropical and extratropical Southern Hemisphere African aerosol properties simulated by a climate model," *Journal of Geophysical Research D*, vol. 114, no. 14, Article ID D14204, 2009.

[82] T. F. Eck, B. N. Holben, D. E. Ward et al., "Variability of biomass burning aerosol optical characteristics in southern

© University of Pretoria

Africa during the SAFARI 2000 dry season campaign and a comparison of single scattering albedo estimates from radiometric measurements," *Journal of Geophysical Research D*, vol. 108, no. 13, pp. 1–21, 2003.

[83] R. J. Swap, H. J. Annegarn, J. T. Suttles et al., "The Southern African Regional Science Initiative (SAFARI 2000): overview of the dry season field campaign," *South African Journal of Science*, vol. 98, no. 3-4, pp. 125–130, 2002.

[84] R. J. Swap, H. J. Annegarn, J. T. Suttles et al., "Africa burning: a thematic analysis of the Southern African Regional Science Initiative (SAFARI 2000)," *Journal of Geophysical Research D*, vol. 108, no. 13, pp. 1–15, 2003.

[85] S. J. Piketh, H. J. Annegarn, and P. D. Tyson, "Lower tropospheric aerosol loadings over South Africa: the relative contribution of aeolian dust, industrial emissions, and biomass burning," *Journal of Geophysical Research D*, vol. 104, no. 1, pp. 1597–1607, 1999.

[86] J. M. Prospero, P. Ginoux, O. Torres, S. E. Nicholson, and T. E. Gill, "Environmental characterization of global sources of atmospheric soil dust identified with the Nimbus 7 Total Ozone Mapping Spectrometer (TOMS) absorbing aerosol product," *Reviews of Geophysics*, vol. 40, no. 1, pp. -1–31, 2002.

[87] O. Dubovik and M. D. King, "A flexible inversion algorithm for retrieval of aerosol optical properties from Sun and sky radiance measurements," *Journal of Geophysical Research D*, vol. 105, no. 16, pp. 20673–20696, 2000.

[88] C. Levoni, M. Cervino, R. Guzzi, and F. Torricella, "Atmospheric aerosol optical properties: a database of radiative characteristics for different components and classes," *Applied Optics*, vol. 36, no. 30, pp. 8031–8041, 1997.

[89] M. I. Mishchenko and L. D. Travis, *Light Scattering by Non-Spherical Particles*, Academic Press, San-Diego, Calif, USA, 2000.

[90] M. Hess, P. Koepke, and I. Schult, "Optical properties of aerosols and clouds: the software package OPAC," *Bulletin of the American Meteorological Society*, vol. 79, no. 5, pp. 831–844, 1998.

[91] E. Andrews, P. J. Sheridan, M. Fiebig et al., "Comparison of methods for deriving aerosol asymmetry parameter," *Journal of Geophysical Research*, vol. 111, no. D5, Article ID D05S04, 2006.

[92] T. Takemura, T. Nakajima, O. Dubovik, B. N. Holben, and S. Kinne, "Single-scattering albedo and radiative forcing of various aerosol species with a global three-dimensional model," *Journal of Climate*, vol. 15, no. 4, pp. 333–352, 2002.

[93] J. H. Seinfeld and S. N. Pandis, *Atmospheric Chemistry and Physics: From Air Pollution to Climate*, Wiley, New York, NY, USA, 2006.

[94] O. Dubovik, A. Smirnov, B. N. Holben et al., "Accuracy assessments of aerosol optical properties retrieved from Aerosol Robotic Network (AERONET) Sun and sky radiance measurements," *Journal of Geophysical Research D*, vol. 105, no. 8, pp. 9791–9806, 2000.

[95] H. Yu, Y. J. Kaufman, M. Chin et al., "A review of measurement-based assessments of the aerosol direct radiative effect and forcing," *Atmospheric Chemistry and Physics*, vol. 6, no. 3, pp. 613–666, 2006.

[96] Y. J. Kaufman, D. Tanré, L. A. Remer, E. F. Vermote, A. Chu, and B. N. Holben, "Operational remote sensing of tropospheric aerosol over land from EOS moderate resolution imaging spectroradiometer," *Journal of Geophysical Research D*, vol. 102, no. 14, pp. 17051–17067, 1997.

[97] P. Chylek, B. Henderson, and M. Mishchenko, "Aerosol radiative forcing and the accuracy of satellite aerosol optical depth retrieval," *Journal of Geophysical Research D*, vol. 108, no. 24, pp. 4–8, 2003.

[98] D. Tanré, Y. J. Kaufman, M. Herman, and S. Mattoo, "Remote sensing of aerosol properties over oceans using the MODIS/EOS spectral radiances," *Journal of Geophysical Research D*, vol. 102, no. 14, pp. 16971–16988, 1997.

[99] R. A. Kahn, B. J. Gaitley, J. V. Martonchik, D. J. Diner, K. A. Crean, and B. Holben, "Multiangle Imaging Spectroradiometer (MISR) global aerosol optical depth validation based on 2 years of coincident Aerosol Robotic Network (AERONET) observations," *Journal of Geophysical Research D*, vol. 110, no. 10, pp. 1–16, 2005.

[100] O. V. Kalashnikova, R. Kahn, I. N. Sokolik, and W.-H. Li, "Ability of multiangle remote sensing observations to identify and distinguish mineral dust types: optical models and retrievals of optically thick plumes," *Journal of Geophysical Research D*, vol. 110, no. 18, Article ID D18S14, pp. 1–16, 2005.

[101] A. De Meij, M. Krol, F. Dentener, E. Vignati, C. Cuvelier, and P. Thunis, "The sensitivity of aerosol in Europe to two different emission inventories and temporal distribution of emissions," *Atmospheric Chemistry and Physics*, vol. 6, no. 12, pp. 4287–4309, 2006.

[102] N. Mahowald, K. Kohfeld, M. Hansson et al., "Dust sources and deposition during the last glacial maximum and current climate: a comparison of model results with paleodata from ice cores and marine sediments," *Journal of Geophysical Research D*, vol. 104, no. 13, pp. 15895–15916, 1999.

[103] Y. J. Kaufman, D. Tanré, and O. Boucher, "A satellite view of aerosols in the climate system," *Nature*, vol. 419, no. 6903, pp. 215–223, 2002.

[104] D. J. Diner, T. P. Ackerman, T. L. Anderson et al., "Paragon: an integrated approach for characterizing aerosol climate impacts and environmental interactions," *Bulletin of the American Meteorological Society*, vol. 85, pp. 14911–11501, 2004.

[105] J. E. Penner, S. Y. Zhang, M. Chin et al., "A comparison of model- and satellite-derived aerosol optical depth and reflectivity," *Journal of the Atmospheric Sciences*, vol. 59, no. 3, pp. 441–460, 2002.

[106] R. E. Dickinson, R. M. Errico, F. Giorgi, and G. T. Bates, "A regional climate model for the western United States," *Climatic Change*, vol. 15, no. 3, pp. 383–422, 1989.

[107] J. T. Kiehl, J. J. Hack, G. B. Bonan et al., "Description of the ncar community climate model (ccm3)," Tech. Rep. NCAR/TN-420+STR, National Center for Atmospheric Research, 1996.

[108] X. Zeng, M. Zhao, and R. E. Dickinson, "Intercomparison of bulk aerodynamic algorithms for the computation of sea surface fluxes using TOGA COARE and TAO data," *Journal of Climate*, vol. 11, no. 10, pp. 2628–2644, 1998.

[109] R. E. Dickinson, A. Henderson-Sellers, and P. J. Kennedy, "Biosphere-atmosphere transfer scheme (bats) version 1e as coupled to the ncar community climate model," Tech. Rep. NCAR/TN-387+STR, National Center for Atmospheric Research, 1993.

[110] F. Giorgi, R. Francisco, and J. Pal, "Effects of a subgrid-scale topography and land use scheme on the simulation of surface climate and hydrology. Part 1: effects of temperature and water vapor disaggregation," *Journal of Hydrometeorology*, vol. 4, pp. 317–333, 2003.

[111] A. A. M. Holtslag, E. I. F. De Bruijn, and H.-L. Pan, "A high resolution air mass transformation model for short-range

© University of Pretoria

weather forecasting," *Monthly Weather Review*, vol. 118, no. 8, pp. 1561–1575, 1990.

[112] G. A. Grell, "Prognostic evaluation of assumptions used by cumulus parameterizations," *Monthly Weather Review*, vol. 121, no. 3, pp. 764–787, 1993.

[113] J. M. Fritsch and C. F. Chappell, "Numerical prediction of convectively driven mesoscale pressure systems. Part I: convective parameterization," *Journal of the Atmospheric Sciences*, vol. 37, no. 8, pp. 1722–1733, 1980.

[114] J. S. Pal, E. E. Small, and E. A. B. Eltahir, "Simulation of regional-scale water and energy budgets: representation of subgrid cloud and precipitation processes within RegCM," *Journal of Geophysical Research D*, vol. 105, no. 24, pp. 29579–29594, 2000.

[115] Y. Huang, W. L. Chameides, Q. Tan, and R. E. Dickinson, "Characteristics of anthropogenic sulfate and carbonaceous aerosols over East Asia: regional modeling and observation," *Advances in Atmospheric Sciences*, vol. 25, no. 6, pp. 946–959, 2008.

[116] D. F. Zhang, A. S. Zakey, X. J. Gao, F. Giorgi, and F. Solmon, "Simulation of dust aerosol and its regional feedbacks over East Asia using a regional climate model," *Atmospheric Chemistry and Physics*, vol. 9, no. 4, pp. 1095–1110, 2009.

[117] M. Santese, M. R. Perrone, A. S. Zakey, F. De Tomasi, and F. Giorgi, "Modeling of Saharan dust outbreaks over the mediterranean by RegCM3: case studies," *Atmospheric Chemistry and Physics*, vol. 10, no. 1, pp. 133–156, 2010.

[118] M. Tesfaye et al., "Mineral dust aerosol distributions, its direct and semi-direct effects over South Africa based on regional climate model simulation," submitted to a peer-reviewed journal and currently, 2013, ftp://ftp.csir.co.za/NLC/EE/.

[119] M. Tesfaye et al., "Simulation of anthropogenic aerosols mass distributions and their direct and semi-direct effects over South Africa using RegCM4," submitted to a peer-reviewed journal and currently, 2013, ftp://ftp.csir.co.za/NLC/EE/.

[120] M. Tesfaye et al., "Simulation of biomass burning aerosols mass distributions and their direct and semi-direct effects over South Africa using a regional climate model," submitted to a peer-reviewed journal and currently, 2013, ftp://ftp.csir.co.za/NLC/EE/.

[121] M. Tesfaye et al., "Simulation of bulk aerosol direct andsemi-direct effects in South Africa using RegCM4," submitted to a peer-reviewed journal and currently, 2013, ftp://ftp.csir.co.za/NLC/EE/.

[122] C. Liousse, F. Dulac, H. Cachier, and D. Tanré, "Remote sensing of carbonaceous aerosol production by African savanna biomass burning," *Journal of Geophysical Research D*, vol. 102, no. 5, pp. 5895–5911, 1997.

[123] S. Fuzzi, M. O. Andreae, B. J. Huebert et al., "Critical assessment of the current state of scientific knowledge, terminology, and research needs concerning the role of organic aerosols in the atmosphere, climate, and global change," *Atmospheric Chemistry and Physics*, vol. 6, no. 7, pp. 2017–2038, 2006.

[124] G. Lesins, P. Chylek, and U. Lohmann, "A study of internal and external mixing scenarios and its effect on aerosol optical properties and direct radiative forcing," *Journal of Geophysical Research D*, vol. 107, no. 9-10, pp. 5–1, 2002.

[125] S. E. Bauer and D. Koch, "Impact of heterogeneous sulfate formation at mineral dust surfaces on aerosol loads and radiative forcing in the Goddard Institute for Space Studies general circulation model," *Journal of Geophysical Research D*, vol. 110, no. 17, Article ID D17202, pp. 91–105, 2005.

[126] M. Z. Jacobson, "Strong radiative heating due to the mixing state of black carbon in atmospheric aerosols," *Nature*, vol. 409, no. 6821, pp. 695–697, 2001.

[127] R. C. Moffet and K. A. Prather, "In-situ measurements of the mixing state and optical properties of soot with implications for radiative forcing estimates," *Proceedings of the National Academy of Sciences of the United States of America*, vol. 106, no. 29, pp. 11872–11877, 2009.

[128] G. McFiggans, P. Artaxo, U. Baltensperger et al., "The effect of physical and chemical aerosol properties on warm cloud droplet activation," *Atmospheric Chemistry and Physics*, vol. 6, no. 9, pp. 2593–2649, 2006.

[129] M. Tesfaye, M. Tsidu, V. Sivakumar, and J. Botai, "Effective single scattering albedo estimation using regional climate model," in *Proceedings of the 27th Annual Conference of the South African Society for Atmospheric Sciences: The Interdependent Atmosphere, Land and Ocean, Hartbeespoort*, pp. 53–54, September 2011.

[130] M. Tesfaye, *Retrival of atmospheric aerosol optical and microphysical parameters from ground base passive remote sensing measurement over Addis Ababa [M.S. thesis]*, Addis Ababa University, Addis Ababa, Ethiopia, 2009.

[131] J.-F. Lamarque, T. C. Bond, V. Eyring et al., "Historical (1850–2000) gridded anthropogenic and biomass burning emissions of reactive gases and aerosols: methodology and application," *Atmospheric Chemistry and Physics*, vol. 10, no. 15, pp. 7017–7039, 2010.

[132] G. R. van der Werf, J. T. Randerson, L. Giglio et al., "Global fire emissions and the contribution of deforestation, savanna, forest, agricultural, and peat fires (1997–2009)," *Atmospheric Chemistry and Physics*, vol. 10, no. 23, pp. 11707–11735, 2010.

[133] L. Giglio, J. T. Randerson, G. R. Van Der Werf et al., "Assessing variability and long-term trends in burned area by merging multiple satellite fire products," *Biogeosciences*, vol. 7, no. 3, pp. 1171–1186, 2010.

[134] G. R. van der Werf, J. T. Randerson, L. Giglio, G. J. Collatz, P. S. Kasibhatla, and A. F. Arellano Jr., "Interannual variability in global biomass burning emissions from 1997 to 2004," *Atmospheric Chemistry and Physics*, vol. 6, no. 11, pp. 3423–3441, 2006.

[135] A. Seth and F. Giorgi, "The effects of domain choice on summer precipitation simulation and sensitivity in a regional climate model," *Journal of Climate*, vol. 11, no. 10, pp. 2698–2712, 1998.

[136] X. Wang, Z. Zhong, Y. Hu, and H. Yuan, "Effect of lateral boundary scheme on the simulation of tropical cyclone track in regional climate model RegCM3," *Asia-Pacific Journal of Atmospheric Sciences*, vol. 46, no. 2, pp. 221–230, 2010.

[137] A. Simmons, S. Uppala, D. Dee, and S. Kobayashi, "ERA-Interim: new ECMWF reanalysis products from 1989 onwards," *ECMWF Newsletter*, vol. 110, pp. 25–35, 2007.

[138] D. P. Dee, S. M. Uppala, A. J. Simmons et al., "The ERA-Interim reanalysis: configuration and performance of the data assimilation system," *Quarterly Journal of the Royal Meteorological Society*, vol. 137, no. 656, pp. 553–597, 2011.

[139] R. W. Reynolds, N. A. Rayner, T. M. Smith, D. C. Stokes, and W. Wang, "An improved in situ and satellite SST analysis for climate," *Journal of Climate*, vol. 15, no. 13, pp. 1609–1625, 2002.

[140] B. N. Holben, T. F. Eck, I. Slutsker et al., "AERONET—a federated instrument network and data archive for aerosol characterization," *Remote Sensing of Environment*, vol. 66, no. 1, pp. 1–16, 1998.

© University of Pretoria

[141] O. Dubovik, M. Herman, A. Holdak et al., "Statistically optimized inversion algorithm for enhanced retrieval of aerosol properties from spectral multi-angle polarimetric satellite observations," *Atmospheric Measurement Techniques*, vol. 4, no. 5, pp. 975–1018, 2011.

[142] D. J. Diner, G. P. Asner, R. Davies et al., "New directions in earth observing: scientific applications of multiangle remote sensing," *Bulletin of the American Meteorological Society*, vol. 80, no. 11, pp. 2209–2228, 1999.

[143] J. V. Martonchik, D. J. Diner, R. A. Kahn et al., "Techniques for the retrieval of aerosol properties over land and ocean using multiangle imaging," *IEEE Transactions on Geoscience and Remote Sensing*, vol. 36, no. 4, pp. 1212–1227, 1998.

[144] J. V. Martonchik, D. J. Diner, K. A. Crean, and M. A. Bull, "Regional aerosol retrieval results from MISR," *IEEE Transactions on Geoscience and Remote Sensing*, vol. 40, no. 7, pp. 1520–1531, 2002.

[145] O. V. Kalashnikova and R. Kahn, "Ability of multiangle remote sensing observations to identify and distinguish mineral dust types: 2. Sensitivity over dark water," *Journal of Geophysical Research D*, vol. 111, no. 11, Article ID D11207, 2006.

[146] A. Sharma, V. Sivakumar, C. Bollig, C. Van Der Westhuizen, and D. Moema, "System description of the mobile LIDAR of the CSIR, South Africa," *South African Journal of Science*, vol. 105, no. 11-12, pp. 456–462, 2009.

[147] V. Sivakumar, M. Tesfaye, W. Alemu et al., "CSIR South Africa mobile LIDAR-first scientific results: comparison with satellite, sun photometer and model simulations," *South African Journal of Science*, vol. 105, no. 11-12, pp. 449–455, 2009.

[148] V. Sivakumar, M. Tesfaye, W. Alemu, A. Sharma, C. Bollig, and G. Mengistu, "Aerosol measurements over South Africa using LIDAR, Satellite and Sun Photometer," in *Advances in Geosciences, 16, Atmospheric Science*, chapter 22, pp. 253–262, World Scientific, 2010.

[149] M. Tesfaye, V. Sivakumar, J. Botai et al., "Retrieval of relative humidity from CSIR-NLC mobile LIDAR backscatter measurements," in *Proceedings of the 25th Annual Conference of South African society for Atmosphere Science*, September 2009.

[150] M. Tesfaye, V. Sivakumar, G. Mengistu et al., "Atmospheric Aerosol load morphological classification and retrieved visibility based on lidar backscatter measurement," in *Proceedings of the 25th International Laser Radar Conference*, pp. 487–490, Saint Pietersburg, Russia, 2010.

[151] J. R. Campbell, E. J. Welton, J. D. Spinhirne et al., "Micropulse lidar observations of tropospheric aerosols over northeastern South Africa during the ARREX and SAFARI 2000 dry season experiments," *Journal of Geophysical Research D*, vol. 108, no. 13, pp. 1–33, 2003.

[152] D. E. Terblanche, M. P. Mittermaier, S. J. Piketh, R. T. Bruintjes, and R. P. Burger, "The Aerosol Recirculation and Rainfall Experiment (ARREX): an initial study on aerosol-cloud interactions over South Africa," *South African Journal of Science*, vol. 96, no. 1, pp. 15–21, 2000.

[153] G.-J. Roelofs, H. Ten Brink, A. Kiendler-Scharr et al., "Evaluation of simulated aerosol properties with the aerosol-climate model ECHAM5-HAM using observations from the IMPACT field campaign," *Atmospheric Chemistry and Physics*, vol. 10, no. 16, pp. 7709–7722, 2010.

[154] V. Ramanathan and M. V. Ramana, "Persistent, widespread, and strongly absorbing haze over the Himalayan foothills and the Indo-Gangetic Plains," *Pure and Applied Geophysics*, vol. 162, no. 8-9, pp. 1609–1626, 2005.

[155] P. Ginoux, M. Chin, I. Tegen et al., "Sources and distributions of dust aerosols simulated with the GOCART model," *Journal of Geophysical Research D*, vol. 106, no. 17, pp. 20255–20273, 2001.

[156] T. Y. Tanaka and M. Chiba, "A numerical study of the contributions of dust source regions to the global dust budget," *Global and Planetary Change*, vol. 52, no. 1-4, pp. 88–104, 2006.

[157] X. Yue, H. Wang, H. Liao, and K. Fan, "Simulation of dust aerosol radiative feedback using the GMOD: 2. Dust-climate interactions," *Journal of Geophysical Research D*, vol. 115, no. 4, Article ID D04201, 2010.

[158] E. M. Wilcox and V. Ramanathan, "The impact of observed precipitation upon the transport of aerosols from South Asia," *Tellus, Series B*, vol. 56, no. 5, pp. 435–450, 2004.

[159] Z. Shi, M. D. Krom, T. D. Jickells et al., "Impacts on iron solubility in the mineral dust by processes in the source region and the atmosphere: a review," *Aeolian Research*, vol. 5, pp. 21–42, 2012.

[160] A. Bhattachan, P. Dodorico, M. C. Baddock, T. M. Zobeck, G. S. Okin, and N. Cassar, "The Southern Kalahari: a potential new dust source in the Southern Hemisphere?" *Environmental Research Letters*, vol. 7, no. 2, Article ID 024001, 2012.

[161] Y. J. Kaufman, D. Tanré, O. Dubovik, A. Karnieli, and L. A. Remer, "Absorption of sunlight by dust as inferred from satellite and ground-based remote sensing," *Geophysical Research Letters*, vol. 28, no. 8, pp. 1479–1482, 2001.

[162] I. Tegen and I. Fung, "Contribution to the atmospheric mineral aerosol load from land surface modification," *Journal of Geophysical Research*, vol. 100, no. 9, pp. 18–726, 1995.

[163] M. T. Freiman and S. J. Piketh, "Air transport into and out of the industrial Highveld region of South Africa," *Journal of Applied Meteorology*, vol. 42, no. 7994, 1002 pages, 2003.

[164] Y. Wang, L. R. Leung, J. L. McGregor et al., "Regional climate modeling: progress, challenges, and prospects," *Journal of the Meteorological Society of Japan*, vol. 82, no. 6, pp. 1599–1628, 2004.

[165] J. Heintzenberg and R. J. Charlson, *Clouds in the Perturbed Climate System*, MIT Press, Cambridge, Mass, USA, 2009.

© University of Pretoria

UNIVERSITEIT VAN PRETORIA
UNIVERSITY OF PRETORIA
YUNIBESITHI YA PRETORIA

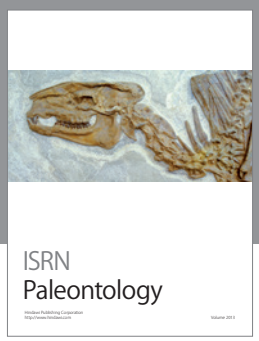

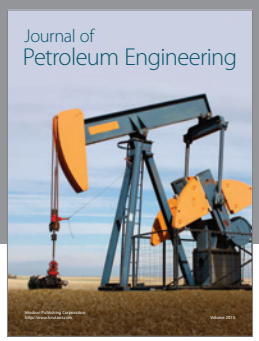

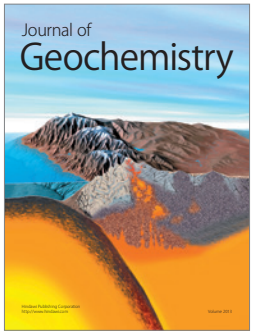

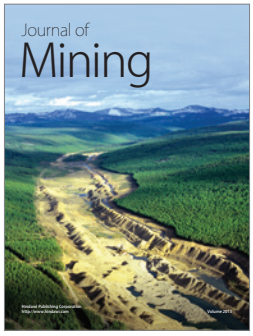

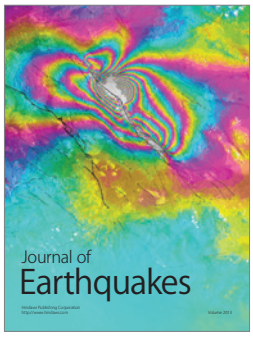

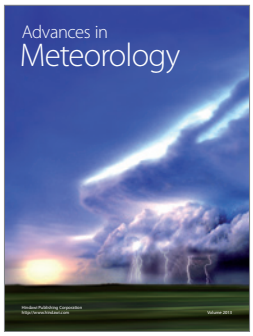

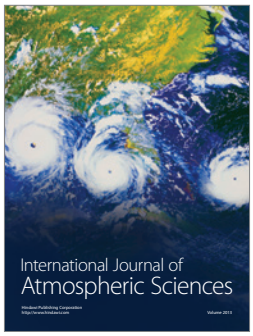

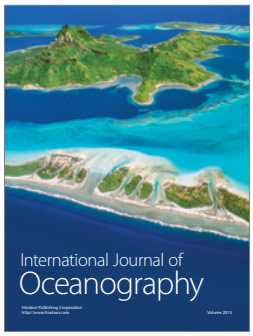

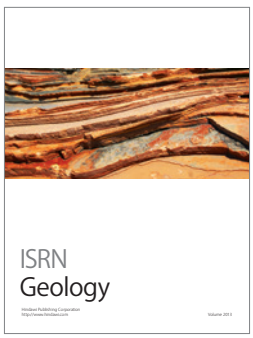

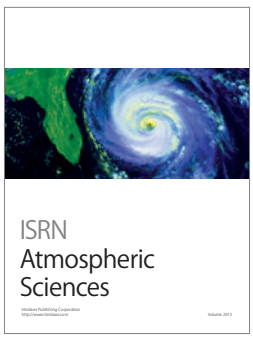

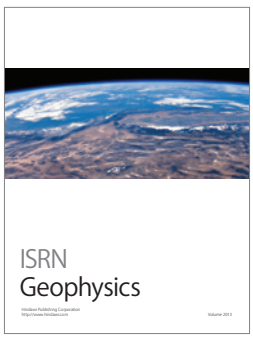

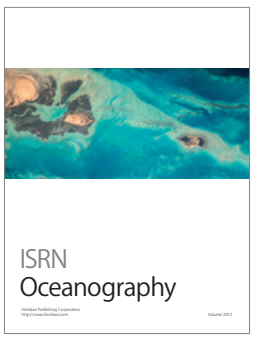

Hindawi
Submit your manuscripts at
http://www.hindawi.com

© University of Pretoria

Chapter 4: Mineral dust aerosol distributions, its direct and semi-direct effects over South Africa based on regional climate model simulation*

*This chapter needs to be cited as:

Tesfaye, M., G. Mengistu Tsidu, J. Botai, and V. Sivakumar (2013b): "Mineral dust aerosol distributions, its direct and semi-direct effects over South Africa based on regional climate model simulation", *J. Arid Environ., in review*.

© University of Pretoria

UNIVERSITEIT VAN PRETORIA
UNIVERSITY OF PRETORIA
YUNIBESITHI YA PRETORIA

Mineral dust aerosol distributions, its direct and semi-direct effects over South Africa based on regional climate model simulation

M. Tesfaye[1,2*], G. Mengistu Tsidu[3], J. Botai[1], V. Sivakumar[1,4]

Abstract: The present contribution investigates the seasonal mean mass distributions, direct and semi-direct climatic effects of desert dust aerosols over South Africa, using the 12 year runs of Regional Climate Model (RegCM4). The simulation results have shown that the arid areas of Northern Cape as well as Namibia and Botswana are the main source regions of desert dust particles, over South Africa. At the surface and within the atmosphere, the SW-Radiative Forcing (RF) and LW-RF of dust showed contrasting effects. However due to the dominant influence on SW, the Net-RF (SW-RF+LW-RF) of dust causes reduction on net radiation absorbed by the surface via increasing radiative heating of the atmosphere. The presence of radiatively interactive desert dust particles predominantly induce positive feedback on atmospheric radiative heating rate, Cloud Cover (CC) and cloud liquid water path. The CC enhancement and RF of dust particles, cooperatively, causes a reduction in surface temperature (up to -1.1 K) and surface sensible heat flux (up to -24W/m^2). The aforementioned dust aerosols' direct and semi-direct influences, jointly, cause the change in regional scale dynamical variables. Overall, the present contribution underscores the importance of including the effects of wind eroded dust particles in climate change studies over South Africa.

[1]*Department of Geography, Geoinformatics and Meteorology, University of Pretoria, Pretoria 0002, South Africa*

[2]*National Laser Centre, Council for Scientific and Industrial Research, Pretoria 0001, South Africa*

[3]*Department of Physics, Addis Ababa University, Addis Ababa, Ethiopia*

[4]*School of physics, University of KwaZulu Natal, Durban 4000, South Africa*

**Correspondence to: M. Tesfaye: mela_20062@yahoo.com*

Keywords: Desert dust; RegCM4; Dust-climate interactions; Dust direct effects; Dust semi-direct effects; South Africa

1 Introduction

Wind eroded dust aerosols which are emitted naturally through different processes such as suspension, saltation, sandblasting and creeping (e.g., Grini et al., 2002; Zakey et al., 2006) are the main aerosol components of arid/semi-arid regions of the world (e.g., Ginoux et al., 2001; Prospero et al., 2002; Tegen et al., 2002). They contribute a large portion of aerosol mass to the total mass of aerosols in the troposphere (e.g., Zender et al., 2004). Even though the arid/semi-arid regions' land surfaces are the main sources of wind-blown dust particles (e.g., Ginoux et al., 2001; Prospero et al., 2002; Tegen et al., 2002); anthropogenic activities induced land surface degradation, land use and plant cover changes for agricultural use, mining activities and many other events, result in an increment in dust production and facilitate their transportation in local to regional scales (e.g., Tegen and Fung, 1994; Tegen et al., 2004; Suh and Lee, 2004; Bessagnet et al., 2008; Bullard et al., 2011). Nonetheless, due to the high variability of anthropogenic events, the estimation of human activities triggered dust production is quite difficult. Therefore, the focus of the present contribution is to analyse effects of naturally induced dust particles on the climatic conditions.

The computation of naturally emitted dust aerosols involves different meteorological fields such as, surface wind speed, as well as numerous criteria of land surface characterization and its conditions such as, soil texture, moisture, the roughness due to the presence of non-erodible elements, vegetation cover and other factors (e.g., Zakey et al., 2006 and references therein). In addition, the dust particle atmospheric processes (i.e., transportation, deposition and aging) are highly reliant on the climatic conditions and mineralogical composition of the particles (e.g., Han and Zender 2010; Han et al., 2012). Though dust concentrations are larger near the desert and semi-arid regions, the smallest dust particles will remain suspended in the atmosphere for a week or more (Tegen and Fung 1994; Han and Zender 2010) and can be transported over large distances from their source region (Prospero, 1999; Prospero et al., 2002; Luo et al., 2003; Engelstaedter et al., 2006; Goudie and Middleton, 2006).

Soil dust aerosols exert substantial influence on the Earth's climatic system through a wide range of interactions. By scattering and partly absorbing solar radiation, as well as - depending on dust particle composition and size (Hess et al., 1998; Miller and Tegen, 1998; Satheesh et al., 2007; Solmon et al., 2008) - by absorbing and re-emitting thermal radiation, dust particles play a significant role in modulating the Earth-atmosphere system radiation budgets (direct effect) (e.g., Weaver et al., 2002; Mallet et al., 2009). As described in different studies, the dust aerosol energy budget perturbation will also induce several climatic implications. Such as, changes in temperature, hydrological cycle (e.g., modification of precipitation and cloud properties), surface heat and moisture fluxes, as well as atmospheric dynamics (semi-direct effect) (e.g., Miller and Tegen 1998; Miller et al., 2004a, 2004b; Yue et al., 2010a; Stanelle et al., 2010; Mallet et al., 2009; Solmon et al., 2012). Further, the dust particle induced climatic variable changes, may modulate the dust production itself (i.e., two way dust-climate interaction) (Perlwitz et al, 2001; Miller et al., 2004a; Stanelle et al., 2010; Yue et al., 2010b). Dust particles, modify the physico-optical properties of clouds, by acting as cloud condensation and ice nuclei (indirect effect) (e.g., Wurzler et al., 2000; Lohmann and Diehl, 2006; Hoose et al., 2008). Goudie and Middleton (2006); Goudie (2009) and references therein provided additional delineation about the role of dust aerosols in various fields.

Associated with the high temporal variability of climatic variables that govern dust emission processes; the soil dust aerosol production exhibits higher temporal heterogeneities. Therefore, quantifying the distributions as a well as different climatic role of dust particles at large-scales directly through field experiments or different observation techniques is very challenging. In this regard, the climate models, which are interactively coupled with a radiatively interactive desert dust module, are a beneficial tool to estimate the dust aerosol distribution along with its direct and

© University of Pretoria

semi-direct radiative effects. The sign and magnitudes of the dust radiative forcing are controlled by its physico–chemical and optical properties (i.e., its concentration, size distribution, mixing state, shape and mineralogical composition (refractive index)) (e.g., Haywood and Boucher, 2000; Balkanski et al., 2007; Wang et al., 2006; McConnell et al., 2008; Osborne et al., 2008; Mishra et al., 2010; Solmon et al., 2008).

Inaccuracies in the model's predicted spatio-temporal distribution of dust aerosol concentrations as well as its microphysical properties, would impose large uncertainties in the model's estimated radiative forcing and related climatic effects of dust aerosols (i.e., the direct and semi-direct radiative effects of dust aerosols) (Perlwitz et al., 2001; Miller et al., 2004b; Yoshioka et al., 2007; Lau et al., 2009; Kim et al., 2010; Zhao et al., 2011; Zakey et al., 2006; Solmon et al., 2008; Konare et al., 2008). Associated with the low grid resolution of the global-scale models, there exists a large bias in simulated meteorological fields and surface variables (e.g., Croft et al., 2012 and reference therein). Subsequently, this will impose remarkable inaccuracies on computations of dust aerosol emission, atmospheric processes and its climatic effects; especially in and around the dust source regions where their influences are more important (e.g., Zender et al., 2003; Tegen et al., 2002; Balkanski et al., 2007; Aoki et al., 2005; Luo et al., 2003; Tegen, 2003; Stanelle et al., 2010; Todd et al., 2012). In this respect, the desert dust module which is interactively coupled with high-resolution regional climate models (such as, the ICTP-RegCM4-dust model) is a noteworthy tool to simulate a small-scale dust process, as well as its climatic effects with better accuracies (e.g., Gong et al., 2003; Suh and Lee, 2004; Wang et al., 2004; Zakey et al., 2006; Han, 2010; Tummon et al., 2010; Konare et al., 2008; Solmon et al., 2008; 2012; Zhang et al., 2009; Giorgi et al., 2012).

It is presumed from the previous studies that the arid/semi-arid regions of South Africa as well as the desert areas of Namibia and Botswana are the most prominent source regions of wind eroded soil dust particles over South Africa (e.g., Bhattachan et al., 2012; Tanaka and Chiba, 2006). Therefore, naturally induced dust particles are one of the main components of atmospheric aerosols in South Africa (e.g., Tesfaye et al., 2011). However, fewer studies have been dedicated to compressive examination of the dust distribution, its radiative and climatic influences over South Africa using interactively coupled regional climate-dust model. For instance, recently reported dust aerosol distribution and influence studies, via employing the art of regional modelling approach, are focused in different parts of the globe, such as, East Asia (Zhang et al., 2009; Ju and Han, 2011), Southwest Asia (Marcella and Eltahir, 2010) and West Africa (Malavelle et al 2011; Zakey et al., 2006; Solmon et al., 2008; Konare et al., 2008; Solmon et al., 2012). It is only Tummon et al., (2010) that has reported the effects of mineral dust and biomass burning particles over the southern African regional climate during the winter season, using the regional climate-aerosol modelling approach. However, following the seasonal variation on local meteorological conditions, the dust emission flux, distribution as well as its radiative and climatic influences will also exhibit a seasonal variation (e.g., Miller et al., 2004b; Zhang et al., 2009). Therefore, to better understand the dust induced radiative perturbations and related climatic implications in a range of different meteorological conditions over South Africa, it is necessary to make an inclusive examination of dust distribution and its various climatic roles in different seasons, based on long-term regional modelling simulations.

The present study investigates the seasonal mean spatial distributions of dust loadings, along with its potential effects on surface and atmospheric radiative budget in different spectral bands (i.e., shortwave, long-wave and the net (sum of shortwave and long-wave)). Subsequently, from several climatic influences of soil dust particles, this study examine changes in terms of surface air temperature, sensible heat fluxes, columnar average net heating rate, cloud cover, cloud liquid water path and atmospheric dynamics; throughout different seasons of the year, over South Africa. This work has been carried out by using interactively coupled Regional Climate Model-anthropogenic/desert dust schemes of the International Centre for Theoretical Physics (ICTP-RegCM4-aerosol model, Giorgi et al., 2012). To our knowledge, this is the first study that has employed aerosol-climate two-way coupled long-term regional scale simulation to examine particularly wind eroded dust particle seasonal distributions, as well as feedbacks among dust, radiation and different meteorological fields, over South Africa. Furthermore, this work enriches the effort of understanding first-degree climatic influences of naturally induced mineral dust aerosols in South Africa. This paper is organized as follows: brief descriptions of the experimental design as well as some important points about the model are given in section 2. In section 3 the simulation results are presented and discussed. The discussion encompasses the seasonal and spatial variation of dust aerosol column burden, along with their direct and semi-direct effects over the area of interest (i.e., South Africa). Finally, the summary of our findings and conclusion are given in section 4.

2 Model and Experiment Design

In this study, interactively coupled regional climate-anthropogenic-desert dust model of the International Centre for Theoretical Physics has been used; to examine the seasonal distribution of desert dust particles, its direct radiative forcings as well the interaction and feedbacks among soil dust aerosols, radiation and climatic fields, in South Africa and the surrounding areas. Before employing the model for such purpose, its performance in simulating the Optical Properties of Aerosols (OPA) in South Africa were evaluated, by comparing with ground-based and satellite observations in Tesfaye et al., (2013). To support this and other studies, Tesfaye et al., (2013) also provided an extended general introduction about the significance of studying the climatic effects of aerosols using interactively coupled RegCM4-aerosol model. The essential steps and mechanisms which are considered in developing and implementing the online dynamical wind-eroded desert dust production scheme into RegCM4 are described in detail by Zakey et al., 2006. The RegCM4 dust emission parameterizations are effective for cells which are dominated by desert and semi-desert land covers as well as the dust scheme of RegCM4 represents the dry dust particle size distribution through size bin approach. The whole size spectrum of dust particles cover a diameter range of 0.01 to 20.0μm, divided into 4 size-bins i.e. the fine (0.01–1.0μm), accumulation (1.0–2.5μm), coarse (2.5–5.0μm), and giant (5.0–20.0μm) particle size modes (Zakey et al., 2006). For further brief description about: RegCM4, interactively coupled desert dust-anthropogenic aerosol modules of RegCM4, its limitations and the emission inventories employed in this study to introduce

© University of Pretoria

anthropogenic and biomass burning activities induced sulfur dioxide (gaseous SO_2), black and organic carbon aerosols into RegCM4, the reader may refer Tesfaye et al., (2013). The selected domain range, resolutions, designated model physics parameterization schemes, dynamical and surface parameter time setups of the model, as well as time-dependent initial and lateral boundary conditions employed in this study are similar with that of Tesfaye et al., (2013). The domain topography and the geographical map of South Africa (with province boundaries) are shown in Fig.1.

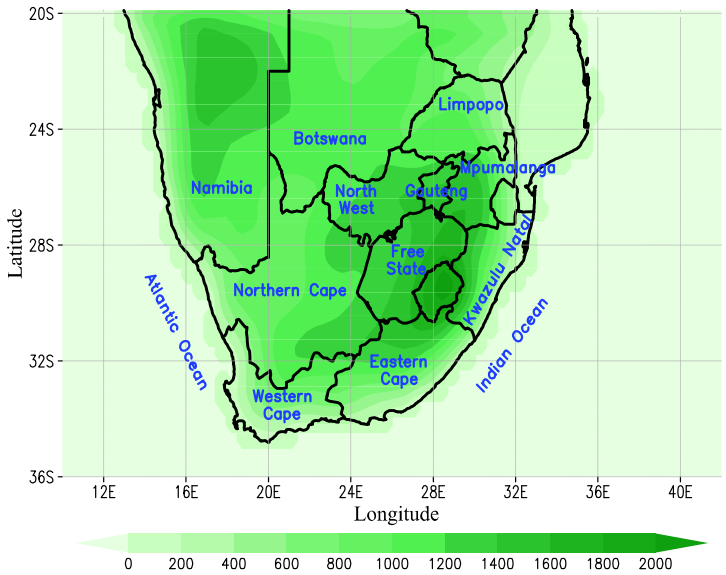

Fig. 1: Model domain, topography (unit: m) and geographical map of South Africa.

In order to extract dust-climate feedback signals from the underlying noise as well as to capture the mineral dust radiative forcing contribution, two long-term parallel simulations encompassing a period from 1997 to 2008 are conducted. Thereafter, the recent 11 years' results were comprehensively analysed in terms of different seasons. Of the two simulations, one is the reference simulation (REF), which includes all radiatively interactive aerosol components of RegCM4 (i.e. interactively coupled interactions among all aerosol components of RegCM4-radiation-climate are accounted). In other words, the REF experiment includes gaseous SO_2, sulfate, hydrophobic and hydrophilic black and organic carbon aerosols, which are induced from anthropogenic and biomass burning activities in and around South Africa; as well as all the four size categories of wind eroded desert dust particles (see Solmon et al., 2006; Zakey et al., 2006; Tesfaye et al., 2013). In the second experiment (i.e., control simulation: CNT) all conditions are the same as in REF except it has been simulated without dust aerosols. The dust aerosol radiative forcing contributions as well as climatic effects was derived from the differences between the REF and CNT runs (i.e. REF minus CNT). In addition, using the results of the REF simulations, we have examined the seasonal variation in dust aerosol column burden spatial distributions.

3 Results and Discussion

In the following subsections, the spatial distributions of dust column loading, as well as its effects on surface and atmospheric radiative budget are presented. Subsequent to these, the dust-radiation-climate interaction induced changes on different atmospheric and surface climatic variables are discussed. All results are presented in terms of four different seasons (Benhin, 2006): summer (November to February: NDJF), early-winter (fall, March to April: MA), winter (May to July: MJJ) and early-summer (spring, August to October: ASO). In addition, even if our domain configuration includes regions outside of South Africa, the simulation result discussions are strictly focused in our region of interest, i.e., South Africa.

3.1 Dust column burden

One of the physical parameters that determine the aerosol radiative forcing via influencing the aerosol optical properties is the particle size. Therefore, we have discussed the different size range of dust particles column burden (i.e, column-integrated mass concentration) seasonal mean spatial distributions. Fig. 2 shows eleven years averaged seasonal distribution of dust particles column loading in different size ranges (a) (0.01–2.5μm) and (b) (2.5–20μm), along with the wind vector at an altitude of 10m above the surface, over South Africa and its surrounding areas (from REF simulation). Generally, the simulation results exhibit that the arid/semi-arid regions of the Northern Cape Province of South Africa as well as Namibia and Botswana are source regions of wind derived soil dust particles, over South Africa. Moreover, because of their relatively short lifetime, dust aerosols are generally concentrated in regional hotspots close to their sources.

Throughout the seasons, the vertical distribution of dust particles mixing ratio exhibit the maximum dust concentration, which is confined below ~ 650hPa (not shown). Therefore, as displayed in Fig. 2 the dust particle columnar spatial distribution in South Africa primarily follows the well-known South African anti-cyclonic (anti-clockwise) surface air circulation. As a result, throughout the year the dust plume predominately sweeps towards the south-eastern and southern parts of the country. These results are consistent with the previous observational based studies (Bhattachan et al., 2012; Tesfaye et al., 2011). Further, the results indicate that the meteorological fields, such as surface wind speed, and the dryness condition seasonal variations are essential in determining the dust emission and distribution.

Across South Africa, the simulation results show that primarily the Northern Cape and the western regions of the North West provinces of South Africa are highly affected by desert dust particles. Following the windy as well as reduced soil moisture conditions (not shown) around the dust aerosol potential source areas, during early-summer (ASO) and summer (NDJF) seasons, over the northern parts of the Northern Cape Province (see Fig. 2), the column burden of dust exhibits its maximum (i.e., up to 440 mg/m^2 for a size range of 2.5–20μm during ASO and 270 mg/m^2 for a size range of 0.01–2.5μm during NDJF). Excluding the Northern Cape arid regions of South Africa, over the rest parts of the country, NDJF is the rainy season (i.e., moisture abundance and precipitation is enhanced in summer). As a result of this situation, the dust particle removals through wet deposition processes are enhanced. Therefore, during summer the dust particle regional scale distribution and build-up over the rest of the areas of the country is constrained.

During MA through to MJJ, associated with the gradual decline of wind speed, the dust loading also illustrate a progressive reduction and reaches its minimum during MJJ. During MJJ, the dust aerosol loading varies from 20 to 225 mg/m^2 (for a size range of 2.5–20μm) and 10 to 150 mg/m^2 (for a size range of 0.01–2.5μm).

© University of Pretoria

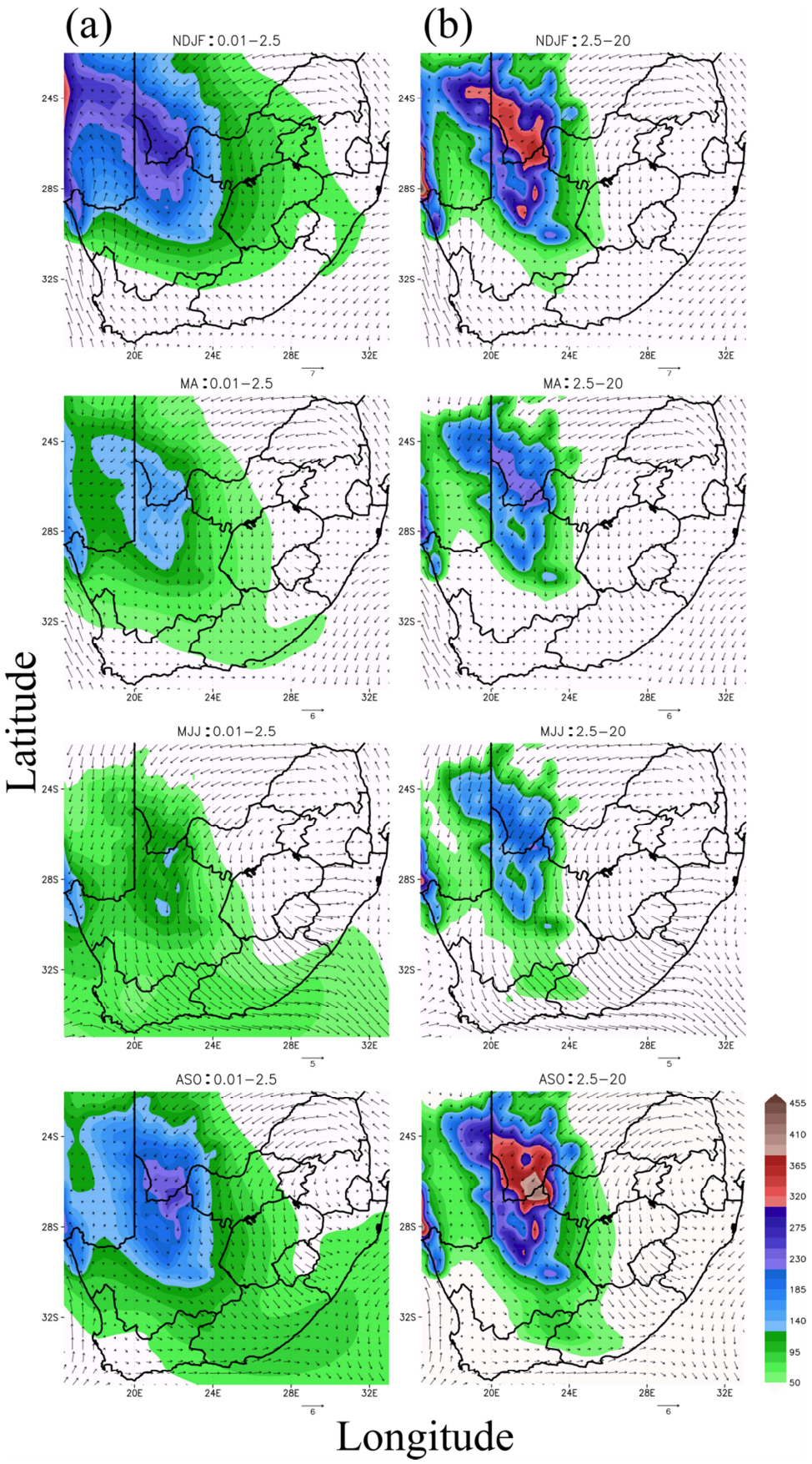

Fig. 2: 1998–2008 averaged seasonal mean spatial distributions of dust aerosol column burden (shaded, unit: mg/m^2) within diameter range of (a) (0.01–2.5μm) and (b) (2.5–20μm) along with the 10 meter wind field (vector; the scale is indicated by the arrow to the lower right; unit: m/s), in and around South Africa.

Overall, during MA and MJJ the dust aerosol column burden exhibit a reduction by about ~ 40% and 45% relative to the maxima, respectively. However, during these seasons (MA and MJJ), as a consequence of gradually enhanced dry situations, the dust particle dispersions beyond their source regions are favoured. In particular, throughout MJJ, the wind current sweeps in a south-westward and southern direction across the dust source regions and flow primarily into the south-eastward direction of the country; influenced by this air flow, the dust particles exhibit a distinct distribution that encompasses wide areas of the southern parts of South Africa and the surrounding ocean. As a consequence of relatively efficient dry deposition processes that take place during the transportation of dust particles which have a diameter larger than 2.5 μm (e.g., Tanaka and Chiba, 2006); these particles' distribution are more constrained compared to particles that have a diameter of less than 2.5 μm. However, we have noticed that the larger sized dust particles' (diameter > 2.5 μm) dispersions are more favoured by the dry situations of the extended winter seasons of South Africa (i.e., MJJ and ASO), especially during spring which exhibit more drier and windy meteorological conditions relative to MJJ. Contribution by each dust particle size category to the annual average dust load show that from ~ 50% to 65% of the total dust mass throughout the northern and central areas of the Northern Cape province are contributed by dust particles which are within the diameter range of 2.5–20 μm (fig. is not shown). Whereas, in other regions of South Africa as well as the remaining areas of the Northern Cape province the contribution of particles with a diameter of < 2.5 μm prevails.

3.2 Direct radiative forcing of dust

The radiative forcing contribution of dust at the surface and in the atmosphere measures the radiative cooling/warming influences of dust aerosols on the surface-atmospheric system before climatic modifications are taking place (i.e., prior to any climatic feedback).

3.2.1 Short-, long-wave and net surface radiative forcings of dust aerosols

The seasonal mean spatial distribution of dust aerosols Shortwave Surface Radiative Forcing (SSRF) are exhibited in Fig. 3 (a). As a result of dust particle solar radiation extinction influences (via both scattering and absorption), the net shortwave radiative flux at the surface is considerably reduced. In general, simulation results show that the dust aerosol SSRF spatial patterns

© University of Pretoria

and seasonal evolutions are similar to that of spatio-seasonal variations of dust aerosol column loads (Fig. 2 and Fig. 3a). Consequently, during the windy seasons of spring and summer (i.e., ASO through NDJF) the SSRF of dust exhibit its maximum (~ -25W/m^2 to -33W/m^2) around the northern areas of the Northern Cape Province. Compared to spring and summer seasons, a continual decline of dust load during autumn and winter induced the weakening of dust SSRF. As a result the lowest negative values of SSRF distributions are noted during MJJ. For MJJ, the maximum range of SSRF's negative values varies from ~ -7W/m^2 to -14W/m^2, around the Northern Cape desert areas. Also, following the widely spread dust particle distribution of winter season (especially dust within a size range of 0.01 –2.5μm, see Fig. 2a), around the central and southern parts of South Africa as well as in the surrounding ocean the SSRF values that varied from ~ -3W/m^2 to -7W/m^2 were noted. Further, the radiative influence of dust particles are more complex because of their ability to interact with both shortwave and longwave radiations.

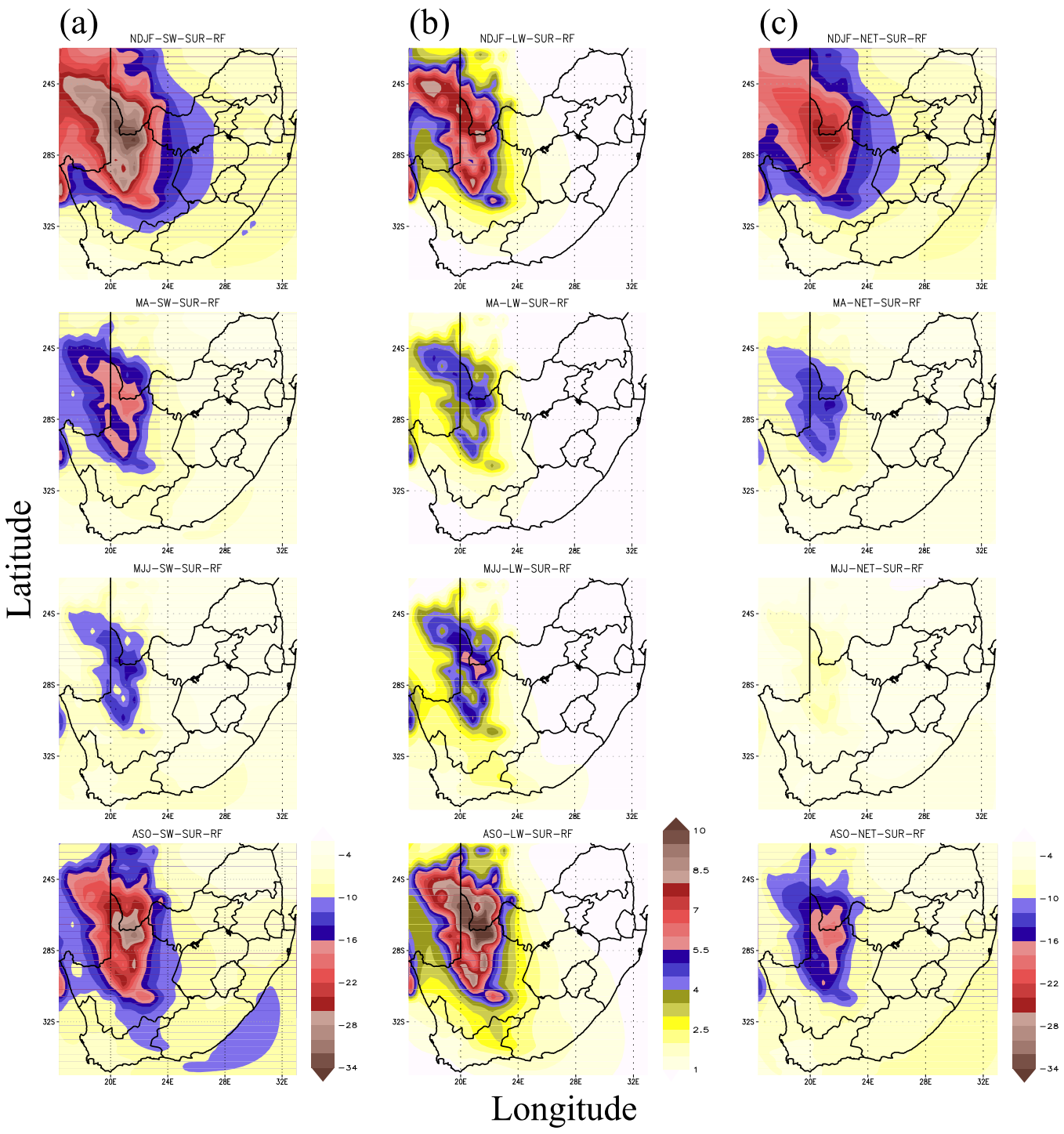

Fig. 3: 1998–2008 averaged seasonal mean spatial distributions of direct radiative forcing contributions of dust aerosols at the surface, in and around South Africa: column (a) shortwave, (b) longwave and (c) net (SW + LW) (units: W/m^2); derived from the difference of REF and CNT simulations (REF-CNT). Each row represent the four seasons of the year, (see the abbreviations at the top of each figure).

Fig. 3b shows the seasonal mean spatial distributions of dust aerosol induced Longwave Surface Radiative Forcing (LSRF). In general, due to the dust aerosol interaction with longwave radiation (especially by those which are large in size), as well as the re-emission of thermal radiation by dust particles, the net surface longwave radiative flux at the surface increased (which is opposite to that of SSRF). These results have shown that the dust LSRF followed the spatio-seasonal patterns of dust particles which have a diameter ≥ 2.5μm. As a result, the dust particles induced LSRF is primarily significant around their source regions (i.e., Northern Cape Province). This is due to various removal processes which specially constrain the large size dust particle dispersions beyond their source regions (see Fig. 2b), as well as the high temperature and arid conditions of the Northern Cape

© University of Pretoria

dust source regions. Over the desert areas of the Northern Cape Province the highest level of dust LSRF (with a maximum range from ~ 8 to 10 W/m^2) are noted during the drier windy season of ASO. During NDJF, the dust LSRF values declined by ~18% compared to ASO season. Aligned with the gradual decline of the dust load, specifically dust particles which are within a diameter range of 2.5–20μm (Fig. 2b), the minimum values of LSRF of dust were noted during MA (the magnitude of dust LSRF, approximately, declines by about 50% during MA, relative to ASO). The gradual advancement of dry conditions from autumn to winter (MJJ) facilitate the dust production and distribution, which as a result slightly enhance the dust LSRF during MJJ, relative to MA.

Lastly, the total role of dust on perturbing the surface net radiative balance, i.e. the Net Surface Radiative Forcing (NSRF = SSRF + LSRF) of dust aerosols, is shown in Fig. 3c. Looking at Fig. 3a and b with the dust mass distribution of Fig. 2, we have shown that where the fraction of large size dust particles are highly concentrated around their source regions; their surface long-wave forcing contribution is relatively large. However, around and away from the dust primary source regions, due to the predominance, longer life time, quick dispersion of small size range dust particles which have the largest cross-sectional area per unit mass; the negative SSRF values of the dust strongly surpass the positive values of the dust's LSRF. In addition, owing to the low temperature conditions and lower surface albedo features of the surrounding oceans (also majority of the coastal regions), enhanced SSRF are noted in these areas. These circumstances cause negative NSRF values of dust throughout the entire seasons (Fig.3c). Therefore, with lower negative values relative to SSRF, the NSRF values of dust exhibit similar spatio-seasonal patterns as the dust SSRF. During the NDJF season, the highest negative values of the NSRF of dust (up to -25 W/m^2) are noted around the northern areas of the Northern Cape Province. Furthermore, the minimum negative value distribution of dust NSRF (varying from -2 W/m^2 to -9 W/m^2) are noticed during winter. In overall, Fig.3c indicates that, owing to a strong reduction of net SW radiation at the surface that offsets the LW surface radiative warming influences of dust aerosols, in and around South Africa the dust particles play a net radiative surface cooling role.

3.2.2 Short-wave, long-wave and net atmospheric radiative forcing of dust aerosols

The change in the atmospheric radiative heating due to aerosols is known as the atmospheric radiative forcing (ARF); which is the difference between the top-of-the-atmosphere (TOARF) and the surface radiative forcing (SRF) (i.e., ARF = TOARF-SRF). The seasonal mean spatial distributions of SW, LW and net ARFs of dust aerosols in and around South Africa are presented in Fig.4 (a) to (c), respectively. Contingent on the dust particles mineralogical composition as well as their particle sizes, the dust aerosols have a partial absorption nature of SW radiation (e.g., Hess et al., 1998; Miller and Tegen, 1998; McConnell et al., 2008; Solmon et al., 2008; Mallet et al., 2009; Mishra et al., 2010). As a result, over the entire domain, the dust aerosol's induced positive values of SWARF (i.e., dust particles induced SW radiative heating in the atmospheric column). Over the upper and central parts of the Northern Cape regions, the maximum range of SWARF values of dust (varying from ~ 20 to 27 W/m^2) are observed during ASO and NDJF. Aligned with the dust burden reduction in and around the neighbouring areas of the Northern Cape Province, the SWARF values that vary from ~ 4 to 14 W/m^2 as well as ~ 2 to 10 W/m^2, were observed during MA and MJJ seasons respectively.

In contrast to the dust SW radiative heating, the dust particle's LW radiative effects exhibit their radiative cooling influences in the atmosphere (i.e., the spatio-seasonal distribution of dust particles LWARF (Fig. 4b) exhibit negative values throughout the entire domain). During ASO and NDJF seasons, the substantial influences of dust particulate LWARF (the highest negative values that vary from ~ -6 to -10 W/m^2), that stretch from the northern to the central areas of the Northern Cape Province are observed. Also, in and around the Northern Cape Province, the LWARF values that vary from ~ -0.5 to -5 W/m^2 and ~ -1 to -6.5 W/m^{2}have been noted respectively during MA and MJJ seasons. When comparing the life time of the small and large sized range of dust particles; the removal processes, such as dry deposition through gravitational and turbulent settling, are more effective in the larger particles (e.g., Zakey et al., 2006). In addition, the lighter mass of the small sized range of dust particles favour their emission and dispersion (this can be also noted by comparing Fig. 2a and b). These factors allow small size range dust particles to dominate, consequently leading to the dominant influence of dust in the SW spectral band.

Additionally, our simulation results show that the magnitude of SWARF is ~ 2 to 3 times higher than that of the LWARF values. As a result, Fig. 4c displays the spatio-seasonal distribution of the dust's net ARF (NARF = SWARF + LWARF) that reflects both the patterns and sign of the SWARF. Therefore, the dust particles' overall role in radiative forcing is to decrease the net radiation absorbed by the surface (Fig.3c), in companion with increasing the radiative heating of the atmosphere (Fig. 4c). In and around the neighbouring areas of the Northern Cape Province, the distribution of the NARF values that vary from ~ 2 to 14 W/m^2 (during spring) and the distribution of the maximum values, which varied from ~ 7 to 18 W/m^2 are found during NDJF. As the seasons progressed, the dust NARF values gradually has declined (during MA it vary from ~ 2 to 9 W/m^2) and reached their minimal values (varying from ~ 0.6 to 5 W/m^2) during MJJ. In spite of the magnitudes of the dust radiative forcing, which are quite reliant on the mineralogical composition of the dust particles, its burden level and other factors; the signs of dust radiative forcing observed in our simulations (i.e., at the surface and atmospheric columns in all SW, LW and net spectral ranges) are in good agreement with other regional and global scale studies (e.g., Yoshioka et al., 2007; Dufresne et al., 2002; Miller et al., 2004b; Yue et al., 2010a; Stanelle et al., 2010; Mallet et al., 2009).

© University of Pretoria

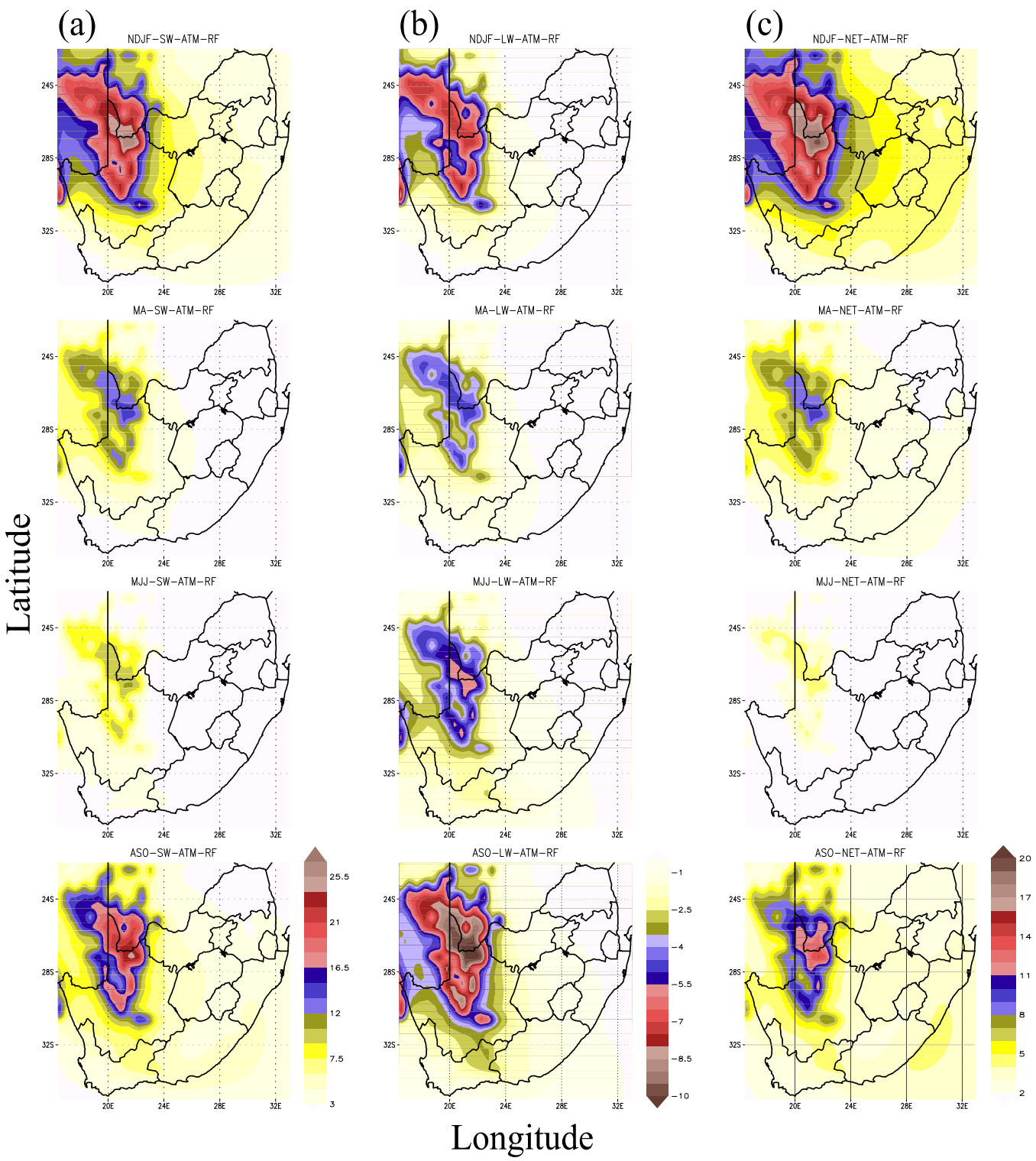

Fig. 4: 1998-2008 averaged seasonal mean spatial distributions of dust aerosol's direct radiative forcing contributions in the atmospheric column, in and around South Africa (a) shortwave, (b) longwave and (c) net (SW + LW) (units: W/m^2); derived from the difference of REF and CNT simulations (REF-CNT). Each row represent the four seasons of the year, (see the abbreviations at the top of each figure).

3.3 Climate responses

In this section, the dust aerosol-radiation-climate interactions induced climatic variables changes, as well as correlations among these alterations are discussed. In the next subsection, the change in Surface Temperature (ΔST) and Surface Sensible Heat Flux (ΔSSHF) will be addressed. In section 3.3.2, the effects of radiatively interactive dust particles on Net Atmospheric radiative Heating Rate (ΔNAHR), as well as on hydrological variables (in terms of Cloud Cover (ΔCC) and Cloud Liquid Water Path (ΔCLWP) changes) are provided. Finally, the influences of dust aerosols on Planetary Boundary Layer height (ΔPBL), Surface Pressure (ΔSP) along with the surface wind field ($\overrightarrow{\Delta W}$) are delineated in section 3.3.3.

3.3.1 The effects of dust aerosol on surface temperature and surface sensible heat flux

The seasonal mean spatial distributions of changes in ST (K) and SSHF (W/m^2) due to the dust-radiation-climate interaction (i.e., differences between REF and CNT simulations), are shown in Fig. 5(a) and (b), respectively. The predicted changes in ST (ΔST) showed a significant seasonal variation. In addition to the negative NSRF effects of dust aerosols (Fig. 3c), their semi-direct effect induced cloud cover enhancement (Fig. 6b, which in turn decrease the amount of solar radiation reaching the surface); furthermore reinforced the dust aerosol's overall surface radiative cooling tendencies (e.g., Haywood and Boucher, 2000; Ramanathan et al., 2001; Zhang, 2008). As a result, predominantly in and around the neighbouring areas of the Northern Cape

Province, reductions in ST are observed (Fig. 5a). Around the northern areas of Northern Cape Province, the pronounced regional cooling effect of dust particles (i.e., higher negative values of ΔST, varying from -0.7 K to -1.1 K) are noticed during the extended summer seasons (from NDJF through MA). Meanwhile, during these seasons, intermediate values of ST reduction (ΔST varying from -0.3 K to -0.7 K) are found in other parts of the Northern Cape, as well as some areas of the neighbouring provinces. Generally, during the spring season (ASO), the South African climatic conditions become dry and windy. Thus, the reinforcement of dust surface radiative cooling effects by the dust particles induced cloud cover increment becomes reduced (Fig. 6b). As a consequence, relative to the extended summer seasons in spring, reduced (moderate) negative values of ΔST (-0.3 K to -0.6 K), which extend from the northern regions of the Northern Cape Province to its central areas, were noted. Associated with the minimal burden (Fig. 2)/reduced direct radiative forcing contribution of dust aerosols (Fig. 3), as well as their dynamical impact (Fig. 7), a minimal ΔST distribution (-0.2 K to -0.5 K) that comprise comparatively wider areas of the downwind dust source regions are observed during MJJ. Generally, the cooling influence of dust aerosols may have a substantial effect on the lower troposphere dynamical processes. This particular issue is discussed in the final subsection of this study (see section 3.3.3).

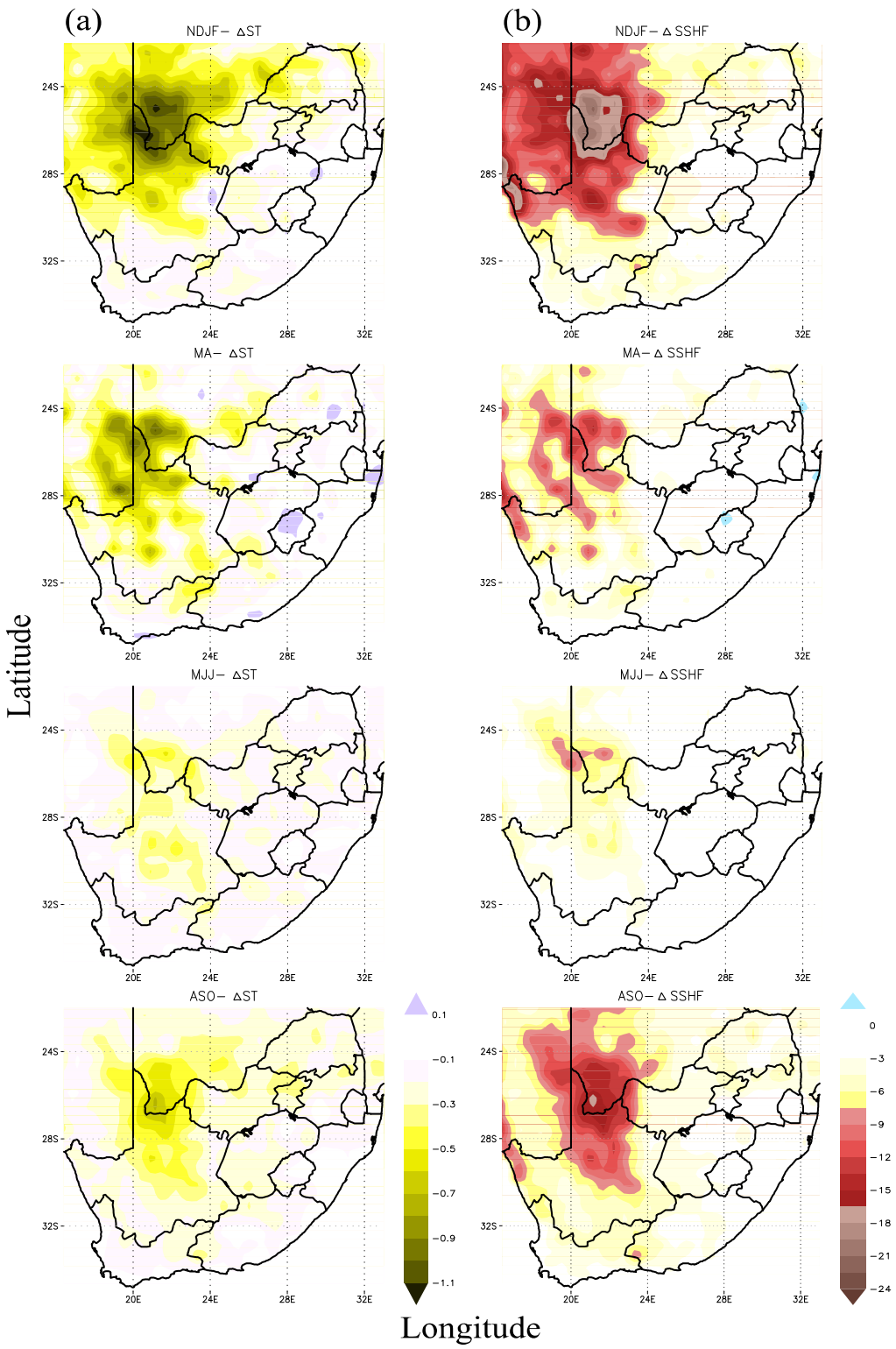

Fig. 5: 1998–2008 averaged seasonal mean spatial distributions of changes in (a) surface temperature (K) and (b) surface sensible heat flux (W/m^2), due to the presence of dust aerosols (REF- CNT). Each row represent the four different seasons of the year, (see the shortened letters at the top of each figure).

In general, atmospheric particulate induced net radiation flux perturbation at the surface, will consequently cause changes on the land-atmosphere system energy exchange (i.e., this will involve alteration of energy transfer from the surface to the atmosphere in the form of net thermal radiation, sensible and latent heat fluxes) (e.g., Ramanathan et al., 2001; Yu et al., 2002; Miller et al., 2004b; Mallet et al., 2009; Yue et al., 2010a; Zhang, 2008). Therefore, the dust aerosol induced negative NSRF (surface radiative cooling) will be compensated by reducing one or all of these surface energy components (e.g., Boer 1993; Yu et al., 2002). Usually, the mechanism through which these surface energy components respond are highly reliant on turbulence activities, changes in surface temperature and, together with these, especially in a case of latent heat on the prior abundance of surface moisture (e.g., Boer 1993; Miller et al., 2004b; Yue et al., 2010b). Thus, as the dust aerosol induced net surface radiation forcing becomes large enough to change the ST (also to some extent the atmospheric dynamics) it will, consequentially, bring a change in the surface energy components (e.g., Miller and Tegen, 1998; Yu et al., 2002; Miller et al., 2004a, 2004b; Zhang, 2008; Mallet et al., 2009; Yue et al., 2010a, 2010b). In addition to these systematic factors, the results from Miller et al., 2004b; Yue et al., 2010b further show that the change in the latent heat flux is more substantial over oceanic regions. Whereas, due to the relative scarcity of water, the modifications of sensible heat and net upward long-wave fluxes are important over the land.

© University of Pretoria

Therefore, in this study, we have examined the dust aerosols' existence induced changes in SSHF (ΔSSHF). Throughout the seasons, as for the ST, the presence of dust particles also induces reductions in SSHF (Fig. 5b). The negative values of ΔSSHF indicated that the cooling at the surface lead to reductions in the upward transport of SSHF from the surface to the atmosphere. Aligned with the spatio-seasonal distributions of ST reductions, across the Northern Cape Province, the maximum negative values of ΔSSHF (~ -6 to -24 W/m^2) and the minimum negative values (~ -2 to -10 W/m^2) are displayed during NDJF and MJJ seasons respectively. Throughout autumn and spring the dust particles induced SSHF reduction varied from ~ -2 to -14 W/m^2. On the other hand, over some narrow scattered areas especially away from the dust source regions, a minor reduction/increase of ST and, consequently, SSHF which are not directly related with the dust aerosol's induced NSRF and/or CC changes were noted. These insignificant changes may be attributed to the dust-climate system's interactions induced background aerosols concentration changes (fig. is not shown here) and/or regional scale atmospheric dynamic alterations (Fig. 7). Nonetheless, both the spatial coverage and magnitudes of these minor changes are quite negligible when compared with the dust-climate interactions induced ST and SSHF changes. Furthermore, even if it is beyond the scope and the concern of this study, we take cognisance of the fact that the change in surface energy budget (such as SSHF-Fig. 5b as well as the upward net longwave radiation) may inflict some alterations on greenhouse gas forcing. Overall, the annually averaged spatial correlations between NSRF of dust with ΔST and ΔSSHF are 0.71 and 0.8, respectively, as well as correlations among ΔST and ΔSSHF are ~ 0.95. The spatial correlations between ΔCC with ΔST and ΔSSHF are -0.81 and -0.65, respectively. These correlations evidently reveal that the dust aerosols' influence on ST and SSHF are not simply associated with their direct radiative effects only, but rather both the dust aerosols' induced direct and semi-direct effects (interactions and feedback among aerosols, radiation, and cloud fields) are accountable for the changes in ST and, in turn, SSHF. This illustrates the necessity of simultaneously considering the direct as well as semi-direct effect of aerosols to get a better understanding of the overall role of aerosols in climate.

3.3.2 The effects of dust aerosols on net atmospheric radiative heating rate, cloud cover and cloud liquid water path

As mentioned previously throughout the seasons, the vertical distribution of dust particles exhibit that the maximum dust concentrations are confined below the altitude of ~ 650hPa. Therefore, the averages over 1998-2008 of the spatio-seasonal distribution of dust induced changes in columnar averaged short- plus long-wave (net) radiative heating rate (K/day, ΔNAHR), column integrated cloud cover (%, ΔCC) and column integrated cloud liquid water path (g/m^2, ΔCLWP) on the lower troposphere (~ below 650hPa), are shown in Fig. 6(a), (b) and (c), respectively. The computation of radiation and climate system interactions induced net atmospheric radiative heating rate include the radiative feedbacks of all climatic components (for example, from aerosols, clouds, water vapour, the underlying surface and other trace gases in the atmospheric column). Therefore, as indicated in section 2.2, the dust aerosols' influences on NAHR are captured based on the differences between REF and CNT simulations. Thus, positive values of ΔNAHR demonstrates that the presence of partially absorbing dust particles in the atmospheric column which results an overall enhancement of net radiative heating rate (i.e., it induced warming in the atmospheric column). In general, the sign convention is such that positive terms specify the dust induced increments on NAHR/CC/CLWP and vice versa for negative terms.

Around the dust burden dominating areas of South Africa (areas that stretch from the northern to the central areas of the Northern Cape Province), the existence of dust aerosols cause net heating of the lower troposphere (below ~ 650 hPa) (Fig. 6a). In these areas, from ASO throughout until NDJF season, the lower-tropospheric columnar averaged net heating influence of dust exhibit large values (the maximum range of ΔNAHR varied from ~ 0.5 to 1.2 K/day). Aligned with the dust loading seasonal variation, the positive value of ΔNAHR gradually declined from MA to MJJ and exhibited its minimum distribution during winter (MJJ). However, over scattered areas which are near and/or away from the dust particles' major warming zones, the changes in the lower troposphere columnar averaged net radiative heating rate showed the net cooling effects of dust (i.e., in Fig. 6a the negative values of ΔNAHR that varied from ~ -0.1 to -0.4 K/day are noted). Our results are in good agreement with previous modelling studies (e.g., Miller et al., 2004b) that exhibit the lower troposphere net heating influences of dust particles, while its column burden exceeded 50 mg/m^2. As highlighted by previous studies, (e.g., Zhang, 2008; Perlwitz and Miller, 2010; Yue et al., 2010b; Solmon et al., 2012), when the atmospheric radiation perturbation by the dust aerosols becomes large enough to change the sign of heating rate of the atmosphere, it will consequently interrupt the vertical dynamics, as well as hydrological variables of the atmosphere. Hence Fig. 6b and c, respectively, show the changes instigated by the dust-radiation-climate interactions in low-level cloud cover (low-clouds which are formed below ~ 650 hPa; ΔCC) and CLWP (ΔCLWP).

Generally, the distribution as well as the sign of ΔCC showed a high degree of consistency with the low-level cloud liquid water amount response (the ΔCC and ΔCLWP showed a 0.94 spatial correlation). Within South Africa there are two main rainy seasons. Excluding the Northern Cape arid region, areas which are north of 30°S summer is their rainy season. Whereas, regions which are south of 30°S (primarily the Western and Eastern Cape regions) display a Mediterranean climate (i.e., from the beginning of MA throughout until MJJ, the cloud cover and amounts of rain exhibits an enhancement). Subsequently, the results show that the magnitudes of ΔCC and ΔCLWP are not only dependent on dust aerosol burden level or their radiation perturbation seasonal variations; but are also reliant on seasonally variable clouds and water vapour abundances. Therefore, during summer (NDJF), encompassing broader areas above 30^{0}S, a CC and CLWP increment with a maximum level range that varied from 2 to 6% (Fig. 6b) and from 0.6 to 2.2 g/m^2 (Fig. 6c), respectively, are noted. During MA to MJJ, primarily in regions which are below 30^{0}S, as well as in and around the Northern Cape arid regions, the ΔCC and ΔCLWP values varies from 1 to 7% (Fig. 6b) and 1 to 2.5 g/m^2 (Fig. 6c), respectively are observed. Owing to the scarcity of cloud and water vapour during spring (i.e., during ASO, which is a dry season of South Africa), minimum positive values of ΔCC (up to 2.1%) and ΔCLWP (up to 0.9 g/m^2) are found over scattered areas in South Africa (Fig. 6b and c).

© University of Pretoria

Aligned with the dust aerosol warming influences some narrow areas experienced minimal reduction in low-level CC and CLWP, which is consistent with the conventional description of the semi-direct effect. Nonetheless, the spatial coverage as well as the magnitudes of these minimal negative values of ΔCC and ΔCLWP are insignificant when compared to the major enhancements of CC and CLWP. Therefore, ruling out these negligible changes generally, the dust aerosol-climatic system interaction in South Africa plays an important role in enhancing low-level (below ~ 650 hPa) CC and CLWP. The enhancements of these hydrological variables are prompted by both net atmospheric heating and cooling influence of dust aerosols under different mechanisms. Subsequent to the major atmospheric heating influence of dust aerosols, an enhancement of low-level (below ~ 650 hPa) column-integrated perceptible water vapour (water vapour mixing ratio) was noted (fig. is not shown). As explained in different studies (e.g., Perlwitz and Miller, 2010; Lau et al., 2009; Solmon et al., 2008, Lau and Kim, 2006), following the dust radiative heating driven water vapour mixing ratio increments, the enhancement in water vapour ascent to the upper regions of the lower-troposphere, as well as an enhanced moisture convergence and higher relative humidity in the upward direction will occur (Perlwitz and Miller, 2010; Zhang, 2008). In this process, the dynamical influences of dust aerosols also have important role (Perlwitz and Miller, 2010; Douville et al., 2002). Overall, attributed to aforementioned circumstances plus other aspects of the climate (Perlwitz and Miller, 2010; Douville et al., 2002; Zhang, 2008) around and away from the dust heating zones, cloudiness and cloud liquid water amount will increase aloft, especially towards the upper level of the lower-troposphere.

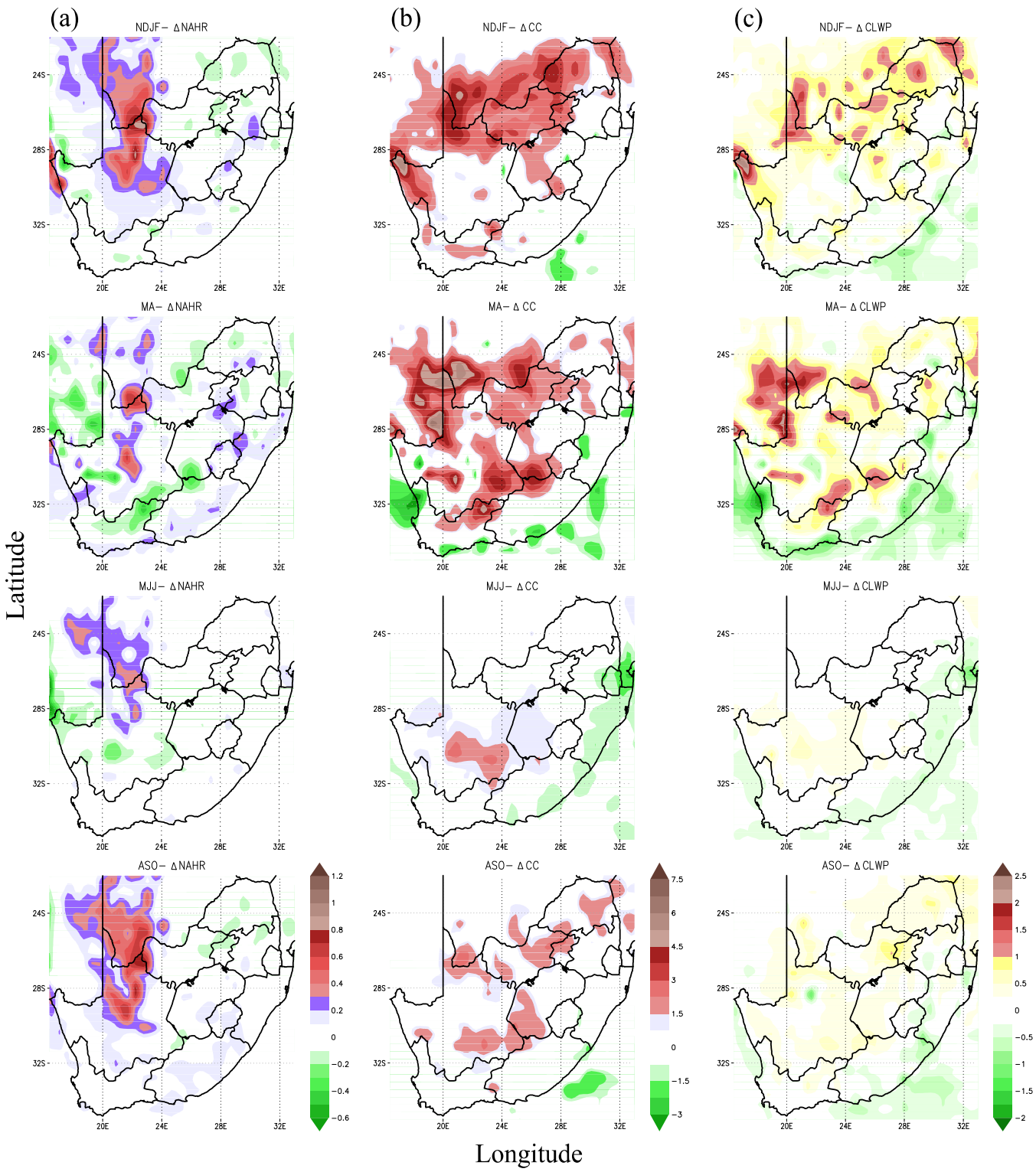

Fig. 6: 1998-2008 averaged seasonal mean spatial distributions of changes in low-level (a) column average net heating rate (K/day), (b) column integrated cloud cover (%) and (c) column integrated cloud liquid water path (g/m^2), due to the presence of dust aerosols (REF- CNT). Each row represent the four seasons of the year, (see the shortened letters at the top of each figure).

© University of Pretoria

Conversely, over areas of South Africa which experience cooling due to the existence of dust particles; the atmospheric background is more favourable and effective for the cloud formation and its liquid water amount amplification. Thus, in these areas (areas that correspond to the dust cooling zones) with minimal influence of dynamical changes, strong and more extended enhancements in CC and CLWP are noted. Since cloud cover generally depends on relative humidity, whereas precipitation depends on the cloud liquid-water amount; therefore, the variation in CLWP mirrors the alterations on precipitation (Pal et al., 2000). Nonetheless, the precipitation change further depends on the atmospheric water holding capacity and other dynamical factors. In addition, even if it is not described here, it is important to remember that dust aerosol promoted modifications on surface energy components, such as changes in latent heat flux (which govern alterations in surface evaporation), in line with other effects of dust, will also affect the overall atmospheric hydrological variable adjustments (e.g., Ramanathan et al., 2001; Rosenfeld, 2006; Cook and Highwood, 2004; Zhang, 2008).

In general, the results have shown that the role the dust particles played on hydrological variables are not only constrained to the radiative influences of dust particles; but rather a result of the complex interaction and feedback among dust, radiation, hydrological and dynamical fields; which are modulated by the dust direct radiative forcing and in turn affect the simulated climate. Furthermore, since clouds are a sustainable water resource for arid and semi-arid regions, our results exhibit that naturally induced dust particles are in favour of maintaining this vital water source of the desert region. However, to draw conclusions on the net role of dust on hydrological parameters, one needs to incorporate the indirect effect of dust; which is not formulated in this study (e.g., Wurzler et al., 2000; Ramanathan et al., 2001; Hoose et al., 2008). The aforementioned dust-induced changes, such as on surface temperature (e.g., Fig. 5a), net energy balances of the surface (e.g., Fig. 5b) and the atmosphere (Fig. 6a), as well as hydrological parameters of the atmosphere (Fig. 6b and c), may have a possible dynamical feedback on atmospheric circulation (e.g., Jacobson and Kaufman 2006; Stanelle et al., 2010; Zhang, 2008; Solmon et al., 2012). This specific issue is discussed in the following sub-section.

3.3.3 The effects of dust aerosols on planetary boundary layer, surface pressure and wind

Seasonally averaged dust-induced changes in planetary boundary layer height (ΔPBL), surface pressure (ΔSP) and 10m surface wind field (ΔW) are shown in Fig. 7. In the course of the extended summer seasons (NDJF throughout until MA), over the dust aerosols' dominating areas of South Africa, the PBL height reduction (with a maximal range that varied from -70 to -90 m) and SP increments (with a maximal range that varied from 0.17 to 0.25 hPa) are noted. Throughout the dry extended winter seasons (relative to the extended summer seasons), reduced values of ΔPBL and ΔSP are observed (for example over the dust aerosols' ruling areas of South Africa the maximal range of ΔPBL and ΔSP varied from -40 to -60 m and 0.07 to 0.17 hPa, respectively). Also, our results show highly consistent spatial correlations of both ΔPBL and ΔSP with ΔST (correlation coefficients of about 0.98 and -0.9, respectively), plus with ΔSSHF (correlation coefficients of about 0.93 and -0.78, respectively); as well as correlations between ΔPBL and ΔSP is ~ -0.9. Subsequent to these relationships, the ΔPBL and ΔSP exhibit a good correlation with the dust induced radiative and hydrological effects, which are the direct/subsidiary prime causes for the change in ST and SSHF. For instance, the correlation between ΔPBL and ΔSP respectively are, with NSRF: -0.76 and 0.7, with NARF: -0.82 and 0.74 and with ΔCC: -0.78 and 0.75.

The dust aerosol direct radiative (Fig. 3 and Fig. 4) and semi-direct atmospheric thermodynamic influences induced the lower-tropospheric heating and CC increments (Fig. 6), as well as the reduction of ST, which in turn, decreases the turbulent flux of sensible heat transfer into the atmosphere (Fig. 5). These situations result a weakening in convectively driven turbulence and surface buoyancy flux (Yu et al., 2002; Miller et al., 2004a; Jiang and Feingold, 2006; Zhang, 2008). As a result, the reduction in PBL height plus the stabilization of the lower troposphere lapse rate (in turn enhancement in SP) will occur (e.g., Zhang, 2008). Accordingly, the results shown in Fig. 7 and the aforementioned correlations (i.e., consistent correlations among ΔPBL and ΔSP with other dust induced radiative and climatic variables changes) evidently clarified these consecutive reasons and mechanisms which were primarily accountable for the observed ΔPBL and ΔSP. Similarly in Fig. 7, seasonally averaged dust-induced changes in the 10m surface wind fields (i.e., $\overrightarrow{\Delta W} = \Delta U + \Delta V$ - the respective differences in zonal (ΔU) and meridional (ΔV) wind components among REF and CNT simulations as a vector arrow) over the land and the neighbouring sea surface are provided. The vector arrows pointing to the eastern and northern directions indicate an increase in ΔU and ΔV, respectively. However, those which point to the western and southern directions specify the reduction in these wind components.

Our simulation results have illustrated that the presence of radiatively interactive dust aerosols caused change in surface wind speed, which is spatio-seasonally highly variable. Relatively larger changes in both zonal and meridional winds (i.e., the surface wind speed increment ~ up to 0.17 m/s and reduction ~ up to 0.22 m/s) are predicted during the extended summer seasons (NDJF and MA). During these seasons, the reductions in meridional component are primarily observed over the west and southwest parts of the country, while for zonal wind experience over the dust aerosol dominating zones. Nonetheless, during the same period, both wind components display an enhancement over the central and northern parts of South Africa. Increments in zonal wind are predicted over the south and southeast areas. Throughout the extended winter seasons (MJJ to ASO), small changes in zonal and meridional winds (i.e., minimal values of $|\overrightarrow{\Delta W}|$ relative to extended summer seasons) are noted. Nonetheless, in these seasons (MJJ, ASO), the $\overrightarrow{\Delta W}$ are found to be more extended to areas which are away from the dust source regions. During this period, in and around the southwest regions of the Northern Cape, both zonal and meridional components show reductions (surface wind speed reductions up to 0.13 m/s). Conversely, an increase of the meridional wind component, primarily over the northern parts of South Africa, and the zonal component - over the southeast regions - are observed (surface wind speed increments up to 0.1 m/s).

© University of Pretoria

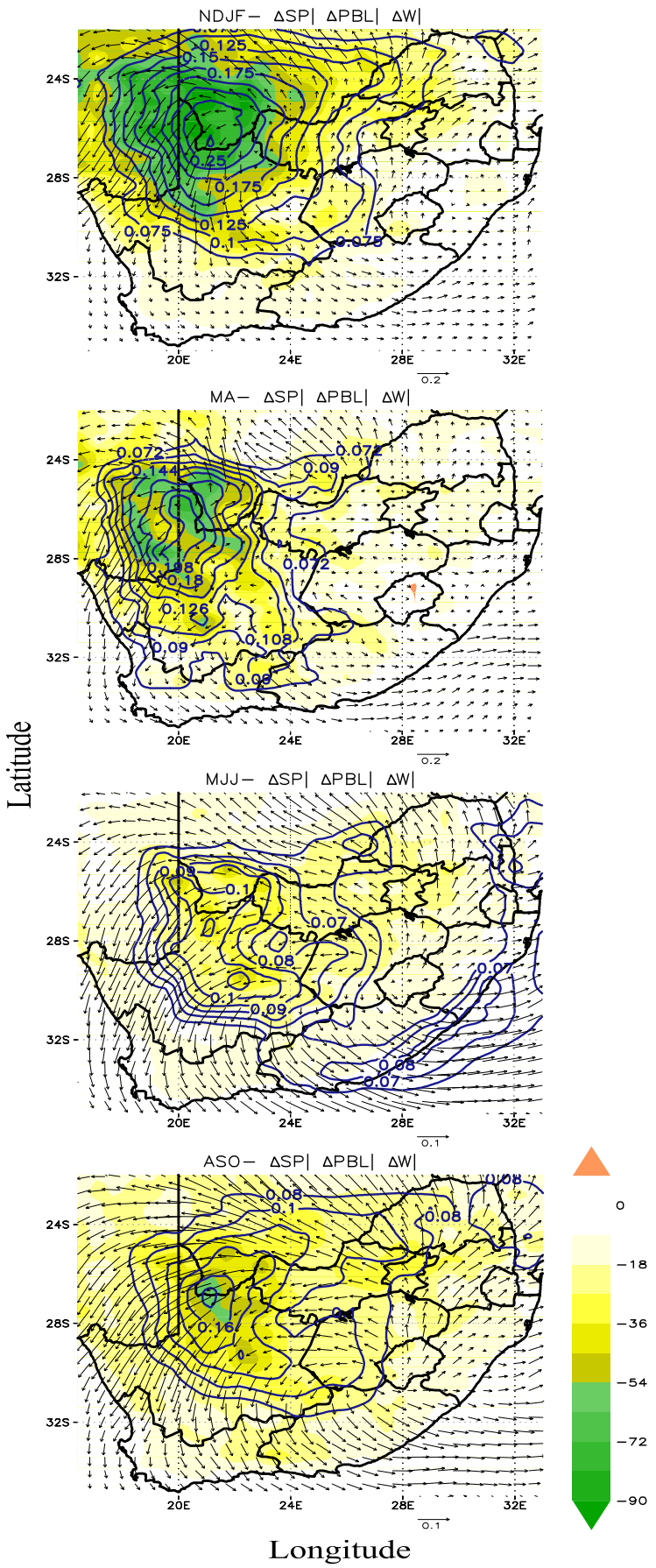

Fig. 7: 1998-2008 averaged seasonal mean spatial distributions of dust aerosol induced changes in planetary boundary layer height (shaded; unit: m), surface pressure (unfilled contour; unit: hPa) and 10m surface wind field (vector; the scale is indicated by the arrow to the lower right; unit: m/s).

Furthermore, comparing the wind directions of CNT simulation (not shown) with the $\overrightarrow{\Delta W}$ (Fig. 7), during summer the dust aerosols influence the northward cold moist air that predominantly flows through the Atlantic Ocean towards the west regions of South Africa. For the rest of the seasons, in areas which are below 30°S, the dust aerosols weakened the southward meridional motions and promoting the eastward anticyclone zonal winds. Over the central, east and northern parts of South Africa, the dust-aerosol induced regional circulation change promoted anti-cyclonic (anti-clockwise) surface air circulation. In general, coinciding with the dust aerosol direct and semi-direct effects induced ST reductions - which reduces the turbulent flux transfer into the atmosphere (Fig. 5) - around the dust aerosol dominating areas of South Africa, the surface wind speed also show reductions (relative to CNT simulations). This further has reinforced the stabilization of the lower troposphere (e.g., Jacobson and Kaufman 2006; Miller et al., 2004a; Zhang, 2008). As a result the reduction in surface wind speed becomes another contributing factor for the enhancement in dust-induced SP around the Northern Cape Province. However, the aforementioned regional atmospheric circulation modifications - due to the inclusion of radiatively interactive dust particles on two-way interactive coupling aerosol-climate simulations (REF-CNT) – would, in turn, influence the dust particle emission and the background aerosol dispersions. In particular, over the dust source regions, the surface wind speed reduction (relative to CNT simulation) would induce a negative feedback on dust emission and transport (e.g., Perlwitz et al., 2001; Miller et al., 2004a; Stanelle et al., 2010). However, in other areas, for example over the central and northern parts of South Africa, which are dominated by the background aerosols (aerosols from anthropogenic and biomass burning activities) we have noted that $\overrightarrow{\Delta W}$ induced a small (minimal) positive feedback in their dispersion (fig. not shown).

4 Summary and Conclusions

Climate simulations using the Regional Climate Model (RegCM4) which is interactively coupled with anthropogenic-desert dust schemes have been carried out to investigate the mass distributions, direct and semi-direct effects of desert dust aerosol, in South Africa. For this purpose, two long-term parallel simulations that encompass a period from 1997 to 2008 were conducted. In the first simulation(REF experiment) - all radiatively interactive aerosol components of RegCM4 were included; while, the second experiment (CNT), all conditions were the same as in REF, except that it was simulated without dust aerosols. Utilizing the results of the REF run and climatic variable differences between the two simulations (i.e., REF-CNT), the spatio-seasonal distributions of the dust aerosol column load and their direct Radiative Forcing (RF) plus semi-direct climatic effects were provided, respectively. A summary and the main conclusions drawn from this study presented as follows:

- The desert dust particles which are primarily emitted from the arid regions of the Northern Cape Province as well as Namibia and Botswana, were concentrated over the western

© University of Pretoria

parts of South Africa. Influenced by the anti-cyclonic air circulation, the dust particles were mainly dispersed towards the south-east and southern parts of the country. The maximum loads of dust particles were found over their source regions, during the windy seasons of spring (440 mg/m^2 for size range 2.5–20μm) and summer (270 mg/m^2 for size range 0.01–2.5μm). Along with the surface wind speed reduction, the dust burden also decline and reach its minimum during winter. Furthermore, the results illustrated that the dry situations of the extended winter season (i.e., May to October) favoured the dispersion of large size dust particles (diameter > 2.5 um). The annual mean dust burden distribution, that varied from ~ 70 to 700 mg/m^2, showed that over the dust source regions, from 45 up to 65% of the total dust mass were donated by dust particles which were within a diameter range of 2.5–20μm.

- Due to the capability of dust aerosols to interact with both Short-Wave (SW) and Long-Wave (LW) radiation, as well as their ability of re-emitting thermal radiation, they perturb the SW and LW radiation balance; both at the SUrface (SU) and in the ATMospheric (ATM) column. The SW-SU-RF and LW-ATM-RF of dust particles showed negative values throughout the entire domain. Additionally, positive values of LW-SU-RF (with maximum up to 10 W/m^2 during spring) and SW-ATM-RF (up to 26 W/m^2 during summer) were observed. Generally, the dust aerosol-RF showed similar spatio-seasonal patterns as that of dust aerosol column loads. The LW influences of dust particles primarily followed the distributions of dust aerosols which have a diameter ≥ 2.5 μm. The SW-RF of dust, both the surface and within the atmosphere was ~ 2 to 3 times higher than that of LW-RF values. As a result, the dust particles net radiative role (SW+LW) becomes decreasing the net radiation absorbed by the surface, along with increasing the radiative heating of the atmosphere.

- As a result of the dust aerosol net surface radiative cooling influence, as well as their semi-direct effects induced cloud cover (CC) enhancements - the reductions in Surface Temperature (ST) and Surface Sensible Heat Flux (SSHF) were occurred. The maximum reductions in ST (~ -0.7 to -1.1 K) and SSHF (~ -15 to -24 W/m^2) were observed across the Northern Cape Province, during summer. The simulations revealed higher degree of spatial correlation among ΔST, ΔSSHF, Net- SW-RF of dust and ΔCC (correlation with magnitude range of 0.67 to 0.95). This implies that the interaction and feedback among aerosols, radiation, and cloud fields were jointly accountable for the changes in ST and SSHF.

- Including the radiative feedbacks of all climatic components, the effects of radiatively interactive dust aerosols on lower tropospheric (~ below 650hPa) columnar averaged Net Atmospheric radiative Heating Rate (NAHR) were computed. The dust aerosols predominantly induced heating; this attributed to the dust aerosol partial SW-absorption nature. The higher values of the ΔNAHR (~ 0.5 to 1.2 K/day) were observed during spring and summer, across the Northern Cape Province. Over some scattered areas that were away from the dust aerosol major warming zones - the presence of desert dust particles induce net radiative cooling (ΔNRHR~ -0.1 to -0.4 K/day). However, the magnitudes as well as the spatial coverage of these cooling effects were small relative to the dust aerosol heating influences.

- The dust aerosol-radiation-climate interactions induced low-level columnar integrated cloud cover (i.e., low-clouds which are formed below ~ 650 hPa) and Cloud Liquid Water Path (low-level CLWP) changes were also addressed. Ruling out some narrow areas that indicated insignificant reductions of CC and CLWP; overall, naturally induced dust particles played a significant role in enhancing the low-level CC (up to 7%) and CLWP (up to 2.5 g/m2). These modifications, seems to favour the availability of water resources in the desert region of the Northern Cape and its surrounding areas. The results also showed that the strength of ΔCC and ΔCLWP were not only dependent on spatio-seasonally variable dust aerosol concentrations and their radiation perturbation levels but they were also reliant on the amount of clouds and water vapour that were available in a region.

- The present study also addressed the dust aerosol induced regional scale dynamic modifications: changes in planetary boundary layer height, surface pressure and the 10m surface wind fields. The dust aerosols' direct and semi-direct effects induced ST and SSHF reductions, jointly, caused Boundary Layer (BL) reduction and Surface Pressure (SP) enhancement. The high level of spatial correlations that were exhibited in our results interrelated with previously reported studies - suggested that the ΔST and ΔSSHF would influence the BL and SP by inducing a weakening on convectively driven turbulence and surface buoyancy flux. Moreover, the reductions of surface wind speed (particularly around dust source regions) also reinforce the stabilization of the lower troposphere lapse rate; thus, it becomes another contributing factor for SP enhancement.

- The change in surface wind fields($\overrightarrow{\Delta W}$) showed that in areas which are below 30°S, the dust aerosols were weakening the southward meridional motions and promoting the eastward anticyclone zonal wind. Over the eastern and northern parts of the country, the dust-aerosols caused regional circulation changes that promoted the anticyclone surface air circulation. Also, during summer the existence of dust aerosols was predicted to reduce the northward cold moist air that predominantly flows through the Atlantic Ocean towards the west regions of South Africa.

- This study only considered direct and semi-direct effects of dust particles, thus it should be taken carefully as a first-degree assessment of the dust aerosols' regional climate effects over South Africa. Nevertheless, our results have critically underscored the importance of including wind eroded dust particles in climate change studies over this region.

- To enrich our understanding of various climatic and ecological roles of dust aerosols with better accuracies, we need to design a strategic approach that consolidates more observational and simulation-based studies. To this end, authors suggest the necessity of establishing continuously

© University of Pretoria

measuring field stations over the western parts of South Africa and its surrounding regions.

Acknowledgements

The authors are grateful to Addis Ababa University, Department of Physics, for providing computational facilities. For the accessibility of RegCM model the authors are thankful to the International Centre for Theoretical Physics (ICTP). We are also indebted to Teresa Faleschini, Tamene Mekonnen, Fiona Tummon and Addisu Gezahegn, for their valuable assistances. This work was supported by African Laser Centre and NRF bi-lateral research grant (UID: 68688/65086), in addition to CSIR National Laser Centre.

References

Aoki, I. et al. (2005). Dust storms generated by mesoscale cold fronts in the Tarim Basin, Northwest China, Geophys. Res. Lett., 32, L06807, doi:10.1029/2004GL021776.

Balkanski,Y. et al. (2007). Reevaluation of mineral aerosol radiative forcings suggests a better agreement with satellite and AERONET data. Atmos. Chem. Phys. 7, 81–95.

Benhin, JKA (2006). Climate change and South African agriculture: Impacts and adaptation options. CEEPA Discussion Paper No. 21. Centre for Environmental Economics and Policy in Africa, University of Pretoria.

Bessagnet, B. et al. (2008). Modelling dust emissions and transport within Europe: the Ukraine March 2007 event, J. Geophys. Res., 113, D15202, doi: 10.1029/2007JD009541.

Bhattachan, A. et al. (2012). The southern Kalahari: a potential new dust source in the southern hemisphere? Environ. Res. Lett. 7 024001, doi:10.1088/1748-9326/7/2/024001.

Boer, G.J. (1993). Climate change and the regulation of the surface moisture and energy budgets.ClimDyn 8:225–239, doi: 10.1007/BF00198617.

Bullard, J. E. et al. (2011). Preferential dust sources: A geomorphological classification designed for use in global dust-cycle models, J. Geophys. Res., 116, F04034, doi:10.1029/2011JF002061.

Christopher, S. A. et al. (2003). Estimation of diurnal shortwave dust aerosol radiative forcing during PRIDE, J. Geophys. Res., 108, 8596, doi:10.1029/2002JD002787, D19.

Cook, J. and Highwood, E. J. (2004). Climate response to tropospheric absorbing aerosols in an intermediate general-circulation model. Q.J.R. Meteorol. Soc., 130: 175–191. doi: 10.1256/qj.03.64.

Croft, B. et al. (2012). Uncertainty associated with convective wet removal of entrained aerosols in a global climate model, Atmos. Chem. Phys., 12, 10725-10748, doi:10.5194/acp-12-10725-2012.

Douville, H. et al. (2002). Sensitivity of the hydrological cycle to increasing amounts of greenhouse gases and aerosols. Climate Dynamics 20, 45–68.

Dufresne, J.-L.et al. (2002). Longwave scattering effects of mineral aerosols. J. Atmos. Sci., 59,1959–1966,doi: http://dx.doi.org/10.1175/1520-0469 (2002) 059<1959:LSEOMA> 2.0.CO;2.

Engelstaedter, S. et al. (2006). North African dust emissions and transport. Earth-Sci Rev; 79:73–100.

Forster, P. et al. (2007). Changes in Atmospheric Constituents and in Radiative Forcing. In: Climate Change 2007: The Physical Science Basis. Contribution of Working Group I to the Fourth Assessment Report of the Intergovernmental Panel on Climate Change [Solomon, S. et al. (eds.)]. Cambridge University Press, Cambridge, United Kingdom and New York, NY, USA.

Giorgi, F. et al. (2012). RegCM4: model description and preliminary tests over multiple CORDEX domains. Clim. Res., 52, 7–29, doi:10.3354/cr01018, 2012. 8474, 8481.

Ginoux, P. et al. (2001). Sources and distributions of dust aerosols simulated with the GOCART model. J. Geophys. Res., 106(D17), 20255–20273, doi:10.1029/2000JD000053.

Gong, S.L. et al. (2003). Characterization of Soil Dust Aerosol in China and its Transport and Distribution during 2001 ACE-Asia: 2. Model Simulation and Validation. J. Geophys. Res. 108: 4262, doi: 10.1029/2002JD002633.

Goudie, A.S. (2009). Dust storms: Recent Developments. Journal of Environmental Management. 90, 89 – 94.

Goudie, A.S., and Middleton, N.J. (2006). Desert dust in the global system, Springer, Berlin.

Grini, A. et al. (2002). Saltation sandblasting behavior during mineral dust aerosol production, Geophys. Res. Lett., 29(18), 1868, doi:10.1029/2002GL015248.

Han, Q. et al. (2012). Global estimates of mineral dust aerosol iron and aluminum solubility that account for particle size using diffusion-controlled and surface-area-controlled approximations, Global Biogeochem. Cycles, 26, GB2038, doi:10.1029/2011GB004186.

Han, Q., and C. S. Zender (2010), Desert dust aerosol age characterized by mass-age tracking of tracers, J. Geophys. Res., 115, D22201, doi:10.1029/2010JD014155.

Han, Z. W. (2010). Direct radiative effect of aerosols over East Asia with a Regional coupled Climate/Chemistry model, Meteor. Z., 19(3), 287–298.

Haywood, J. and Boucher, O. (2000). Estimates of direct and indirect radiative forcing due to tropospheric aerosols: a review, Rev. Geophys., 38, 513–543.

Hess, M. et al. (1998). Optical properties of aerosols and clouds: The software package OPAC. Bulletin of American Meteorological Society 79, 831–844.

Hoose, C. et al. (2008). Global influence of dust mineralogical composition on heterogeneous ice nucleation in mixed-phase clouds, Environ. Res. Lett., 3, 025003, doi:10.1088/1748-9326/3/2/025003.

Jacobson, M. Z., and Kaufman, Y. J. (2006). Wind reduction by aerosol particles, Geophys. Res. Lett., 33, L24814, doi:10.1029/2006GL027838.

Jiang, H., and Feingold, G. (2006). Effect of aerosol on warm convective clouds: Aerosol-cloud-surface flux feedbacks in a new coupled large eddy model, J. Geophys. Res., 111, D01202, doi:10.1029/2005JD006138.

Ju, L.-X., and Han, Z.-W. (2011). Direct radiative forcing and climatic effects of aerosols over East Asia by RegCM3. Atmos. Oceanic Sci. Lett., 4, 363–367.

Kim, K.-M.et al. (2010). Influence of aerosol-radiativeforcings on the diurnal and seasonal cycles of rainfall over West Africa and Eastern Atlantic Ocean using GCM simulations, Clim.Dynam., 35, 115–126, doi:10.1007/s00382-010-0750-1.

Konare, A. et al. (2008). A regional climate modeling study of the effect of desert dust on the West African monsoon. J GeophysRes 113:D12206. doi:10.1029/2007JD009322.

Lau, K. M., and Kim, K. M. (2006).Observational relationships between aerosol and Asian monsoon rainfall, and circulation, Geophys. Res. Lett.. 33, L21810, doi:10.1029/2006GL027546.

Lau, K.M. et al. (2009). A GCM study of the response of the atmospheric water cycle of West Africa and the Atlantic to Saharan dust radiative forcing. Ann Geophys 27:4023−4037.

Lohmann, U. and Diehl, K. (2006). Sensitivity studies of the importance of dust ice nuclei for the indirect aerosol effect on stratiformmixedphase clouds, J. Atmos. Sci, 63, 968–982.

Luo, C. et al. (2003). Sensitivity study of meteorological parameters on mineral aerosol mobilization, transport and distribution, J. Geophys. Res., 108(D15), 4447, doi:10.1029/2003JD003483.

© University of Pretoria

Malavelle, F. et al. (2011). Simulation of aerosol radiative effects over West Africa during DABEX and AMMA SOP-0. J GeophysRes 116:D08205. doi:10.1029/ 2010 JD014829.

Mallet, M. et al. (2009). Impact of dust aerosols on the radiative budget, surface heat fluxes, heating rate profiles and convective activity over West Africa during March 2006.AtmosChemPhys 9:7143−7160.

Marcella, M. P., and Eltahir, E. A. B. (2010). Effects of mineral aerosols on the summertime climate of Southwest Asia: Incorporating subgrid variability in a dust emission scheme. J. Geophys. Res., 115, D18203, doi:10.1029/2010JD014036.

McConnell, C. L. et al. (2008). Seasonal variations of the physical and optical characteristics of Saharan dust: results from the dust outflow and deposition to the ocean (DODO) experiment, J. Geophys. Res., 113, D14S05, doi:10.1029/2007jd009606.

Miller, R. L. et al. (2004a). Feedback upon dust emission by dust radiative forcing through the planetary boundary layer, J. Geophys. Res., 109, D24209, doi:10.1029/2004JD004912.

Miller, R.L. et al. (2004b). Surface radiative forcing by soil dust aerosols and the hydrologic cycle. J GeophysRes 109:D04203. doi:10.1029/2003JD004085.

Miller, R.L. and Tegen, I. (1998). Climate response to soil dust aerosol. J. Climate, 11, 3247-3267.

Mishra, S. K. et al. (2010). Effects of particle shape, hematite content and semi-external mixing with carbonaceous components on the optical properties of accumulation mode mineral dust, Atmos. Chem. Phys. Discuss., 10, 31253-31300, doi:10.5194/acpd-10-31253-2010.

Osborne, S. R. et al. (2008). Physical and optical properties of mineral dust aerosol during the dust and biomass-burning experiment, J. Geophys. Res., 113, D00C03, doi:10.1029/2007jd009551.

Pal, J. S. et al. (2000). Simulation of regional-scale water and energy budgets: Representation of subgrid cloud and precipitation processes within RegCM, J. Geophys. Res.-Atmospheres, 105(D24), 29,579–29,594.

Perlwitz, J. and Miller, R. L. (2010).Cloud cover increase with increasing aerosol absorptivity: A counterexample to the conventional semi-direct aerosol effect, J. Geophys. Res., 115, D08203, doi:10.1029/2009JD012637.

Perlwitz, J. et al. (2001). Interactive soil dust aerosol model in the GISS GCM: Part I: Sensitivity of the soil dust cycle to radiative properties of soil dust aerosols, J. Geophys. Res., 106, 18167–18192, doi:10.1029/2000JD900668.

Prospero, J. M. (1999). Long-term measurements of the transport of African mineral dust to the southeastern United States: Implications for regional air quality, J. Geophys. Res., 104(D13), 15917–15927, doi:10.1029/1999JD900072.

Prospero, J. M. et al. (2002). Environmental Characterization Of Global Sources Of Atmospheric Soil Dust Identified With The Nimbus 7 Total Ozone Mapping Spectrometer (TOMS) Absorbing Aerosol Product, Rev. Geophys., 40(1), 1002, doi:doi:10.1029/2000RG000095.

Ramanathan, V. et al. (2001). Aerosol, climate, and hydrological cycle.Science 294, 2119-2124.

Rosenfeld, D. (2006). Aerosol–cloud interactions control of earth radiation and latent heat release budgets. Space Sci. Rev. 125 (1–4), 149–157. doi:10.1007/s11214-006-9053-6.

Rosenfeld, D. et al. (2001). Desert dust suppressing precipitation: A possible desertification feedback loop, Proc. Natl. Acad. Sci. U.S.A., 98, 5975 – 5980, doi:10.1073/pnas.101122798.

Satheesh, S. K. et al. (2007). Atmospheric warming due to dust absorption over Afro-Asian regions.Geophys. Res. Lett., 34, L04805, doi: 04810.01029/02006GL028623.

Sherwood, S. (2002). A microphysical connection among biomass burning, cumulus clouds and stratospheric moisture, Science, 295, 1272–1275.

Solmon, F. et al. (2008). Dust aerosol impact on regional precipitation over western Africa, mechanisms and sensitivity to absorption properties. Geophys. Res. Lett. 35(L24705). Doi:10.1029/2008GL035900.

Solmon, F. et al. (2012). Radiative and climatic effects of dust over West Africa, as simulated by a regional climate model, Clim. Res., 52, 97–113, doi:10.3354/cr01039.

Stanelle, T. et al. (2010). Feedback between dust particles and atmospheric processes over West Africa during dust episodes in March 2006 and June 2007.AtmosChemPhys 10: 10771−10788.

Suh, M.-S., and Lee, D.-K. (2004). Impacts of land use/cover changes on surface climate over east Asia for extreme climate cases using RegCM2, J. Geophys. Res., 109, D02108, doi:10.1029/2003JD003681.

Tanaka, T. Y., and Chiba, M. (2006).A numerical study of the contributions of dust source regions to the global dust budget, Global Planet. Change, 52, 88 – 104.

Tegen, I. (2003). Modeling soil dust aerosol in the climate system: An overview.Quarternary Science Reviews, 22, 1821-1834.

Tegen, I. and Fung, I. (1994).Modeling of Mineral Dust in the Atmosphere – Sources, Transport, and Optical-Thickness, J. Geophys. Res. Atmos., 99(D11), 22897–22914, doi:10.1029/94JD01928.

Tegen, I. et al. (2002). Impact of vegetation and preferential source areas on global dust aerosol: Results from a model study. J. Geophys. Res. 107, 4576,doi:10.1029/2001JD000963.

Tegen, I. et al. (2004). Relative importance of climate and land use in determining present and future global soil dust emission. Geophys. Res. Lett., 31, L05105, doi:10.1029/2003GL019216.

Tesfaye, M. et al. (2011). Aerosol climatology over South Africa based on 10 years of Multiangle Imaging Spectroradiometer (MISR) data, J. Geophys. Res., 116, D20216, doi:10.1029/2011JD016023.

Tesfaye, M. et al. (2013). Evaluation of Regional Climatic Model Simulated Aerosol Optical Properties over South Africa Using Ground-Based and Satellite Observations, ISRN Atmospheric Sciences, vol. 2013, Article ID 237483, 17 pages, 2013. doi:10.1155/2013/237483.

Todd, M.C. et al. (2008). Quantifying uncertainty in estimates of mineral dust flux: An inter-comparison of model performance over the Bodélé Depression, northern Chad. J. Geophys. Res., 113, D24107, doi:10.1029/2008JD010476.

Tummon, F. et al. (2010). Simulation of the direct and semi-direct aerosol effects on the southern Africa regional climate during the biomass burning season, J. Geophys. Res., 115(D19), doi:10.1029/2009JD013738.

Wang, H. et al. (2006). The impacts of optical properties on radiative forcing due to dust aerosol. Advances in Atmospheric Sciences, 23(3), 431–441.

Wang, Y. et al. (2004). Regional climate modeling: Progress, Challenges, and Prospects. J. Meteor. Soc. Japan., 82, 1599-1628.

Weaver, C. J. et al. (2002). Radiative Forcing of Saharan Dust: GOCART Model Simulations Compared with ERBE Data. J. Atmos. Sci., 59, 736–747.

Wurzler, S. et al. (2000). Modification of mineral dust particles by cloud processing and subsequent effects on drop size distributions, J. Geophys. Res., 105(D4), 4501–4512, doi:10.1029/1999JD900980.

Yoshioka, M. et al. (2007). Impact of desert dust radiative forcing on Sahel precipitation: Relative importance of dust compared to sea surface temperature variations, vegetation changes, and greenhouse gas warming. J. Climate, 20, 1445–1467.

Yu, H. et al. (2002). Radiative effects of aerosols on the evolution of the atmospheric boundary layer, J. Geophys. Res., 107(D12), 4142, doi:10.1029/2001JD000754.

Yue, X. et al. (2010a). Direct climatic effect of dust aerosol in the NCAR Community Atmosphere Model Version 3 (CAM3). Adv. Atmos. Sci., 27(2), 230–242, doi:10.1007/s00376-009-8170-z.

© University of Pretoria

Yue, X. et al. (2010b). Simulation of dust aerosol radiative feedback using the GMOD: 2. Dust-climate interactions, J. Geophys. Res., 115, D04201, doi:10.1029/2009JD012063.

Zakey, A. S. et al. (2006). Implementation and testing of a desert dust module in a regional climate model, Atmos. Chem. Phys., 6, 4687-4704, doi:10.5194/acp-6-4687-2006.

Zender, C. S. et al. (2003). Mineral Dust Entrainment and Deposition (DEAD) model: Description and 1990s dust climatology. J. Geophys. Res., 108, 4416, doi: 4410.1029/2002JD002775.

Zender, C. S. et al. (2004). Quantifying mineral dust mass budgets: Terminology, constraints, and current estimates, Eos Trans. AGU, 85(48), 509–512, doi:10.1029/2004EO480002.

Zhang, D. F. et al. (2009). Simulation of dust aerosol and its regional feedbacks over East Asia using a regional climate model, Atmos. Chem. Phys., 9, 1095–1110.

Zhang, Y. (2008). The Radiative Effect Of Aerosols From Biomass Burning On The Transition From Dry To Wet Season Over The Amazon As Tested By A Regional Climate Model: PhD thesis. Georgia Institute of Technology, United State.

Zhao, C. et al. (2011). Radiative impact of mineral dust on monsoon precipitation variability over West Africa, Atmos. Chem. Phys., 11, 1879–1893, doi:10.5194/acp-11-1879-2011.

© University of Pretoria

Chapter 5: Simulation of anthropogenic aerosols mass distributions and their direct and semi-direct effects over South Africa using RegCM4*

*This chapter needs to be cited as:

Tesfaye, M., V. Sivakumar, J. Botai, and G. Mengistu Tsidu (2013c): "Simulation of anthropogenic aerosols mass distributions and their direct and semi-direct effects over South Africa using RegCM4", *Int. J. Climatol., in review.*

© University of Pretoria

UNIVERSITEIT VAN PRETORIA
UNIVERSITY OF PRETORIA
YUNIBESITHI YA PRETORIA

Simulation of anthropogenic aerosols mass distributions and their direct and semi-direct effects over South Africa using RegCM4

M. Tesfaye[1,2*], V. Sivakumar[1,3], J. Botai[1], G. Mengistu Tsidu[4]

Abstract: The seasonal mean mass distributions, direct and semi-direct effects of different Anthropogenic Aerosols (AAs) [i.e., sulfate, Black Carbon (BC), Organic Carbon (OC) and all together (SBO)] in South Africa are investigated using the 12 year runs of the Regional Climate Model-RegCM4. We have found that the AAs which primarily originated from the Highveld zones of Gauteng and Mpumalanga are distributed in the northern, central and eastern areas of South Africa, influenced by the anti-cyclonic air circulation. The maximum Surface Radiative Forcing (SRF) values are found over AA source regions: up to -12 W/m^2 for sulfate and -14 W/m^2 for SBO during summertime, as well as, up to -2 W/m^2 for BC and -0.68 W/m^2 for OC during austral winter. In contrary to sulfate, the reduction of surface solar flux by BC and OC particles are occurred through enhancing atmospheric radiative heating. The climatic feedbacks of AAs resulted change in background aerosol concentrations. Thus, climatic effects of AAs are also found in regions which are away from the AA loading zones. Across the northern and eastern parts, the inclusion of sulfate and OC reduced the low-level columnar averaged Net Atmospheric radiative Heating Rate (NAHR) by about -0.3 K/day; whereas, over the west parts of South Africa, they have enhanced NAHR by about +0.2 K/day. Enhancements in NAHR, which cover large areas of South Africa, are found during BC and SBO cases. The change in Surface Temperature (ST) and sensible heat flux are more closely correlated with the cloud cover change than SRF of AAs. Aligned with the spatial patterns of ST reductions (and enhancements) respectively we have found that the PBL height decreases (or increases) along with surface pressure increases (or decreases). Overall, the results have revealed that the nonlinear feedbacks of cloud fields are more important in inducing other climatic anomalies.

[1]*Department of Geography, Geoinformatics and Meteorology, University of Pretoria, Pretoria 0002, South Africa*

[2]*National Laser Centre, Council for Scientific and Industrial Research, Pretoria 0001, South Africa*

[3]*School of physics, University of KwaZulu Natal, Durban 4000, South Africa*

[4]*Department of Physics, Addis Ababa University, Addis Ababa, Ethiopia*

**Correspondence to: M. Tesfaye: mela_20062@yahoo.com*

Keywords: Anthropogenic aerosols; Aerosol-climate interactions; Radiative forcing; Semi-direct effects; Regional climate model; South Africa

1 Introduction

The Earth's climate system includes several components which are intensely coupled with each other. The major components of this system include the atmosphere, the hydrosphere/cryosphere (oceans and land hydrology/sea and land ice), the biosphere and the chemosphere (e.g., Giorgi, 1995; Baede *et al.*, 2001). Changes in one or more of these coupled components of the Earth system may affect processes in other constituents of the Earth's climate system. Furthermore, changes on the Earth's climate system may have an influence on human socio-economic activities and the natural ecosystems (Baede *et al.,* 2001). Atmospheric aerosols, which are induced from natural processes/anthropogenic activities, are one of the constituents of the atmosphere. Due to their direct, semi-direct and indirect influences, they can affect our climate system in several ways (Denman *et al.,* 2007 and references therein). Compared to the pre-industrial times, due to the expansion of industrialization and other human activities, the anthropogenic emissions are enhanced (e.g., Schultz *et al.,* 2006). Emissions from human activities which considerably amplified the quantities of particulate matters in the atmosphere have become one of the common concerns to various researchers across the globe (Schultz *et al.,* 2006; Penner *et al.,* 2001; Ramanathan et al, 2005; IPCC 2007 and references therein). Therefore, evaluating the climatic roles of anthropogenic aerosol components which arise from different human activities have become one of the crucial subjects which has received wider attention in climatic change studies, as well as in view of addressing the impact of human activities on climate variation.

Among several species of primary/secondary anthropogenic aerosols, sulfates, nitrates and carbonaceous aerosols have been found to be the major constituents (Penner *et al.,* 2001; Ghan and Schwartz, 2007). Anthropogenically induced sulfate aerosols are predominantly formed in the atmosphere via the chemical conversion of its precursor gas (sulfur dioxide, SO_2, which is emitted through anthropogenic activities), primarily through two oxidation pathways: one in gaseous phase and the other in aqueous phase (Haywood and Boucher 2000; Qian and Giorgi, 1999; Roeckner et al. 1999; Qian *et al.,* 2001; Penner *et al.,* 2001). Whereas, Black Carbon (BC) and Organic Carbon (OC) aerosols are ejected directly into the atmosphere from various anthropogenic combustion activities, such as, the combustion of different fossil fuels for industrial, transportation, domestic usages and several other purposes (e.g., Penner *et al.,* 2001; Jacobson, 2002; Bond *et al.,* 2013). These carbonaceous particles age in the atmosphere via different physico-chemical transformation processes, they attain hydrophilic properties. This process may also modify the optical properties of these particles as well as their radiative and climatic roles (e.g., Eck *et al.,* 2003; Jacobson, 2006; Fan *et al.,* 2008; Tesfaye *et al.,* 2011b).

As presumed from previous studies, the scattering of solar radiation back to space, predominantly by sulfate aerosols as well as organic carbon particles (Pilinis et al. 1995; Penner *et al.,* 2001; Bond, 2001; Jacobson, 2001b) induce radiative cooling in the Earth-atmospheric system (e.g., Adams *et al.,* 2001; Mitchell and Johns 1997). The Shortwave (SW) absorption, mainly by BC and moderately via OC aerosols (Andreae and Gelencser, 2006), reduces the amount of solar radiation reaching the surface and simultaneously, enhances radiative heating in the atmosphere. These radiative influences of both sulfate and carbonaceous aerosols cause various significant semi-direct effects (Lohmann and Feichter 2001; Penner *et al.,* 2001; Koch and Del Genio, 2010 and references therein). Additionally, the deposition of BC

© University of Pretoria

aerosols onto snow/ice surfaces may reduce their surface albedo, thereby increase the melting rate of the snow/ice surfaces (Jacobson 2004; 2010; Hansen and Nazarenko 2004; Flanner et al. 2007; 2009). Sulfate and aged carbonaceous aerosols, being efficient source of cloud condensation nuclei (or associated into cloud droplets through scavenging), play an important role in modulating the cloud radiative and microphysical properties (indirect effects) (e.g., Menon *et al.,* 2002a; Giorgi *et al.,* 2003; Rosenfeld and Woodley 2001; Huang *et al.,* 2007; Penner *et al.,* 2001).

Generally, owing to aforementioned and other complicated climatic forcing roles of anthropogenic aerosols; the distribution, physico-chemical properties, atmospheric processes and regional/global climate effects of these aerosols have increasingly become an intense research topic in many observational and modelling studies (e.g., Ramanathan and Carmichael, 2008; IPCC, 2007 and references therein).

In the past decade, a number of studies, using different global models, have reported several valuable results regarding the radiative and climatic forcing of anthropogenic aerosols (e.g., Jacobson 2001a; 2001b; Liu *et al.,* 2005; Posselt and Lohmann, 2009; Penner *et al.,* 2001; Ghan and Schwartz, 2007 and reference therein). However, the coarse spatial resolution and longer computational time demands of global scale models (relative to regional scale models) becomes a challenge for regional scale simulations of anthropogenic aerosol distributions and climatic influences, with higher spatial and temporal resolution. On the other hand, owing to the short atmospheric life time of anthropogenic aerosols (e.g., Shindell *et al.,* 2008a, 2008b) their concentration and effects predicted to be significant at a regional scale (e.g., Giorgi et al. 2002, 2003; Roeckner et al. 2006; Solomon *et al.,* 2006; Wu *et al.,* 2008). Due to the aforementioned circumstances, the high-resolution Regional Climate Models (RCM) turn out to be important tool towards simulating the regional scale radiative as well as climatic effects of anthropogenic aerosols (Solomon *et al.,* 2006; Zhang and Yin, 2008; Han, 2010; Gao et al. 2006, 2008; Zhou and Yu 2006).

South Africa being one of the most industrialized countries on the continent, the climatic and air quality changes that are caused by anthropogenic emissions are progressively become one of the major concerns in and around South Africa. The majority of particulate/aerosol precursor gas emissions from South Africa are related with the mining industries and the extensive consumption of coal for electrical power generation, fuel production, and different domestic and industrial usages. Due to these and other human activities, various observational (e.g., Queface *et al.,* 2011; Magi 2009; Tesfaye *et al.,* 2010; Tesfaye *et al.,* 2011a; Tummon, 2011 and references therein) and modelling studies (Magi *et al.,* 2009; Tummon *et al.,* 2010; Tesfaye *et al.,* 2011b; Tummon, 2011 and references therein) noted that South Africa is one of the country that has a higher load of anthropogenic aerosols. Furthermore, most of the above studies indicate that the power plants and various industrial and mining activities in the northern parts of South Africa are the major source of anthropogenic aerosols in the sub-continent. So far to our knowledge there has been no comprehensive study which has been devoted to examine the potential local climatic influences of the South African anthropogenic aerosols, via employing the art of RCM. Most of the recently reported studies, which evaluate various climatic effects of anthropogenic aerosols (via applying the RCM approach) are focused in different regions of the globe: such as South-eastern Europe (Zanis 2009); East Asia (Qian *et al.,* 2001, Giorgi *et al.,* 2002; 2003 and Huang *et al.,* 2006) as well as China (Wang *et al.,* 2003 and Li *et al.,* 2009).

Based on long-term regional modelling simulations, the present study has examined the total (i.e., sulfate + BC + OC) and individual components of anthropogenic aerosols' seasonal mean column burden spatial distributions, along with their direct and semi-direct effects over South Africa. Among several semi-direct impacts of anthropogenic aerosols, this study has addressed their role in terms of influencing the Surface Temperature (ST), Surface Sensible Heat Flux (SSHF), Net Atmospheric radiative Heating Rate (NAHR), Cloud Cover (CC), Planetary boundary Layer height (PBL), Surface Pressure (SP) and surface wind fields (W). This work has been conducted using version 4 of interactively coupled regional climate-anthropogenic-desert dust model of the International Centre for Theoretical Physics (ICTP-RegCM4-aerosol model, Giorgi *et al.,* 2012). To our knowledge, this is the first study that has employed an aerosol-climate two-way interactively coupled long-term regional scale simulation to examine particularly the individual and total anthropogenic aerosol species' spatio-seasonal distributions, in companion with the interactions and feedback among the anthropogenic aerosols, radiation and climatic fields, over South Africa. The paper is organized as follows: brief descriptions of the experimental design as well as some important points about the model are given in section 2. While in section 3, the simulation results on South Africa are presented and discussed. Lastly, the summary of our findings and concluding points are provided in section 4.

2 Model and experimental design

In this study; the ICTP-RegCM4 model, which is interactively coupled with chemistry/anthropogenic aerosol-desert dust modules (e.g., Solmon et al. 2006; Giorgi *et al.,* 2012) is used to simulate the spatio-seasonal distribution of anthropogenic aerosols, as well as their radiative forcing and climate signals, over South Africa and the surrounding areas. A brief description about RegCM4 and the coupled aerosol modules, as well as the recently updated emission inventories which are employed in our simulations are presented in Tesfaye *et al.* (2013a). The selected domain range, resolutions, designated model physics parameterization schemes, dynamical and surface parameter time setups of the model, as well as time-dependent initial and lateral boundary conditions implemented in this study are the same with that of Tesfaye *et al. (*2013a). The domain topography and the geographical map of South Africa (with province boundaries) are shown in Fig.1.

To attain our purpose, five basic long-term experiments are conducted; each covering the period from 1 January 1997 to 31 December 2008; from which, only the recent 11 year results are comprehensively analysed in terms of different seasons. The first experiment (hereafter referred to as Exp1) is the control experiment, which do not encompass any of the anthropogenic aerosols (i.e., a baseline simulation where RegCM4 only incorporate interactively coupled radiatively-interactive desert dust particles and gaseous SO_2, particulate SO_4^{-2}, hydrophobic and hydrophilic black carbon, as well as organic carbon aerosols which are induced from biomass burning activities).

© University of Pretoria

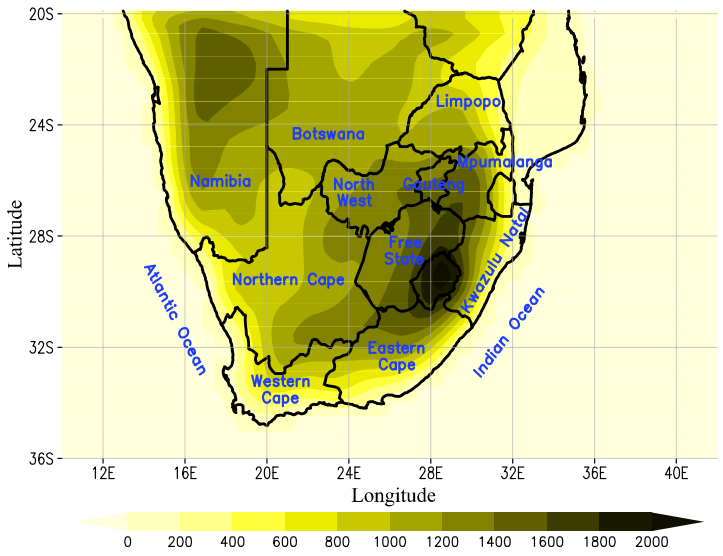

Fig. 1: Model domain, topography (unit: m) and geographical map of South Africa.

The second experiment (hereafter Exp2) is designed such that all conditions are the same as in Exp1, except for the inclusion of the emission of anthropogenic gaseous SO_2 (i.e., particulate SO_4^{-2}), while the rest of the anthropogenic emissions are set to zero. In a similar manner as in Exp2, the anthropogenic BC and OC emissions are included separately to RegCM4 in the third and fourth experiments (hereafter Exp3 and Exp4), respectively. Lastly, in the fifth experiment (hereafter Exp5), keeping the RegCM4 setup the same as the baseline simulation, in addition to the background aerosols, all radiatively interactive anthropogenic aerosol components (i.e., sulfate, hydrophobic and hydrophilic BC as well as OC aerosols which are induced from anthropogenic emissions) are taken into account together. Afterward, the individual and total anthropogenic aerosol species' column burden spatio-seasonal variations plus the climatic feedbacks for the existence of radiatively-interactive anthropogenic aerosols are derived from the differences between the results of Exp2 through Exp5 versus Exp1. In addition, the direct radiative forcing contributions of total/individual anthropogenic aerosol species are also computed in additional experiments.

Although there are several processes in the atmosphere that changes an external mixture of particles into an internal mixture (e.g., Jacobson, 2001c; Myhre and Nielsen, 2004; Fuzzi *et al.*, 2006), throughout our studies, considering the relative humidity influence on the optical properties of hydrophilic aerosols (Solmon et al. 2006); the external mixture assumption is used. Furthermore, to perceive some of the other limitations of the model, the reader is referred to Tesfaye *et al.* (2013a). This paper only has considered the direct and semi-direct effects of anthropogenic aerosols, thus it has to be viewed as a first-degree assessment of anthropogenic aerosols and their influence on the climate, in South Africa.

3 Results and discussion

By comparing the simulation results obtained from Exp2 through Exp5 with the Exp1; in the following subsections we present the column burden spatial distributions (see section 3.1), the radiative perturbations (see section 3.2) as well as semi-direct climatic implications (see section 3.3) of anthropogenic sulfate, BC and OC aerosols, separately, and all three combined. For the sake of brevity, all results are presented in terms of two contrasting seasons of South Africa (Tummon, 2011): the wet season [summer (November to February)] and dry season [austral winter (June-September)]. Although our domain configuration includes regions outside of South Africa, the discussions of this study are particularly focused on our region of interest, i.e., South Africa.

3.1 Anthropogenic aerosols (sulfate and carbonaceous aerosols) column burden

Fig. 2, (a to d) respectively show the eleven years averaged seasonal mean spatial distributions of anthropogenic activities induced sulfate, BC, OC and the total (SBO) aerosol column burden, along with the wind vector at an altitude of 10m above the surface, over South Africa and its surrounding areas. These anthropogenic aerosol column loadings are extracted by comparing the results of their corresponding experiments with Exp1 (see section. 2); whereas, the wind fields are obtained directly from Exp2 to Exp5 with their corresponding orders. Generally, the results show that the most populated and highly industrialized regions of the country (i.e., the Highveld zones of Gauteng and Mpumalanga provinces, where ~75% of the South African industrial infrastructures are situated) (e.g., Wells *et al.*, 1996) are the major source areas of anthropogenic aerosols in and around South Africa. The central and southwest areas of Mpumalanga are highly saturated with coal-fired power stations (e.g., Eskom, 1996; Spalding-Fecher and Matibe, 2003; Mills et al. 2012); accordingly the largest sulfate aerosol loads are found in these regions. Similarly, related with some power sectors that are operating on the Highveld areas of Gauteng, as well as various industries and mines which are concentrated in this province (e.g., Freiman and Piketh, 2003; Scheifinger and Held, 1997; Mills et al. 2012); intense regional values of anthropogenically induced carbonaceous particle loading (i.e., BC and OC) have been noted over broader areas of Gauteng. As the particles disperse from their source regions, through various atmospheric processes, their concentrations decline substantially (see Fig. 2).

The dynamical situations of the atmosphere are essential in determining the aerosol's distribution (e.g., Solmon *et al.*, 2012). Therefore, as shown in Fig. 2, the spatial distribution of the anthropogenic plume that originates from Gauteng and Mpumalanga basically follows the well-known southern African subtropics region dominating lower tropospheric anticyclone air circulation pattern (Freiman and Piketh 2003 and references therein). Influenced by this familiar air flow pattern, the anthropogenic aerosols are dispersed towards the northern, central and eastern areas of South Africa. Thereafter, driven by the anti-clockwise air circulation and westerly disturbances, the aerosols' dispersion are curved through the central areas of South Africa and exit the country through the east and southeast direction towards the Indian Ocean. The surface wind circulation and anthropogenic aerosol dispersion patterns presented in our study are highly consistent with previous studies, such as Freiman and Piketh, 2003, which presented a similar lower tropospheric flow of aerosol pollution from the Highveld areas of South Africa. Therefore, throughout the year the column burden of sulfate, BC, OC as well as the total SBC anthropogenic aerosols exhibited a similar spatial distribution pattern, with a moderate and considerable seasonal variation on carbonaceous and sulfate aerosol concentrations, respectively (see Fig. 2).

© University of Pretoria

UNIVERSITEIT VAN PRETORIA
UNIVERSITY OF PRETORIA
YUNIBESITHI YA PRETORIA

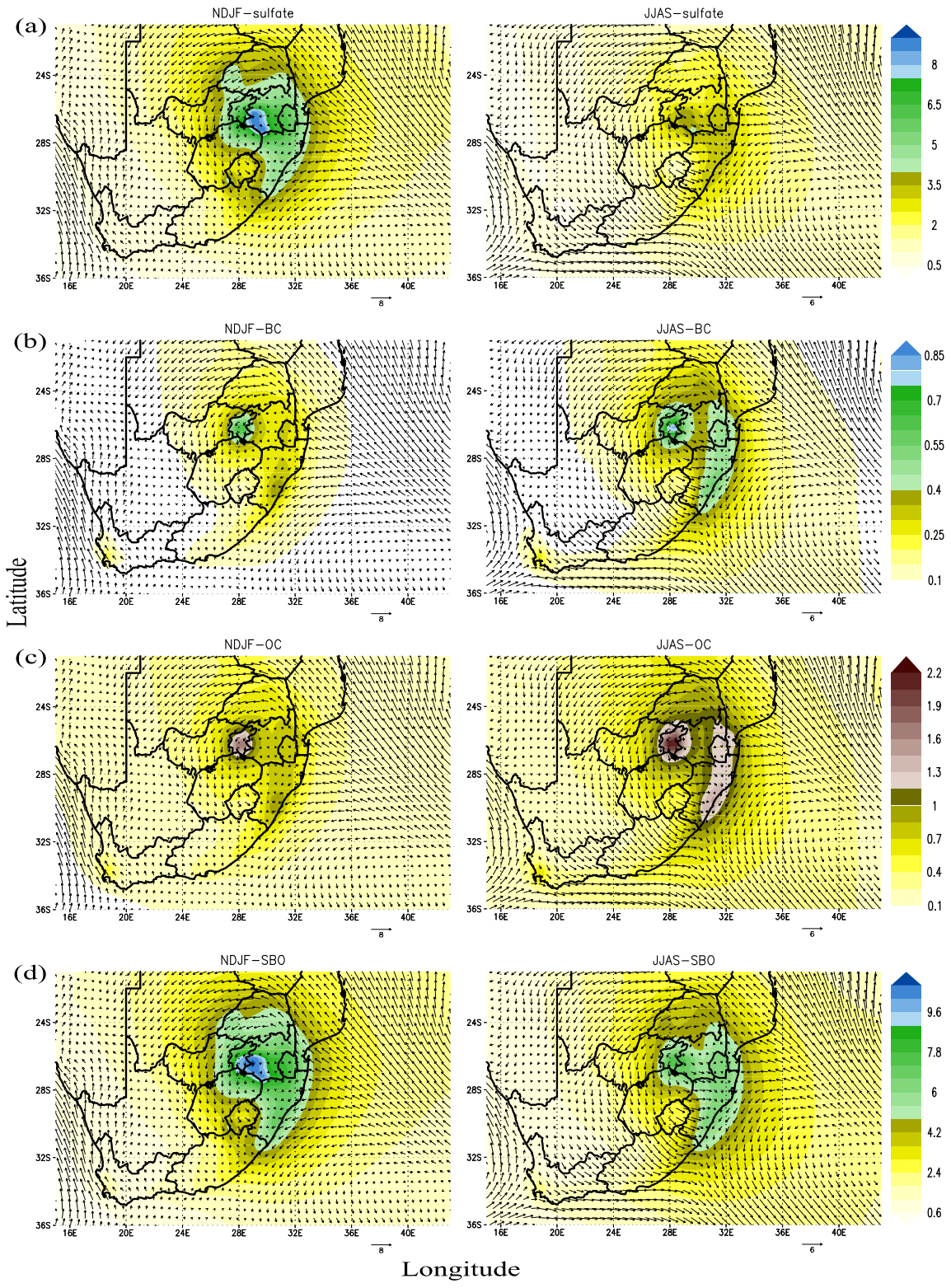

Fig. 2: 1998–2008 averaged seasonal mean spatial distributions of anthropogenic activities induced sulfate, BC, OC and the total (sulfate+BC+OC) aerosol column burden (shaded, unit: mg/m^2), from row (a) to (d), respectively, superposed with the 10 meter wind field (vector; the scale is indicated by the arrow to the lower right; unit: m/s), in and around South Africa. The first row is for the summer; whereas, the second row is for the austral winter.

The column burden of carbonaceous aerosols' seasonal variations, relative to their annual average, is ~ ±14% for BC and ~ ±12% for OC. These variations are found to be far smaller when they are compared with that of sulfate particles, which exhibit a variation of ~ ±35%. As stated in section 1, sulfate aerosols are primarily formed in the atmosphere via gas-phase and aqueous phase SO_2 to SO_4^{-2} chemical conversion pathways (Qian and Giorgi 1999; Qian *et al.*, 2001); consequently, their concentration becomes highly reliant on seasonally variable meteorological fields. Due to this, considerable seasonal variations in sulfate aerosol concentration, relative to the other anthropogenic aerosol components are found (see Fig. 2). The enhanced air temperature and moist meteorological conditions of the summer season offer advantageous situations for the formation of secondary sulfate particles (e.g., Ganzeveld *et al.*, 1998; Roelofs *et al.*, 2001). Thus, the maximum column load of sulfate aerosols, in South Africa, has been noted during this season; particularly around the Highveld areas of South Africa, their concentration varied from 5.5 to 10 mg/m^2(Fig. 2a). Predominantly, freshly emitted carbonaceous aerosols (especially BC particles) are hydrophobic; however as they stay in the atmosphere, due to complex physico-chemical ageing processes, they may gradually evolve into hydrophilic particles (Solmon *et al.*, 2006; Cooke *et al.*, 1999; Liu *et al.*, 2005). As a result wet deposition becomes one of the main removal processes for BC and OC aerosols; especially for their hydrophilic components (Cooke and Wilson, 1996; Jacobson, 2010). Abundant moisture and rainy conditions of summer generally enhance the ageing process of carbonaceous particles from hydrophobic to hydrophilic states (i.e., a fraction of carbonaceous aerosol that evolves from hydrophobic to hydrophilic state in the atmosphere increases). This situation has reduced the local build-up (atmospheric life time) and regional transport of these carbonaceous particles through enhanced removal by wet deposition (Cooke and Wilson, 1996). Therefore,

© University of Pretoria

relative to the austral winter, reduced column burden values of BC (hydrophobic-BC + hydrophilic-BC) and OC (hydrophobic-OC + hydrophilic-OC), that varied from 0.1 to 0.65 mg/m^2 and 0.2 to 1.7 mg/m^2, respectively are found during the summer season (see Fig. 2b and 2c).

Reduced air temperature and dry weather situations of the austral winter season, constrain the oxidation processes of SO_2; which in turn, result in unfavourable situations for the formation of secondary sulfate aerosols. Nevertheless, these meteorological circumstances, to some extent, enhance the atmospheric residence time and the dispersion of anthropogenic aerosols (Shindell *et al.*, 2008a, 2008b). Accordingly, relative to summer, the decline in sulfate aerosol concentration by up to 52% (i.e., its column burden varied from 0.8 to 4.4 mg/m^2, Fig. 2a) as well as a slight enhancement in carbonaceous aerosol loadings (by about 20% for BC and 22% for OC, Fig. 2b and 2c) has been noted during the austral winter. Owing to the predominant anticyclone air circulation patterns, throughout the year, an insignificant load of anthropogenic particles have been observed in the Northern and Western Cape Provinces (see Fig. 2). This excludes the southwest corner of the Western Cape (~ 18°E, -34°S) which exhibited a minimal load of carbonaceous aerosols that are induced through some local activities.

The annual mean regional average total anthropogenic aerosol burden (averaged over the areas of South Africa: -35° – -22°S, 16° – 33°E) is 3.5 mg/m^2 with the sulfate, BC and OC aerosols accounting for ~ 72%, ~ 10% and ~ 18% of the burden, respectively. This indicated that, in and around South Africa, among these three species of anthropogenic aerosols, the scattering components on a mass basis contributed the largest fraction. The bulk aerosol effective optical properties are not only dependent on physico-optical properties of its aerosol constituents; but also highly reliant on the fractional contributions of each aerosol species to the bulk aerosols. Therefore, these aforementioned total anthropogenic aerosol fractional configurations have far-reaching implications in determining the overall radiative and climatic influence of anthropogenic aerosols.

3.2 The shortwave radiative forcing of anthropogenic aerosols at the surface and in the atmospheric column

The sign and magnitude of aerosols' radiative forcing, at the surface and within the atmospheric column, indicate their role in inducing radiative cooling/warming on the surface-atmospheric system, along with the level of their influence. Therefore, in the following subsection the radiative forcing contributions of sulfate, BC, OC, and all three anthropogenic aerosols combined, are presented.

The eleven year (1998–2008) seasonally-averaged direct shortwave surface and atmospheric radiative forcing contributions of anthropogenically induced sulfate, BC, OC and SBO (i.e., sulfate+BC+OC) aerosols, over South Africa and its surrounding areas, are depicted in Fig. 3.1 and Fig. 3.2, respectively. Generally, for all anthropogenic aerosol species, the spatio-seasonal evolution of surface (Fig. 3.1) and atmospheric (Fig. 3.2) radiative forcing are quite similar to their corresponding column burden seasonal and spatial variations. However, there is a minor shift in the peaks of forcing away from the maximum of their column burden, which is due to the relative humidity dependence of radiative forcing (Kiehl *et al.*, 2000; Kiehl and Rodhe, 1995; Markowicz *et al.*, 2003). Throughout the seasons, the anthropogenic aerosol radiative forcing predominantly cover: the central, upper and east coast regions of South Africa, as well as the surrounding Indian Ocean. Owing to the lowest level of anthropogenic aerosol abundance over the west and southwest areas of the country (see Fig. 2), the lowest anthropogenic aerosol radiative forcing values appeared in the Northern and Western Cape provinces of South Africa. This excludes the southwest corner of Western Cape that has showed a minimal influence of carbonaceous aerosols (Fig. 3.1 and Fig. 3.2).

Overall, the simulation outcomes in Fig. 3.1 showed that both absorbing and scattering components of anthropogenic aerosols lead to a reduction of net solar radiation at the surface. The uptake of water by hygroscopic particles, such as sulfate aerosols, increases their scattering efficiency and, in turn, strengthens their radiative forcing (e.g., Haywood *et al.*, 1997). This, associated with the moist situation of the summer season and the higher load of secondary sulfate particles (see Fig. 2), consequently result the largest negative values of Sulfate aerosol Surface Radiative Forcing (SSRF) that varied from ~ -3 to -12 W/m^2 (Fig. 3.1a). Whereas, in conjunction with the reduction of the column load of sulfate particles, as well as the dry conditions of the austral winter season, the minimal negative values of SSRF (varying from -0.4 to -3.9 W/m^2) are noted during this season (Fig. 3.1a). In both seasons the maximum influence of SSRF are noted in areas which are in and nearby their source regions (Fig. 3.1a), due to the short residence time (e.g., Seinfeld and Pandis, 2006; Shindell *et al.*, 2008a).

Generally, the atmospheric radiative forcing of aerosols is computed based on the differences between the aerosol radiative forcing at the top-of-the-atmosphere and surface. As stated in section 1, the sulfate aerosols have a strong scattering effect. As a result, throughout the seasons, Sulfate aerosol Atmospheric Radiative Forcing (SARF) values have illustrated a minimal value (varying from -0.05 to 0.06 W/m^2, Fig. 3.2a). This indicates that the sulfate aerosols reduce the net solar flux at the surface, by entirely scattering the solar radiation that enters the atmospheric column back to space. All over the domain as well as throughout all the seasons, the surface and atmospheric radiative forcing values of carbonaceous aerosols (i.e., BC and OC particles) display negative and positive signs, respectively (Fig. 3.1b, c and Fig. 3.2b, c). The peak minima of carbonaceous aerosols' Surface Radiative Forcing (CSRF) (i.e., BC ~ -2 W/m^2 and OC ~ -0.68W/m^2) occurred around Gauteng and its adjacent areas during the austral winter season (Fig. 3.1b and 3.1c). Additionally, within the same areas and season, the peak values of carbonaceous aerosol Atmospheric Radiative Forcing (CARF) (i.e., BC ~ +2.7 W/m^2, Fig. 3.2b and OC ~ +0.33 W/m2, Fig. 3.2c) are observed. As seen in section 3.1, the column burden of carbonaceous particles seasonal variations are small relative to the sulfate aerosols. Therefore, the magnitude of CSRF and CARF, relative to their annually average values only varied respectively by about ±6% and ±5% for BC, as well as ±11% and ±3% for OC aerosols. These seasonal variations are quite small when compared with the magnitude of SSRF seasonal variations. The simulated positive CARF and negative CSRF values endorse that the solar radiation absorption by carbonaceous aerosols (primarily by BC as well as slightly via OC particles e.g., Andreae and Gelencser, 2006) cause a reduction of the net shortwave radiation flux at the surface by increasing the reception in the atmosphere (by enhancing the radiative heating within atmospheric column).

© University of Pretoria

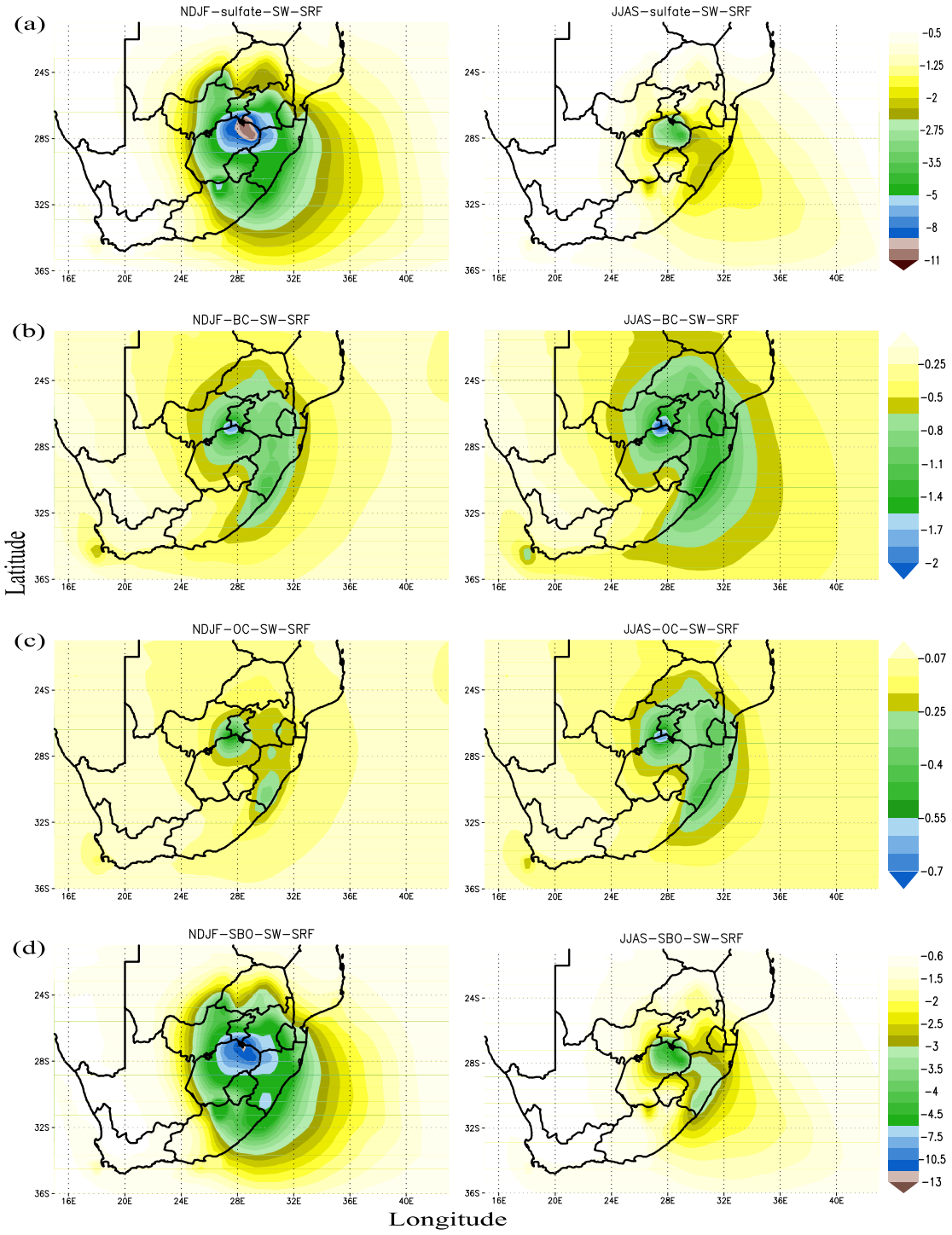

Fig. 3.1: The seasonal mean spatial distribution of anthropogenic activities induced aerosols' shortwave Surface direct Radiative Forcing (SRF), in and around South Africa; (units: W/m^2): row (a) sulfate (b) BC (c) OC and (d) SBO. The first column represent summer; whereas, the second column represent austral winter, for SRF. The seasons and aerosol types are indicated at the top of each figure.

The BC particles account only for 10% of the total anthropogenic aerosol mass burden (refer section 3.1), nevertheless, due to their enhanced solar radiative absorption nature; the BC aerosol surface and atmospheric forcings are almost 3 and 7 times stronger than that of OC particles (which account for 18% of anthropogenic aerosol burden). The total anthropogenic aerosol (i.e., sulfate+BC+OC), surface (TSRF) and columnar (TARF) radiative forcing are shown in Fig. 3.1d and Fig. 3.2d, respectively. Throughout the seasons, the SW scattering and absorbing influences of anthropogenic aerosols, cooperatively, induced radiative cooling and heating, at the surface and in atmosphere respectively. i.e., over the entire domain, negative and positive values of TSRF and TARF, respectively are noted. In and around the Highveld zones of Gauteng and Mpumalanga, extreme values of TSRF (that varied from -7 to -14 W/m^2) and TARF (that varied from +2.5 to +3.2 W/m^2) are observed during the summer and austral winter, respectively. Whereas, during the summer season, away from the Highveld zones of South Africa, reduced values of TSRF (that varies from -0.7 to -6.5 W/m^2) are found (Fig. 3.1d). The seasonal variation in TARF is quite small in comparison to TSRF values, which show a variation by about 50%.

© University of Pretoria

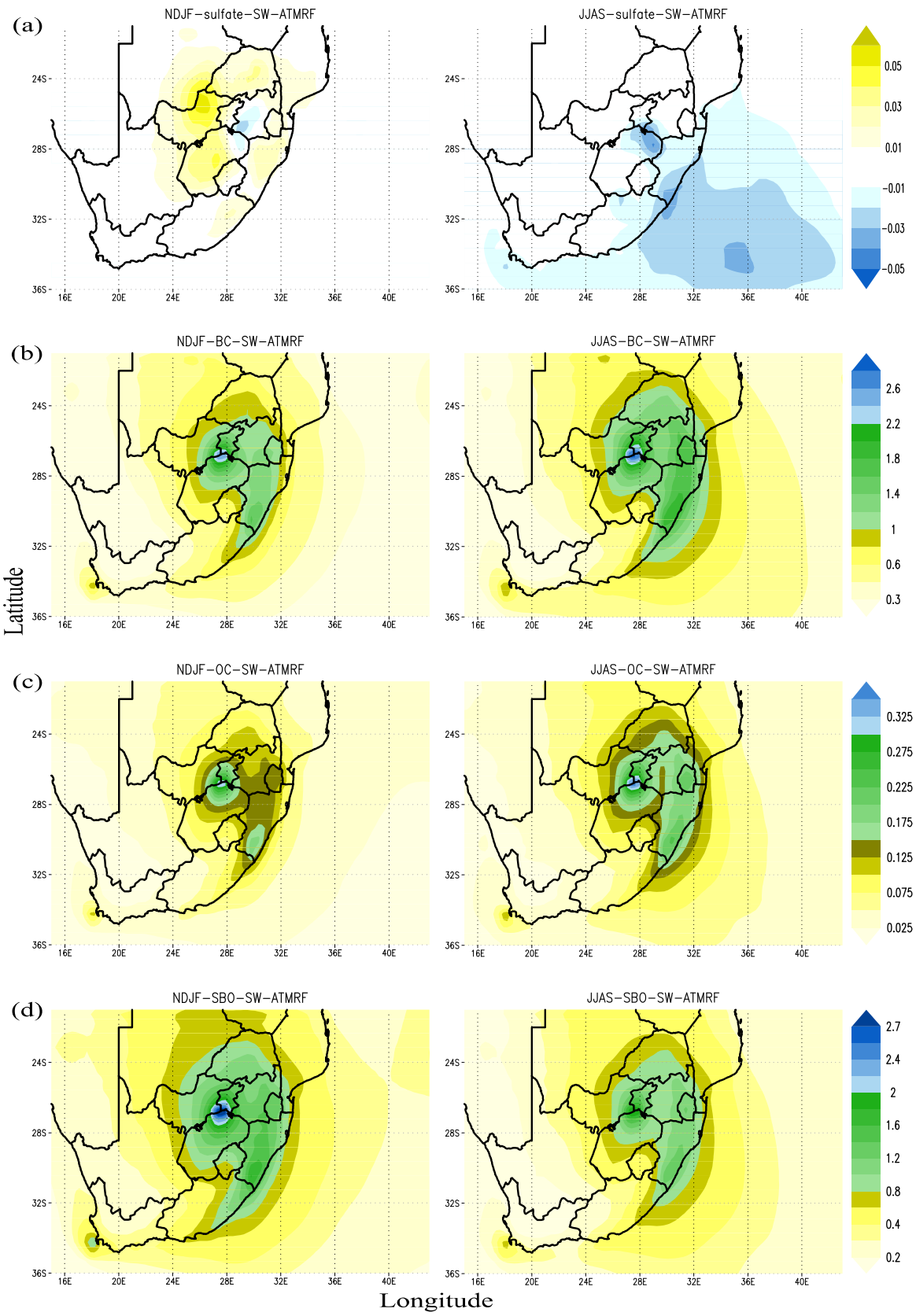

Fig. 3.2: The same as Fig. 3.1 but for atmospheric radiative forcing; (units: W/m^2): row (a) sulfate (b) BC (c) OC and (d) SBO.

The comparison of the magnitudes, the signs, as well as, spatio-seasonal variations of TSRF (Fig. 3.1d) with that of Fig. 3.1 (a), (b), (c), clearly illustrates that scattering influences of sulfate aerosols are the main contributor to the TSRF values (about 81%). The same comparison for TARF (Fig. 3.2d) also indicate that the shortwave absorption influences of BC particles with a minor contribution of OC aerosols are the key donor of the total anthropogenic aerosol atmospheric forcing. The simulation results show that the magnitudes of aerosol radiative forcing are primarily contingent on the aerosols' concentrations and their physico-optical characteristics. However, we would like to remark that the incoming solar radiation intensity and surface albedo spatio-seasonal variations also have some influences in determining the magnitude of the aerosols' radiative forcing (e.g., Kumar and Devara 2012; Stier *et al.*, 2007; Forster *et al.*, 2007 and references therein).

3.3 Climate responses

In this section, the changes in different climatic variables due to the presence of radiatively interactive anthropogenic aerosols, as well as the correlations among these alterations are discussed. As stated in section 2, the climatic feedbacks associated with the presence of radiatively interactive anthropogenic aerosol species are captured by comparing the simulation results obtained from Exp2 through Exp5 with that of the baseline simulation (Exp1). In the next section, the change in Surface Temperature (ΔST) and Surface Sensible Heat Flux (ΔSSHF) is addressed. In section 3.3.2, the influences of anthropogenic aerosols' on Net

© University of Pretoria

Atmospheric radiative Heating Rate (ΔNAHR) as well as on Cloud Cover (ΔCC) are provided. Lastly, the effects of anthropogenic aerosols' on Planetary Boundary Layer height (ΔPBL), Surface Pressure (ΔSP) along with the surface wind field ($\overrightarrow{\Delta W}$) are discussed in section 3.3.3.

3.3.1 The effects of anthropogenic aerosols on surface temperature and surface sensible heat flux

Relative to the control simulation (Exp1), changes on ST and SSHF due to the existence of different anthropogenic aerosol species, in and around South Africa are shown in Fig. 4.1 and Fig. 4.2, respectively. Both ST and SSHF responses show a significant seasonal variation. These ST and SSHF changes are induced by different processes which involve aerosols-radiation and climate interactions. Such as, in and around the anthropogenic aerosol loaded areas, the ΔST and ΔSSHF are associated with the anthropogenic aerosol radiative forcing (see section 3.2). Furthermore, the anthropogenic aerosol semi-direct effects induced CC alterations (section 3.3.2) and to some extent regional scale circulation changes (section 3.3.3) also plays important role in inducing the ΔST and ΔSSHF. Generally, following the enhancement (or reduction) of cloudiness, the amount of solar radiation which is reflected by clouds respectively be enhanced (or reduced). Correspondingly, the solar flux that reaches the surface may be reduced (or enhanced), which means that the ΔCC (section 3.3.2) may significantly influence the ST as well as the SSHF (e.g., Haywood and Boucher, 2000; Ramanathan *et al.*, 2001a; Zhang, 2008).

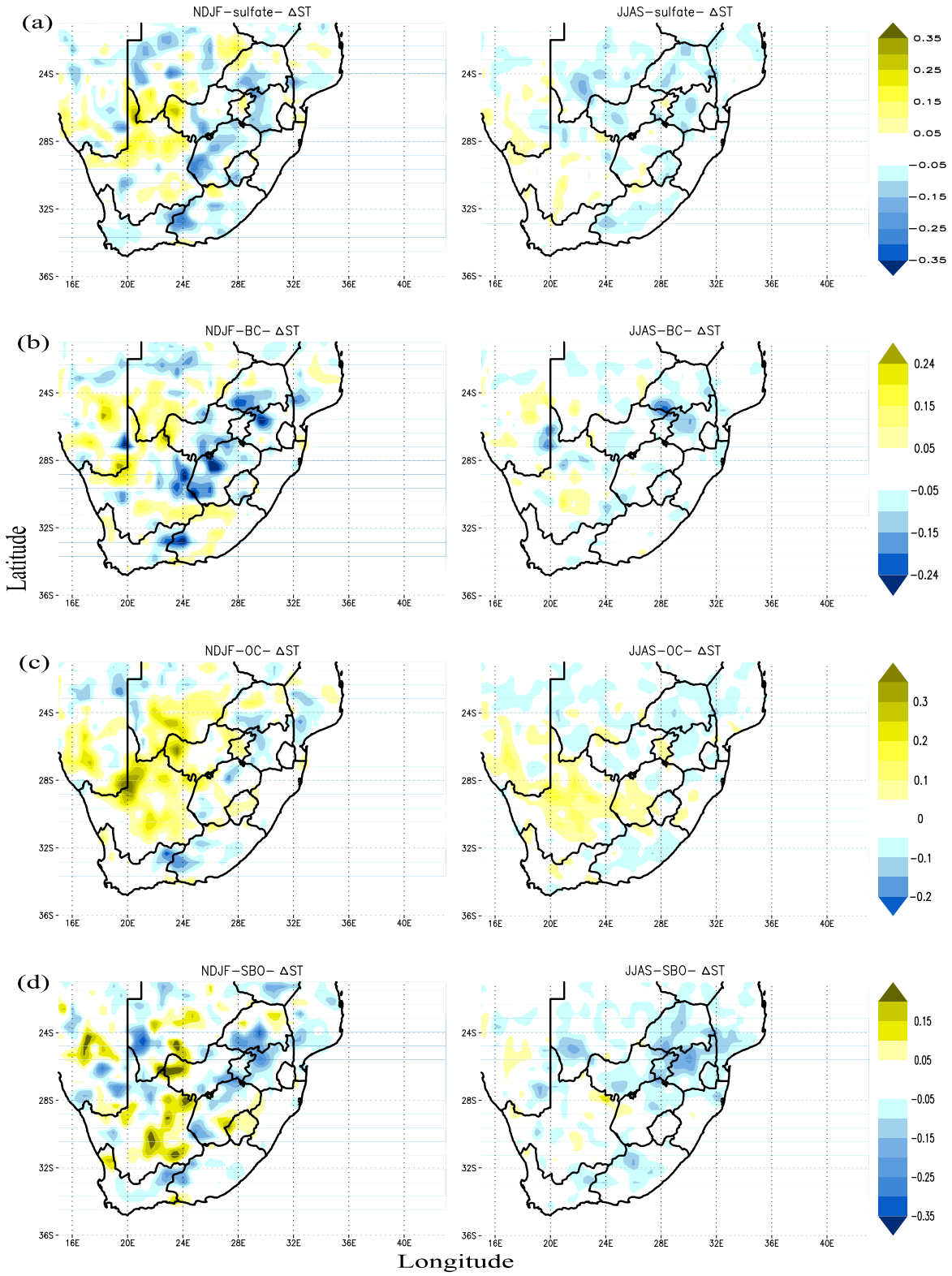

Fig. 4.1: Simulated seasonal mean changes in surface temperature (ΔST, unit: K) in the presence of anthropogenic activities induced aerosols: row (a) sulfate [Exp2- Exp1] (b) BC [Exp3- Exp1] (C) OC [Exp4- Exp1] and (d) SBO [Exp5- Exp1]. All results were averaged over 1998–2008; as well as, the first column represent summer; whereas, the second column represent austral winter, for ΔST.

Moreover, the results in Fig. 4.1 and Fig. 4.2 show that the ΔST (ΔSSHF) are not limited in areas where anthropogenic aerosols are dominant. Though the loads as well as the radiative forcing of anthropogenic particles over the west and southwest

© University of Pretoria

areas of the country (i.e., the Northern and Western Cape Provinces) are insignificant (see Fig. 2 and Fig. 3.1) - the inclusions of anthropogenic aerosols also induce a ΔST and ΔSSHF in these regions as well. These changes are basically related with the meteorological field modifications that are induced due to the enclosure of radiatively interactive anthropogenic aerosols, which, in turn, influence the background aerosol concentration. The changes in surface wind speed (see Fig. 6), surface humidity and other meteorological situations of the climate, due to the inclusion of different components of anthropogenic aerosols, consequently modify the desert dust emission and burden level, in and around the Northern Cape arid/semi-arid regions (e.g., Yue *et al.,* 2010b) (figure is not shown). Attributed to this modification (i.e., the dust aerosol burden level alterations), some changes in the background dust aerosol radiative influence as well as local atmospheric thermal structure adjustments take place. Which subsequently, lead to the change in cloud cover in and around the Northern Cape Province (Fig. 5.2; also see Ramanathan *et al.,* 2001a; 2001b; Miller *et al.,* 2004a). Since the anthropogenic aerosols' radiative forcing in the Northern and Western Cape Provinces are very insignificant; a small change in CC in these areas provide a pronounced variation on ΔST (ΔSSHF), by reducing (or enhancing) the surface solar flux.

In the course of the summer season, around Mpumalanga, Limpopo, the central areas of South Africa (Free State), the western parts of the Eastern Cape province as well as over some other narrow scattered areas of South Africa; the inclusion of sulfate, BC, OC and SBO aerosols induce ST reduction that varied from -0.1 K to -0.3 K, -0.06 K to -0.25 K, -0.05 K to -0.21 K and -0.07 K to -0.36 K, respectively. In contrast to this, in and around the Northern Cape arid/semi-arid regions as well as Gauteng (during the inclusion of OC particles), it is also found that the enclosure of sulfate, BC, OC and SBO aerosols ensued an enhancement in ST that varied from +0.1 K to +0.3 K, +0.06 K to +0.24 K, +0.1 K to +0.35 K and +0.07 K to +0.22 K, respectively (see Fig. 4.1). The enhancement in ST is mainly caused by the reductions in CC; which have attributed to the anthropogenic aerosols' atmospheric heating (see Fig. 5.1), as well as the thermodynamical influences of changes in background aerosol concentrations (especially changes on the dust particles' burden level; e.g., Yue *et al.,* 2010b). Particularly, around the potential source region of carbonaceous particles (i.e., Gauteng; Fig. 2b and 2c), our simulation show that, in contrast to BC aerosols, the inclusion of OC particles promote the reduction in low-level cloud cover (Fig. 5.2). Concurrently, this semi-direct effect increase the amount of solar flux reaching the surface; which in turn, counteract the OC aerosols induced negative SRF (e.g., Ramanathan *et al.,* 2001a; Denman *et al.,* 2007 and references therein). Our results exhibit the SRF of OC particles are small enough (see Fig. 3.1c) to be surpassed by the CC reduction induced surface solar flux increases; therefore during the enclosure of OC aerosols, around Gauteng, a slight enhancement in ST varied from +0.05 K to +0.2 K have occurred (Fig. 4.1c).

As described in different studies (e.g., Ramanathan and Ramana, 2005; Boer 1993; Slingo *et al.,* 2006; Mallet *et al.,* 2009; Yu et al. 2002), the direct and semi-direct effects of atmospheric aerosols induced radiation flux perturbations at the surface - beside influencing the ST - may also consequently impose a disruption on the surface-atmospheric energy exchange. Especially over the land, the surface cooling (or heating) incidences that are noted above (Fig. 4.1), correspondingly lead to the reduction (or increment) in upward transport of SSHF from the surface into the atmosphere (e.g., Miller and Tegen, 1998; Shell and Somerville, 2007; Yue *et al.,* 2010a, 2010b; Zhang, 2008). As a result, particularly aligned with the spatial patterns of ST reductions (or enhancements), correspondingly the ΔSSHF that varies from -1 to -4 W/m^2 (+1 to +4 W/m^2), -0.7 to -4.2 W/m^2 (+0.7 to +3.5 W/m^2), -0.8 to -4 W/m^2 (+0.8 to +4.8 W/m^2) and -0.8 to -4 W/m^2 (+0.8 to +3.3 W/m^2) respectively occur due to the presence of sulfate, BC, OC and SBO anthropogenic aerosols (Fig. 4.2).

During the austral winter the ΔST and ΔSSHF that covered analogous geographical locations as the summer season are noted (see the second column of Fig. 4.1 and Fig. 4.2). However, relative to the summer, the amplitudes of ΔST and ΔSSHF during the austral winter season were reduced approximately by half. In addition during austral winter, the spatial distributions of ΔST (and ΔSSHF) are slightly modified. Moreover, except for sulfate aerosols, for other cases, the areal coverage of ΔST (and ΔSSHF) are comparably less than that of the summer season. The physical processes through which the inclusion of anthropogenic aerosols induced changes in ST as well as SSHF are the same as described for the summer season. During the austral winter, encompassing a wider area of Mpumalanga, Limpopo, Eastern Cape as well as some other narrow scattered areas in South Africa; sulfate aerosols induce ST (and SSHF) reduction that varies from -0.05 K to -0.15 K (and -0.5 to -2.5 W/m^2). Conversely, over some constricted areas of the Northern Cape arid/semi-arid regions, the inclusion of sulfate aerosols induce positive ST (and SSHF) changes that varies from +0.05 K to +0.1 K (and +0.5 to +2 W/m^2). Within the same season, the BC, OC and SBO aerosols resulted the ST (and SSHF) drops which varies from -0.03 K to -0.18 K (and -1 to -3.5 W/m^2), -0.03 K to -0.12 K (and -0.5 to -2.5 W/m^2) and -0.08 K to -0.21 K (and -1 to -3.2 W/m^2), respectively. These reductions in ST (and SSHF) are mainly located around the Free State, Limpopo, Highveld zones and its adjacent areas of South Africa (see the second column of Fig. 4.1 and Fig. 4.2). Meanwhile, around the Northern Cape Province, Gauteng (during the inclusion of OC particles) as well as over some parts of South Africa, the BC, OC and SBO aerosols promoted a small enhancement in ST (and SSHF) that varies, from +0.03 K to +0.15 K (and +0.5 to +2.1 W/m^2), +0.06 K to +0.19 K (and +0.5 to +2.5 W/m^2) and +0.04 K to +0.13 K (and +0.5 to +1.5 W/m^2).

© University of Pretoria

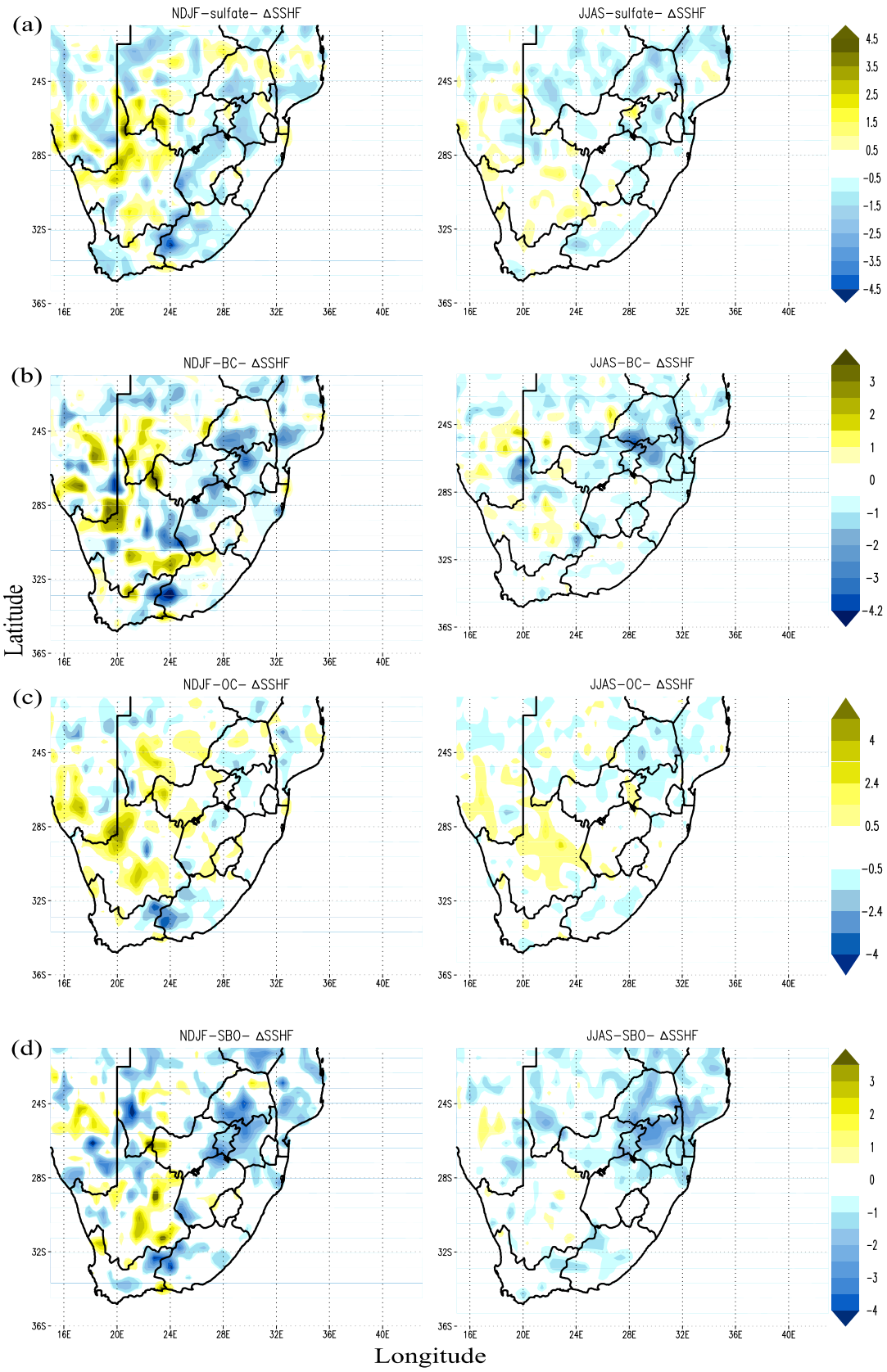

Fig. 4.2: The same as Fig. 4.1 but for changes in surface sensible heat flux (ΔSSHF, unit: W/m^2).

Throughout the seasons, the amplitude as well as the spatial coverage of ST enhancement - during the inclusion of radiatively interactive OC particles - are comparatively large and wider than the other anthropogenic aerosol species (see Fig. 4.1). In contrast, the least pronounced ST enhancement is observed when sulfate, BC, and OC are considered together (i.e., during SBO case, Fig. 4.1d). The annual mean regional average ST (and SSHF) changes for sulfate, BC, OC and SBO have shown the values of -0.012 K (-0.125 W/m^2), -0.01 K (-0.6 W/m^2), +0.04 K (+0.2 W/m^2) and -0.06 K (-0.7 W/m^2) respectively. These regionally averaged values (which are averaged over the areas of South Africa) indicate that the net effect of these anthropogenic activities induced aerosols are slightly promoting surface cooling over the region, except for that of the OC particles. The ΔST and ΔSSHF influence the lower tropospheric dynamics (e.g., Zhang, 2008); this significant issue is discussed in section 3.3.3. The above findings have shown that beside the direct and semi-direct effect of anthropogenic aerosols, their climatic feedbacks induced background aerosol concentration variation and its consequential impacts are also important in promoting changes in different climatic variables over a regional scale.

3.3.2 The effects of anthropogenic aerosols on net atmospheric radiative heating rate and cloud cover

BC aerosols are primarily hydrophobic during their emission (e.g., Cooke *et al.*, 1999), as well as comparatively anthropogenic aerosols have lighter mass, thus they easily rise to the upper level of the atmosphere (e.g., Cook and Highwood, 2004). However, the concentration profile of our results show that

© University of Pretoria

most of the anthropogenic aerosols are predominantly confined in the lower parts of the troposphere (i.e., below ~ 650hPa altitude) (figure not shown). Therefore, even if, the magnitudes plus the sign of aerosol semi-direct effects (especially the cloud response for carbonaceous aerosols) are highly dependent on the atmospheric altitude where aerosols mainly reside (e.g., Johnson *et al.*, 2004; Cook and Highwood, 2004; Fan *et al.*, 2008; Koch and Genio, 2010); this study only examine the anthropogenic aerosol columnar influences. Seasonally averaged changes in low-level (below ~ 650hPa): column integrated cloud cover (ΔCC) and columnar average net (short- plus long-wave) atmospheric radiative heating rate (ΔNAHR), due to the presence of different types of anthropogenic aerosols, are shown in Fig. 5.1. The computation of net atmospheric radiative heating rate comprise the radiative influences of all climatic components (i.e., different types of aerosols, clouds, water vapour, the underlying surface and other trace gases in the atmospheric column). By comparing the NAHRs obtained from Exp2 through Exp5 with that of the baseline simulation (Exp1), the influence of anthropogenic aerosols on NAHR are assessed.

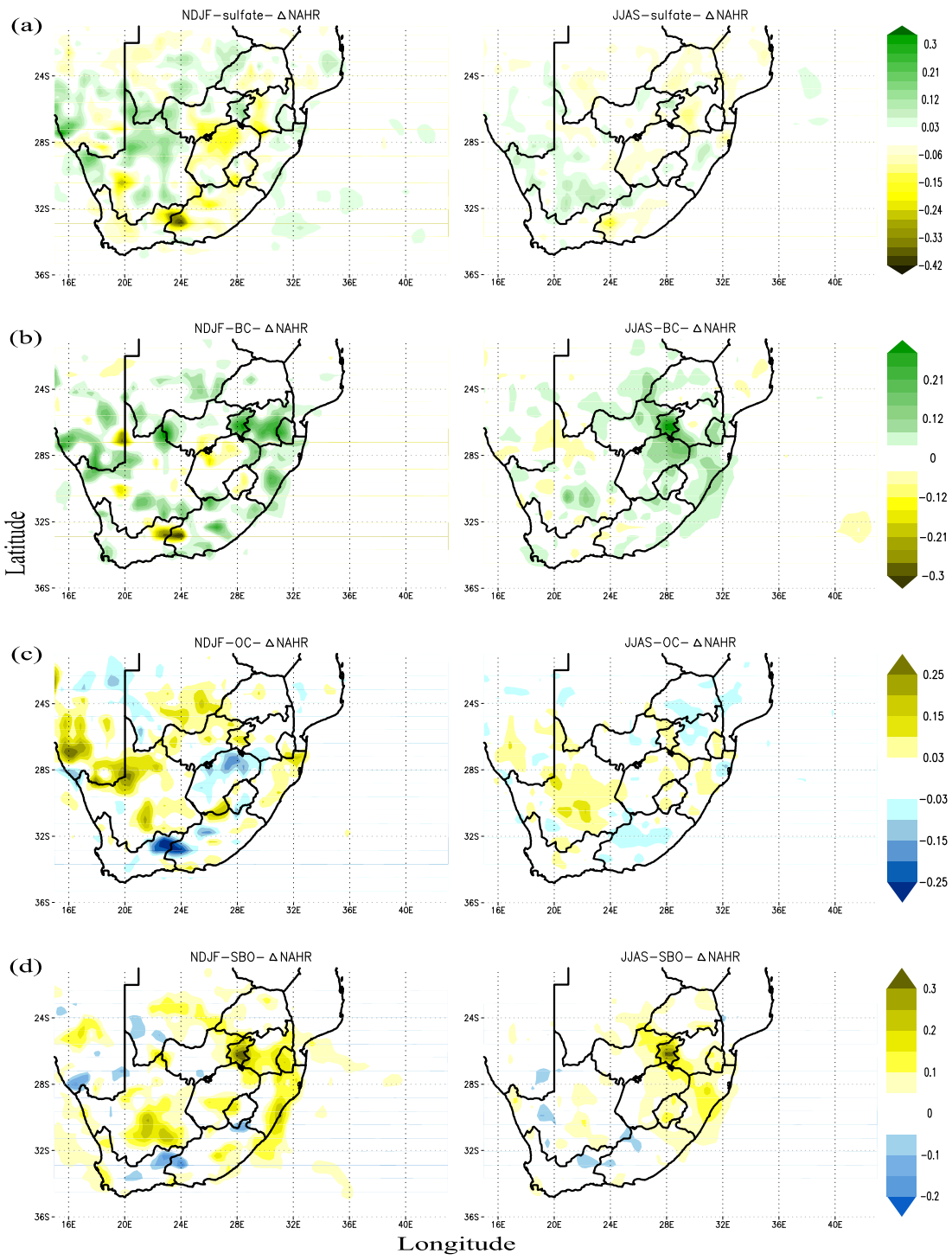

Fig. 5.1: Changes in low-level columnar average net atmospheric radiative heating rate (ΔNAHR, unit: K/day), due to the existence of anthropogenically induced: row (a) sulfate, (b) BC, (C) OC and (d) SBO aerosols. The results were averaged over 1998–2008. The first column represent summer; whereas, the second column represent austral winter, for ΔNAHR.

During the enclosure of sulfate and OC aerosols, mainly around Mpumalanga, Limpopo, Free State and the Eastern Cape, as well as over scattered areas of the Northern Cape region, the ΔNAHR that varies from -0.08 to -0.42 K/day for sulfate (OC: -0.05 to -0.26 K/day) and -0.03 to -0.17 K/day for sulfate (OC: -0.03 to -0.13 K/day), are found in the course of the summer and austral winter, respectively (see Fig. 5.1a and c). Largely over the Northern Cape Province, coastal areas of KwaZulu-Natal (during the inclusion of OC particles) as well as over some scattered areas of South Africa, in these corresponding seasons, positive values of ΔNAHR that varies from +0.08 to +0.32 K/day for sulfate (OC: +0.05 to +0.25 K/day) and +0.03 to +0.09 K/day for sulfate (OC: +0.03 to +0.15 K/day) were predicted. In the case of sulfate aerosols, the spatial coverage of the ΔNAHR during the austral winter was comparatively wider than that of the summer season. The above columnar cooling influences (especially around the sulfate and OC aerosol loaded areas, see Fig. 2) were basically caused by the predominant SW scattering nature of the sulfate

© University of Pretoria

aerosols as well as weakly absorbing OC particles. Furthermore, as stated in section 3.3.1, interaction and feedbacks among the anthropogenic aerosols, radiation and climate, consecutively, induced changes in background aerosol concentrations. The climatic feedbacks of sulfate and OC aerosols also induce both reductions (and enhancements) of the background desert dust aerosol concentrations; this correspondingly attribute to the columnar cooling (and heating) effects, that are noted in and around the Northern Cape region, during the inclusion of these anthropogenic aerosols.

The BC (SBO) aerosol-radiation-climatic interactions primarily result in an enhancement in the net atmospheric radiative heating rate (see Fig. 5.1b and d). The inclusion of BC (and SBO) aerosols induced atmospheric heating that correspondingly varied from +0.06 to +0.27 K/day (+0.05 to +0.32 K/day) during summer and from +0.06 to +0.32 K/day (+0.05 to +0.3 K/day) throughout winter. These heating influences of BC and SBO aerosols are mainly located around the Highveld regions of Gauteng and Mpumalanga and their adjacent areas, such as the coastal regions of KwaZulu-Natal, along with some parts of Northern Cape Province (Fig. 5.1b and d). During the summertime, over the central areas of South Africa, western regions of the Eastern Cape as well as over some scattered areas of the Northern Cape, the presence of BC aerosols results a ΔNAHR that varies from -0.04 to -0.3 K/day (Fig. 5.1b). In both cases (during BC and SBO inclusions), a minimal negative values of ΔNAHR, which encompassed only some narrow scattered areas of the Northern Cape, are noted during the dry season (austral winter). Over the anthropogenic aerosol dominating areas (see Fig. 2), the columnar heating influences BC and SBO aerosols are primarily attributed to the SW absorbing nature of the BC aerosols as well as, the effect of BC in cooperation with the slightly absorbing OC particle contributions (in the case of SBO inclusion). Similar to other anthropogenic aerosols, the climatic feedbacks of BC and SBO aerosols also triggered reductions (or enhancements) on the desert dust particle burden level, which correspondingly induced both decreases (and increases) in the NAHR, in and around arid/semi-arid regions of South Africa.

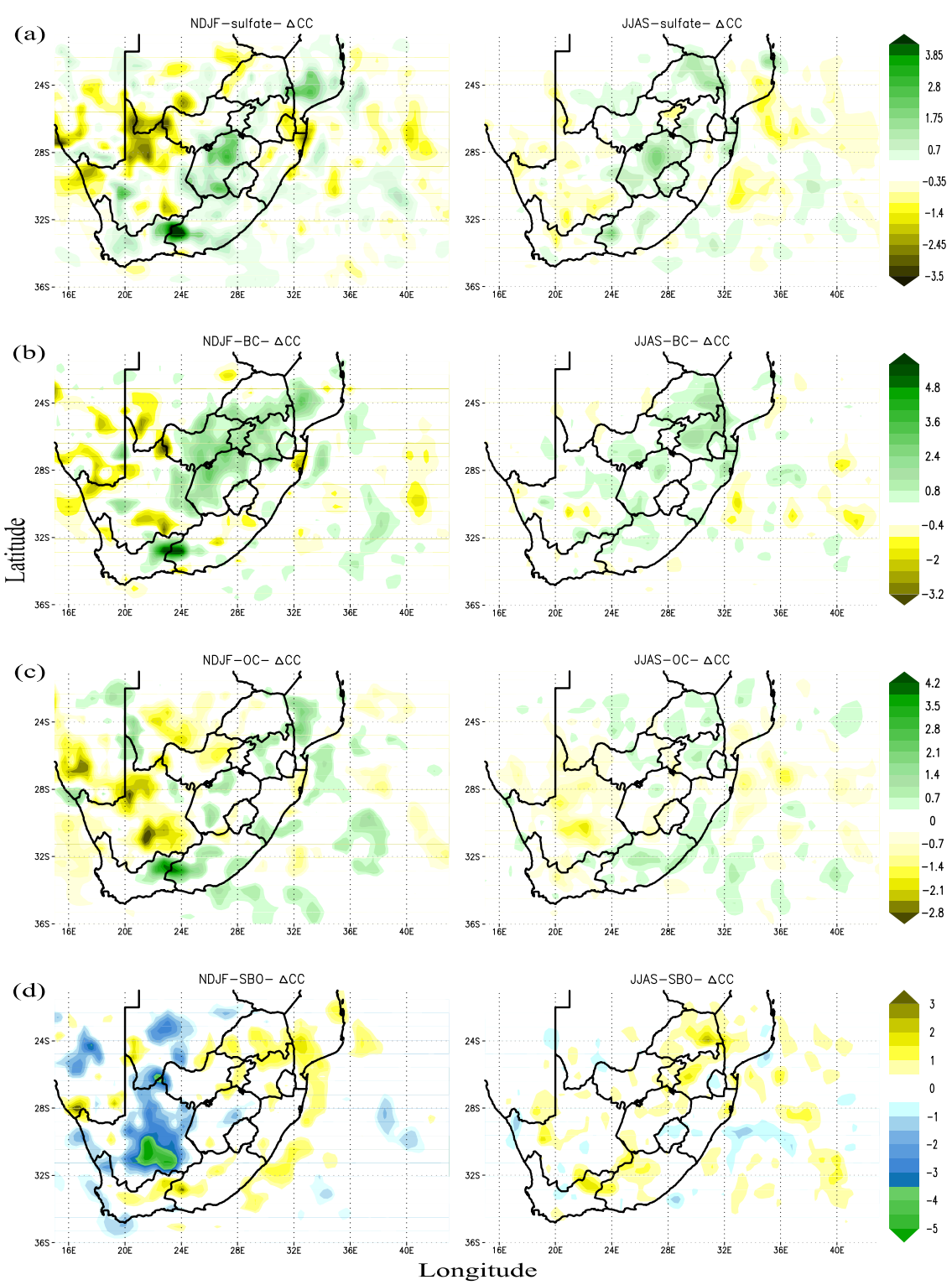

Fig. 5.2: The same as that of Figure 5.1 except that here the change in low-level column integrated cloud cover (ΔCC, unit: %) are depicted.

© University of Pretoria

In response to the ΔNAHR, various alterations on the thermal structure of the atmosphere (in turn on atmospheric stability), dynamical situations and hydrological variables of the atmosphere occur (Menon *et al.*, 2002b; Ramanathan et al. 2001a; 2001b; 2005; Zhang, 2008). Fig. 5.2 displays one of the hydrological parameter (i.e., cloudiness) which is highly sensitive to the change in the net atmospheric heating rate. When aerosols induce NAHR reduction within the atmosphere which has higher relative humidity, the situation is more favourable for cloud formation (e.g., Ramanathan et al, 2001a). Thus, our results have shown that, throughout the seasons, the low-level CC (clouds which are formed below ~ 650 hPa) are enhanced in all areas of South Africa where the anthropogenic aerosols induced NAHR reductions. Accordingly, in the course of summer, consistent with the spatial distributions of NAHR reductions, the enhancement in low-level CC in the range from + 0.7 to +4.2 %, + 0.8 to +5.6 %, + 0.7 to +4.2 % and + 1 to +3.2 % are found in the case of sulfate, BC, OC and SBO, respectively. Similarly, during the austral winter season, over areas of South Africa that correspond to the anthropogenic aerosols cooling zones, CC enhancements which varies from + 0.2 to +1.9 %, + 0.4 to +1.5 %, + 0.35 to +1.1 % and + 0.6 to +2.5 % are found in the case of sulfate, BC, OC and SBO, respectively (see Fig. 5.2).

When the inclusion of anthropogenic aerosols trigger the enhancement of NAHR - depending on the region considered and its meteorological conditions - the overall CC response becomes more complex (e.g., Koch and del Genio 2010). For instance, during the presence of sulfate and OC aerosols, over areas that exhibit NAHR enhancement, ΔCC displayed values that varied from -0.7 to -3.6 % for sulfate (OC: -0.7 to -2.9 %) and -0.2 to -1.1 % for sulfate (OC: -0.35 to -1.8 %), in the course of the summer and austral winter, respectively (Fig. 5.2a and c). These CC responses are found to be quite consistent with the conventional description of the semi-direct effects of aerosols (e.g., Hansen et al. 1997; Ackerman *et al.*, 2000). Whereas, the NAHR enhancements, which are induced during the inclusion of BC and SBO aerosols are comparatively stronger and wider than the other anthropogenic aerosol species (Fig. 5.2b and d). In such case, different studies have shown that depend on various climatic factors the cloud response can be either positive or negative (e.g., Koch and del Genio 2010 and references therein). Such as, the vertical location of absorbing aerosols with respect to clouds (e.g., Johnson *et al.*, 2004; Feingold et al. 2005), the underlying surface properties (e.g., Allen and Sherwood, 2010), the moisture flux transport adjustments (e.g., Douville et al. 2002; Perlwitz and Miller, 2010; Zhang, 2008) and other issues are important here. Our results indicate that the BC and SBO aerosols are concentrated in the lower parts of the troposphere, thus their influence in enhancing NAHR may improve the instability of the atmosphere (e.g., Feingold et al. 2005; Zhang, 2008). This, accompanied by these complex climatic factors discussed so far, results an increment in low-level CC, around the central, north and eastern regions of South Africa which are the wet and semi-wet parts of the country (Fig. 5.2b and d). Attributed to the involvements of various local meteorological conditions, the distribution of BC (and SBO) aerosols caused NAHR and CC enhancements are slightly shifted in their spatial analogies, over these wet and semi-wet regions (see Fig. 5.1 and 5.2).

Unlike the above incidence, in and around the arid and semi-arid regions, in line with the spatial distributions of BC and SBO aerosols induce NAHR enhancement; the low-level fractional cloud cover exhibited a reduction (Fig. 5.2b and d). Overall, in agreement with the aforementioned studies, our results also highlighted that during the inclusion of BC and SBO aerosols, the CC response could be either positive or negative, not only governed by the NAHR effects of these aerosols, but also through a significant involvement of various regional scale climatic factors. Our results also show that the magnitude of ΔCC were quite significant during the wet season (summer) than that of the dry winter season (see Fig. 5.2). This put forward that the amplitude of anthropogenic aerosols' semi-direct influence-induced ΔCC, are not only reliant on the seasonal variations of aerosol burden level and its radiation perturbations; but are also highly dependent on seasonal availability of cloud and water vapour. We have noted that the signs and spatio-seasonal patterns of anthropogenic aerosols induced cloud liquid water path changes are generally analogous to those of the ΔCC (figures are not shown).

The annual mean regionally averaged ΔCC (i.e., averaged over the areas of South Africa: -35° – -22°S, 16° – 33°E) showed that the presence of anthropogenic aerosols slightly enhance the regional CC: by about +0.13% for sulfate, +0.21% for BC and +0.07% for SBO; except for OC aerosols which slightly reduce the regional CC by about -0.15%. The sign of these regionally averaged ΔCC are opposite to that of their corresponding ΔST (ΔSSHF) (see section 3.3.1). Furthermore, annually averaged spatial correlations between ΔST (ΔSSHF) with that of ΔCC are found to be -0.67 (-0.64) for sulfate, -0.78 (-0.77) for BC, -0.76 (-0.74) for OC and -0.56 (-0.53) for SBO. The above fairly consistent negative correlations confirm that the increases/decreases in CC are also accountable for the ST (and for SSHF) reductions/enhancements, by promoting the reduction/enhancement of solar flux reaching the surface. It is apparent that all the above alterations which are attributed by anthropogenic aerosols (i.e., changes that are described in section 3.3.1 and 3.3.2) have possible dynamical feedbacks (e.g., Jacobson and Kaufman 2006; Stanelle *et al.*, 2010; Solmon *et al.*, 2012; Zhang, 2008). This specific issue will be discussed in the following sub-section.

3.3.3 The effects of anthropogenic aerosols on planetary boundary layer, surface pressure and wind field

The seasonal mean spatial distribution of different anthropogenic aerosol species induced changes in planetary boundary layer height (ΔPBL), surface pressure (ΔSP) and 10m surface wind field ($\overrightarrow{\Delta W}$) are shown in Fig. 6. During summer, areas of South Africa that experience ST reduction due to the existence of anthropogenic aerosols (see section 3.3.1), also illustrate the PBL height reduction (and SP increments) which respectively varies from -5 to -20 m (+0.008 to +0.024 hPa) for sulfate, from -4 to -16 m (+0.01 to +0.03 hPa) for BC, from -5 to -20 m (+0.01 to +0.015 hPa) for OC and from -5 to -30 m (+0.008 to +0.024 hPa) for SBO (see Fig. 6). In contrast, in alignment with the regions of South Africa that display ST enhancements (see section 3.3.1), increase in PBL height (and reductions in SP) that respectively varies from +5 to +20 m (-0.008 to -0.04 hPa) for sulfate, from +4 to +24 m (-0.01 to -0.05 hPa) for BC, from +5 to +35 m (-0.01 to -0.08 hPa) for OC and from +5 to +20 m (-0.008 to -0.032 hPa) for SBO are found (Fig. 6). Similarly, during

© University of Pretoria

austral wintertime the enhancement of PBL height along with SP reduction, or vice versa results, are noted over the areas of South Africa which show ST increases/decreases (section 3.3.1), respectively.

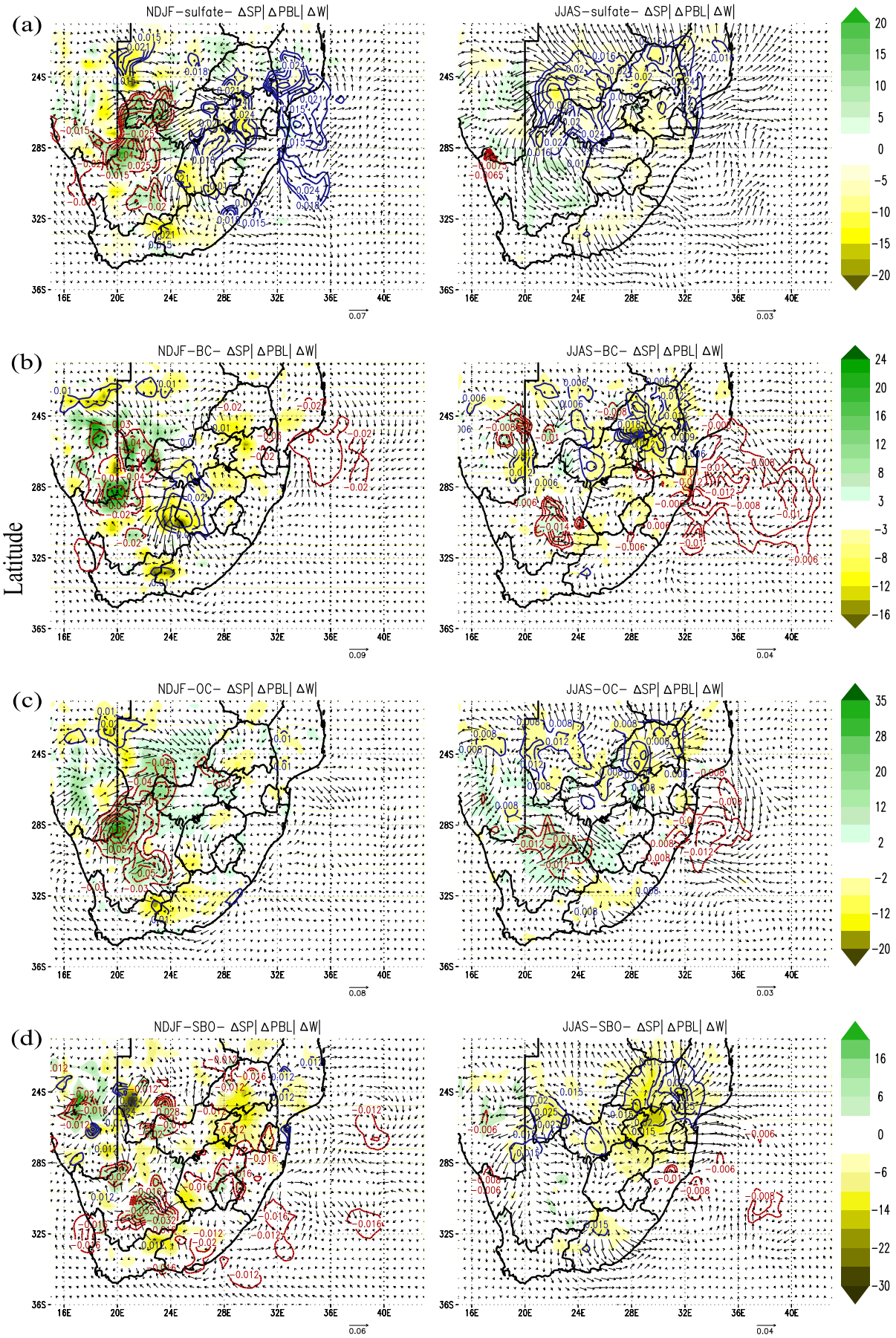

Fig. 6: Anthropogenic aerosols: row (a) sulfate, (b) BC, (c) OC and (d) SBO induced changes in PBL height (shaded; unit: m), SP (unfilled contour; unit: hPa) and 10m surface wind field- $\vec{W}$ (vector; the scale is indicated by the arrow to the lower right; unit: m/s). The results were averaged over 1998–2008. The first column represent summer; whereas, the second column represent austral winter.

It has also been found that in all cases (i.e., sulfate, BC, OC and SBO) the magnitudes of ΔPBL and ΔSP during the austral winter season are relatively smaller (by about ~ 35 to 62 %) than their corresponding summertime values (see Fig. 6). Annually averaged spatial correlations between ΔPBL (ΔSP) with that of ΔST are correspondingly found to be +0.9 (-0.7) for sulfate, +0.93 (-0.76) for BC, +0.94 (-0.8) for OC and +0.94 (-0.81) for SBO. Likewise, for all different types of anthropogenic aerosols the correlations among ΔPBL (ΔSP) with that of ΔSSHF are respectively within the range of +0.9 to +0.94 (-0.67 to -0.8); as well as the correlations among ΔPBL and ΔSP are ~ -0.82. In addition, in each cases, the ΔPBL (and ΔSP), respectively, display a negative (and positive) correlation that varies from 0.55 to 0.77 with that of anthropogenic aerosols induced cloud cover changes,

© University of Pretoria

which is one of the important cause for the ΔST and ΔSSHF (see section 3.3.1 and 3.3.2).

Previously reported studies (e.g., Yu *et al.,* 2002; Menon *et al.,* 2002b; Miller et al. 2004b; Jacobson and Kaufman 2006; Jiang and Feingold, 2006; Zhang, 2008) indicated that the aerosols-radiation-climate interactions induce ST and SSHF reductions/enhancements, would correspondingly result a weakening/strengthening of Convectively Driven Turbulence (CDT) and Surface Buoyancy Fluxes (SBF). Following these (i.e., the adjustments in CDT and SBF), a decreases/increases in PBL height may respectively occur. Furthermore, these CDT and SBF alterations also correspondingly improve/decline the stability of the lower troposphere; thus, they consequently promote the SP enhancement/reduction, respectively (e.g., Zhang, 2008; Yu *et al.,* 2002). The sign and higher level of correlations, which are found in our simulations, clearly reflect these successive circumstances and mechanisms which are predominantly responsible for the alteration of PBL height and SP (Fig. 6). A similar situation has been also noted in Zhang, 2008. Here we would like to remark that for all types of anthropogenic aerosols, the spatial correlations among ΔSP and ΔST (ΔSSHF) are found to be a bit smaller (by about ~ 20%) than that of ΔPBL. This suggests that, other than the ΔST (and ΔSSHF) induced CDT and SBF modifications, the influences of anthropogenic aerosols on regional circulation also have some contribution in tuning the SP (Jacobson and Kaufman 2006; Miller et al. 2004b; Zhang, 2008).

The wind vector in Fig. 6 shows the changes in surface wind fields, due to anthropogenic aerosols. The $\overrightarrow{\Delta W} = \Delta U + \Delta V$ are computed based on the respective differences in zonal (ΔU) and meridional (ΔV) wind components among Exp2 through Exp5 with that of the baseline simulation (Exp1). The $\overrightarrow{\Delta W}$ pointing to the eastern and northern direction indicates an increase in zonal and meridional wind components, respectively. However, those which point to the western and southern directions indicate the contrary. The results have illustrated that the presence of different anthropogenic aerosol species caused both a reduction and rise of surface wind speed, which are spatio-seasonally highly variable. In all cases (i.e., for sulfate, BC, OC and SBO; Fig. 6), the largest changes in both zonal and meridional wind components have been predicted during the course of the summer season. The maximum amplitudes of surface wind speed increment (and reduction) that are noted in summer are respectively ~ up to 0.072 m/s (0.071 m/s) for sulfate, 0.05 m/s (0.09 m/s) for BC, 0.08 m/s (0.05 m/s) for OC and 0.06 m/s (0.04 m/s) for SBO).

During summer, primarily in the North West and some parts of the Free State provinces, the inclusion of sulfate aerosols result in a reduction of both zonal and meridional components (Fig. 6a). In addition to these, during the presence of sulfate aerosols, the reduction of zonal wind has been also noted around Gauteng and Limpopo regions in conjunction with the decrease of meridional components over the eastern parts of the Eastern Cape Province. In contrast, across KwaZulu Natal and the Northern Cape (over some areas of the Eastern Cape Province), respectively, the enhancement of zonal (and meridional) wind components have been noted during this case (Fig. 6a). During the same period (summer), in the case of BC aerosols (Fig. 6b), over most areas of South Africa the zonal wind show a decline, except around the northern regions of the Northern Cape Province. Additionally, over the southern parts of the Free State, the meridional component exhibits a reduction, and in some areas of the Northern Cape and Limpopo provinces it shows an enhancement. During the enclosure of OC aerosols (Fig. 6c), over the North West, Free State as well as around the southern parts of the Northern Cape regions the zonal component display weakening. Besides these, in and around Gauteng, Limpopo and Free State areas, a reduction in the meridional wind has been noted. However, in the case of OC, the strengthening of both zonal and meridional components is also noted over most parts of the Northern Cape Province. Finally, during the inclusion of SBO (in the course of summertime), across Free State, North West and eastern parts of Limpopo (over the central regions of the Northern Cape and Limpopo Provinces) correspondingly the reduction (and enhancement) of zonal wind are observed. In addition, excluding some scattered areas in Mpumalanga and the Northern Cape Province, over most areas of South Africa, the meridional component display an enhancement (Fig. 6d).

The dynamical influences of anthropogenic aerosols during the austral winter season are different from that of the summertime (see Fig. 6). For instance, during the austral wintertime, apart from the Northern Cape and southern areas of the Eastern Cape where the meridional components are reduced, almost in all areas of South Africa, the presence of sulfate aerosols strengthen both zonal and meridional components (Fig. 6a). Similarly, during austral winter the inclusion of other anthropogenic aerosols also induce different spatial distributions of $\overrightarrow{\Delta W}$ than that of the summertime. In all cases, the amplitudes of $\overrightarrow{\Delta W}$ during the course of the austral winter are much weaker than that of summer season (i.e., during austral wintertime $|\overrightarrow{\Delta W}|$ were reduced by about 52% for sulfate, 45% BC, 58% for OC and 25% for SBO than their corresponding summertime values).

The dynamical effects of anthropogenic aerosols, in turn, influence the background aerosol concentrations (e.g., Yue *et al.,* 2010b). Such as, the $\overrightarrow{\Delta W}$ around the north and eastern parts of the country have some influence on anticyclonic dispersions of biomass burning aerosols, which are mostly emitted from these regions of South Africa (e.g., Magi *et al.,* 2009; Tesfaye *et al.,* 2011a; Tummon *et al.,* 2011. During the inclusion of sulfate, BC and predominantly OC aerosols (Fig. 6c), the changes of both zonal and meridional components in and around the Northern Cape regions may have some influence on desert dust emission and dispersion. As a result of these background aerosol concentration changes, the effects of anthropogenic aerosols on different meteorological fields are also noted in areas where their loadings are insignificant (see section 3.3.1 and 3.3.2). Depending on the magnitude of surface wind speed intensification (or decrease), the dynamical alterations will correspondingly suppress (or reinforce) the stabilization of the lower troposphere (e.g., Jacobson and Kaufman 2006; Zhang, 2008; Yu *et al.,* 2002). Therefore, the anthropogenic aerosols induce dynamical adjustments respectively become another factor that promote the reduction (or enhancement) of SP.

Here we would like to remark that - owing to the complexity of the non-linear feedback mechanisms of the climate system to the aerosol radiative influences - the physical reasons for the $\overrightarrow{\Delta W}$ in different spatial locations are very complicated (Jacobson and Kaufman 2006; Zhang, 2008). Thus, investigating the specific physical processes of the phenomenon has been left for our future research. Furthermore, though this study focused only on columnar changes, it is well known that their role in

© University of Pretoria

altering the atmospheric radiative heating rate may consequently promote various changes on different layers of the atmosphere (e.g., Dickerson *et al.,* 1997; Ott *et al.,* 2010; Johnson *et al.,* 2004; Koch and Genio, 2010). The impact of anthropogenic aerosols on vertical profile of the atmosphere and other related issues will be addressed in our future work.

4 Summary and conclusions

In this paper, we examined the regional scale mass distribution, direct and semi-direct influences of anthropogenically induced sulfate, Black Carbon (BC), Organic Carbon (OC) aerosols and all three together (SBO), over South Africa. The present contribution used the 12 year runs of Regional Climate Model (RegCM4) which is interactively coupled with anthropogenic-desert dust schemes. The simulations of this study employed recently updated particulate (aerosol precursor gases) emission inventories Tesfaye *et al.* (2013a). Considering aforementioned anthropogenic aerosols as an additional component to atmospheric aerosols, different climatic simulations were conducted and the last 11 years results were analysed and discussed in terms of two contrasting seasons: summer and austral winter. A summary and the main conclusions drawn from this study are presented as follows:

- Influenced by the anticyclonic air circulation, all anthropogenic aerosols which primarily originated from the Highveld zones of Gauteng and Mpumalanga provinces were distributed in the northern, central and eastern areas of South Africa. Enhanced air temperature and moist meteorological conditions of summertime offered beneficial circumstances for the secondary sulfate particle formations. Therefore, during this season the maximum column burdens of sulfate (up to 10 mg/m^2) and SBO (12.5 mg/m^2) were observed. The seasonal variations of carbonaceous aerosols were less important when compared with that of the sulfate particles. The annual mean regional averaged total anthropogenic aerosol burden (averaged over the areas of South Africa) was ~ 3.5 mg/m^2 - with the sulfate, BC and OC aerosols accounting for ~ 72%, ~ 10% and ~ 18% of the burden, respectively.

- Both absorbing and scattering components of anthropogenic aerosols lead to a reduction of net solar radiation at the surface (i.e., all anthropogenic aerosols caused negative Surface Radiative Forcing (SRF)). The maximal influence of SRF, up to -12 W/m^2 for sulfate and -14 W/m^2 for SBO during summertime, as well as -2 W/m^2 for BC and -0.68 W/m^2 for OC during austral wintertime, were noted nearby their source regions. In contrast to sulfate aerosols, the atmospheric radiative forcing of BC, OC and SBO illustrate that the Short-Wave (SW) absorption primarily by BC and slightly via OC particles caused the reduction of SW radiation flux at the surface, by enhancing the radiative heating within the atmospheric column.

- In most cases, due to the presence of radiatively interactive anthropogenic aerosols, the northern, central and eastern areas of South Africa experienced Surface Temperature (ST: -0.05 K to -0.36 K) and Sensible Heat Flux (SSHF: -0.5 to -4.2 W/m^2) reductions. Except during the inclusion of OC particles, slight enhancements of ST (and SSHF) were observed around Gauteng. Over the west areas of South Africa, the enclosure of different anthropogenic aerosols induced ST (and SSHF) enhancement which were within a range of +0.05 K to +0.35 K (+0.5 to +4.8 W/m^2), respectively.

- The primary physical processes which were accountable for these ST (and SSHF) changes were: the anthropogenic aerosol direct radiative forcings and their semi-direct effects induced Cloud Cover (CC) change. In addition to these, the climatic feedbacks of anthropogenic aerosols also induced the change in background aerosol concentrations. This, in turn, produced local atmospheric thermal structure adjustments and consequently cloudiness alterations. These physical process were another important cause for the ΔST (and ΔSSHF), especially over areas of South Africa which were away from the anthropogenic aerosol loading zones, such as across Northern Cape arid/semi-arid regions.

- Largely, across Mpumalanga, Limpopo, Free State and the Eastern Cape provinces, the annual mean low-level (below ~ 650 hPa) columnar average Net Atmospheric radiative Heating Rate changes (ΔNAHR)showed values that varied from -0.05 to -0.3 K/day for sulfate and -0.04 to -0.2 K/day for OC. Whereas, around the Northern Cape Province as well as over the coastal areas of KwaZulu-Natal (for the case of OC) the annual mean ΔNAHR showed values that varied from +0.05 to +0.2 K/day for sulfate and +0.04 to +0.2 K/day for OC. Excluding some narrow scattered areas of the Northern Cape Province which showed insignificant negative values of ΔNAHR, overall, the inclusion of BC (and SBO) aerosols predominantly induced the enhancement of ΔNAHR that correspondingly varied from +0.03 to +0.3 K/day (+0.05 to +0.31 K/day).

- In all cases, aligned with the spatial distribution of NAHR reductions, the annual mean low-level column integrated cloud cover change (ΔCC) showed an enhancement that varied from +0.2 to +3.5 %, +0.4 to +3.1 %, +0.3 to +2.7 % and +0.5 to +2.9 %; for sulfate, BC, OC and SBO, respectively. In the case of sulfate and OC aerosols, areas that displayed NAHR improvements also showed a reduction in CC, that varied from -0.2 to -2.2 % for sulfate and -0.3 to -2.5 for OC. Whereas in the case of BC and SBO aerosols, the NAHR enhancement associated with other regional climatic factors caused dual influences: over the wet and semi-wet parts of the country it resulted in the strengthening of CC. While, around the arid/semi-arid regions it weakened the CC. Overall, our results showed that the magnitudes and even in some cases the sign of CC responses, were not only dependent on anthropogenic aerosols induced ΔNAHR, but was also greatly reliant on local meteorological situations of the background atmosphere.

- In-line with the spatial patterns of ST (SSHF) reductions, the Boundary Layer height (ΔBL) and Surface Pressure (ΔSP) changes respectively showed decreases and increases. Similarly, in all cases, along with the spatial distributions of ST (SSHF) enhancements, the ΔBL and ΔSP showed increases and decreases, respectively. Overall, the spatial correlations of ΔST (ΔSSHF) with that of ΔPBL were within a range of +0.9 to +0.94 as well as with ΔSP were within a range of -0.67 to -0.81. Additionally, the magnitudes of the spatial correlation among both of ΔPBL and ΔSP with that of ΔCC were within a range of 0.55 to 0.77. These correlations reflected that the anthropogenic aerosols' direct and semi-direct effects induced ΔST and ΔSSHF were cooperatively played a major role in promoting the change in BL plus SP; via modulating a weakening/strengthening of convectively driven turbulence and surface buoyancy fluxes.

© University of Pretoria

UNIVERSITEIT VAN PRETORIA
UNIVERSITY OF PRETORIA
YUNIBESITHI YA PRETORIA

- The presence of radiatively interactive anthropogenic aerosols also caused both a reduction and rise of surface wind speed, which were geographically and seasonally highly variable. The annual mean surface wind speed increase (decrease) respectively showed ~ up to 0.025 m/s (0.015 m/s) for sulfate, 0.025 m/s (0.025 m/s) for BC, 0.03 m/s (0.025 m/s) for OC and 0.03 m/s (0.025 m/s) for SBO. Both zonal and meridional wind changes, depending on their magnitudes and regional conditions, suppress (or reinforce) the anti-cyclonic surface air circulation and the background aerosol burden level.
- The spatial correlations of anthropogenic aerosols induce ΔCC with other climatic variable changes mirror the far-reaching role of the nonlinear feedback of cloud fields in the climate system.
- Even if we have used the external mixture assumption, our results have shown that the climatic influences of each anthropogenic aerosol components (i.e., sulfate, BC and OC) were somewhat different from their combined effects (i.e., SBO). This indicates that one cannot simply sum-up the individual aerosol climatic effects to predict the overall influences of multiple aerosols.
- Lastly, we would like to remark that addressing the interactions and feedbacks among anthropogenic aerosols, radiation and climatic fields - by involving: other species of anthropogenic aerosols, their indirect effects and heterogeneous reactions, were left as the subject of our future research.

Acknowledgements

The authors are grateful to Addis Ababa University, Department of Physics, for providing computational facilities. For the accessibility of RegCM model the authors are thankful to the International Centre for Theoretical Physics (ICTP). We are also indebted to Teresa Faleschini, Tamene Mekonnen, Fiona Tummon and Addisu Gezahegn, for their valuable assistances. This work was supported by African Laser Centre and NRF bi-lateral research grant (UID: 68688/65086), in addition to CSIR National Laser Centre.

References

Ackerman, A. S. et al. (2000). Reduction of tropical cloudiness by soot, Science, 288, 1042–1047.

Adams, P. J. et al. (2001). General circulation model assessment of direct radiative forcing by the sulfate-nitrate-ammonium-water inorganic aerosol system, J. Geophys. Res., 106, 1097–1111.

Allen, R. J., and Sherwood, S. C. (2010). Aerosol-cloud semi-direct effect and land-sea temperature contrast in a GCM, Geophys. Res. Lett., 37, L07702, doi:10.1029/2010GL042759.

Andreae, M. O., and Gelencser, A. (2006). Black carbon or brown carbon? The nature of light-absorbing carbonaceous aerosols, Atmos. Chem. Phys., 6, 3131 – 3148.

Baede, A. et al. (2001). The climate system: an overview. In: IPCC Report 2001 (eds Houghton JT, Ding Y, Griggs DJ et al.), pp. 87–98. Cambridge University Press, Cambridge, UK and New York, NY, USA.

Boer, G.J. (1993). Climate change and the regulation of the surface moisture and energy budgets. Clim Dyn 8:225–239, doi: 10.1007/BF00198617.

Bond T. C. et al. (2013). Bounding the role of black carbon in the climate system: A scientific assessment, J. Geophys. Res., doi: 10.1002/jgrd.50171.

Bond, T. C. (2001). Spectral dependence of visible light absorption by carbonaceous particles emitted from coal combustion, Geophys. Res. Lett., 28, 1075 – 4078.

Cook, J. and Highwood, E. J. (2004). Climate response to tropospheric absorbing aerosols in an intermediate general-circulation model. Q.J.R. Meteorol. Soc., 130: 175–191. doi: 10.1256/qj.03.64.

Cooke, W.F., and Wilson, J.J.N. (1996). A global black carbon aerosol model. J. Geophys. Res. 101. 19,395-19,409.

Cooke, W.F. et al. (1999). Construction of a 1x1 fossil fuel emission data set for carbonaceous aerosol and implementation and radiative impact in the ECHAM4 model. J. Geophys. Res. 104. 22137-22162.

Denman, K. L. et al. (2007). Couplings Between Changes in the Climate System and Biogeochemistry. In: Climate Change 2007: The Physical Science Basis. Contribution of Working Group I to the Fourth Assessment Report of the Intergovernmental Panel on Climate Change [Solomon, S. et al. (eds.)]. Cambridge University Press, Cambridge, United Kingdom and New York, NY, USA.

Dickerson, R. R. et al. (1997). The impact of aerosols on solar ultraviolet radiation and photochemical smog, Science, V. 278, 827-830.

Douville, H. et al. (2002). Sensitivity of the hydrological cycle to increasing amounts of greenhouse gases and aerosols. Climate Dynamics 20, 45–68.

Eck, T. F., et al. (2003), Variability of biomass burning aerosol optical characteristics in southern Africa during the SAFARI 2000 dry season campaign and a comparison of single scattering albedo estimates from radiometric measurements, J. Geophys. Res., 108(D13), 8477, doi:10.1029/2002JD002321.

Eskom, (1996). Effects of atmospheric pollution on the Mpumalanga Highveld. Power Technology No. 70. Eskom Technology Group, Cleveland.

Fan, J. et al. (2008). Effects of aerosol optical properties on deep convective clouds and radiative forcing, J. Geophys. Res., 113(D8), D08209, doi:10.1029/2007JD009257.

Feingold, G. et al. (2005). On smoke suppression of clouds in Amazonia, Geophys. Res. Lett., 32, L02804, doi:10.1029/2004GL021369.

Flanner, M. G. et al. (2007). Present day climate forcing and response from black carbon in snow, J. Geophys. Res., 112, D11202, doi:10.1029/2006JD008003.

Flanner, M. G. et al. (2009). Springtime warming and reduced snow cover from carbonaceous particles, Atmos. Chem. Phys., 9, 2481-2497.

Forster, P. et al. (2007). Changes in Atmospheric Constituents and in Radiative Forcing. In: Climate Change 2007: The Physical Science Basis. Contribution of Working Group I to the Fourth Assessment Report of the Intergovernmental Panel on Climate Change [Solomon, S. et al. (eds.)]. Camb. Univ. Press, Camb., United Kingdom and New York, NY, USA.

Freiman, M. T., and Piketh, S. J. (2003). Air transport into and out of the industrial Highveld region of South Africa, J. Appl. Meteorol., 42, 994–1002, doi:10.1175/1520-0450(2003)042<0994:ATIAOO>2.0.CO2.

Freiman, M.T. et al. (2002). The state of the atmosphere over South Africa during the Southern African Regional Science Inititatve (SAFARI 2000). S. Afr. J. Sci. 98. 91-96.

Fuzzi, S. et al. (2006). Critical assessment of the current state of scientific knowledge, terminology, and research needs concerning the role of organic aerosols in the atmosphere, climate, and global change. Atmos. Chem. Phys., 6, 2017-2038.

Ganzeveld, L. et al. (1998). A dry deposition parameterization for sulfur oxides in a chemistry and general circulation model. J. Geophys. Res. 103. 5679–5694.

Gao, X.J. et al. (2006). Projected changes in mean and extreme precipitation over the Mediterranean region from high resolution double nested RCM simulations. Geophysical Research Letters, 33, L03706, doi:10.1029/2005GL024954.

Gao, X.J. et al. (2008). Reduction of future monsoon precipitation over China: comparison between a high resolution RCM simulation and the driving GCM. Meteorol. Atmos. Phys. 100, 73e86.

Ghan, S.J. and Schwartz, S.E. (2007). Aerosol properties and processes: a path from field and laboratory measurements to global climate models. Bull. Am. Meteorol. Soc. 88: 1059−1083.

© University of Pretoria

Giorgi, F. (1995). Perspectives for regional earth system modelling. Global Planet. Change 10: 23-42.

Giorgi, F. et al. (2003). Indirect vs. direct effects of anthropogenic sulfate on the climate of east Asia as simulated with a regional coupled climate-chemistry/aerosol model. Climatic Change, 58, 345-376.

Giorgi, F. et al. (2002). Direct radiative forcing and regional climatic effects of anthropogenic aerosols over East Asia: A regional coupled climate-chemistry/aerosol model study. J. Geophys. Res., 107, 4439, doi:10.1029/2001JD001066.

Giorgi, F. et al. (2012). RegCM4: model description and preliminary tests over multiple CORDEX domains. Clim. Res., 52, 7–29, doi:10.3354/cr01018, 2012. 8474, 8481.

Han, Z. W. (2010). Direct radiative effect of aerosols over East Asia with a Regional coupled Climate/Chemistry model, Meteor. Z., 19(3), 287–298.

Hansen, J. and Nazarenko, L. (2004). Soot climate forcing via snow and ice albedos, Proc. Nat. Acad. Sci. USA, 101, 423–428.

Hansen, J. et al. (1997). Radiative forcing and climate response, J. Geophys. Res., 102(D6), 6831–6864, doi:10.1029/96JD03436.

Haywood, J. and Boucher, O. (2000). Estimates of the direct and indirect radiative forcing due to tropospheric aerosols: a review, Rev. Geophys., 38(4), 513–543.

Haywood, J. M. et al. (1997). A limited-area model case study of the effects of subgrid scale variations in relative humidity and cloud upon the direct radiative forcing of sulfate aerosol. Geophys. Res. Lett., 24, 143–146.

Huang, Y. et al. (2007). Direct and indirect effects of anthropogenic aerosols on regional precipitation over East Asia. J Geophys Res 112:D03212. doi:03210.01029/02006JD007114.

Huang, Y. et al. (2006). Impact of aerosol indirect effect on surface temperature over East Asia. Proc. Nat. Acad. Sci., United States of America, 103(12), 4371-4376.

IPCC, (2007). Climate Change 2007: The Physical Science Basis. Contribution of Working Group I to the Fourth Assessment Report of the Intergovernmental Panel on Climate Change [Solomon, S. et al. (eds.)]. Camb. Univ. Press, Camb., UK and NY, USA, 996 pp.

Jacobson, M. Z. (2001a). GATOR-GCMM: A global- through urban-scale air pollution and weather forecast model: 1. Model design and treatment of subgrid soil, vegetation, roads, rooftops, water, sea ice, and snow, J. Geophys. Res., 106(D6), 5385–5401, doi:10.1029/2000JD900560.

Jacobson, M. Z. (2001b), Global direct radiative forcing due to multi-component anthropogenic and natural aerosols, J. Geophys. Res., 106(D2), 1551–1568, doi:10.1029/2000JD900514.

Jacobson, M. Z. (2001c). Strong radiative heating due to the mixing state of black carbon in atmospheric aerosols, Nature, 409(6821), 695–697, doi:10.1038/35055518.

Jacobson, M. Z. (2006). Effects of externally through-internally mixed soot inclusions within clouds and precipitation on global climate, J. Phys. Chem. A, 110(21), 6860–6873, doi:10.1021/jp056391r.

Jacobson, M. Z., and Kaufman, Y. J. (2006). Wind reduction by aerosol particles, Geophys. Res. Lett., 33, L24814, doi:10.1029/2006GL027838.

Jacobson, M. Z. (2004). Climate response of fossil fuel and biofuel soot, accounting for soot's feedback to snow and sea ice albedo and emissivity, J. Geophys. Res., 109, D21201, doi:10.1029/2004JD004945.

Jacobson, M. Z. (2002). Control of fossil-fuel particulate black carbon and organic matter, possibly the most effective method of slowing global warming, J. Geophys. Res., 107, 4410, doi:10.1029/2001JD001 376.

Jacobson, M. Z. (2010). Short-term effects of controlling fossil-fuel soot, biofuel soot and gases, and methane on climate, Arctic ice, and air pollution health, J. Geophys. Res., 115(D14), D14209, doi:10.1029/2009JD013795.

Jiang, H., and Feingold, G. (2006). Effect of aerosol on warm convective clouds: Aerosol-cloud-surface flux feedbacks in a new coupled large eddy model, J. Geophys. Res., 111, D01202, doi:10.1029/2005JD006138.

Johnson, B. T. et al. (2004). The semi-direct aerosol effect: Impact of absorbing aerosols on marine stratocumulus, Quat. J. Roy. Meteor. Soc., 130(599), 1407–1422, doi:10.1256/qj.03.61.

Kiehl, J.T. and Rodhe, H. (1995). Modelling geographical and seasonal forcing due to aerosols. In: Aerosol Forcing of Climate [Charlson, R.J. and J. Heintzenberg (eds.)]. J. Wiley and Sons Ltd, pp. 281-296.

Kiehl, J.T. et al. (2000). Radiative forcing due to sulfate aerosols from simulations with the National Center for Atmospheric Research Community Climate Model, Version 3. J. Geophys. Res., 105, 1441-1457.

Koch, D., and Genio, A. D. (2010). Black carbon semi-direct effects on cloud cover: review and synthesis, Atmos. Chem. Phys., 10, 7685-7696, doi:10.5194/acp-10-7685-2010.

Kumar, S., and Devara, P.C.S (2012). A long-term study of aerosol modulation of atmospheric and surface solar heating over Pune, India: Tellus B 2012, 64, 18420, http://dx.doi.org/10.3402/tellusb.v64i0.18420.

Li, S. et al. (2009). Indirect radiative forcing and climatic effect of the anthropogenic nitrate aerosol on regional climate of China. Advances in Atmospheric Sciences, 26(3), 543-552.

Liu, X. H. et al. (2005). Global modeling of aerosol dynamics: Model description, evaluation, and interactions between sulfate and nonsulfate aerosols, J. Geophys. Res., 110(D18), D18206, doi:10.1029/2004JD005674.

Lohmann, U. and Feichter, J. (2001). Can the direct and semi-direct aerosol effect compete with the indirect effect on a global scale?, Geophys. Res. Lett., 28, 159–161.

Magi, B. I et al. (2009). Evaluation of tropical and extratropical Southern Hemisphere African aerosol properties simulated by a climate model, J. Geophys. Res., 114, D14204, doi:10.1029/2008JD011128.

Magi, B. I. (2009). Chemical apportionment of Southern African aerosol mass and optical depth, Atmos. Chem. Phys. 9, 7643–7655.

Mallet, M. et al. (2009). Impact of dust aerosols on the radiative budget, surface heat fluxes, heating rate profiles and convective activity over West Africa during March 2006. Atmos. Chem. Phys. 9:7143−7160.

Markowicz, K. M. et al. (2003). Influence of relative humidity on aerosol radiative forcing: An ACE-Asia experiment perspective, J. Geophys. Res., 108, 8662, doi:10.1029/2002JD003066, D23.

Menon, S. et al. (2002a). GCM simulations of the Aerosol Indirect Effect: Sensitivity to Cloud Parameterization and Aerosol Burden. J. Atmos. Sci., 59, 692-713.

Menon, S. et al. (2002b). Climate effects of black carbon aerosols in China and India, Science, 297, 2250 – 2253.

Miller, R. L.et al. (2004a). Surface radiative forcing by soil dust aerosols and the hydrologic cycle. J Geophys Res 109:D04203. doi:10.1029/2003JD004085.

Miller, R. L. and Tegen, I. (1998). Climate response to soil dust aerosols. J. Climate 11, 3247–3267.

Miller, R. L. et al. (2004b). Feedback upon dust emission by dust radiative forcing through the planetary boundary layer, J. Geophys. Res., 109, D24209, doi:10.1029/2004JD004912.

Mills, A. J. et al. (2012). Aerosol capture by small trees in savannas marginal to treeless grassland in South Africa. Geoderma. doi: 10.1016/j.geoderma.2012.05.006.

Mitchell, J. F. B. and Johns, T. C. (1997). On modification of global warming by sulfate aerosols. J. Clim, 10, 245–267.

Myhre, C. E. L. and Nielsen, C. J. (2004). Optical properties in the UV and visible spectral region of organic acids relevant to tropospheric aerosols, Atmos. Chem. Phys., 4, 1759–1769.

Ott, L. et al. (2010). Influence of the 2006 Indonesian biomass burning aerosols on tropical dynamics studied with the GEOS-5 AGCM, J. Geophys. Res., 115, D14121, doi:10.1029/2009JD013181.

Penner, J. E. et al. (2001). Aerosols, their Direct and Indirect Effects, in: Climate Change 2001: The Scientific Basis, edited by: Houghton, J. T. et al. Report to IPCC from the Scientific Assessment Working Group (I), Camb. Univ. Press, 289–416.

Perlwitz, J. and Miller, R. L. (2010). Cloud cover increase with increasing aerosol absorptivity: A counter example to the conventional

© University of Pretoria

semidirect aerosol effect, J. Geophys. Res., 115, D08203, doi:10.1029/2009JD012637.

Pilinis, C. et al. (1995). Sensitivity of direct climate forcing by atmospheric aerosols to aerosol size and composition. Journal of Geophysical Research, 100, D9, 18739-18754.

Posselt, R. and Lohmann, U. (2008). Influence of Giant CCN on warm rain processes in the ECHAM5 GCM, Atmos. Chem. Phys., 8, 3769-3788, doi:10.5194/acp-8-3769-2008.

Qian, Y., and Giorgi, F. (1999). Interactive coupling of regional climate and sulfate aerosol models over eastern Asia, J. Geophys. Res., 104(D6), 6477–6499, doi:10.1029/98JD02347.

Qian, Y. et al. (2001). Regional simulation of anthropogenic sulfur over East Asia and its sensitivity to model parameters. Tellus. 53B. 171-191.

Queface, A. J. et al. (2011), Climatology of aerosol optical properties in southern Africa, Atmos. Environ., 45, 2910–2921, doi:10.1016/j. atmosenv.2011.01.056.

Ramanathan, V., Carmichael, G. (2008). Global and regional climate changes due to black carbon. Nat Geosci 1:221–227.

Ramanathan, V. et al. (2005). Atmospheric brown clouds: impact on South Asian climate and hydrologic cycle. Proc. Nat. Acad. Sci. USA 102:5326–5333. doi:10.1073/pnas.0500656102.

Ramanathan, V., and Ramana, M. V. (2005). Persistent, widespread, and strongly absorbing haze over the Himalayan foothills and the Indo-Gangetic Plains. Pure Appl. Geophys., 162, 1609–1626, ,doi 10.1007/s00024-005-2685-8.

Ramanathan, V. et al. (2001a). Aerosol, climate, and hydrological cycle. Science 294, 2119-2124.

Ramanathan, V. et al. (2001b). Indian ocean experiment: an integrated analysis of the climate forcing and effects of the great Indo-Asian haze. Journal of Geophysical Research 106, 28371-28398.

Reid, J. S. et al. (1999). Use of the Angstrom exponent to estimate the variability of optical and physical properties of ageing smoke particles in Brazil, J. Geophys. Res., 104, 27473–27489.

Roeckner, E. et al. (1999). Transient climate change simulations with a coupled atmosphere-ocean GCM including the tropospheric sulfur cycle. J. Clim., 12, 3004–3032.

Roeckner, E. et al. (2006). Impact of carbonaceous aerosol emissions on regional climate change, Clim. Dynamics, 27, 552–571.

Roelofs, G. J. et al. (2001). Analysis of regional budgets of sulfur species modeled for the COSAM exercise. Tellus Ser. B, 53(5), 673 – 694.

Rosenfeld, D., and Woodley, W. (2001). Pollution and clouds, Phys. World, 14, 33 – 37.

Scheifinger, H., Held, G. (1997). Aerosol behaviour on the South African Highveld. Atmospheric Environment 31, 3497–3509.

Schulz, M. et al. (2006). Radiative forcing by aerosols as derived from the AeroCom present-day and pre-industrial simulations. Atmos. Chem. Phys., 6, 5225-5246, doi:10.5194/acp-6-5225-2006.

Seinfeld, J.H. and Pandis, S.N. (2006). Atmospheric chemistry and physics: from air pollution to climate. Wiley. New York.

Shell, K. M., and Somerville, R. C. J. (2007). Direct radiative effect of mineral dust and volcanic aerosols in a simple aerosol climate model. J. Geophys. Res., 112, D03206, doi: 03210.01029/02006JD007198.

Shindell, D.T. et al. (2008a). Multi-model projections of climate change from short-lived emissions due to human activities. J. Geophys. Res., 113, D11109, doi:10.1029/2007JD009152.

Shindell, D.T. et al. (2008b). A multi-model assessment of pollution transport to the Arctic. Atmos. Chem. Phys., 8, 5353-5372, doi:10.5194/acp-8-5353-2008.

Slingo, A. et al. (2006). Observations of the impact of a major Saharan dust storm on the atmospheric radiation balance, Geophys. Res. Lett., 33, L24817, doi:10.1029/2006GL027869.

Solmon, F. et al. (2012). Radiative and climatic effects of dust over West Africa, as simulated by a regional climate model, Clim. Res., 52, 97–113, doi:10.3354/cr01039.

Solmon, F. et al. (2006). Development of a regional anthropogenic aerosol model for climate studies: Application and validation over a European/African domain. Tellus B, 58, 51-72.

Spalding-Fecher, R., Matibe, D.K., (2003). Electricity and externalities. Energy Policy 31, 721–734.

Stanelle, T. et al. (2010). Feedback between dust particles and atmospheric processes over West Africa during dust episodes in March 2006 and June 2007. Atmos Chem Phys 10: 10771−10788.

Stier, P. et al. (2007). Aerosol absorption and radiative forcing, Atmos. Chem. Phys., 7, 5237–5261.

Tesfaye, M. et al. (2010). Latitudinal Variations of Aerosol Optical Parameters over South Africa Based on MISR Satellite Data; 26th Annual conference of South African society for atmosphere science, ISBN 978 0 620 47333 0, South Africa, 20-22 September 2010, Pg,105-106.

Tesfaye, M. et al. (2011a). Aerosol climatology over South Africa based on 10 years of Multiangle Imaging Spectroradiometer (MISR) data, J. Geophys. Res., 116, D20216, doi:10.1029/2011JD016023.

Tesfaye, M. et al. (2011b). Effective Single Scattering Albedo Estimation using Regional Climate Model. In: South African Society for Atmospheric Sciences 27th Annual Conference 22 - 23 September 2011: The Interdependent Atmosphere, Land and Ocean, Pp 53-54.

Tesfaye, M. et al. (2013a). Evaluation of Regional Climatic Model Simulated Aerosol Optical Properties over South Africa Using Ground-Based and Satellite Observations, ISRN Atmospheric Sciences, vol. 2013, Article ID 237483, 17 pages, 2013. doi:10.1155/2013/237483.

Tummon, F. (2011). Direct and semi-direct aerosol effects on the southern African regional climate during the austral winter season: PhD thesis. University of Cape Town, South Africa.

Tummon, F. et al. (2010). Simulation of the direct and semi-direct aerosol effects on the southern Africa regional climate during the biomass burning season, J. Geophys. Res., 115(D19), doi:10.1029/2009JD013738.

Wang, T. J. et al. (2003). Seasonal variations of anthropogenic sulfate aerosol and direct radiative forcing over China. Meteorology and Atmospheric Physics, 84, 185-198.

Wells, R.B. et al. (1996). National air pollution source inventory - Inventory of scheduled processes, [Held, G. et al. (eds)], Air pollution and its impacts on the South African Highveld, Environ. Sci. Assoc., Cleveland.

Wu, J. et al. (2008). Simulation of direct effects of black carbon aerosol on temperature and hydrological cycle in Asia by a Regional Climate Model. Meteorol. Atmos. Phys., 100, 179-193.

Yu, H. et al. (2002). Radiative effects of aerosols on the evolution of the atmospheric boundary layer, J. Geophys. Res., 107(D12), 4142, doi:10.1029/2001JD000754.

Yue, X. et al. (2010a). Direct climatic effect of dust aerosol in the NCAR Community Atmosphere Model Version 3 (CAM3). Adv. Atmos. Sci., 27(2), 230–242, doi:10.1007/s00376-009-8170-z.

Yue, X. et al. (2010b). Simulation of dust aerosol radiative feedback using the GMOD: 2. Dust-climate interactions, J. Geophys. Res., 115, D04201, doi:10.1029/2009JD012063.

Zanis, P. (2009). A study on the direct effect of anthropogenic aerosols on near surface temperature over Southeastern Europe during summer 2000 based on regional climate modeling, Ann. Geophys., 27, 3977-3988.

Zhang, J., and Yin, Y. (2008). Numerical simulations of effect of black carbon aerosol on regional climate in China, J. Nanjing Institute Meteor. (in Chinese), 31(6), 852–859.

Zhang, Y. (2008). The Radiative Effect Of Aerosols From Biomass Burning On The Transition From Dry To Wet Season Over The Amazon As Tested By A Regional Climate Model: PhD thesis. Georgia Institute of Technology, United State.

Zhou, T., and Yu, R. C. (2006). Twentieth-century surface air temperature over China and the Globe simulated by coupled climate models, J. Climate, 19, 5843–5858.

© University of Pretoria

Chapter 6: Simulation of biomass burning aerosols mass distributions and their direct and semi-direct effects over South Africa using a regional climate model *

*This chapter needs to be cited as:

Tesfaye, M., J. Botai, V. Sivakumar and G. Mengistu Tsidu (2013d): "Simulation of biomass burning aerosols mass distributions and their direct and semi-direct effects over South Africa using a regional climate model", *J. Meteorol. Atmos. Phys., in review*.

© University of Pretoria

UNIVERSITEIT VAN PRETORIA
UNIVERSITY OF PRETORIA
YUNIBESITHI YA PRETORIA

Simulation of biomass burning aerosols mass distributions and their direct and semi-direct effects over South Africa using a regional climate model

M. Tesfaye[1,2*], J. Botai[1], V. Sivakumar[1,3], G. Mengistu Tsidu[4]

Abstract: In this study, we examine the mass distributions, direct and semi-direct effects of different Biomass Burning Aerosols (BBAs) over South Africa using the 12 year runs of the Regional Climate Model (RegCM4). The results were analyzed and presented for the main BB season (July to October). The results show that Mpumalanga, KwaZulu Natal and the eastern parts of Limpopo are the main local source areas of BBAs in South Africa. In comparison to carbonaceous aerosols, BB induced sulfate aerosol mass loading and climatic effects were found to be negligible. All carbonaceous aerosols reduce solar radiation at the surface by enhancing local atmospheric radiative heating. The climatic feedback caused by BBAs, resulted changes in background aerosol concentrations. Thus, on a regional scale, climatic effects of BBAs were also found in areas far away from the BBA loading zones. The feedback mechanisms of the climate system to the aerosol radiative effects, resulted both positive and negative changes to the low-level columnar averaged Net Atmospheric radiative Heating Rate (NAHR). Areas which experienced a NAHR reduction showed an increase in Cloud Cover (CC). During the NAHR enhancement, CC over arid areas decreased; whereas CC over the wet/semi-wet regions increased. The changes in Surface Temperature (ST) and surface sensible heat flux are more closely correlated with BBA semi-direct effects induced CC alteration than their direct radiative forcing. Furthermore, decreases (or increases) in ST respectively lead to the reductions (and enhancements) in boundary layer height and the vice versa on surface pressure. The direct and semi-direct effects of BBAs also jointly promoted a reduction and rise in surface wind speed which was spatially highly variable. Overall, the results suggest that the CC response to changes in BBA-induced NAHR is important in determining changes in other climatic variables.

[1]*Department of Geography, Geoinformatics and Meteorology, University of Pretoria, Pretoria 0002, South Africa*

[2]*National Laser Centre, Council for Scientific and Industrial Research, Pretoria 0001, South Africa*

[3]*Department of Physics, Addis Ababa University, Addis Ababa, Ethiopia*

[4]*School of physics, University of KwaZulu Natal, Durban 4000, South Africa*

**Correspondence to: M. Tesfaye: mela_20062@yahoo.com*

Keywords: Biomass burning aerosols; Aerosol-climate interactions; Direct radiative forcing; Semi-direct effects; RegCM4; South Africa

1 Introduction

Both regionally and globally, biomass burning (BB) resulting from natural and anthropogenic fires, has been identified as an important source of atmospheric trace gases and a mixture of aerosols (e.g., Sinha et al., 2003; Andreae and Merlet, 2001; Lamarque et al., 2010). In particular, open BB activities, such as deforestation and crop residue burnings are major sources of carbonaceous aerosols (e.g., Andreae and Merlet, 2001). The most important and distinct property of BB activity is that their occurrence is strongly dependent on the seasons as well as numerous BB triggering processes, thus, exhibiting substantial temporal and geographical variability (e.g., Liousse et al., 2004; Roberts et al., 2009). For instance, the main BB months in the southern hemisphere are between June and October, which is the dry season of this hemisphere; while, in the northern hemisphere it falls between December and April (e.g., Duncan et al., 2003; Torres et al., 2010). Moreover, within the same hemispherical region, BB activities show a disparity in their temporal occurrences; such as in the extra-tropical regions of southern Africa, intense BB activities occurred during spring (August to October), whereas in the tropical regions of Southern Africa, the peak BB activities began early (i.e., during June) (e.g., Roberts et al., 2009; Magi et al., 2009; Tesfaye et al., 2011a, 2011b).

The type and amount of trace gases/aerosols emitted from BB activities are determined by several factors including: the nature, burning phases and combustion efficiency of the specific biomass/vegetation as well as numerous climatic factors of the region (e.g., Cooke et al., 1999; Barbosa et al., 1999; Sinha et al., 2003; Liousse et al., 2010; van der Werf et al., 2010). The quantification of BB emissions is supported mainly by different ground-based measurements and active fire/environmental products of earth observation satellites (e.g., Reid et al., 2004, 2009; Roberts et al., 2005; van der Werf et al., 2006, 2010; Zhang et al., 2012 and references therein). The space born systems characterize the active fires spectral signatures based on the thermal emissions of the fires, burnt area surface albedo and spectral reflectance changes as well as other parameterizations (e.g., Fraser et al., 2000; Giglio et al., 2009 and references therein).

Aerosols resulting from BB activities exert a substantial influence on the Earth's climatic system through a wide range of interactions. Either through scattering or absorption of solar radiation, BB aerosols play an important role in modulating both the regional/global scale radiation budget (direct effect) (e.g., Zhang, 2008; Randles and Ramaswamy, 2010; Tummon et al., 2010). The influence of BB aerosols on atmospheric shortwave scattering and absorption reduces the amount of solar radiation reaching the surface. As a result, the surface radiative forcing of BB aerosols may induce various feedbacks on the land-atmosphere energy exchange (see section 3.3.1). Particularly, the absorbing components of BB aerosols induce surface radiative cooling by enhancing radiative heating in the atmosphere (e.g., Randles and Ramaswamy, 2010). This radiative heating in turn creates another effect which is known as semi-direct effect of aerosols (e.g., Hansen et al., 1997). The semi-direct effect is the overall feedback of the thermal, hydrological and dynamical fields of the atmosphere to the atmospheric heating induced by light-absorbing BB aerosols (see section 3.3; Tummon et al., 2010; Randles and Ramaswamy, 2010 and references therein). Due to this, BB aerosols have an important influence on hydrological cycle (e.g., modification of precipitation efficiency and cloud

© University of Pretoria

cover) and circulation patterns of the atmosphere (e.g., Koren et al., 2004; Tummon et al., 2010; Randles and Ramaswamy, 2010). Moreover, these semi-direct effects of BB aerosols may have far-reaching effects on other climatic components (e.g., see section 3; Randles and Ramaswamy, 2010 and references therein).

For further information about other climatic implications of BB aerosols, such as their influences on cloud formation and microphysical properties by acting as cloud condensation nuclei (indirect effects), regional scale atmospheric chemistry and others, the reader is referred to Forster et al., 2007 and references therein. Inaccuracies associated with the quantifications of BB emissions as well as their physico-chemical and optical properties have become a major source of uncertainty in quantifying the climatic implications of BB induced aerosols (Liousse et al., 2004, 2010; Langmann et al., 2009). Previous studies have presumed that both direct and semi-direct effects of BB aerosols occur almost simultaneously (e.g., Koch and Del Genio, 2010 and references therein). Therefore, depending on various circumstances, these two effects sometimes reinforce each other and occasionally offset each other (see section 3 and references therein). Thus, to better understand the overall radiative role of BB aerosols, their direct and semi-direct influences need to be examined concurrently.

On a continental scale, many studies (e.g., Swap et al., 2003; Liousse et al., 2004; van der Werf et al., 2006, 2010, Magi et al., 2009 and references therein) recognized Africa as one of the major source of BB emissions. In Africa, human activities are the main causes of BB. These include forest-clearing (deforestation fires to accommodate the population and increasing agricultural lands), dry plant material burning or agricultural burning (intended for the preparation of crop lands and land use changes) and residential combustion for energy sources (Scholes et al., 1996; Andreae, 2001 and references therein). These and other practices are a significant source of BB-induced primary/secondary aerosols and therefore contribute to air pollution on both a regional and global scale (Andreae, 2001; Edwards et al., 2006; Lewis et al., 2013 and references therein).

According to the results of Magi et al. (2009), BB from southern Africa contributes approximately 21% of the global active fire counts. In the past, a number of field experiments were conducted in southern Africa to examine the regional emissions from BB activities and its different climatic aspects. These include dry season campaigns such as Southern African Fire-Atmosphere Research Initiative (SAFARI-92) (e.g., Piketh et al., 1996) and South African Regional Science Initiative (SAFARI 2000) (e.g., Swap, 2002, 2003; Sinha et al., 2003). These measurements, in cooperation with different models, provide important information about BB emissions, its regional scale transportation processes along with some of its implications on air quality and climate. Focusing on the region of our interest (i.e., South Africa), the aerosol climatology study of Tesfaye et al. (2011a) as well as the regional scale BB aerosol transportation by Winkler et al.(2008), both indicated that South Africa experiences radical turbidity during August to October due to high levels of BB aerosol loading. Furthermore, Tesfaye et al. (2011a) based on MISR retrieval products and the MODIS fire counts in Magi et al. (2009), pointed out that the east and northeast parts of South Africa are the main local sources of BB aerosols. Moreover, it is presumed from previous studies that the radiative and climatic implications of aerosols are more important on a regional scale, particularly nearby their source regions (e.g., Tummon et al., 2010). Therefore, the energy budget and climatic influences of aerosols which are produced from such important spatio-seasonally variable activities such as BB, needs to be addressed separately.

Including dust, anthropogenic aerosols and different BB inventories on RegCM3, Tummon et al., (2010) have analyzed the effects of bulk aerosol over southern Africa for a six-year period (2001-2006) during the austral winter season (June-September). This study has provided important information about the total aerosol direct and semi-direct effects, as well as its sensitivity to different BB inventories. However, it has not provided segregated climatic implications of the individual and total BB induced aerosols. In addition, encompassing almost the same domain range as Tummon et al. (2010), simulations using an atmospheric general circulation model (AGCM) by Randles and Ramaswamy (2010) have shown various direct and semi-direct climatic impacts of BB induced absorbing (BC and OC) aerosols during the dry season (August to October). Other than the radiative perturbations of these BB induced aerosols, this study investigated their critical impact on the hydrologic cycle. However, relying on the coarse resolution of AGCM (which is ~ 2.5º longitude x 2.0º latitude resolution) to make a detailed spatial analysis about the implications of these aerosols on various atmospheric and surface processes in a particular region is rather difficult. The present contribution uses a high resolution Regional Climate Model (RegCM4) to assess the mass distribution, direct and semi-direct climatic effects of different species of BB aerosols (individually/collectively) over South Africa. For BB emission estimates, this study has employed the Global Fire Emissions Database version 3 [GFED3: which has a temporal (monthly) and spatial (0.5º x 0.5º) resolution; van der Werf et al., 2010] on RegCM4.

The BB aerosols, which have been incorporated in our simulation as an additional component to atmospheric aerosols, are sulfates, hydrophobic (newly emitted) and hydrophilic (aged) components of both black carbon (BC) and organic carbon (OC) particles. The primary source of BB induced sulfate aerosols are driven from the oxidation of sulfur dioxide (SO_2) which is emitted from biomass combustion (Solmon et al., 2006; Qian et al., 2001). Predominantly BC and OC particles are directly emitted through incomplete and complete combustion processes, respectively (e.g., Bond et al., 2013 and references therein). To our knowledge, this is the first study, which examines the interactions and feedbacks among the individual/total BB aerosol species, radiation and climatic fields, over South Africa using the aerosol-RegCM4 two-way interactively coupled regional scale simulation. The paper has been organized as follows: in the next section a brief description of the experimental design as well as some essential points about the model are provided. The simulation results: the BB aerosol column burden and their direct and semi-direct effects are presented and discussed in section 3. Following these, a summary of our findings and concluding points are provided in section 4.

2 Model and Experiment Design

In this study, the International Centre for Theoretical Physics (ICTP)-RegCM4, which is interactively coupled with chemistry/anthropogenic aerosol-desert dust modules (e.g., Giorgi et al., 2012), is used to assess the mass distribution of BB aerosols as well as their direct and semi-direct radiative influences in South

© University of Pretoria

Africa. As is the practice before employing the model for such a purpose, Tesfaye et al. (2013a) first evaluated its aerosol optical property simulating performance in South Africa via comparing with ground-based and satellite observations. To assist this and other studies, Tesfaye et al. (2013a) also provided an extended general introduction about the significance of studying the climatic effects of aerosols using interactively coupled RegCM4-aerosol model. Furthermore, a brief description of RegCM4, the coupled aerosol modules and the emission inventories used in this study to introduce anthropogenic and BB activities induced gaseous SO_2, BC and OC aerosols into RegCM4 [i.e., for anthropogenic – MACCity (Lamarque et al., 2010) and for BB - GFED3 (van der Werf et al., 2010)], were given in Tesfaye et al. (2013a). These emission date sets were found from Global Emissions InitiAtive - Atmospheric Composition Change European Network (GEIA-ACCENT) emission data portal (http://accent.aero.jussieu.fr/database_table_inventories.php).

Beyond the descriptions of these emission inventories on Tesfaye et al. (2013a) and references therein, the readers can also see the spatio-temporal profiles of aerosol/precursor gases emission in South Africa using the data manipulation tools of GEIA-ACCENT emission database (found on aforementioned link). Following Qian et al. (2001), the RegCM4-aerosol model takes into account the chemical conversion of SO_2 to SO_4^{2-} through both the gaseous and aqueous-phase pathways. Moreover, following Cooke et al. (1999), the model considered the ageing process of BC and OC aerosols (i.e., the transformation of hydrophobic carbonaceous aerosols into hydrophilic particles). Overall, for further discretion about RegCM4-aerosol schemes, its aerosol optical property parameterizations, shortcomings and other related issues, the reader may refer to Tesfaye et al. (2013a) and references therein. The selected domain range, its resolutions, the model physics parameterization schemes, its dynamical and surface parameter time setups as well as time-dependent initial and lateral boundary conditions employed in this study are the same as Tesfaye et al. (2013a). The domain topography and geographical map of South Africa (with province boundaries) is shown in Fig.1.

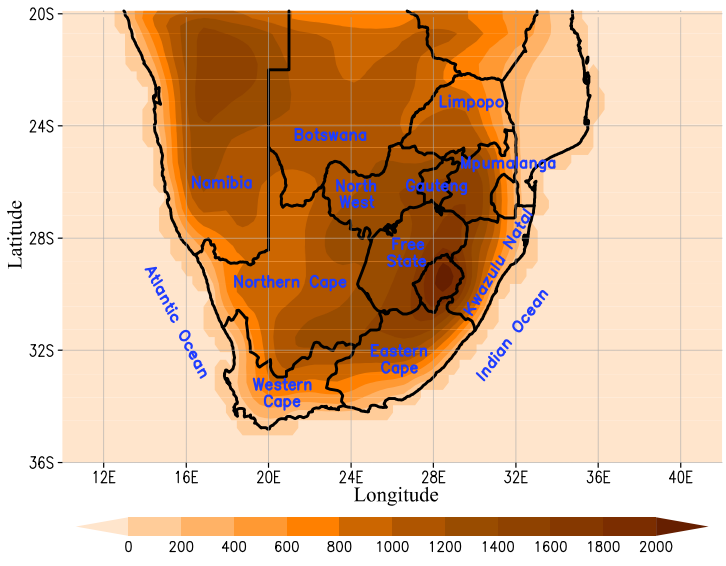

Fig. 1: Model domain, topography (unit: m) and geographical map of South Africa.

A series of five basic experiments - which extend from 1 January 1997 to 31 December 2008 - were conducted and results from the recent 11 years were thoroughly analyzed. The baseline simulation (Exp1), did not encompass any of the BB aerosols [i.e., it is a control experiment which only incorporates radiatively interactive desert dust particles as well as gaseous SO_2 (i.e., particulate SO_4^{2-}), hydrophobic and hydrophilic carbonaceous aerosols which are induced from anthropogenic activities]. For Exp2, all conditions were the same as in Exp1, however in addition to the background aerosols, BB induced SO_2 emissions were also included (i.e., particulate SO_4^{2-}), while the rest of BB emissions were set to zero. In a similar manner as Exp2, BC and OC aerosols, which are introduced from BB activities, were added separately in RegCM4 under Exp3 and Exp4, respectively. Finally in Exp5, in addition to the background aerosols, all three kinds of BB aerosols (i.e., sulfate+BC+OC) were considered.

The individual as well as the total BB aerosol column loadings and climatic signals which are associated with their existence, were captured by comparing the outcomes of the BB aerosol-comprising simulations (Exp2 through Exp5) with that of Exp1. Throughout our studies, considering the relative humidity influences on optical properties of hydrophilic aerosols (Solmon et al., 2006); the external mixture routine was used. Therefore, the direct radiative forcing contributions of the total/individual components of BB aerosols were computed using additional experiments. In these additional experiments, all conditions were kept the same as aforementioned five experiments (i.e., Exp1 to Exp5), however here the climatic feedback of both the background and BB aerosols were excluded. Thus, similar to the climatic signal computation, the individual as well as the total BB aerosol direct radiative forcing contributions were computed by comparing the results of these additional experiments which are simulated without the climatic feedbacks aerosols. This study only considered the direct and semi-direct effects of BB aerosols, thus it need be considered as a first-order climatic influence assessment of BB aerosols in South Africa.

3 Results and Discussion

While our domain configuration encompasses regions outside South Africa, results reported here focus on South Africa only. In South Africa there are two dry seasons. The main dry season for large areas of South Africa, approximately north of 30°S, is July to October (JASO). Whereas regions which are approximately south of 30°S (i.e., the southern part of the country) experience dry climatic conditions from November to February (NDJF). Accordingly, the spatio-seasonal distributions of open BB activities in South Africa have illustrated distinctive features. Over the southern part of the country, biomass combustion appeared during NDJF; whereas over the rest of the country (excluding the Northern Cape arid region) intense biomass burning activities occur during JASO. However, emissions from BB in areas which are south of 30°S (during NDJF) are much smaller than that of BB emissions which occur in areas that are north of 30°S (during JASO). Therefore, in this study, the BB aerosol mass distributions and their climatic influences are reported only for the main dry season (i.e., JASO).

Furthermore, as indicated previously, sulfate aerosols are predominantly formed in the atmosphere via the gaseous/aqueous phase oxidation pathways of its precursor gas (i.e., SO_2) (e.g., Qian and Giorgi, 1999; Qian et al., 2001). Nevertheless, compared to other events such as various anthropogenic activities in South Africa (e.g., Tesfaye et al., 2013b), open BB activities emit lower amounts of SO_2. In addition, the reduced air temperature and dry weather situations of the BB seasons create inconvenient conditions for SO_2 oxidation processes which in turn causes

© University of Pretoria

unfavorable situations for secondary sulfate aerosol formation (e.g., Roelofs et al., 2001; Qian and Giorgi, 1999; Khoder, 2002). As a result, the column loading, radiative and climate influences of BB induced secondary sulfate particles that are extracted from the comparison of Exp2 and Exp1 were found to be very small (almost negligible) relative to the other cases. This simulation result concurs with the observational based studies of Tesfaye et al. (2011a) and Magi (2009), which clearly point out the dominant radiative influences of BB induced carbonaceous aerosols, in and around South Africa. Therefore, the present study discusses only the column integrated mass distribution (section 3.1), radiative perturbations (section 3.2) and climatic feedbacks (section 3.3) of BC, OC and total aerosols which are driven from BB activities, during JASO.

3.1 Biomass burning aerosols column burden

In Fig. 2, rows (a) to (c) respectively show the JASO average (between 1998-2008) spatial distribution of BB aerosols (BC, OC and SBO) column burdens superposed with the corresponding surface wind fields ($\vec{W}$). The column mass distributions of BB aerosols were extracted by comparing the results of their corresponding experiments with Exp1 (see section 2). The surface wind field is taken from Exp3 (for BC), Exp4 (for OC) and Exp5 (for SBO). Generally, the results illustrate that the eastern parts of Mpumalanga (which is the hot-spot) as well as the northeast regions of KwaZulu Natal and eastern areas of Limpopo are the major local source areas of BB aerosols in South Africa (Fig. 2). The maximum load of BB aerosols (~ 0.33 mg/m^2, 2.35 mg/m^2 and 2.7 mg/m^2 for BC, OC and SBO, respectively) is observed in these major local source areas. The dry meteorological conditions of BB seasons offer advantageous circumstances for aerosols to travel far from their source locations into remote regions (e.g., Oshima et al. 2012). Thus, all BB aerosols which primarily originate from the aforementioned regions are distributed in the northern, central and eastern areas of South Africa (Fig. 2). Moreover, due to the influence of anticyclonic air circulation, the BB plume curved over the central areas of South Africa and exited the country towards the Indian Ocean (see Fig. 2). Through various aerosol removal processes (i.e., wet and dry depositions: Solmon et al., 2006; Oshima et al. 2012), the BB aerosol concentration declines during transportation. However, in areas which are in the vicinity of the BB aerosol source regions, such as Gauteng, Limpopo, KwaZulu Natal and northern areas of the Free State, the loading of BC, OC and SBO varied from 0.1 to 0.24 mg/m^2, 0.7 to 2 mg/m^2 and 0.8 to 2.3 mg/m^2, respectively. Over the arid areas of South Africa, the population distribution is too small, the availability of biomass for burning is inadequate and the anticyclone air flow bends the BB aerosol dispersion over the central areas of South Africa (Fig. 2). Due to these factors, the lowest BB aerosol burden is seen in and around the Northern Cape arid regions.

Natural events that occur occasionally such as veld fires and anthropogenic activities which are related with agricultural practices are the main causes of biomass combustion in South Africa (e.g., Scholes et al., 1996). For instance, as the dry season progresses, vegetation dries out thus several agricultural burning activities occur for the preparation of the coming growing season. These practices are the main cause of strong biomass combustion in the northern regions of the country (Helas and Pienaar, 1996; Sinha et al., 2003).

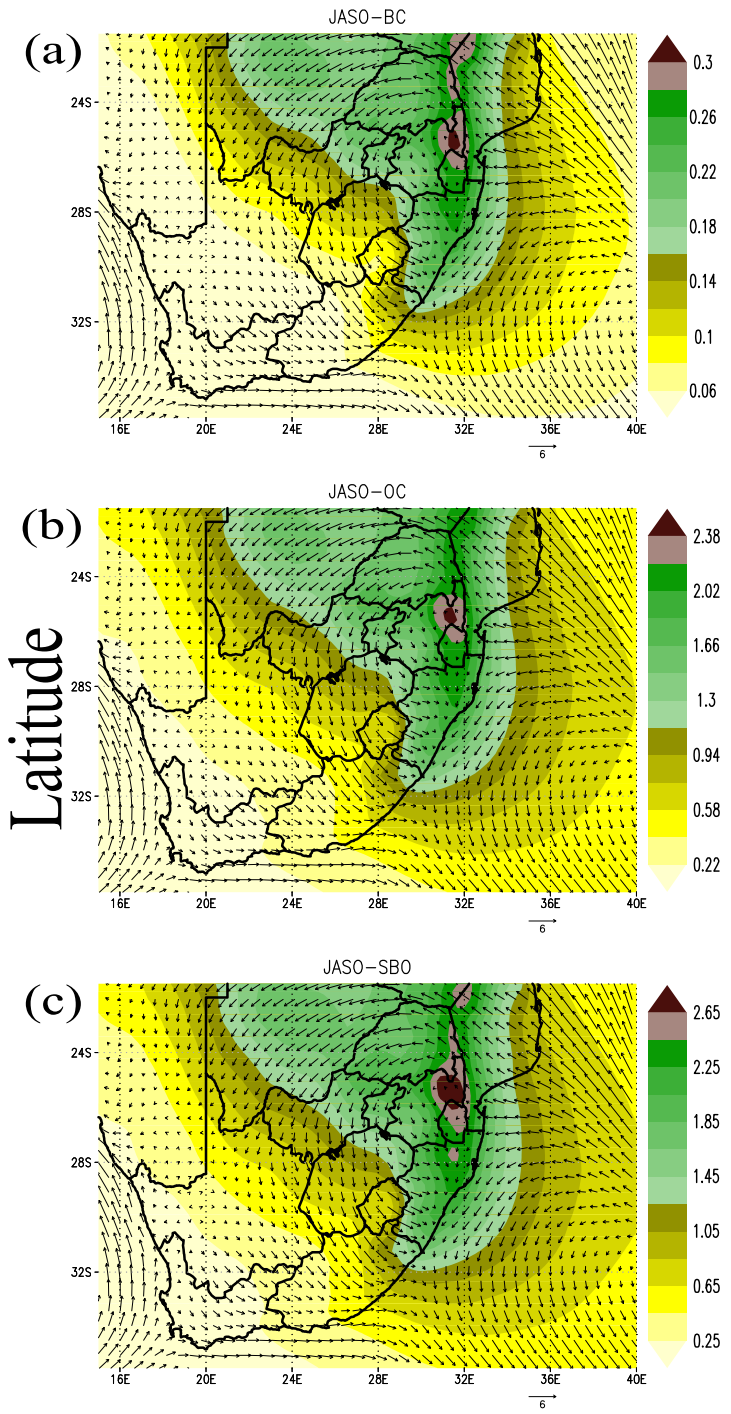

Fig. 2: The spatial distribution of BB activities induced BC, OC and total (Sulfate+BC+OC: SBO) aerosol column burden (shaded, unit: mg/m^2), respectively from row (a) to (c), superposed with the 10 meter wind field (vector arrow with its scale indicated at the lower right in unit of m/s), in and around South Africa. All results were averaged over 1998–2008 for the JASO season. In order to show the detailed spatial variability of each BB aerosol mass loading, the scale legend in Fig. 2a – Fig. 2c are kept different.

Sugarcane farming and refineries are commonly found in KwaZulu Natal and its surrounding areas. In these regions it is a conventional practice, before the end of the main dry season (i.e., JASO), to burn the sugarcane field prior to harvesting as well as for pre-industrial processing purposes. This becomes another main domestic cause for high level BB aerosol loading. The regional mean total BB aerosol burden (averaged over the areas of South Africa: -35° – -22°S, 16° – 33°E) was 1.2 mg/m^2 with BC and OC aerosols accounting for ~ 12.2 % and ~ 86.2 % of the burden, respectively. These fractional arrangements might have a significant implication on the magnitude of total BB aerosol radiative perturbations and climatic effects. The comparison of the aforementioned percentage contributions with the corresponding

© University of Pretoria

anthropogenic aerosol fractional configurations, reported in Tesfaye et al. (2013b), clearly indicate that the anthropogenic emissions are the main sources of sulfate particles in and around South Africa.

3.2 The shortwave surface and atmospheric radiative forcings of biomass burning aerosols

Eleven years averaged spatial distributions of BC, OC and SBO aerosols-induced Shortwave (SW) direct radiative forcing at the surface (SRF) and within the atmosphere (ATMRF) for the JASO season are shown in Fig. 3(a) to (c). In general, the spatial pattern of SRF and ATMRF of all BB aerosol species, resemble their corresponding column burden spatial distribution (Fig. 2). However, the aging of carbonaceous particles (i.e., their evolvement from hydrophobic to hydrophilic state) and the relative humidity influences on optical properties of hydrophilic aerosols (Cooke et al., 1999; Markowicz et al., 2003; Zhang et al., 2008) jointly induce a slight shift in the peaks of forcing away from the maximum column burden. Substantial radiative influences of BB aerosols are observed around their potential source areas, which correspond to the eastern parts of Mpumalanga and Limpopo as well as northeast regions of KwaZulu Natal (see Fig. 3). Additionally moderate influences appeared in nearby these regions. Over the west and southwest areas of the country, minimum radiative influences of BB aerosols are noted due to the lowest BB aerosols loading being present (see Fig. 2). Here we would like to remark that apart from the column burden of BB aerosols, the spatial variation of surface albedo may have some role in determining the magnitudes of their RF (e.g., Stier et al., 2007; Forster et al., 2007 and references therein).

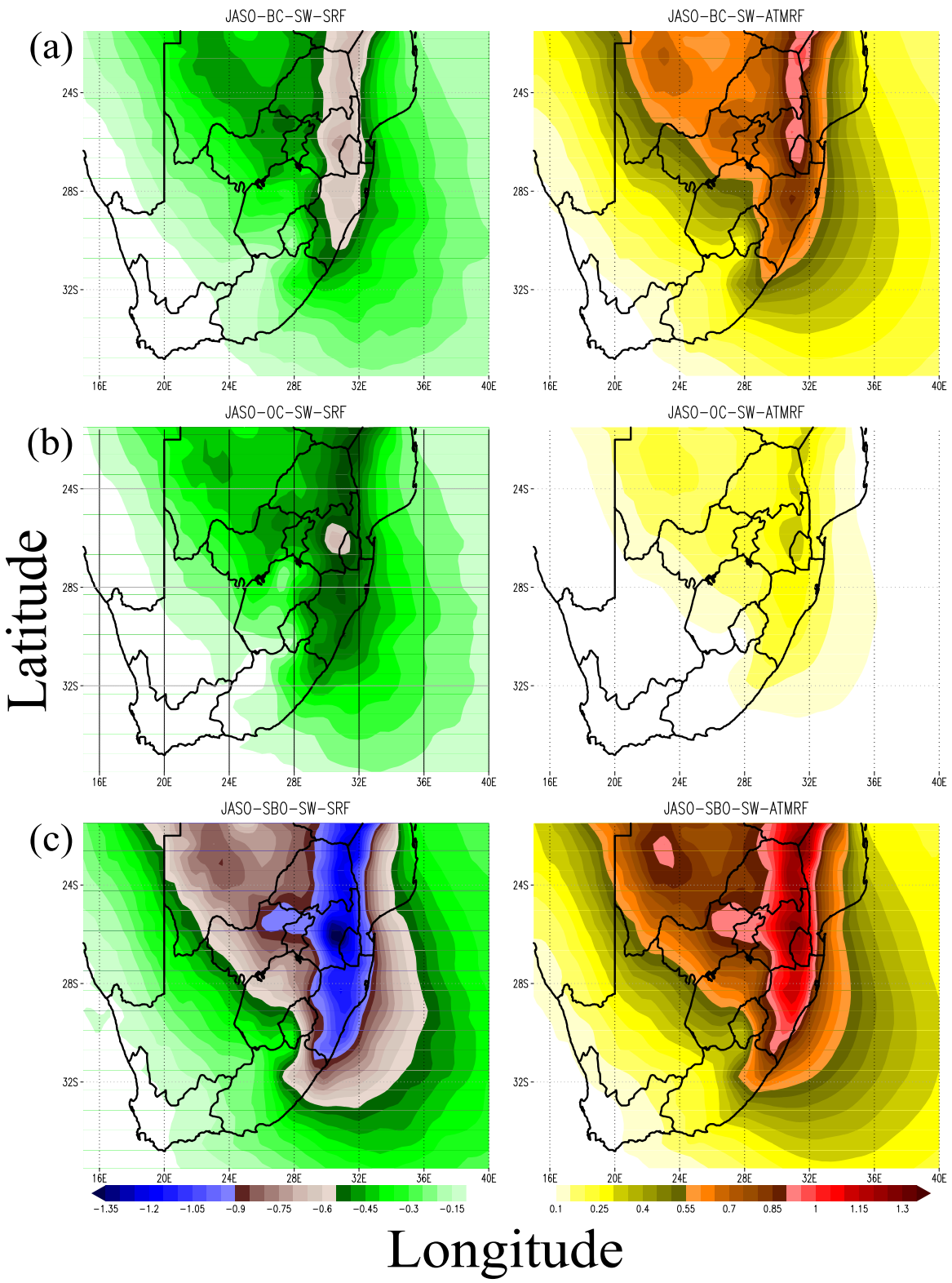

Fig. 3: the same as that of Fig. 2 but for BB aerosols induced shortwave surface (first column) and atmospheric (second column) direct radiative forcing (units: W/m^2): row (a) BC (b) OC and (c) SBO. In order to show the detailed spatial variability of each BB aerosol induced SRF and ATMRF, the scale legend in the first and second column of Fig. 3 are plotted in different colors and range.

© University of Pretoria

UNIVERSITEIT VAN PRETORIA
UNIVERSITY OF PRETORIA
YUNIBESITHI YA PRETORIA

As depicted in Fig. 3, the SW absorption primarily by BC and slightly by OC particles (e.g., Andreae and Gelencser, 2006) lead to a reduction of solar flux at the surface (known as negative SRF), by enhancing atmospheric radiative heating (positive ATMRF). The regional means (averaged over the areas of South Africa:-35° – -22°S, 16° – 33°E) and extreme values of SRF are as follows: BC: -0.37 W/m^2 (extreme: -0.7 W/m^2), OC: -0.35 W/m^2 (extreme: -0.65 W/m^2) and SBO: -0.73 W/m^2 (extreme: -1.35 W/m^2). Similarly, the regional mean and extreme values of ATMRF are: BC: +0.53 W/m^2 (extreme: +0.93 W/m^2), OC: +0.18 W/m^2 (extreme: +0.3 W/m^2) and SBO: +0.71 W/m^2 (extreme: +1.23 W/m^2).

Although BC particles account only for ~12.2 % of the regional mean total BB aerosol mass burden (refer section 3.1), the BC aerosol surface and atmospheric forcings are almost 1.2 and 3 times stronger than that of OC particles (which account for ~ 86.2 % of the regional mean total BB aerosol burden). This is due to the strong visible solar radiation absorbing nature of BC aerosols (the BC particles extinction cross section at 550 nm is ~3 times stronger than that of OC particles) (e.g., Solmon et al., 2006; Ramanathan and Carmichael, 2008). Therefore, the comparison of regional average radiative flux perturbations of BC and OC aerosols with that of the SBO illustrate that almost 53 % and 74 % of the total BB aerosol SRF and ATMRF, respectively are caused by BC particles. The OC aerosols almost contributed the remaining amount of the total RF (i.e., OC made a contribution of ~ 47 % and 26 % of the total BB aerosol's SRF and ATMRF, respectively). These simulation outcomes (particularly the total ATMRF fractional configurations) are in good agreement with the southern Africa BB observational analysis of Magi (2009), which exhibited that 27% and 73% of aerosol absorption optical depth are donated from OC and BC particles, respectively. If we compare the RFs of the individual/total anthropogenic aerosols species (from the results of Tesfaye et al., (2013b) with their corresponding BB aerosols induced RFs values over South Africa, the anthropogenic particles' radiative perturbations are found to be more significant than the BB aerosols. As mentioned previously, BB emissions are the main source of carbonaceous aerosols. Subsequently, we have seen that the SW absorption of these regionally concentrated carbonaceous particles extinguished the solar radiation flux reaching the Earth's surface, via promoting atmospheric radiative heating (Fig. 3a to 3c). This could consequently perturb various climatic variables such as the surface temperature, cloud cover, the regional circulation patterns and others (e.g., Ramanathan et al., 2005; Ramanathan and Carmichael, 2008). These and other climatic feedbacks will be discussed in the next section.

3.3 Climate responses

In this section, the BB aerosols' (BC/OC/SBO)-radiation-climate interactions induced climatic variables changes, as well as correlations among these alterations are discussed. In the next section, the change in Surface Temperature (ΔST) and Surface Sensible Heat Flux (ΔSSHF) are addressed. Thereafter, the effects of radiatively interactive BB aerosols on Net Atmospheric radiative Heating Rate (ΔNAHR) and Cloud Cover (ΔCC) are provided in section 3.3.2. Finally, alterations on Planetary Boundary Layer height (ΔPBL), Surface Pressure (ΔSP) in conjunction with the surface wind field ($\overrightarrow{\Delta W}$) are delineated in section 3.3.3.

3.3.1 The effects of BB aerosols on surface temperature and surface sensible heat flux

The changes in ST and SSHF that are induced due to the inclusion of different BB aerosols species are shown in Fig.4. The results have shown that, around the BB aerosol burdened regions (such as Mpumalanga, Limpopo, KwaZulu Natal and North West provinces, see Fig. 2) as well as over some other smaller scattered areas of South Africa – the inclusion of BC, OC and SBO aerosols induced a reduction in ST within a range of -0.03 K to -0.21 K, -0.03 K to -0.15 K and -0.05 K to -0.3 K, respectively. The maximum drop in ST has appeared during the case of SBO (Fig. 4c) in the upper reaches of Mpumalanga, which is one of the main source areas of BB aerosols (see Fig. 2). The ΔST is not consistently correlated with the respective pattern of BB aerosol SRFs (Fig. 3). Instead, the spatial correlation has indicated that the physical reason for these ST reductions were primarily associated with the BB aerosols' semi-direct effects induce cloud cover enhancement (Fig.5, see section 3.3.2) as well as it is moderately connected with their negative SRF (Fig. 3). Change in cloudiness is one of the feedback mechanisms of the climate system to the radiative effects of aerosols; thus, an enhancement (or reduction) of CC correspondingly result in a decrease (or increase) on the incoming solar radiation at the surface (e.g., Zhang, 2008). Therefore, the change in cloudiness (depending on the sign and the level of ΔCC) by reinforcing/offsetting the surface radiative cooling tendencies of BB aerosols – it plays an important role in prompting the ST as well as the SSHF alterations (e.g., Haywood and Boucher, 2000; Ramanathan et al., 2001; Zhang, 2008; Randles and Ramaswamy, 2010). Furthermore, the spatial correlations among the ΔST (Fig. 4) and the dynamical feedback of BB aerosols ($\overrightarrow{\Delta W}$) (Fig.6, see section 3.3.3) reflect that there is a small involvement of regional circulation changes in facilitating ST modifications. The aforementioned correlations have pointed out that the changes on surface variables due to aerosols cannot simply be explained by relating these changes with the respective patterns of aerosols' radiative influences, but rather these changes are the net product of complex feedback mechanisms of the overall climate system to the aerosol radiative effects.

The climatic feedback of BB aerosols influence the emissions of desert dust particles across the Northern Cape Province as well as the overall background aerosol burden level (see Fig. S1 of the supplementary document). Concurring with our results, different two-way coupled aerosol-climate modeling studies also reported the consequential influences of aerosol climatic feedback on atmospheric particulate burden levels (especially on dust emissions). For instance, Yue et al. (2010b) which examined the dust aerosol radiative feedback, using the Global Transport Model of Dust (GMOD), reported such incidences. The changes in background aerosol concentration (especially the dust burden level around the Northern Cape arid/semi-arid regions) may affect the local thermodynamical processes and cloudiness of these regions (see Fig. 5; also see Miller et al., 2004a, Perlwitz and Miller, 2010; Yue et al., 2010b). Especially in our case, the loads (Fig. 2) as well as the radiative influences (Fig. 3) of BB particles are insignificant in and around the Northern Cape Province. Thus CC changes, which are generated by the aforementioned background dust aerosol

© University of Pretoria

concentration variation, can easily provide a noticeable alteration on ST and SSHF. As depicted in Fig. 4, following this incidental ΔCC (in our case which displayed reduction: see Fig. 5) across the Northern Cape plus over some scattered areas, the inclusion of BC, OC and SBO aerosols resulted ΔST that varies from +0.03 K to +0.15 K, +0.03 K to +0.15 K and +0.05 K to +0.1 K, respectively. The maximum ST increases are found during both BC (Fig. 4a) and OC (Fig. 4b) cases. However the spatial coverage of ST increase in case in the OC case (especially around the Northern Cape) was found to be more extended than that of the BC case.

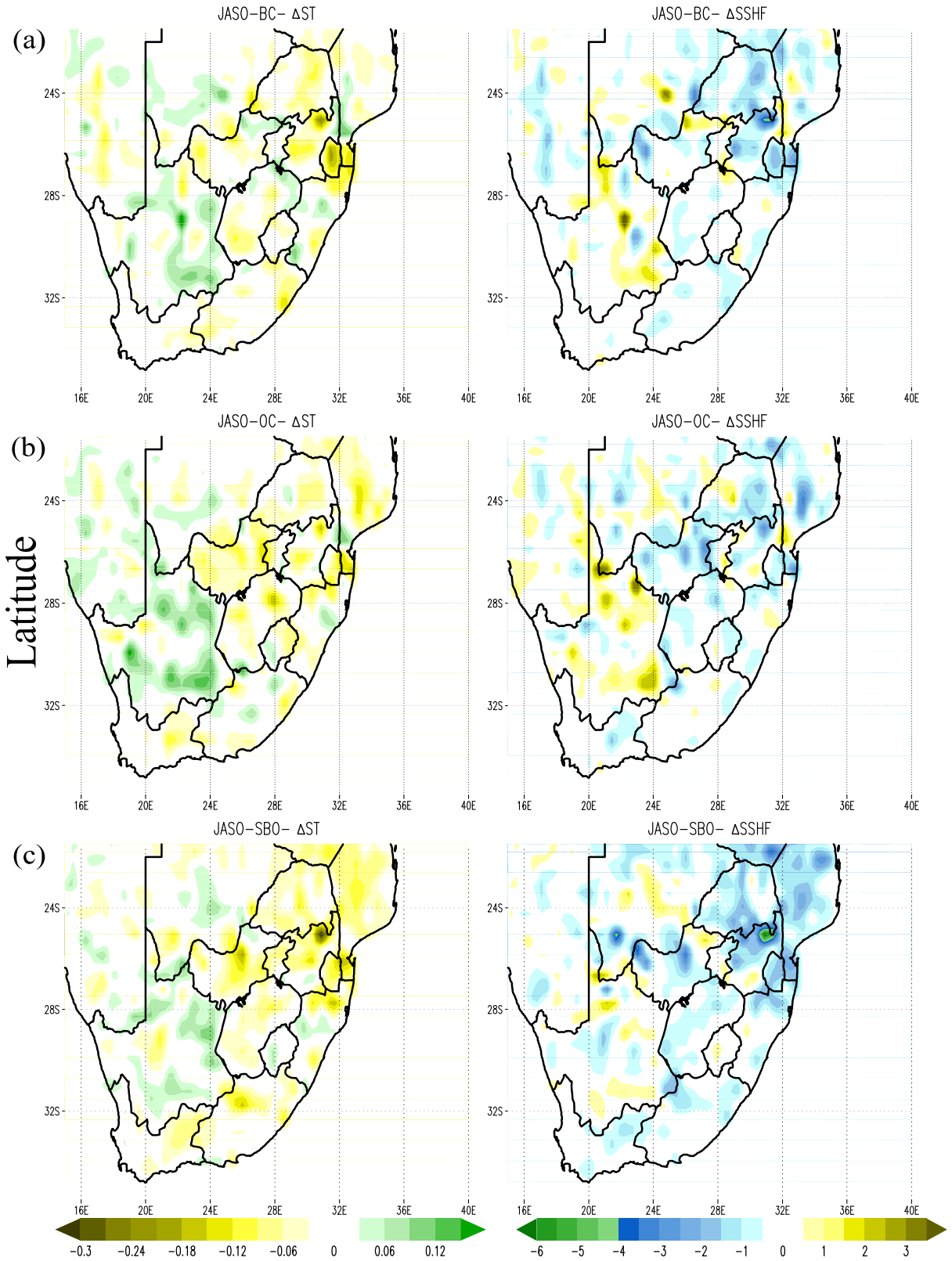

Fig. 4: Surface temperature (first column, unit: K) and surface sensible heat flux (second column, unit: W/m^2) responses during the presence of BB activities induced: row (a) BC, (b) OC and (c) SBO aerosols, in South Africa. All results were averaged over 1998–2008 for the JASO season.

The incidents of surface radiative cooling (or heating), caused by the direct and semi-direct influences of BB aerosols, subsequently induce the adjustment in land–atmosphere energy exchange (e.g., Zhang, 2008; Mallet et al., 2009). This includes the change in energy transfer from the surface into the atmosphere in the form of net thermal radiation, sensible and latent heat fluxes (e.g., Boer, 1993; Yu et al. 2002; Zhang, 2008; Mallet et al., 2009; Yue et al., 2010a, 2010b). Due to different circumstances such as the availability of water and other conditions, the change in SSHF and net upward long-wave fluxes are significant over the land than the oceanic regions (Miller et al., 2004a; Zhang, 2008). Therefore, as stated previously in this study, we have presented the BB aerosols' existence induced ΔSSHF (Fig. 4). Areas of South Africa which displayed a ST reduction (or enhancement) correspondingly shows the ΔSSHF that varied from -0.5 to -4 W/m^2 (+1 to +3.5 W/m^2), -0.5 to -2.5 W/m^2 (+0.5 to +3 W/m^2) and -0.7 to -6.3 W/m^2

© University of Pretoria

(+0.7 to +1.4 W/m^2), during the presence of BB induced BC, OC and SBO aerosols, respectively (Fig. 4). Overall, for different cases (i.e., for BC, OC and SBO), the spatial correlation between ΔST and ΔSSHF are within the range from 0.87 to 0.9. These higher values of spatial correlation coefficients confirm that the ΔSSHF is predominantly contingent on ΔST as well as slightly on other factors such as turbulence activities (e.g., Boer, 1993; Miller and Tegen, 1998; Ramanathan and Ramana, 2005; Zhang, 2008).

In all cases, the regional mean of both ΔST and ΔSSHF (i.e., averaged over all areas of South Africa) showed very small negative values. This indicates that on a regional context, these BB aerosols are slightly promoting surface cooling and are also decreasing the turbulent flux of sensible heat transfer into the atmosphere. As discussed above, the presence of BB aerosols have a contradictory role in different areas of South Africa. Therefore, these regional mean values did not necessarily reflect the local role of BB aerosols. This implies the main necessity for a high resolution climatic model in order to capture the actual role of atmospheric aerosols on a local scale. The above results have also showed that, in addition to the direct and semi-direct climatic effects of BB aerosols on regional scale, the BB aerosol climatic feedbacks induced background aerosol concentration variations and its consequential impacts are also considered to be important.

3.3.2 The effects of BB aerosols on net atmospheric radiative heating rate and cloud cover

The vertical profile of BB aerosols showed that they were primarily confined in the lower part of the troposphere (i.e., below ~ 650hPa altitude - not shown). Therefore, even though different studies have illustrated that the BB aerosol semi-direct effects were highly reliant on vertical location of aerosols (especially with respect to clouds) (e.g., Feingold et al., 2005; Koch and Genio, 2010), this study has examined their columnar influences, specifically over the lower part of the troposphere. Changes in the low-level (below ~ 650hpa) columnar averaged net (short- plus long-wave) atmospheric radiative heating rate (ΔNAHR) and column integrated cloud cover (ΔCC), which are engendered by different kinds of BB aerosols-radiation-climate interactions, are provided in Fig. 5. All the climatic component radiative feedbacks (i.e., different types of aerosols, clouds, water vapor, the underlying surface and other trace gases in the atmospheric column) are accounted for during the computation of NAHR. Attributed to various feedback mechanisms of the climate system to the aerosol radiative effects (especially the cloud responses), the spatial distribution of ΔNAHR for each species of BB aerosols are quite different from each another (see Fig. 5a, b and c).

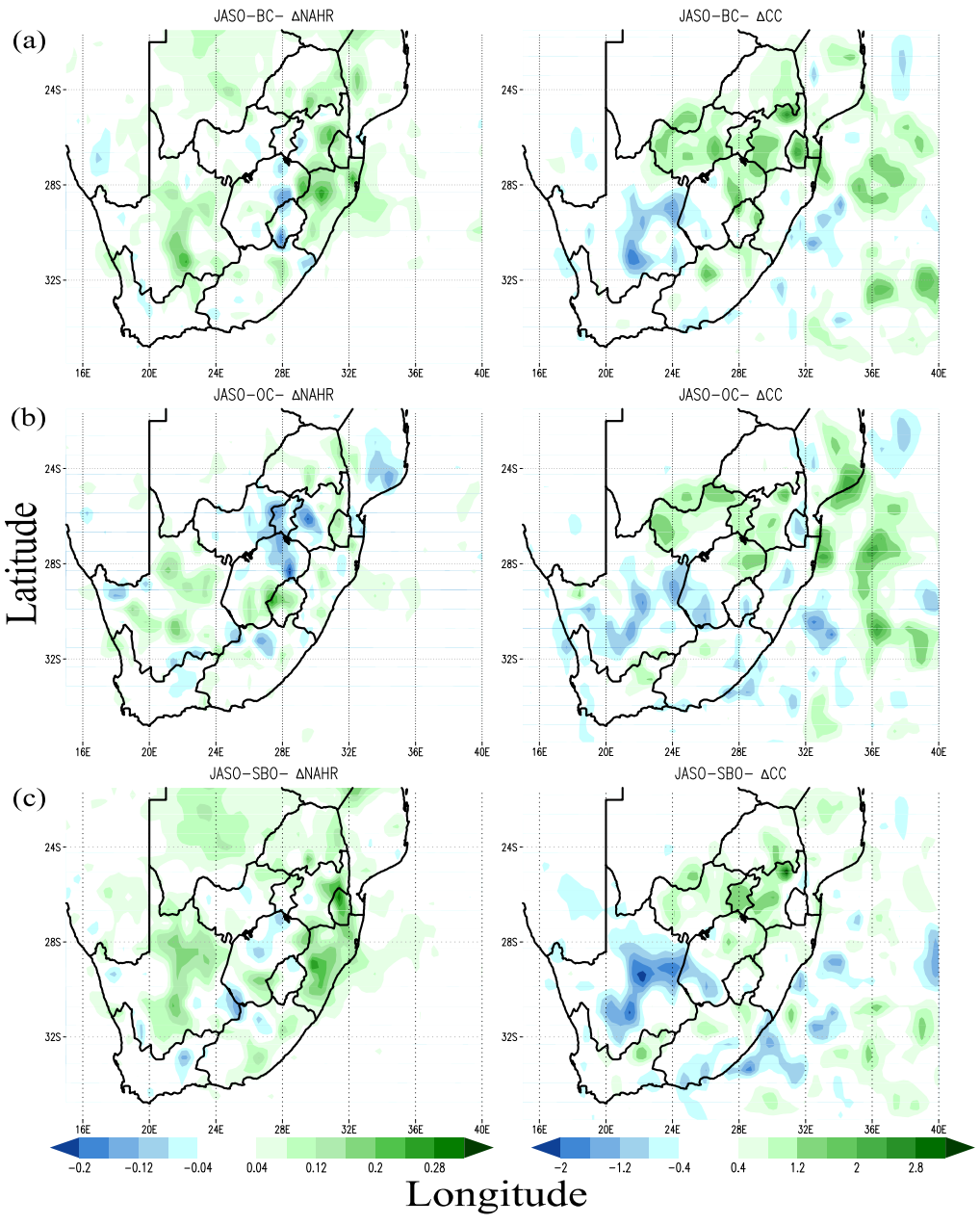

Fig. 5: Same as Fig. 4 but for changes in low-level: columnar average NAHR (first column, unit: K/day) and column integrated CC (second column, unit: %) during the presence of BB activities induced: row (a) BC, (b) OC and (c) (SBO) aerosols.

During the inclusion of BC (Fig. 5a), extending from the central areas of KwaZulu Natal up to the northern regions of Mpumalanga as well as over central parts of Northern Cape and southern areas of Limpopo provinces, we found the ΔNAHR varies from +0.06 to +0.25 K/day. The pronounced values (~ +0.21 to +0.25 K/day) are situated around the central areas of KwaZulu Natal. On the other hand, mainly in the northeastern parts of the Free State and over some scattered areas of South Africa, a reduction in NAHR from -0.04 K/day to -0.16 K/day was observed. In the case of OC aerosols (Fig. 5b), we have found positive values of ΔNAHR that varied from +0.04 to +0.24 K/day, largely in the Northern Cape and southern parts of the Free State as well as over limited areas of Mpumalanga and Limpopo. In contrast, over large areas of the Highveld zones of South Africa as well as in some scattered regions, the inclusion of OC aerosols generated a reduction of NAHR that was within a magnitude range of -0.04 to -0.2 K/day. Apart from some confined areas which exhibited an insignificant reduction of NAHR, the total BB aerosols (i.e., SBO case, Fig. 5c) predominantly caused a widely spread NAHR enhancement that varied from+0.05 to +0.31 K/day.

© University of Pretoria

These heating influences have been noted in wider areas of the BB aerosols' potential source regions (see Fig. 2) as well as over the border areas of the Northern Cape and other scattered areas of South Africa. The net radiative heating effects which were noted in areas dominated by BB aerosols were primarily attributed by the strong and partial SW absorbing nature of BC and OC aerosols, respectively. Furthermore, as previously mentioned, owing to the regional climatic feedbacks of BB aerosols, the desert dust particle burden levels exhibited both a reduction and enhancement in and around the Northern Cape region (see Fig. S1 of the supplementary document), which congruently became one of the causes for the reduction and enhancement in NAHR. Likewise, the inclusion of radiatively interactive BB aerosols also caused a slight variation in the background anthropogenic aerosol concentrations especially over areas such as the industrial Highveld region of South Africa, which are potential sources regions of anthropogenic aerosols (e.g., Freiman and Piketh, 2003). This phenomenon might also cause some modification in the radiative feedback of the overall climatic system (which in turn changes in NAHR), in these regions (e.g., Ramanathan et al., 2001). Overall, due to the complexity of the feedback mechanisms of the climate system to the aerosol radiative influences, the physical reasons for the ΔNAHR in different spatial locations are very complicated. The specific physical processes of the phenomenon need to be investigated comprehensively in a future work.

As reported in different studies (e.g., Ramanathan et al. 2001; Menon et al., 2002; Zhang, 2008; Randles and Ramaswamy, 2010), following changes on heating rate of the atmosphere, the adjustment of hydrological variables as well as dynamical circumstances of the atmosphere will take place. Accordingly, the changes on low-level CC (clouds which are formed below ~ 650 hPa) that have been generated by the presence of different species of BB aerosols are presented in Fig. 5. The ΔCC is one of the feedback mechanisms of the climate system to the radiative effects of aerosols. Nonetheless as reported in Kaufman and Koren, 2006; Zhang, 2008, the CC response is not dependent only on aerosol burden levels and their radiation perturbations. Particularly in the case of carbonaceous aerosols, the change in cloudiness was also greatly reliant on the atmospheric altitude, where these aerosols mainly reside, (e.g., Cook and Highwood, 2004; Johnson et al., 2004; Feingold et al., 2005) and on various other climatic conditions of the region (e.g., Douville et al., 2002; Allen and Sherwood, 2010; Koch and Genio, 2010).

Depending on water vapor availability in the background atmosphere (e.g., Koch and Genio, 2010), amplification of low-level CC occurred over areas of South Africa which experience a reduction in NAHR due to the existence of BB aerosols (see Fig. 5, first and second column). Conversely, contingent on the region considered and its meteorological features, the heating influences of BB aerosols causes both a positive and negative ΔCC. Over the wet/semi-wet zones, when aerosols induce radiative heating in the lower parts of the troposphere, the water vapour mixing ratio and atmospheric instability might increase (e.g., Feingold et al., 2005; Koch and Genio, 2010; Perlwitz and Miller, 2010). Subsequently, depending on moisture flux dynamics, an enhancement in low-level moisture convergence and relative humidity in the upward direction arises (e.g., Zhang, 2008; Kaufman and Koren, 2006; Randles and Ramaswamy, 2010). Attributed to these and other dynamical features of the region, in and around the BB aerosol heating zones, cloudiness increases, especially towards the upper region of the lower-troposphere (e.g., Douville et al., 2002; Perlwitz and Miller, 2010; Feingold et al., 2005). Due to the aforementioned complex climatic factors that follows the enhancement of NAHR, the increments in low-level CC (+ 0.5 to +2.5 %, + 0.4 to +2 % and + 0.5 to +3 %, for BC, OC and SBO, respectively) appeared around the central, north and eastern regions of South Africa; which are the wet and semi-wet parts of the country (see Fig. 5, first and second column). These results are in good agreement with previously reported studies such as Feingold et al. (2005) and Randles and Ramaswamy (2010) that showed similar effects of BB aerosols around Amazonia and southern Africa regions, respectively.

Contrarily, in-line with the enhancements of NAHR over arid/semi-arid areas of South Africa (i.e ., in and around the Northern Cape province), the change in low-level CC exhibited a reduction that varied from -0.5 to -1.5 %, -0.4 to -1.2 % and -0.5 to -2 %, for BC, OC and SBO, respectively (see Fig. 5). In general, over the arid areas of the country, the BB aerosols induced ΔNAHR and ΔCC, showed an opposite relation. These results are consistent with the conventional description of the semi-direct effects of aerosols (e.g., Hansen et al., 1997). However, over the wet/semi-wet regions, the responses of CC for NAHR enhancements involve various climatic factors (e.g., Feingold et al., 2005; Koch and Genio, 2010); thus, the resulted relation of NAHR enhancement and ΔCC are contrary to the conventional description of the semi-direct effects. The regionally averaged ΔCC (i.e., averaged over the areas of South Africa) showed that in a regional context, the BB aerosols slightly increased the CC, which is opposite to the regional mean results of ΔST (and ΔSSHF) (see section 3.3.1). This illustrated that the increase/decrease in CC was one of the factors that accounted for the reductions/enhancements in ST (and SSHF) (see section 3.3.1). These changes which were described in this section, as well as in section3.3.1, jointly induced regional scale dynamical alterations (e.g., Jacobson and Kaufman 2006; Zhang, 2008; Stanelle et al., 2010; Randles and Ramaswamy, 2010; Solmon et al., 2012). This particular issue will be discussed in the next section.

3.3.3 The effects of BB aerosols on planetary boundary layer, surface pressure and wind field

Changes in planetary boundary layer height: ΔPBL, surface pressure: ΔSP and 10m surface wind field: $\overrightarrow{\Delta W}$ that were produced by inclusion of BB aerosols are depicted in Fig. 6. Areas of South Africa, which experienced surface cooling and SSHF reduction (Fig. 4, see section 3.3.1), exhibited a reduction of PBL height plus enhancement of SP which respectively ranges from -4 to -16 m (+0.005 to +0.01 hPa) for BC, from -2 to -12 m (+0.005 to +0.015 hPa) for OC and from -2 to -20 m (+0.01 to +0.025 hPa) for SBO (see Fig. 6a, b and c). In contrast, areas that exhibited an enhancement in the ST and SSHF (Fig. 4, see section 3.3.1), also experienced a reduction in the SP along with increase in PBL height within a range of +4 to +16 m (-0.02 to -0.005 hPa) for BC, +2 to +10 m (-0.02 to -0.005 hPa) for OC and +2 to +6 m (-0.015 to -0.005 hPa) for SBO. In all cases, the spatial correlations among the ΔPBL (ΔSP) with that of ΔST were correspondingly within a range of +0.85 to +0.87 (-0.7 to -0.72); as well as with that of ΔSSHF, respectively varying from +0.88 to +0.91 (-0.62 to -0.65). The signs and the higher level of correlations found above mirror

© University of Pretoria

the mechanisms through which the ΔPBL and ΔSP occurred (e.g., Zhang, 2008).

The direct and semi-direct effects of BB aerosols induced ST and SSHF reductions/enhancements. This will correspondingly cause the weakening/strengthening of Convectively Driven Turbulence (CDT) as well as Surface Buoyancy Fluxes (SBF) (e.g., Yu et al., 2002; Jacobson and Kaufman, 2006; Zhang, 2008; Menon et al., 2002; Miller et al. 2004b; Jiang and Feingold, 2006). These adjustments (i.e., weakening/strengthening of CDT and SBF) respectively cause a drop/rise in PBL height as well as the advancement/weakening in stability of the lower troposphere (Ramanathan et al., 2005; Mallet et al., 2009; Zhang, 2008; Yu et al., 2002); in turn, the enhancement/reduction of SP (e.g., Yu et al., 2002; Zhang, 2008; Randles and Ramaswamy, 2010). In general, our results and clarifications (regarding the ΔPBL height and ΔSP) are also consistent with the findings of Randles and Ramaswamy (2010); which studied the climate effects of BB aerosols using GFDL-AGCM that has a much coarser resolution than our RCM simulation. As noted above, the correlation among ΔSP with that of ΔST as well as ΔSSHF were slightly smaller (on average, respectively, by about ~ 18% and ~ 28%) than the corresponding correlations between ΔPBL and ΔST/ΔSSHF. Ultimately, this suggests that other than the adjustments in CDT and SBF, the dynamical feedbacks of BB aerosols (especially on surface wind fields) also play some role in adjusting the ΔSP.

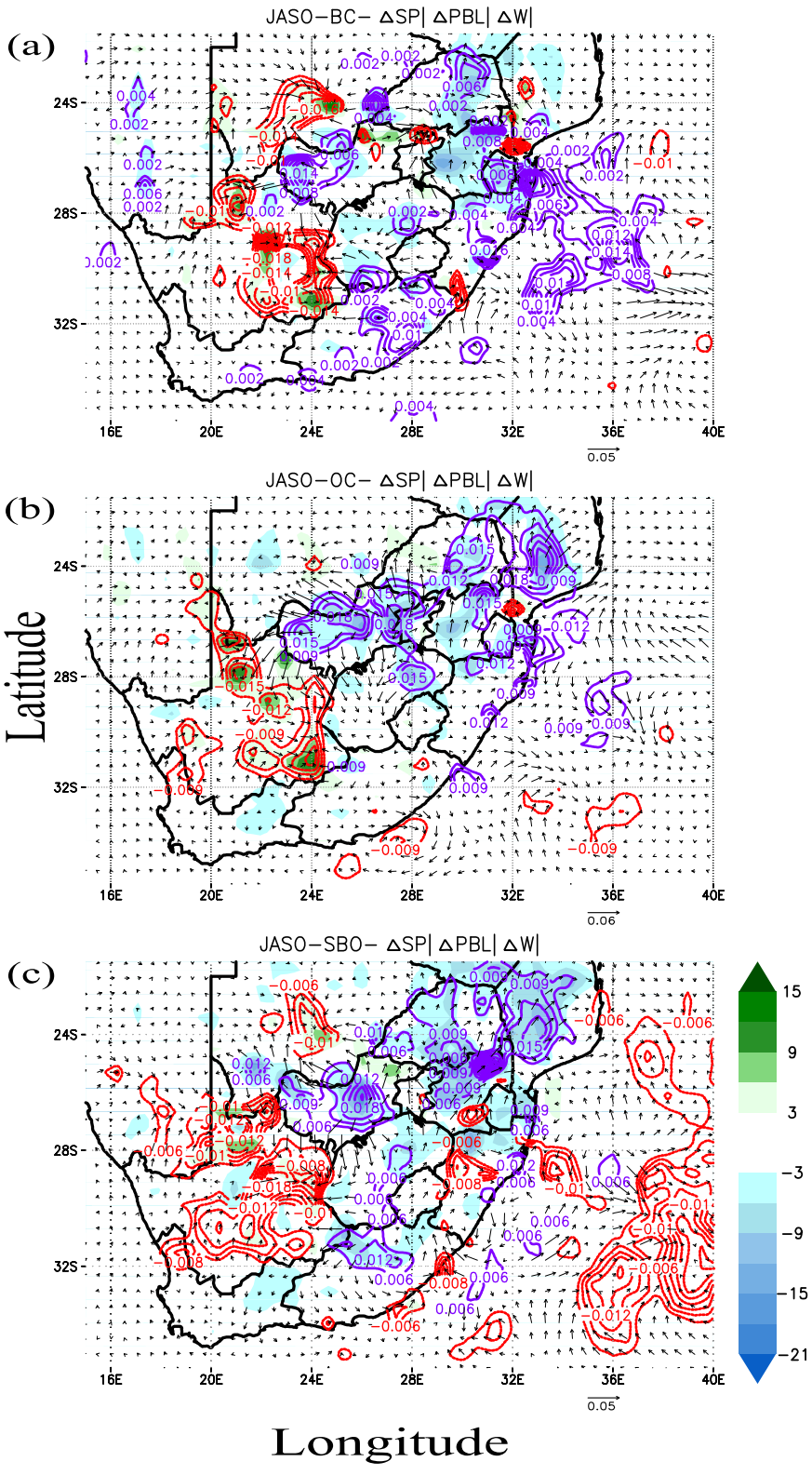

Fig. 6: Same as Fig. 4 but for changes in PBL height (shaded; unit: m), SP (unfilled contour: unit hPa; the red and purple contour lines show the negative and positive ΔSP, respectively) and 10m surface wind field: $\overrightarrow{\Delta W}$ (vector arrow with its scale indicated at the lower right; unit: m/s) during the presence of BB activities induced: row (a) BC, (b) OC and (c) (SBO) aerosols.

The vector arrows in Fig. 6 represent changes in surface wind fields (i.e., $\overrightarrow{\Delta W} = \Delta U + \Delta V$ - changes in zonal (ΔU) and meridional (ΔV) wind components), which were induced due to the presence of radiatively interactive BB aerosols. The vector arrows which point in the east and north directions correspondingly indicate a positive change (increase) in zonal and meridional wind components. The maximum amplitudes of surface wind speed increments (and reductions) which were predicted in our simulation are respectively ~ up to 0.04 m/s (0.05 m/s) for BC, 0.047 m/s (0.06 m/s) for OC and 0.032 m/s (0.05 m/s) for SBO. Moreover, the spatial distributions of $\overrightarrow{\Delta W}$ for each species of BB aerosols were quite different from one another (see Fig. 6a, b and c). During the inclusion of BC (Fig. 6a): extending from the central areas of the Eastern Cape up to the eastern parts of the Free State as well as across the North West province, zonal components exhibited a reduction. Whereas, around Limpopo and over some narrow scattered areas of South Africa an increase in zonal winds were found. Apart from the North West province and other confined areas, predominantly the OC aerosols generated an enhancement in ΔU (Fig. 6b). During the inclusion of SBO (Fig. 6c), reduction in zonal winds are found in confined areas of the Free State, eastern parts of Mpumalanga and the North West province.

In all cases (i.e., during the presence of BC, OC and SBO; Fig. 6a, b and c), across the eastern parts of Mpumalanga, Gauteng, North West province and over the west parts of Limpopo, the ΔV exhibited an enhancement. Additionally, during the inclusion of BC and SBO (Fig. 6a and c), an improvement in meridional wind has been also noted in the southwest areas of the Northern Cape and some parts of the Eastern Cape provinces. On the other hand, in all cases, largely in the western areas of the Free State and across the northern regions of the Northern Cape Province, the ΔV displays a reduction.

© University of Pretoria

These regional circulation changes discussed so far, will have some impact on burden level and dispersions of the background aerosols. Particularly, the change in surface wind fields around the arid/semi-arid regions of the Northern Cape Province ($\overrightarrow{\Delta W}$) incorporated with other climatic feedbacks of BB aerosols, will influence the emission and dispersions of desert dust particles (e.g., Yue et al., 2010b; Stanelle et al., 2010). Furthermore, the $\overrightarrow{\Delta W}$ may induce some adjustment on stability of the lower troposphere (e.g., Jacobson and Kaufman, 2006; Zhang, 2008); therefore, this become another contributing factor for BB aerosols' induced ΔSP. Overall, changes in regional circulation are the net product of various climatic effects of BB aerosols (Jacobson and Kaufman, 2006; Zhang, 2008); thus, the physical reasons for the $\overrightarrow{\Delta W}$ are quite complex. Similar to the ΔNAHR, this phenomenon also needs to be examined more thoroughly in future research.

4 Summary and Conclusions

In this study, we examined the mass distribution, direct and semi-direct effects of different species of Biomass Burning (BB) aerosols: sulfate, Black Carbon (BC), Organic Carbon (OC) aerosols and all three together (SBO), using 12 years of the Regional Climate Model-RegCM4, over South Africa. The simulations showed that biomass combustions were occurring throughout the seasons in different locations; however, the most intense BB activities occurred from July to October (JASO). Moreover, a lower amount of SO_2 was emitted from open BB and the dry weather situation of the main BB season (JASO) created unfavorable conditions for secondary sulfate aerosol formation. Accordingly, the load and climate signal of sulfate particles that resulted from open BB activities were almost negligible (relative to carbonaceous aerosols which were emitted from the same events). Owing to the above circumstances, this study only discussed the JASO season (averaged over 1998-2008) column loading, radiative and climate effects of BB activities induced BC, OC and SBO aerosols. Summary of the main results and conclusions drawn from this study are presented as follows:

- Influenced by the anticyclonic air circulation, the BB aerosols which primarily originate from Mpumalanga, KwaZulu Natal and the eastern areas of Limpopo were distributed in the northern, central and eastern regions of South Africa. Due to the air mass movement as well as insufficiency of biomass for burning, the lowest BB aerosol burdens appeared in and around the Northern Cape arid regions. The maximum load of BC (up to 0.33 mg/m^2), OC (up to 2.35 mg/m^2) and SBO (up to 2.7 mg/m^2), were noted in their source regions. Overall, the regional mean total BB aerosol column burden was 1.2 mg/m^2 – with the BC and OC aerosols accounting for ~ 12.2 % and ~ 86.2 % of the burden, respectively.

- Due to the strong shortwave absorption by BC and slight absorption by OC, aerosols emitted from BB reduced solar radiation at the surface and locally heated the atmospheric column. The maximum contribution of BB aerosol Surface Radiative Forcing (SRF) [atmospheric radiative forcing] was observed around their source regions; which is respectively: -0.7 W/m^2 [+0.93 W/m^2] for BC, -0.65 W/m^2 [+0.3 W/m^2] for OC and -1.35 W/m^2 [+1.23 W/m^2] for SBO. Moderate radiative influences of BB aerosols were found in areas which are adjacent to their source regions and minimum influences appeared in the Northern and Western Cape provinces of South Africa.

- The inclusion of radiatively interactive BB aerosols as an additional component to atmospheric aerosols resulted in both a reduction and enhancement of Surface Temperature (ST) as well as Surface Sensible Heat Flux (SSHF). In general, the BB aerosol loaded areas (i.e., Mpumalanga, Limpopo, KwaZulu Natal and North West provinces) experienced reductions in the ST (within a range of -0.03 K to -0.3 K) and SSHF (within a range of -0.5 to -6.3 W/m^2). Whereas, over the western areas of South Africa, the BB aerosols induced ST and SSHF enhancements, that respectively varied from +0.03 K to +0.15 K and +0.5 to +3.5 W/m^2. Overall, the results demonstrate that the BB aerosols which are induced over South Africa have an insignificant influence on the ST and SSHF but could have foreseeable climatic impacts.

- The spatial correlation of ΔST (ΔSSHF) with that of BB aerosol radiative and climatic influences showed that changes in cloud cover (CC) caused by the semi-direct effects of BB aerosols were the primary physical process accountable for ΔST (ΔSSHF). In addition, BB aerosol SRFs and dynamical feedback mechanisms also have a moderate and slight involvement in persuading ST (SSHF) adjustments, respectively.

- The interaction and feedback among BB aerosols, radiation and climate generated alterations in the background aerosol concentrations, especially on desert dust emission and burden levels, around the Northern Cape arid/semi-arid regions. This, in turn, produced local atmospheric thermal structure adjustments and CC changes, mainly over areas of South Africa which were away from the BB aerosol loading zones. These results also suggested that the climatic feedback of aerosols, which are produced from one activity sector, at least on a regional level, impose important changes on atmospheric processes of other aerosols (i.e., emission, aging, transport) that are produced from different sectors.

- Over different areas in South Africa, such as Mpumalanga, Limpopo, KwaZulu Natal, Northern Cape and Free State, the inclusion of BC, OC and SBO aerosols resulted changes on low-level columnar average Net Atmospheric radiative Heating Rate (ΔNAHR: ~ below 650hPa) which varied from +0.04 to +0. 31 K/day. Whereas, the inclusion of BC (over the northern parts of Free State) and OC (over wide areas of Highveld zones of South Africa); caused a ΔNAHR that varied from -0.04 to -0. 2 K/day.

- Areas of South Africa which experienced a reduction in NAHR due to the existence of BB aerosols also showed an increase in low-level columnar integrated CC. However, depending upon the region and its climatic features, the heating influences of BB aerosols resulted in both the enhancement and reduction of CC. Over the wet/semi-wet regions of South Africa (i.e., around the central, north and eastern regions of South Africa), the enhancement of NAHR generated an increment in CC which varied from +0.4 to +3

© University of Pretoria

%. Whereas, over the arid regions of South Africa (i.e., Northern Cape Province), the existence of BB aerosols induced NAHR enhancements cause a reduction of CC. In general, our results suggest that over the wet/semi-wet regions, apart from the enhancements of NAHR, various climatic factors also play a prominent role in determining the ΔCC.

- In all cases (i.e., during the inclusion of BC, OC and SBO aerosols), areas of South Africa which experienced ST (and SSHF) reductions also exhibited the reduction of Boundary Layer height (BL: -2 to -20 m) along with the enhancement of Surface Pressure (SP: +0.005 to +0.025 hPa). In contrast, areas which exhibited enhancements in the ST (and SSHF) also displayed BL increases (+2 to +16 m) along with SP reductions (-0.005 to -0.02 hPa).
- The presence of radiatively interactive BB aerosols also promoted a change in surface wind fields ($\overrightarrow{\Delta W}$) that were spatially highly variable. However, clarifying the physical mechanisms through which the $\overrightarrow{\Delta W}$ occurred was beyond the scope of this study. The investigations of this phenomenon, ΔNAHR and the indirect effects of BB aerosols have been left as a subject of our future research.

Acknowledgements

The authors are grateful to Addis Ababa University, Department of Physics, for providing computational facilities. For the accessibility of RegCM model the authors are thankful to the International Centre for Theoretical Physics (ICTP). We are also indebted to Teresa Faleschini, Tamene Mekonnen, Fiona Tummon and Addisu Gezahegn, for their valuable assistances. Authors thank Ameeth Sharma for proof reading and language correction in the manuscript. This work was supported by African Laser Centre and NRF bi-lateral research grant (UID: 68688/65086), in addition to CSIR National Laser Centre.

References

Allen, R. J., and Sherwood, S. C. (2010). Aerosol-cloud semi-direct effect and land-sea temperature contrast in a GCM, Geophys. Res. Lett., 37, L07702, doi:10.1029/2010GL042759.

Andreae, M. O. and Gelencser, A. (2006).Black carbon or brown carbon? The nature of light-absorbing carbonaceous aerosols, Atmos. Chem. Phys., 6, 3131-3148, doi:10.5194/acp-6-3131-2006.

Andreae, M. O. and Merlet, P. (2001). Emission of trace gases and aerosols from biomass burning, Global Biogeochem. Cycles, 15, 955–966.

Barbosa, P. M. et al. (1999). An assessment of vegetation fire in africa (1981–1991): Burned areas, burned biomass, and atmospheric emissions, Global Biogeochem. Cycles, 13, 933–950.

Boer, G.J. (1993). Climate change and the regulation of the surface moisture and energy budgets.ClimDyn 8:225–239, doi: 10.1007/BF00198617.

Bond, T. C. et al. (2013), Bounding the role of black carbon in the climate system: A scientific assessment, J. Geophys. Res. Atmos., 118, 5380–5552, doi:10.1002/jgrd.50171.

Cook, J. and Highwood, E. J. (2004). Climate response to tropospheric absorbing aerosols in an intermediate general-circulation model. Q.J.R. Meteorol. Soc., 130: 175–191. doi: 10.1256/qj.03.64.

Cooke, W.F. et al. (1999). Construction of a 1x1 fossil fuel emission data set for carbonaceous aerosol and implementation and radiative impact in the ECHAM4 model. J. Geophys. Res. 104.22137-22162.

Douville, H. et al. (2002). Sensitivity of the hydrological cycle to increasing amounts of greenhouse gases and aerosols. Climate Dynamics 20, 45–68.

Duncan, B. N. et al. (2003). Interannual and seasonal variability of biomass burning emissions constrained by satellite observations, J. Geophys. Res., 108(D2), 4100, doi:10.1029/2002JD002378.

Edwards, D. P., et al. (2006). Satellite-observed pollution from Southern Hemisphere biomass burning, J. Geophys. Res., 111, D14312, doi:10.1029/2005JD006655.

Feingold, G. et al. (2005). On smoke suppression of clouds in Amazonia, Geophys. Res. Lett., 32, L02804, doi:10.1029/2004GL021369.

Forster, P. et al. (2007). Changes in Atmospheric Constituents and in Radiative Forcing. In: Climate Change 2007: The Physical Science Basis. Contribution of Working Group I to the Fourth Assessment Report of the Intergovernmental Panel on Climate Change [Solomon, S. et al. (eds.)]. Camb.Univ. Press, Camb., United Kingdom and New York, NY, USA.

Fraser, R.H. et al. (2000). Hotspot and NDVI differencing synergy (HANDS): A new technique for burned area mapping over boreal forest. Remote Sensing of Environment, 74, 362–376.

Freiman, M. T., and Piketh, S. J. (2003). Air transport into and out of the industrial Highveld region of South Africa, J. Appl. Meteorol., 42, 994–1002, doi:10.1175/1520-0450(2003)042<0994:ATIAOO>2.0.CO2.

Giglio, L. et al. (2009). An active-fire based burned area mapping algorithm for the MODIS sensor, Remote Sens. Environ., 113, 408–420, doi:10.1016/j.rse.2008.10.006.

Giorgi, F. et al. (2012). RegCM4: model description and preliminary tests over multiple CORDEX domains. Clim Res 52:7–29.

Hansen, J. et al. (1997), Radiative forcing and climate response, J. Geophys. Res., 102(D6), 6831–6864, doi:10.1029/96JD03436.

Haywood, J., and O. Boucher (2000). Estimates of the direct and indirect radiative forcing due to tropospheric aerosols: A review, Rev. Geophys., 38(4), 513–543, doi:10.1029/1999RG000078.

Helas, G and Pienaar, J.J. (1996). Biomass burning emissions. (Chapter 3 in: Air pollution and its impacts on the South African highveld, G Held, BJ Gore, AD Surridge, GR Tosen, CR Turner and RD Walmsley, eds), 12-15, Environ. Sci. Assoc., Cleveland, 144 pp.

Jacobson, M. Z., and Kaufman, Y. J. (2006). Wind reduction by aerosol particles, Geophys. Res. Lett., 33, L24814, doi:10.1029/2006GL027838.

Jiang, H., and Feingold, G. (2006). Effect of aerosol on warm convective clouds: Aerosol-cloud-surface flux feedbacks in a new coupled large eddy model, J. Geophys. Res., 111, D01202, doi:10.1029/2005JD006138.

Johnson, B. T. et al. (2004). The semi-direct aerosol effect: Impact of absorbing aerosols on marine stratocumulus, Quat. J. Roy. Meteor.Soc., 130(599), 1407–1422, doi:10.1256/qj.03.61.

Kaufman, Y. J., and Koren, I. (2006). Smoke and pollution aerosol effect on cloud cover, Science, 313, 655– 658.

Khoder, M. I. (2002). Atmospheric conversion of sulfur dioxide to particulate sulfate and nitrogen dioxide to particulate nitrate and gaseous nitric acid in an urban area.Chemosphere 49, 675-684.

Koch, D. and Genio, A. D. (2010). Black carbon semi-direct effects on cloud cover: review and synthesis, Atmos. Chem. Phys., 10, 7685–7696, doi:10.5194/acp-10-7685-2010.

Koren, I. et al. (2004). Measurement of the effect of Amazon smoke on inhibition of cloud formation, Science, 303(5662), 1342 – 1345, doi:10.1126/science.1089424.

Lamarque, J.-F.et al. (2010). Historical (1850–2000) gridded anthropogenic and biomass burning emissions of reactive gases and aerosols: methodology and application, Atmos. Chem. Phys., 10, 7017–7039, doi:10.5194/acp-10-7017-2010.

Langmann, B. et al. (2009). Vegetation fire emissions and their impact on air pollution and climate, Atmos. Environ., 43, 107–116.

Lewis, A. C. et al. (2013). The influence of biomass burning on the global distribution of selected non-methane organic compounds, Atmos. Chem. Phys., 13, 851-867, doi:10.5194/acp-13-851-2013.

© University of Pretoria

Liousse C. et al. (2004). Deriving Global Quantitative Estimates for Spatial and Temporal Distributions of Biomass Burning Emissions, In "Emissions of Atmospheric Trace Compounds", edited by: Granier, C., Artaxo, P., and Reeves, C., Kluwer Academic Publishers, Dordrecht, The Netherlands, 544 pp.

Liousse, C. et al. (2010). Updated African biomass burning emission inventories in the framework of the AMMA-IDAF program, with an evaluation of combustion aerosols, Atmos. Chem. Phys., 25 10, 9631–9646, doi:10.5194/acp-10-9631-2010.

Magi, B. I. et al. (2009). Evaluation of tropical and extratropical Southern Hemisphere African aerosol properties simulated by a climate model, J. Geophys. Res., 114, D14204, doi:10.1029/2008JD011128.

Mallet, M. et al. (2009). Impact of dust aerosols on the radiative budget, surface heat fluxes, heating rate profiles and convective activity over West Africa during March 2006.AtmosChemPhys 9:7143−7160.

Markowicz, K. M. et al. (2003). Influence of relative humidity on aerosol radiative forcing: An ACE-Asia experiment perspective, J. Geophys. Res., 108, 8662, doi:10.1029/2002JD003066, D23.

Menon, S. et al. (2002).Climate effects of black carbon aerosols in China and India, Science, 297, 2250 – 2253.

Miller, R. L. and Tegen, I. (1998). Climate response to soil dust aerosols. J. Climate 11, 3247–3267.

Miller, R. L. et al. (2004b). Feedback upon dust emission by dust radiative forcing through the planetary boundary layer, J. Geophys. Res., 109, D24209, doi:10.1029/2004JD004912.

Miller, R.L. et al. (2004a).Surface radiative forcing by soil dust aerosols and the hydrologic cycle. J Geophys Res 109:D04203. doi:10.1029/2003JD004085.

Oshima, N. et al. (2012). Wet removal of black carbon in Asian outflow: Aerosol Radiative Forcing in East Asia (A-FORCE) aircraft campaign, J. Geophys. Res., 117, D03204, doi:10.1029/2011JD016552.

Perlwitz, J. and Miller, R. L. (2010). Cloud cover increase with increasing aerosol absorptivity: A counterexample to the conventional semi-direct aerosol effect, J. Geophys. Res., 115, D08203, doi:10.1029/2009JD012637.

Piketh, S.J. et al. (1996). Regional scale impacts of biomass burning emissions over southern Africa, Biomass Burning and Global Change, J. S. Levine (ed.), MIT Press, Cambridge, 320-326.

Qian, Y. et al. (2001). Simulation of anthropogenic sulphur over east Asia with a regional coupled chemistry-climate model. Tellus 53B, 171–191.

Qian, Y., and Giorgi, F. (1999). Interactive coupling of regional climate and sulfate aerosol models over eastern Asia, J. Geophys. Res., 104(D6), 6477–6499, doi:10.1029/98JD02347.

Ramanathan, V. et al. (2001). Aerosol, climate, and hydrological cycle.Science 294, 2119-2124.

Ramanathan, V. et al. (2005). Atmospheric brown clouds: impacts on South Asian climate and hydrological cycle. Proceedings of the National Academy of Sciences 102:5326–5333.

Ramanathan, V., and Ramana, M. V. (2005).Persistent, widespread, and strongly absorbing haze over the Himalayan foothills and the Indo-Gangetic Plains. Pure Appl. Geophys., 162, 1609–1626, ,doi 10.1007/s00024-005-2685-8.

Ramanathan, V., Carmichael, G. (2008). Global and regional climate changes due to black carbon. Nat Geosci 1:221–227.

Randles, C. A. and Ramaswamy, V. (2010). Direct and semi-direct impacts of absorbing biomass burning aerosol on the climate of southern Africa: a Geophysical Fluid Dynamics Laboratory GCM sensitivity study. Atmos. Chem. Phys. 10, 9819–9831.

Reid, J. S. et al. (2004). Real-time monitoring of South American smoke particle emissions and transport using a coupled remote sensing/box-model approach, Geophys. Res. Lett., 31, L06107, doi:10.1029/2003GL018845.

Reid, J. S. et al. (2009). Global monitoring and forecasting of biomass-burning smoke: Description and lessons from the Fire Locating and Modeling of Burning Emissions (FLAMBE) program, J. Sel. Topics Appl. Earth Obs. Rem. Sens., 2, 144–162.

Roberts, G. et al. (2005). Retrieval of biomass combustion rates and totals from fire radiative power observations: Application to southern Africa using geostationary SEVIRI imagery. J. Geophys. Res., 110, D21111, doi:10.1029/2005JD006018.

Roberts, G. et al. (2009). Annual and diurnal african biomass burning temporal dynamics, Biogeosciences, 6, 849–866, doi:10.5194/bg-6-849-2009.

Roelofs, G.J. et al. (2001). Analysis of regional budgets of sulfur species modeled for the COSAM exercise. Tellus Ser. B, 53(5), 673 – 694.

Scholes, R. J. et al. (1996). Emissions of trace gases and aerosol particles due to vegetation burning in southern hemisphere Africa, J. Geophys. Res., 101(D19), 23677–23682, doi:10.1029/95JD02049.

Sinha, P. et al. (2003). Distributions of trace gases and aerosols during the dry biomass burning season in southern Africa, J. Geophys. Res., 108(D17), 4536, doi:10.1029/2003JD003691.

Solmon, F. et al. (2006). Development of a regional anthropogenic aerosol model for climate studies: Application and validation over a European/African domain. Tellus B, 58, 51-72.

Stier, P. et al. (2007). Aerosol absorption and radiative forcing, Atmos. Chem. Phys., 7, 5237-5261, doi:10.5194/acp-7-5237-2007.

Streets, D. G. et al. (2003). An inventory of gaseous and primary aerosol emissions in Asia in the year 2000, J. Geophys. Res., 108, 8809, doi:10.1029/2002jd003093.

Swap, R. J. et al. (2002). The Southern African Regional Science Inititatve (SAFARI 2000): overview of the dry season field campaign. S. Afr. J. Sci. 98. 125-130.

Swap, R. J. et al. (2003). Africa burning: A thematic analysis of the Southern African Regional Science Initiative (SAFARI 2000), J. Geophys. Res., 108, 8465, doi:10.1029/2003JD003747.

Tesfaye, M. et al. (2011a). Aerosol climatology over South Africa based on 10 years of Multiangle Imaging Spectroradiometer (MISR) data, J. Geophys. Res., 116, D20216, doi:10.1029/2011JD016023.

Tesfaye, M. et al. (2011b). Effective Single Scattering Albedo Estimation using Regional Climate Model. In: South African Society for Atmospheric Sciences 27th Annual Conference 22 - 23 September 2011: The Interdependent Atmosphere, Land and Ocean, Pp 53-54.

Tesfaye, M. et al. (2013a). Evaluation of Regional Climatic Model Simulated Aerosol Optical Properties over South Africa Using Ground-Based and Satellite Observations, ISRN Atmospheric Sciences, vol. 2013, Article ID 237483, 17 pages, 2013. doi:10.1155/2013/237483.

Tesfaye, M. et al. (2013b). "Simulation of anthropogenic aerosols mass distributions and their direct and semi-direct effects over South Africa using RegCM4", in review.

Torres, O. et al. (2010). OMI and MODIS observations of the anomalous 2008–2009 Southern Hemisphere biomass burning seasons Atmos. Chem. Phys. 10 2505–13.

Tummon, F. et al. (2010). Simulation of the direct and semi-direct aerosol effects on the southern Africa regional climate during the biomass burning season, J. Geophys. Res., 115(D19), doi:10.1029/2009JD013738.

van der Werf, G. R. et al. (2006).Interannual variability in global biomass burning emissions from 1997 to 2004, Atmos. Chem. Phys., 6, 3423-3441, doi:10.5194/acp-6-3423-2006.

van der Werf, G. R. et al. (2010). Global fire emissions and the contribution of deforestation, savanna, forest, agricultural, and peat fires (1997–2009), Atmos. Chem. Phys., 10, 11707-11735, doi:10.5194/acp-10-11707-2010.

Winkler, J. et al. (2008).Evidence for large scale transport of biomass burning aerosols from sunphotometry at a remote South African site, Atmos. Environ., 42, 5569–5578, doi:10.1016/j.atmosenv. 2008.03.031.

Yu, H. et al. (2002). Radiative effects of aerosols on the evolution of the atmospheric boundary layer, J. Geophys. Res., 107(D12), 4142, doi:10.1029/2001JD000754.

Yue, X. et al. (2010a). Direct climatic effect of dust aerosol in the NCAR Community Atmosphere Model Version 3 (CAM3). Adv. Atmos. Sci., 27(2), 230–242, doi:10.1007/s00376-009-8170-z.

© University of Pretoria

Yue, X. et al. (2010b). Simulation of dust aerosol radiative feedback using the GMOD: 2. Dust-climate interactions, J. Geophys. Res., 115, D04201, doi:10.1029/2009JD012063.

Zhang, R. Y. et al. (2008). Variability in morphology, hygroscopicity, and optical properties of soot aerosols during atmospheric processing, P. Natl. Acad. Sci. USA, 105(30), 10291–10296.

Zhang, X. et al. (2012). Near-real-time global biomass burning emissions product from geostationary satellite constellation, J. Geophys. Res., 117, D14201, doi:10.1029/2012JD017459.

Zhang, Y. (2008). The Radiative Effect Of Aerosols From Biomass Burning On The Transition From Dry To Wet Season Over The Amazon As Tested By A Regional Climate Model: PhD thesis. Georgia Institute of Technology, United State.

© University of Pretoria

Chapter 7: Simulation of bulk aerosol direct and semi-direct effects in South Africa using RegCM4*

*This chapter needs to be cited as:

Tesfaye, M., J. Botai, V. Sivakumar and G. Mengistu Tsidu (2013e): "Simulation of bulk aerosol direct and semi-direct effects in South Africa using RegCM4", *J. Aerosol Air Qual Res., in review.*

© University of Pretoria

UNIVERSITEIT VAN PRETORIA
UNIVERSITY OF PRETORIA
YUNIBESITHI YA PRETORIA

Simulation of bulk aerosol direct and semi-direct effects in South Africa using RegCM4

M. Tesfaye[1,2*], J. Botai[1], V. Sivakumar[1,3], , G. Mengistu Tsidu[4]

Abstract: This study has used the 12 year runs of the Regional Climate Model RegCM4 to simulate the direct and semi-direct climatic effects of bulk aerosol over South Africa. The contribution of each constituent of the bulk aerosol to the total aerosol optical thickness (at 550 nm) showed that over the west and southwest areas of South Africa, desert dust particles are dominant. However, secondary sulfate aerosols and carbonaceous particles are mostly distributed over the eastern and northern regions of South Africa. The Short-Wave (SW) and Long-Wave (LW) Radiative Forcing (RF) of bulk aerosol shows a contrasting effect. Nevertheless, the magnitude of SW-RF exceeds that of the LW; therefore, the Net-RF (SW-RF+LW-RF) of bulk aerosol reduced the radiation absorbed by the surface via enhancing atmospheric radiative heating. In all the seasons, the bulk aerosol-radiation-climate interaction induced a positive feedback on net atmospheric radiative heating rate (up to +1 K/day). Over most areas of South Africa, the feedbacks from cloud cover are predominantly positive (up to +7 %) - with exceptions over southeast coastal areas that exhibited minimal reductions in CC (~ -0.5 to -2.2 %). The cloud cover enhancement and RF of aerosols cooperatively, induce a reduction in Surface Temperature (ST: ~ -0.2 K to -1 K) and Surface Sensible Heat Flux (SSHF: ~ -2 to -24 W/m^2). The ST and SSHF decreases lead to the reduction in PBL height (up to -100 m) and the surface pressure enhancement (up to +0.16 hPa). In all seasons, the maximum values of direct and semi-direct effects of aerosols have been noted across the Northern Cape Province. This area is dominated by the wind-eroded desert dust particles; thus, the South Africa environmental affairs need to give significant concern for mitigating the expansion of aridity and environmental degradations, in and around the Northern Cape regions.

[1]*Department of Geography, Geoinformatics and Meteorology, University of Pretoria, Pretoria 0002, South Africa*

[2]*National Laser Centre, Council for Scientific and Industrial Research, Pretoria 0001, South Africa*

[3]*Department of Physics, Addis Ababa University, Addis Ababa, Ethiopia*

[4]*School of physics, University of KwaZulu Natal, Durban 4000, South Africa*

**Correspondence to: M. Tesfaye: mela_20062@yahoo.com*

Keywords: Bulk aerosol; Aerosol-climate interactions; Aerosol radiative forcing; Aerosol semi-direct effects; Regional climate model; South Africa

1 Introduction

Studies reported elsewhere by the authors, examined the distribution, direct and semi-direct climatic effects of naturally induced desert dust particles (Tesfaye et al., 2013b), different species of aerosols which were induced from anthropogenic sectors (Tesfaye et al., 2013c) and biomass burning activities (Tesfaye et al., 2013d), in South Africa. These studies showed that the northern and eastern parts of South Africa (i.e., Gauteng, Mpumalanga, Limpopo and KwaZulu-Natal provinces) were the major local source areas for anthropogenic and biomass burning aerosols. Additionally, the authors have reported in Tesfaye et al., 2013b that the arid/semi-arid regions of the Northern Cape as well as the neighboring countries (particularly Namibia and Botswana) were the main source regions of wind eroded desert dust particles, in South Africa.

The above studies have also illustrated that, predominantly, the scattering of solar radiation by sulfates and small dust particles, as well as the shortwave absorption by Black Carbon (BC) and partially by dust and Organic Carbon (OC) particles (Tegen and Lacis, 1996; Andreae and Gelencser, 2006) were the main causes for the reduction of shortwave radiative flux at the surface. On the other hand, these absorptions enhance the atmospheric radiative heating. The work reported in Tesfaye et al. (2013b) also illustrates that the dust aerosol-long-wave interaction (especially those which were large in size: diameter $\geq$ 2.5 μm) plus their re-emission of thermal radiation, caused the enhancement and reduction of long-wave radiative flux at the surface and within the atmospheric column, respectively.

When we compare the radiative effects of different species of aerosols over South Africa (i.e., using the results of Tesfaye et al., 2013b, 2013c and 2013d), the maximal radiative forcing values (both at the surface and within the atmospheric column) were caused by dust particles. Subsequent to these, aerosols that were generated by anthropogenic activities showed an advanced radiative influence around the northern, central and eastern parts of South Africa than those particles from biomass burning sectors. Additionally, Tesfaye et al. (2013c and 2013d) showed that the total aerosol radiative forcing were not only dependent on physico-optical properties of its aerosol constituents; but also highly reliant on the fractional contributions of each aerosol species to the total (bulk) aerosol. Furthermore, these studies also illustrated that the climatic modifications that are induced, due to the presence of aerosols, were not reliant only on the aerosol burden level and its radiation perturbations; but they are rather a net product of complex and non-linear interactions and feedbacks among aerosols, radiation, and climatic fields.

Overall, the aforementioned studies (i.e., Tesfaye et al., 2013b, 2013c and 2013d) have provided insightful information regarding the direct and semi-direct effects of different aerosols which were attributed from particular sources, over South Africa. However, tropospheric aerosols which originated from different natural processes and anthropogenic activities never actually occur as individual species; but rather exist as a complex mixture with high variability in their spatial and temporal distributions (e.g., Jacobson, 2001). Therefore, the combined effects of all aerosols take place at the same time, but not necessarily in the same place. Moreover, when two or more aerosol types mix together, one may reinforce/outweigh the other aerosol's radiative effect (e.g., Haywood and Boucher 2000; Reddy et al., 2005a, 2005b; Jacobson, 2001). Thus, the magnitude (even sometimes the sign) of total (bulk) aerosol net radiative forcing is different from the individual aerosol species - which constitute the aerosol mixture (e.g., Jacobson, 2001). Apart from this, in Tesfaye et al. (2013c and 2013d), we have also noted that due to the non-linear feedback mechanisms of the climate system (especially cloud

© University of Pretoria

fields) to the aerosol radiative effects, one cannot simply sum-up the individual aerosol climatic effects to predict the overall consequence of multiple aerosol types. This means that the bulk aerosol direct and semi-direct climatic effects display another outcome which might concur/contrast with the individual aerosol climatic roles (e.g., Haywood and Boucher, 2000). Therefore, as indicated in previous studies (for e.g., Leibensperger et al., 2012; Giorgi et al., 2012 and references therein), in order to generate more realistic climatic role of aerosols and to reproduce the observed climate trends, it is important to consider all types of aerosols which originate from different activity sectors.

In this context, it becomes crucial to study the bulk aerosol climatic influences, over South Africa. Accordingly, in this study, using simulations with the Regional Climate Model version 4 (RegCM4; Giorgi et al., 2012); we have examined the seasonal mean direct and semi-direct effects of the total aerosols over South Africa. Unlike our previous studies (Tesfaye et al., 2013b, 2013c and 2013d), the present contribution provide the combined climatic influences of sulfate, BC and OC aerosols which originated from both anthropogenic and biomass burning activities together with wind-eroded desert dust particles. Thus, this study enriches the effort of understanding first-degree climatic influences of the total aerosols, in South Africa. Among several semi-direct impacts of aerosols, the present study particularly provides their climatic roles in terms of influencing: Surface Temperature (ST), Surface Sensible Heat Flux (SSHF), Net Atmospheric radiative Heating Rate (NAHR), Cloud Cover (CC), Planetary Boundary Layer height (PBL), Surface Pressure (SP) and surface wind fields ($\vec{W}$). The paper is organized as follows: brief descriptions of the experimental design plus some essential points about the model are given in section 2. While focusing on our area of interest (i.e., South Africa) the simulation results and discussion are presented in section 3. Finally, the summary of our findings and concluding points are given in section 4.

2 Model and Experimental Design

The International Centre for Theoretical Physics (ICTP)-RegCM4, which is interactively coupled with chemistry/anthropogenic aerosol-desert dust modules (Giorgi et al., 2012 and references therein), were used to examine the direct and semi-direct effects of bulk aerosol, in South Africa. A brief description of the model and emission inventories employed in this study (i.e., for anthropogenic emission: MACCity; Lamarque et al., 2010 and biomass burning: GFED3; van der Werf et al., 2010) were given by Tesfaye et al. (2013a). The simulation domain, resolutions, selected model physics parameterization schemes, dynamical and surface parameter time setups of the model plus time-dependent initial and lateral boundary conditions, implemented in this study, are the same as that of Tesfaye et al. (2013a). The domain topography and the geographical map of South Africa (with province boundaries) are shown in Fig.1. Our simulation includes various externally-mixed aerosol species that are primarily emitted from different activities, as well as aerosols that are formed in the atmosphere via chemical reactions/ageing processes. I.e., the simulation incorporates all four size categories of wind eroded desert dust particles (Zakey et al., 2006), different anthropogenic and biomass burning activities induced sulfur dioxide, SO_2 - which is a precursor of sulfate particles (SO_4^{-2}), hydrophobic and hydrophilic BC and OC aerosols (Solmon et al., 2006).

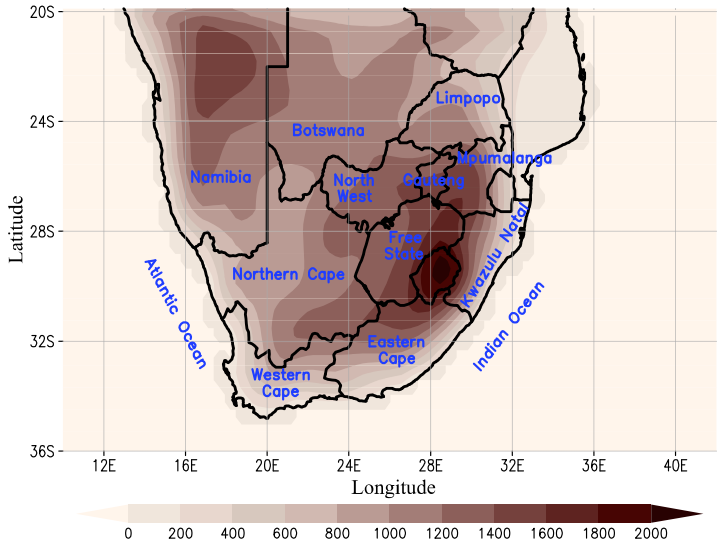

Fig. 1: Model domain, topography (unit: m) and geographical map of South Africa.

In order to capture the bulk aerosol radiative influences and their climatic signals, two parallel simulations which encompass a period from 1997 to 2008 were conducted. Afterward, the recent 11 year results were analysed in terms of different seasons. Of the two simulations one is the reference simulation (CNT), which includes all aforementioned aerosols but they are not radiatively interactive (i.e., CNT is the baseline simulation where aerosols are effectively inert tracers). Whereas, in the second experiment (AERO) all conditions were the same as in CNT, except that it considered the aerosol radiative effects and its climatic feedbacks (i.e. interactively coupled interactions among all aerosol components of RegCM4-radiation-climate were taken into account in AERO simulation). The aerosol radiative and climatic effects were captured using the differences between AERO and CNT runs (AERO minus CNT). Though our domain configuration includes regions outside South Africa (Fig. 1), the results discussed in this study are solely focused on the South African regions. Furthermore, we would like to note that the present study did not take into account the atmospheric chemical processes of aerosols that change an external mixture of particles into an internal mixture (e.g., Lesins et al., 2002; Fuzzi et al., 2006); this subject has been left for our future research. For additional information on the limitations of the RegCM4-aerosol model, the reader is referred to Tesfaye et al. (2013a).

3 Results and Discussion

In the following subsections: the contribution of individual aerosol species to the total bulk Aerosol Optical Depth (AOD at 550nm) (section 3.1), the bulk aerosol influence on surface and atmospheric radiative budget (section 3.2), as well as the change in different climatic variables in response to the bulk aerosol radiative effects (section 3.3) have been discussed. The radiative and climatic influences of aerosols are presented in terms of four different seasons, namely: summer (November to February: NDJF), early-winter (fall, March to April: MA), winter (May to July: MJJ) and early-summer (spring, August to October: ASO).

© University of Pretoria

3.1 The contribution of individual aerosols to the total AOD

Fig. 2 shows the eleven years' averaged results of the dust, sulfate and carbonaceous aerosol contributions to the total AOD (at 550nm), in South Africa. The sulfate particles' maximal contributions to the total AOD (~ 70 to 80%) were noted around the north-eastern parts of the Free State (Fig. 2b). Also, around its adjacent areas such as Gauteng, Mpumalanga, KwaZulu-Natal, central parts of the Free State and over the northern regions of the Eastern Cape Province, sulfate particles have contributed about 30 to 70% of the total AOD. While, over the eastern parts of Mpumalanga, the northern areas of Limpopo and in most areas of Gauteng, ~ 8.5 to 10% of the total AOD is due to carbonaceous (BC + OC) aerosols (Fig. 2c). Furthermore, over the remaining areas of these provinces plus in the wider region of KwaZulu-Natal and in some parts of North West and Free State; the carbonaceous particles contribute from 4 up to 8.5% of the total AOD. The results also have indicated that, in the Northern and Western Cape provinces, ~ 60 to 100% of the total AOD are due to wind eroded desert dust particles (Fig. 2a). In addition to these, over the remaining areas of South Africa (especially over the western parts of the Free State and North West provinces as well as in the northern parts of Limpopo), naturally induced dust particles contribute from 40 up to 60% of the total AOD. In general, due to the disparities in potential source regions of aerosols (Tesfaye et al., 2013b, 2013c and 2013d) and anticyclonic air mass movement (Fig. 2, also see Freiman and Piketh, 2003); the spatial distributions of aerosols in South Africa exhibited a unique feature.

Sulfate and carbonaceous aerosols are mostly distributed over the east and northern regions of South Africa (Fig. 2b and c). However, over the west and southwest areas of South Africa the sulfate and carbonaceous aerosol contributions are found to be negligible, but rather wind eroded desert dust particles becomes the dominant aerosol in these regions (Fig. 2a). Some provinces of South Africa, such as Limpopo, North West and Free State, are in-between the potential source regions of dust and industrial/biomass burning aerosols; therefore, these areas are exposed to a complex mixture of natural and anthropogenic aerosols which vary with season as a result of different prevailing winds. Even if the seasonal variation of dust, sulfate and carbonaceous aerosol contributions to the total AOD is not exhibited here, during our analysis we have seen that the spatial distribution of these aerosol contributions to the total AOD are similar to Fig. 2. However, in different seasons, the magnitude of dust, sulfate and carbonaceous aerosol contributions have shown a disparity of ~ ±6%, ~ ±13% and ~ ±45% respectively, relative to their annually averaged values. Since Biomass Burning (BB) activities are a major source of carbonaceous aerosols (Andreae and Merlet, 2001; Tesfaye et al., 2013d); the enhanced seasonal variation in carbonaceous aerosol optical depth contribution rises from the strong seasonal reliance of BB events.

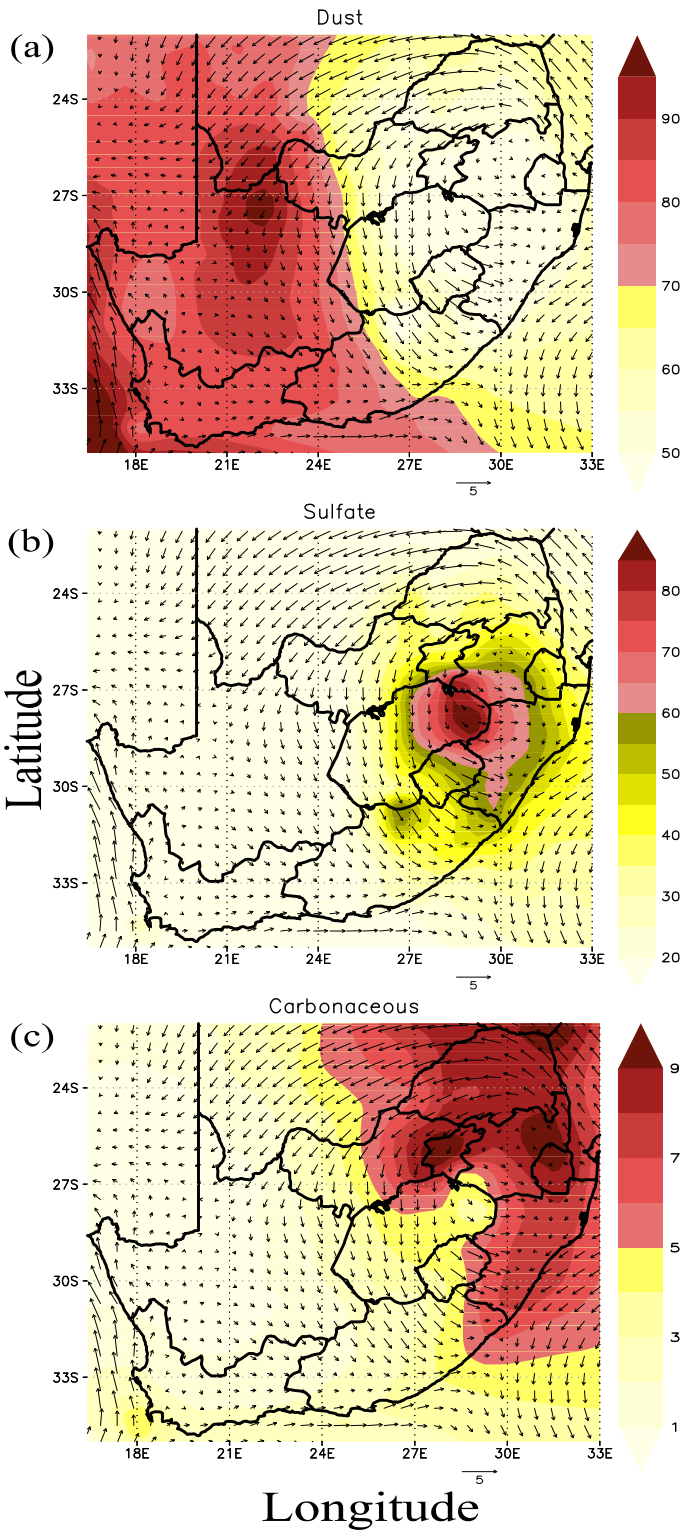

Fig. 2: The annual mean spatial distributions of (a) dust, (b) sulfate and (c) carbonaceous (BC + OC) aerosol contributions to the visible bulk aerosol optical depth (unit: %), superposed with the surface wind field (vector; the scale is indicated by the arrow to the lower right in unit of m/s). All results are averaged over 1998-2008.

3.2 Direct radiative forcing of aerosols

The signs plus the magnitudes of aerosols' direct radiative forcing indicate the level and the role of aerosols in inducing radiative cooling/warming on the surface-atmospheric system. In the following subsections the Short-Wave (SW), Long-Wave (LW) and the net (SW+LW) Radiative Forcing of aerosols at the SURface (SUR-RF) (section 3.2.1) and within ATMospheric column (ATM-RF) (section 3.2.2) are presented.

3.2.1 Short-, long-wave and net surface radiative forcing of aerosols

The seasonal mean spatial distributions of the total aerosols' SW, LW and net (SW + LW) surface radiative forcing

© University of Pretoria

over South Africa are depicted in column-(a) to column-(c) of Fig. 3, respectively. The results indicate that influences of both SW scattering and absorption of aerosols (e.g., Penner et al., 2001) jointly induce a reduction of net solar radiative flux at the surface (Fig. 3a). The maximal SW-SUR-RF of aerosols appeared during the course of spring and summer seasons. During fall and winter seasons, the aerosol SW-SUR-RF (Fig. 3a) exhibit moderate and minimal values, respectively. Throughout the seasons, the maximum negative values of SW-SUR-RF are observed in the northern and central regions of the Northern Cape Province. Around this region, during ASO and NDJF, the SW-SUR-RF of aerosols was in the range of -25 W/m^{2}to -35 W/m^2. Whereas, moderate (~ -15 W/m^2 to -20 W/m^2) and minimal (~ -8 W/m^2 to -15 W/m^2) negative values of SW-SUR-RF of aerosols are found during MA and MJJ, respectively. Over the northern areas of the Free State, the southern regions of Limpopo, the coastal areas of KwaZulu-Natal and across the Highveld zones of Gauteng and Mpumalanga; starting from ASO throughout summer and fall, the SW-SUR-RF of aerosols in the range of ~ -8 W/m^2 to -21 W/m^2 are found. However, over these areas, reduced values of SW-SUR-RF (~ -3 W/m^2 to -8 W/m^2) are appeared during MJJ (Fig. 3a).

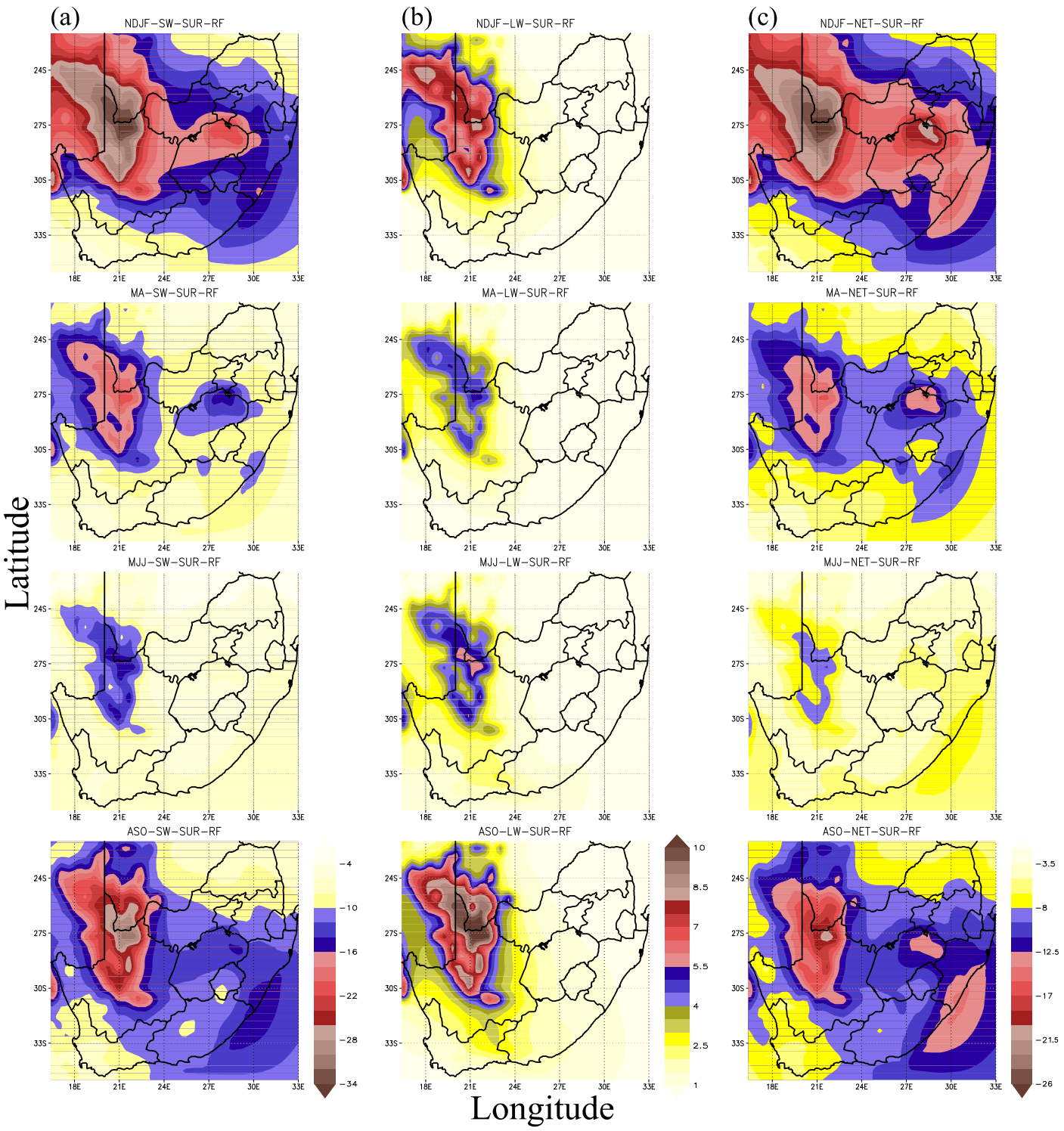

Fig. 3: Eleven year averaged (i.e., 1998-2008) seasonal mean spatial distributions of surface radiative forcing of total aerosols, in South Africa; column: (a) SW, (b) LW and (c) net (SW+ LW) (units: W/m^2). Each row represent the four seasons of the year (see the abbreviated words at the top of each figure).

Overall, by correlating the results of Fig. 2 and Fig. 3a; it is clearly shown that the highest level of SW-SUR-RF over South Africa is due to naturally-induced desert dust particles. Following dust dominating regions, a significant SW radiative flux perturbation of aerosols are found in areas of South Africa which are dominated by sulfate aerosols (see Fig. 2) as well as over the east coastal zones of South Africa, where anticyclonically driven aerosol plumes exit South Africa towards the Indian Ocean (e.g., Freiman and Piketh, 2003). As stated in different studies (e.g., Hess et al. 1998; Highwood et al. 2003; Tesfaye, 2009), the long-

© University of Pretoria

wave direct radiative forcing of aerosols are considerably important for particles which are larger in size. Thus, the dust particles, in addition to their effect on solar radiative transfer, also have a significant role in perturbing the long-wave radiation (e.g., Highwood et al., 2003; 2005; Solmon et al., 2008; Tesfaye et al., 2013b). Our simulation encompassed the dust particles' LW emissivity/absorptivity influences (Solmon et al., 2008). The results in Fig. 3b show that the interaction between the dust aerosols and LW radiation, plus their re-emission of thermal radiation, cooperatively, induced the enhancement of LW radiative flux at the surface; which contrast the SW-SUR-RF of aerosols.

In general, the spatio-seasonal variations of LW-SUR-RF - displayed in Fig. 3b - are quite similar with that of the results which are found in Tesfaye et al. (2013b). Throughout the year, the maximum LW-SUR-RF of dust particles have been noted around their source regions (i.e., over the northern and central areas of the Northern Cape Province). The highest levels of LW-SUR-RF (with magnitude in ranges of ~ 6.5 to 10 W/m^2) are found during the drier season of ASO and windy period of NDJF. During the course of MA, aligned with the gradual decline of the dust load (e.g., Tesfaye et al., 2013b) - the LW-SUR-RF of dust particles also exhibit its reduced values. The dry weather conditions of winter (relative to autumn) facilitate the production and distribution of dust particles (Tesfaye et al., 2011); thus, the LW-SUR-RF in MJJ is slightly larger than MA (Fig. 3b). Further clarifications in association with the seasonal variation of LW-SUR-RF of dust particles, the reader are referred to Tesfaye et al. (2013b).

The overall role of aerosols on perturbing the total radiative flux balance at the surface (NSUR-RF = SW-SUR-RF + LW-SUR-RF) are shown in Fig. 3c. Owing to the dominant SW influences of small size particles which have the largest cross-sectional area per unit mass; the negative SW-SUR-RF of aerosols strongly exceeds the positive values of LW-SUR-RF throughout the seasons (see Fig. 3a and b). Thus, over the entire domain the total (bulk) aerosol NSUR-RF exhibited a negative value which is analogous in its spatio-seasonal variations as that of the SW-SUR-RF, except in magnitude (Fig. 3c). In the Northern Cape Province, where the dust particles are the principal constituent of the bulk aerosol (Fig. 2), the higher level of NSUR-RF of aerosols which are within the ranges of ~ -14 to -20.5 W/m^2 and ~ -21 to -26 W/m^2 are found during spring and summertime, respectively. Whereas, the least pronounced values of NSUR-RF of aerosols are observed during MJJ (i.e., the magnitude of NSUR-RF during MJJ is reduced by about 60% relative to NDJF). Furthermore, in areas of South Africa which are found within the longitudinal range of 25°E to 33°E, the LW-SUR-RF of dust particles are insignificant (relative to the west and southwest areas of South Africa, Fig. 3b). Therefore, the magnitudes and distributions of NSUR-RF of aerosols, in these longitudinal ranges, are found to be quite comparable with their SW-SUR-RF (Fig. 3c). Finally, we would like to remark that, all the aforementioned seasonal variations of the total aerosols' direct radiative influences are primarily correlated with the burden levels of the individual aerosols which constituent the bulk aerosol. Therefore, for more information regarding the spatio-seasonal variations of different aerosol species which are attributed from natural/anthropogenic activities over South Africa and other related issues, the readers are referred to Tesfaye et al. (2013b, 2013c and 2013d).

3.2.2 Short-, long-wave and net atmospheric radiative forcing of aerosols

Generally, the aerosol atmospheric radiative forcing (ATM-RF) is computed based on the difference in aerosol radiative forcing at the Top-Of-the-Atmosphere (TOA-RF) and at the surface (SUR-RF) (i.e., ATM-RF = TOA-RF - SUR-RF). The spatio-seasonal variation of the SW, LW and net atmospheric radiative forcing of the bulk aerosol are presented in Fig. 4column (a), (b) and (c), respectively. As shown in Fig. 4a, over the entire domain, the SW-ATM-RF of aerosols exhibited positive values (i.e., the interaction of aerosols with SW radiation induce radiative heating within the atmospheric column). The atmospheric radiative heating of aerosols in South Africa are primarily contributed by BC as well as dust and OC particles, which have a partial SW radiation absorption nature (e.g., Miller and Tegen, 1998; Andreae and Gelencser, 2006;Solmon et al., 2008). As previously stated, our simulation includes the long-wave influences of wind-eroded dust particles. Thus, the results in Fig. 4b show that in contrast to the SW-ATM-RF of aerosols, the dust particles rather promote LW-radiative cooling within the atmosphere.

Similar to the SW-SUR-RF of aerosols (Fig. 3a), throughout the seasons, the SW-ATM-RF (Fig. 4a) also illustrate its highest values around the Northern Cape areas of South Africa. Over this province, starting from the dry season of ASO through the windy period of summertime, the higher values of SW-ATM-RF that are within maximum ranges of ~ 15 to 26 W/m^2 are found. On the other hand, during these seasons (i.e., ASO and NDJF), in areas of South Africa which are bounded within the longitudinal range of 25°E to 33°E, the SW-ATM-RF exhibit values that varies from 2 to 8 W/m^2. Also, within this longitudinal range (i.e., 25°E to 33°E) the maximal values of SW-ATM-RF of aerosols that varies from 5 to 8 W/m^2 have been noted in the southern areas of Limpopo, the coastal regions of the Eastern Cape and over wider areas of Highveld regions and KwaZulu-Natal (Fig. 4a).

Over the central and northern parts of the Northern Cape Province, the high level of LW-ATM-RF, in the range of -6 to -10 W/m^2, is observed during ASO and NDJF (Fig. 4b). In the course of fall and winter, in and around the Northern Cape areas, the LW-ATM-RF that varies from -2 to -6 W/m^2 are found. The LW-ATM-RF primarily depends on the spatial distribution of dust particles, especially in dust particles that are large in size (e.g., Tegen and Lacis, 1996; Tesfaye et al. 2013b). Nevertheless, due to various removal processes of aerosols that are more effective in larger particles, such as dry deposition through gravitational and turbulent settling (e.g., Zakey et al., 2006; Seinfeld and Pandis, 2006); the distribution of large-size dust particles are more confined in and around their source regions (Tesfaye et al. 2013b). As a result, throughout the climatic seasons, in areas of South Africa, which are within the longitudinal range of 25°E to 33°E, the LW-ATM-RF values varied from -0.5 to -1.7 W/m^2. These values are exceedingly lower (~ by about 82%) than the magnitudes of LW-ATM-RF, that are noted in the west and southwest parts of South Africa (Fig. 4b).

© University of Pretoria

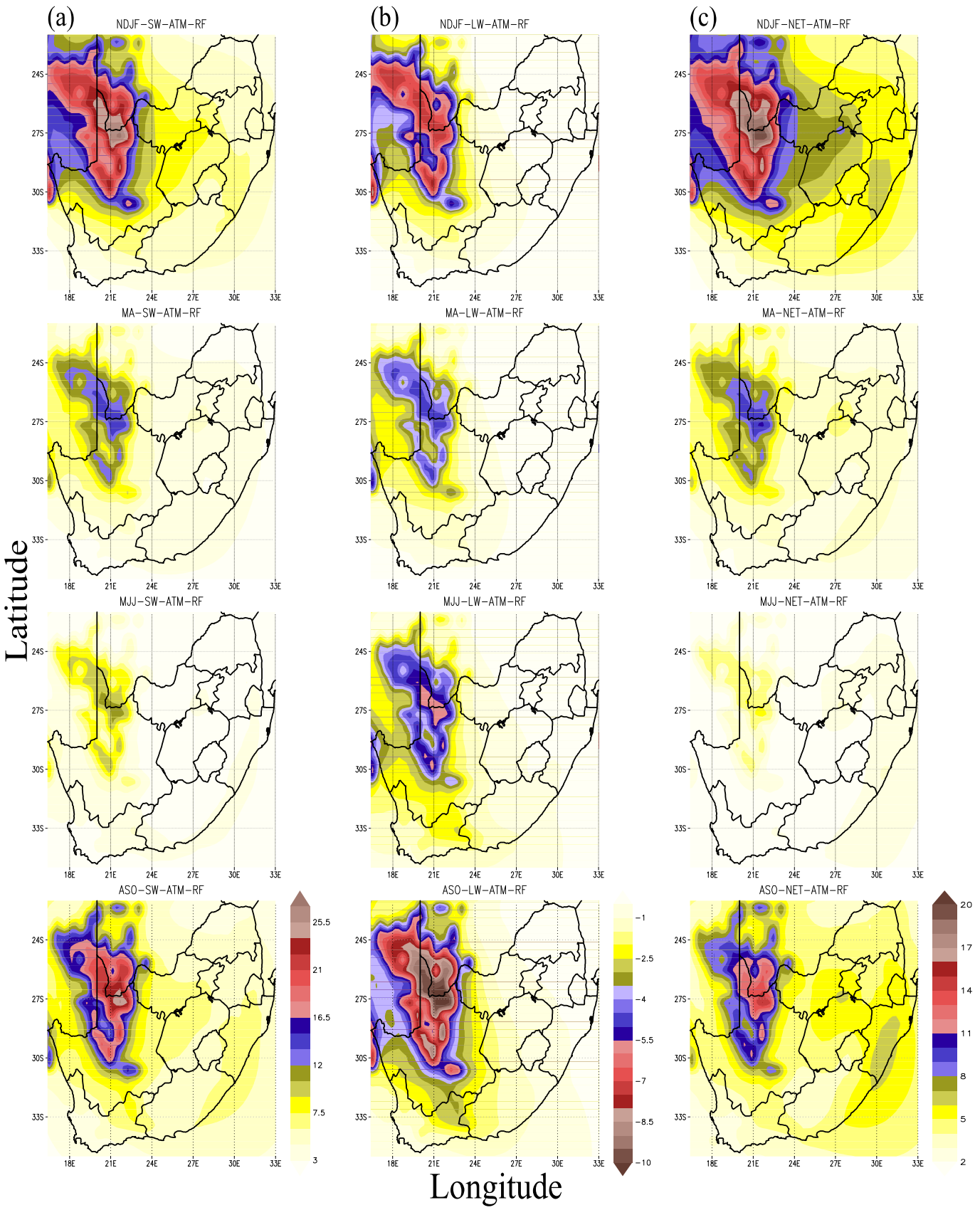

Fig. 4: The same as Fig. 3, but for the radiative forcing of aerosols within the atmospheric column: (a) SW, (b) LW and (c) net (SW + LW) (units: W/m^2).

The results in Fig. 4a and b also have shown that throughout the seasons, the magnitude of SW-ATM-RF is ~ 2.5 times higher than that of LW-ATM-RF. As a result, over the entire domain the Net ATMospheric Radiative Forcing (NATM-RF = SW-ATM-RF + LW-ATM-RF) of aerosols illustrate positive values (Fig. 4c). This mirrors that the overall radiative role of the bulk aerosol in South Africa: reducing the net radiation is absorbed by the surface (Fig. 3c) and enhancing the radiative heating within the atmosphere (Fig. 4c). Regarding the magnitudes of the NATM-RF, higher values are still noted in areas where the desert dust particles are dominant (i.e., areas which are in and around the Northern Cape: Fig. 2). During the course of spring and summertime, over these arid/semi-arid regions of South Africa, high values of NATM-RF - which are within a maximal range of 8 to 19 W/m^2 - are found. During this season (ASO and NDJF), in areas of South Africa which are burdened by anthropogenic and biomass burning aerosols (i.e., over Highveld regions, Limpopo and KwaZulu-Natal: Fig. 2) as well as over the coastal areas of Eastern Cape; NATM-RF values within a range of 2 to 8 W/m^2 are noted (Fig. 4c).

The LW-ATM-RF - in areas of South Africa which are within longitudinal range of 25°E to 33°E - is found to be insignificant (see Fig. 4b); thus, the magnitudes and distributions of NATM-RF of aerosols, in these areas, are almost similar with their SW-ATM-RF. Furthermore, throughout the whole domain,

© University of Pretoria

moderate and minimal values of NATM-RF are found during MA and MJJ, respectively (Fig. 4c). Here, we would like to remark that further than the aerosol physico-optical characteristics and their spatio-seasonally variable concentrations, the incoming solar radiation intensity and surface albedo spatio-seasonal variations also have some influence in determining the magnitude of aerosol-RF (e.g., Forster et al., 2007; Di Biagio et al., 2012). Generally, in response to these radiative effects of aerosols, the adjustment in different climatic variables take place (e.g., Miller and Tegen, 1998; Miller et al., 2004a; Ramanathan and Carmichael, 2008; Zhang, 2008). Some of the climate feedbacks of the bulk aerosol are discussed in the next section.

3.3 Climate responses

In this section the feedbacks of the climate system to the aerosol radiative effects are addressed. Changes in different climatic variables due to the presence of radiatively interactive aerosols are captured by comparing the results of AERO and CNT simulations (see section 2). In the next subsection, the change in Surface Temperature (ΔST) and Surface Sensible Heat Flux (ΔSSHF) are addressed. The alteration in Net Atmospheric radiative Heating Rate (ΔNAHR) and Cloud Cover (ΔCC) are provided in section 3.3.2. Finally, the effects of aerosols on Planetary Boundary Layer height (ΔPBL), Surface Pressure (ΔSP) along with the 10m wind field ($\overrightarrow{\Delta W}$) are discussed in section 3.3.3.

3.3.1 The effects of aerosols on surface temperature and surface sensible heat flux

The aerosol-radiation-climate interaction induced ST (K) and SSHF (W/m^2) changes are depicted in Fig. 5 column-(a) and (b), respectively. The results show that, in response to the negative NSUR-RF of aerosols as well as their semi-direct effect induced CC enhancement (Fig. 6b) which reinforce the aerosols' surface radiative cooling tendencies (e.g., Haywood and Boucher, 2000; Ramanathan et al., 2001; Zhang, 2008), both ST and SSHF displayed a reduction (Fig. 5a and b). The largest range of cooling (i.e., ΔST ~ -0.5 K to -1 K) appeared around the Northern Cape regions, during extended summer (i.e., NDJF and MA). Also during these seasons, over wide areas of the North West province, in eastern parts of Mpumalanga as well as across Free State and Limpopo, intermediate values of the reduction in ST that varied from -0.1 K to -0.5 K are predicted (Fig. 5a).

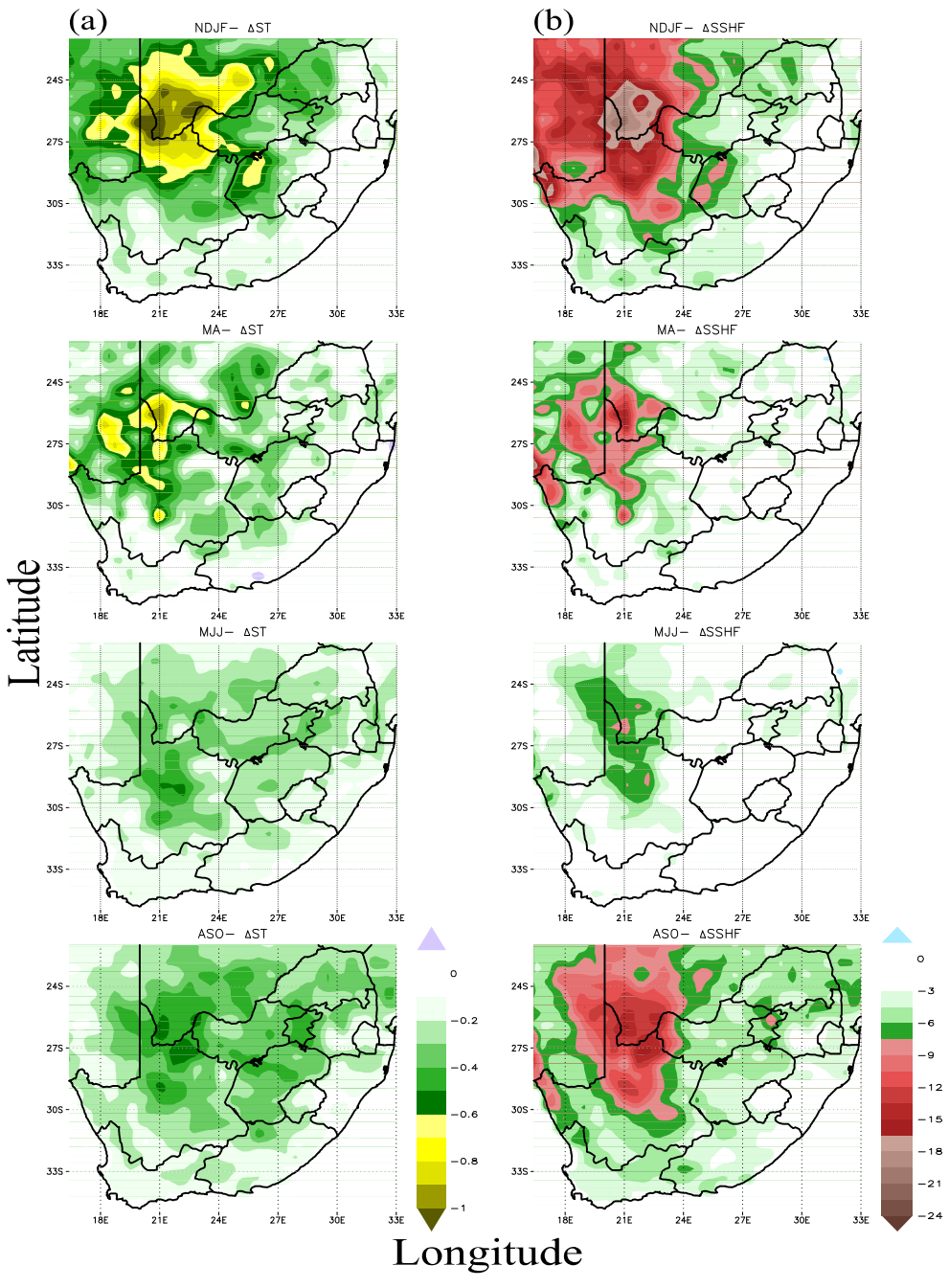

Fig. 5: Seasonal mean spatial distributions of changes in (a) surface temperature (K) and (b) surface sensible heat flux (W/m2). All results are averaged over 1998-2008 and, each row represent the four seasons of the year (see the abbreviated words at the top of each figure).

Spring and winter (i.e., extended winter: MJJ and ASO) in South Africa are more dry than the extended summer seasons. Therefore, during extended winter the reinforcement of surface radiative cooling by the aerosols' semi-direct effects induced cloud cover enhancement is not as much as that of the extended summer season (see Fig. 6b for the seasonal variation of ΔCC). Due to this phenomenon, even if the higher values of NSUR-RF of aerosols are noted during ASO (Fig. 3c), the ΔST during extended winter are generally moderate relative to the extended summer seasons (Fig. 5a). The spatial correlation between the dynamical feedbacks of aerosols and ΔST/ΔSSHF are found to be relatively high during MJJ and ASO (see, section 3.3.3). Particularly, the spatial correlation among the change in zonal component of the surface wind field (i.e., ΔU) with that of ΔST and ΔSSHF is ~ 0.75 and 0.8, respectively; thus, the ΔST and ΔSSHF during extended winter encompassed a wider area than the extended summer seasons. Therefore, over wider areas of South Africa (excluding the east and south east coastal regions), the ΔST in the range of -0.1 K to -0.56 K are noted during MJJ and ASO (Fig. 5a). During this period, the maximal values of ΔST that varies from -0.42 K to -0.56 K are noted in the northern parts of the Northern Cape as well as across the North West, Gauteng and Free State provinces.

© University of Pretoria

The surface radiation flux perturbations which are induced by the direct and semi-direct effects of atmospheric aerosols, also trigger changes on the land-atmosphere system energy exchange (e.g., Ramanathan and Ramana, 2005; Tesfaye et al., 2013b, 2013c and 2013d; Zhang, 2008). This includes changes on the energy transfer from the surface to the atmosphere in the form of net thermal radiation as well as sensible and latent heat fluxes (e.g., Miller et al., 2004a). Generally, the mechanism through which the surface energy components respond to the direct and semi-direct radiative influences of aerosols involves various conditional circumstances (e.g., Miller et al., 2004a; Ramanathan and Ramana, 2005; Boer, 1993). Over the land, the change in sensible heat and net upward long-wave fluxes are more important (e.g., Miller et al., 2004a; Zhang, 2008).

The surface cooling (or heating) incidences that are promoted due to the radiative influences of aerosols may correspondingly, cause the reduction (or increment) in upward transport of SSHF (e.g., Liu et al., 2004; Tesfaye et al., 2013b, 2013c and 2013d; Zhang, 2008; Boer 1993; Miller and Tegen, 1998; Yu et al. 2002; Slingo et al., 2006; Shell and Somerville, 2007; Mallet et al. 2009; Yue et al., 2010a, 2010b). Therefore, in alignment with the spatial patterns of ST reductions throughout NDJF, MA, MJJ and ASO, respectively, a change in SSHF that varied from -2 to -24 W/m^2, -2 to -16 W/m^2, -1 to -8 W/m^2 and -2 to -14 W/m^2 are found (Fig. 5b). For all seasons, the maximal negative amplitudes of ΔSSHF are mainly located in the northern and central areas of the Northern Cape Province, similar to that of the ΔST. Meanwhile, the intermediate and minimal negative values of the ΔSSHF are found in the southwest areas of South Africa and in regions which are bounded within the longitudinal range of 25°E to 33°E (Fig. 5b).

The annual averaged spatial correlation between NSUR-RF of aerosols with ΔST and ΔSSHF is 0.67 and 0.72, respectively; also correlations among ΔST and ΔSSHF is ~ 0.9. In addition, the spatial correlation of ΔCC with ΔST and ΔSSHF, correspondingly, illustrate values of -0.87 and -0.72. The change in cloudiness is one of the feedback mechanisms of the climate system to the radiative effects of aerosols (Fig. 6b, see section 3.3.2). Thus, as previously indicated, the enhancement in CC correspondingly results in the reduction of incoming solar radiation; which in turn, reinforce the surface radiative cooling tendencies of aerosols (e.g., Gu et al., 2006; Zhang, 2008). The above correlations also confirmed that along with the aerosols' direct radiative influence, their semi-direct effect induced ΔCC also have a crucial role in promoting the change in ST plus SSHF. The annual mean regionally averaged (i.e., averaged over the areas of South Africa: -35° – -22°S, 16° – 33°E) values of ΔST (and ΔSSHF), respectively, showed values of -0.23 K (-4.4 W/m^2). These regionally average values indicate that, the overall role of aerosols in South Africa is to promote surface cooling and reduce the upward transport of SSHF from the surface into the atmosphere.

3.3.2 The effects of aerosols on net atmospheric radiative heating rate and cloud cover

Aerosol induced changes in columnar averaged Net (short- plus long-wave) Atmospheric radiative Heating Rate (ΔNAHR) and column integrated Cloud Cover (ΔCC) in the lower troposphere (~ below 650hPa) are, correspondingly, shown in Fig. 6a and b. The computation of net atmospheric radiative heating rate include the radiative feedbacks of all climatic components (i.e., aerosols, clouds, water vapor, the underlying surface and other trace gases in the atmospheric column). Therefore, by comparing the NAHR obtained from AERO to that of the CNT simulation, the influences of radiatively interactive aerosols on NAHR are captured. Due to the predominant shortwave absorption influences of aerosols (see section 3.2.2); their radiative feedbacks results in an enhancement of NAHR within the lower parts of troposphere (Fig. 6a). Throughout the season, maximal values of the ΔNAHR appeared around the dust aerosol dominating zones of South Africa (Fig. 2), particularly in areas that stretch from the northern to the central parts of the Northern Cape Province. Tesfaye et al. (2013b) demonstrated that the dust aerosol concentrations are higher during ASO and NDJF; therefore, during these seasons the ΔNAHR exhibit advanced values which vary from 0.4 to 1 K/day (Fig. 6a). Moreover, across the Highveld zones of South Africa, the southern parts of Limpopo as well as over the coastal regions of KwaZulu-Natal and Eastern Cape, the ΔNAHR which varied from ~ 0.1 to 0.3 K/day are noticed, during the ASO and NDJF. Relative to the aforementioned seasons, reduced values of ΔNAHR are found during MA and MJJ. Throughout fall and winter - in the northern and central regions of the Northern Cape Province - the ΔNAHR displayed values that varied from ~ 0.3 to 0.5 K/day (Fig. 6a). In addition, over wide areas of Gauteng and KwaZulu-Natal - the ΔNAHR illustrate values that vary from ~ 0.05 to 0.3 K/day. Beside these, during MJJ, over a narrow area in the southern part of the Northern Cape, a minimal reduction in ΔNAHR (~ -0.07 to -0.14 K/day) is noted.

In response to the ΔNAHR and other climatic feedbacks of aerosols, the adjustment in thermal structure, hydrological fields and dynamical states of the atmosphere may occur (e.g., Menon et al., 2002;Ramanathan et al., 2001; 2005; Jiang and Feingold, 2006; Zhang, 2008). Changes in columnar integrated low-level cloud cover (clouds which are formed below ~ 650 hPa; ΔCC) that are induced by the aerosol-radiation-climate interactions are shown in Fig. 6b. Our results (Fig. 6b) show that over wide areas of the Northern Cape, North West, Free State, Limpopo and Gauteng provinces, the presence of radiatively interactive aerosols has resulted in an enhancement of CC, during summer (~ 1 to 7%), fall (~ 1 to 6%) and spring (~ 0.5 to 3.5%). The increases in CC during winter (~ 0.5 to 3.5%) mainly include broader areas of the Northern Cape and Free State provinces. In contrast, in some areas of Mpumalanga as well as over the boundaries of Free State and KwaZulu-Natal, a slight reduction in CC (~ -0.7 to -1.4 %) appeared during NDJF. Also, during the course of fall, negative values of the ΔCC (with ~ -1 to -2.2 % ranges) are noted in the west and southwest areas of the Northern Cape Province and other narrow scattered areas of South Africa. Across the western parts of Mpumalanga and, the coastal areas of KwaZulu-Natal and the Eastern Cape Province, the reduction in CC (~ -0.5 to -2.2 %) are noticed during extended winter seasons (especially throughout MJJ, Fig. 6b).

MJJ and ASO are the dry seasons in South Africa (i.e., there is a scarcity of cloud and water vapour during extended winter); therefore, as indicated above the CC responses are higher during the wet seasons of extended summertime than that of the extended dry seasons (see Fig. 6b). This shows that the amplitudes of aerosols' semi-direct influences on CC are not only dependent on the seasonal variations in aerosol radiation perturbations (Fig. 3 and 4); however are also reliant on seasonally variable cloud and

© University of Pretoria

water vapour abundances. These results are similar with the findings of Tesfaye et al. (2013b and 2013c). Besides these, we have noted that, the spatial correlation among ΔCC and ΔNAHR are not strong (i.e., their spatial correlation coefficient is < 0.5).

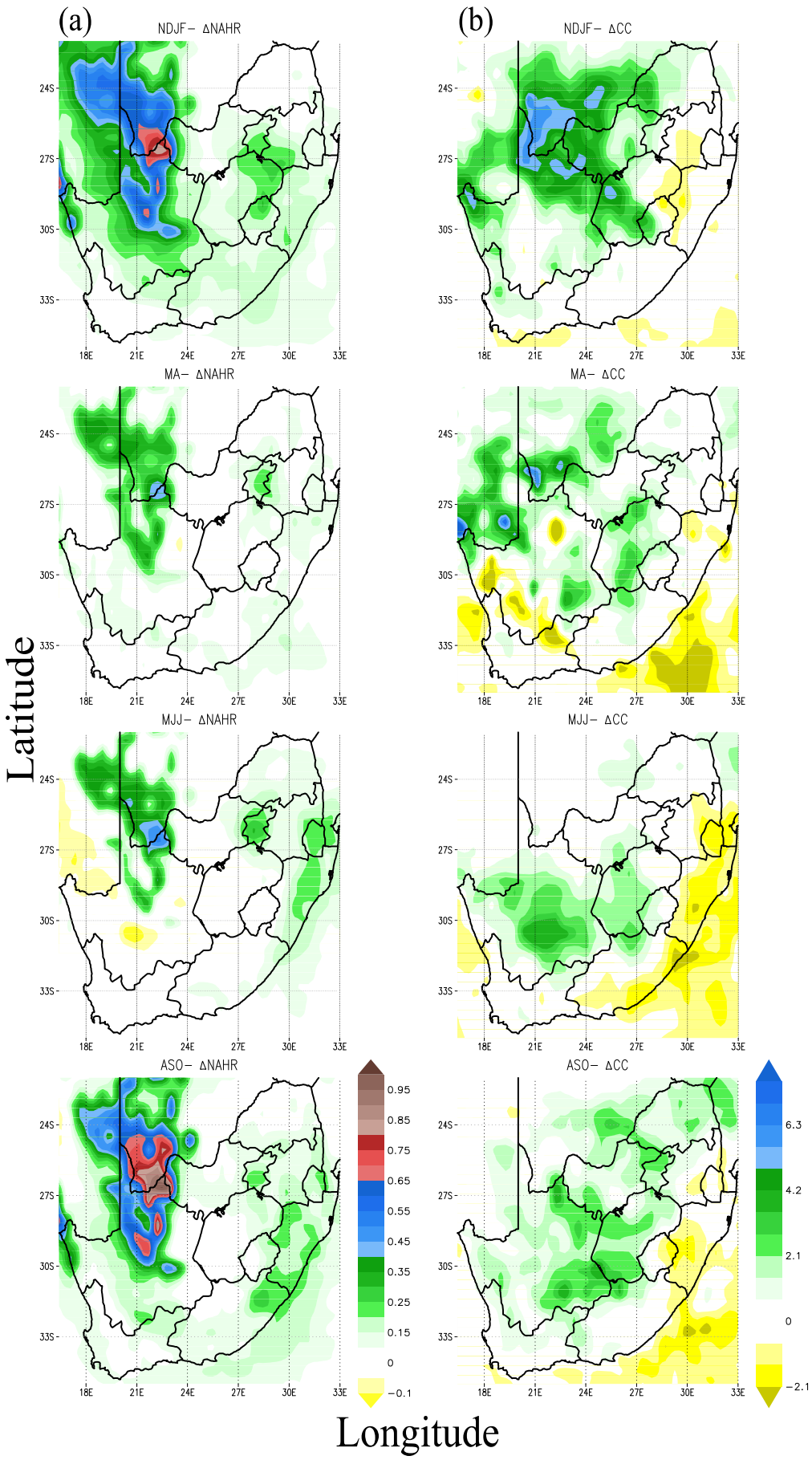

Fig. 6: Same as Figure 5 but for the change on low-level (a) column average net atmospheric radiative heating rate (K/day), (b) column integrated cloud cover (%).

As shown in Fig. 6a, attributed to the SW absorbing nature of BC, dust and OC particles, the bulk aerosol in South Africa predominantly stimulate the enhancement of NAHR. In such occasions, the nonlinear feedbacks of clouds are not only dependent on ΔNAHR; but rather also reliant on the vertical location of the aerosol layer with respect to clouds (e.g., Cook and Highwood, 2004; Johnson et al., 2004; Feingold et al., 2005) as well as various climatic conditions of the region considered (e.g., Allen and Sherwood, 2010; Koch and Genio, 2010). In addition, the studies of Ramanathan et al. (2001), Menon et al. (2002); Douville et al. (2002), Feingold et al. (2005), Jiang and Feingold (2006) and Perlwitz and Miller (2010); Zhang, (2008) illustrated that the influences of aerosols on moisture flux and pressure gradient (atmospheric instability) also have a significant role in determining the overall CC responses to the aerosol heated layers. For further details of the complex physical mechanisms through which the ΔCC occurs, please refer to Perlwitz and Miller (2010), Koch and Genio (2010) and references therein.

As mentioned previously, seasonally variable cloud and water vapour amounts are one of the factors that determine the magnitudes of ΔCC. Thus, in areas north and south of ~ 30°S the maximal ΔCC were noted during NDJF and MJJ, respectively (see Fig. 6b). These results are in conjunction with the two main rainy seasons of South Africa; i.e., areas of South Africa that are north of ~ 30°S - NDJF (summer) is their rainy season. Whereas, regions that are south of ~ 30°S have a Mediterranean climatic feature, therefore, MJJ is their rainy season. Additionally, the simulation results illustrate that the signs plus spatio-seasonal distributions of changes in low-level Cloud Liquid-Water amount (ΔCLW) is similar to that of ΔCC (i.e., the spatial correlation coefficient among ΔCC and ΔCLW is 0.93) (not shown).

The change in precipitation depends on various factors such as the change in CLW amount, atmospheric water holding capacity, latent heat flux and other dynamical issues (e.g., Cook and Highwood, 2004; Pal et al., 2000; Jiang and Feingold, 2006; Solmon et al., 2012). Therefore, the above consistent correlation between ΔCC and ΔCLW, to a certain extent, reflect the influences of radiatively interactive aerosols in precipitation. However, to draw conclusions regarding the role of aerosols on hydrological parameters and the mechanisms through which they influence these parameters; we need further analysis on

© University of Pretoria

interactions and feedbacks mechanisms of aerosol-radiation-hydrological and dynamical fields (e.g., Perlwitz and Miller, 2010; Solmon et al., 2012). Besides this, it is also important to incorporate the indirect effect of aerosols (Wurzler et al., 2000; Rosenfeld et al., 2001; Lohmann and Feichter, 2001; Jiang and Feingold, 2006; Lohmann et al., 2007), which is not accounted in this study. Some of the above tasks are a subject of our future research.

Annually averaged regional mean values of ΔCC (averaged over the areas of South Africa: -35° – -22°S, 16° – 33°E) showed that the presence of radiatively interactive aerosols in South Africa induced slight enhancements in CC (by about +1%). The regional mean ΔCC exhibited an opposite sign while being compared with the corresponding results of ΔST (and ΔSSHF) (see section 3.3.1). This result along with the highly consistent spatial correlations which are noted in section 3.3.1 (among ΔST/ΔSSHF with that of ΔCC), cooperatively, indicate that the aerosols semi-direct effect induced CC enhancement is one of the main factor which is accountable for the ST (and SSHF) reductions in South Africa. As reported in different studies (e.g., Jacobson and Kaufman 2006; Zhang, 2008; Stanelle et al., 2010; Solmon et al., 2012), all aforementioned changes which are attributed by radiatively interactive aerosols (i.e., see section 3.3.1 and 3.3.2) jointly induce a dynamical alteration in the lower parts of the troposphere. The next section is devoted to address this particular issue.

3.3.3 The effects of aerosols on Planetary Boundary layer, surface pressure and surface wind field

The spatio-seasonal distributions of total aerosol-induced changes in Planetary Boundary layer height (ΔPBL), surface pressure (ΔSP) and the 10m surface wind field ($\overrightarrow{\Delta W}$) are shown in Fig. 7. In all seasons, the interaction and feedbacks among the bulk aerosol-radiation-climate results in the reduction and enhancement of PBL height and SP, respectively. Also when comparing the simulation results of Fig. 7 with that of Fig. 5a, the seasonal patterns and the spatial distribution of ΔPBL/ΔSP are found to be quite consistent with the spatio-seasonal distributions of ΔST. Throughout extended summer, almost all regions of South Africa which experience a reduction in ST (see section 3.3.1); also exhibited a reduction in the PBL height (within the range of -5 to -100 m) and increments in SP (within the range of +0.02 to +0.16 hPa). Similarly, during the dry seasons (MJJ and ASO), in the areas of South Africa that display ST reductions (Fig. 5a), negative and positive changes in PBL height and SP are found, respectively (Fig. 7). The magnitudes of ΔPBL height and ΔSP during the extended winter season are relatively smaller (respectively by about ~ 50 to 35 %) than their corresponding summertime values. Similar to the ΔST (Fig. 5a), in all seasons the largest range of ΔPBL height and ΔSP are found in the northern and central areas of the Northern Cape as well as over the west and southwest regions of the North West Province. Meanwhile, almost throughout the seasons, intermediate values of ΔPBL height and ΔSP are predicted in the broader areas of Limpopo as well as over the Highveld zones of South Africa (see Fig. 7). Minimal changes in PBL height and SP are, however, noted in all coastal regions of South Africa, that are surrounded by the Indian and Atlantic Ocean.

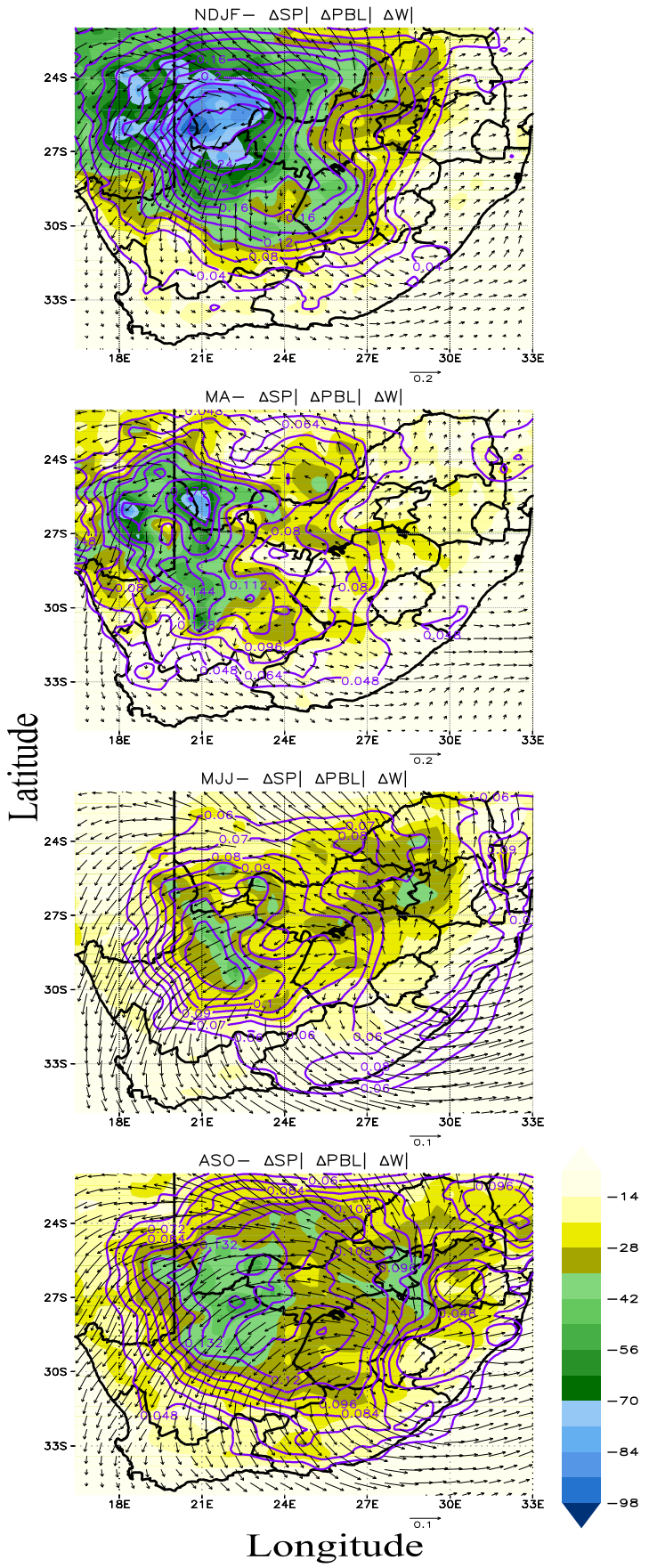

Fig. 7: Same as Figure 5 but for the changes on planetary boundary layer height-ΔPBL (shaded; unit: m), surface pressure-ΔSP (unfilled contour; unit: hPa) and 10m surface wind field-$\overrightarrow{\Delta W}$ (vector; the scale is indicated by the arrow to the lower right; unit: m/s).

The annual averaged spatial correlations between ΔST with that of ΔPBL (ΔSP) correspondingly displayed correlation coefficients of ~ 0.97 (~ -0.91). Similarly, correlation coefficients among ΔSSHF with that of ΔPBL (and ΔSP) are respectively ~ 0.9 (and ~ -0.76) as well as the spatial correlation coefficient of ~ -0.9 (between ΔPBL height and ΔSP) were also found. As we have already discussed in section 3.3.1, the aerosols' direct SRF and their semi-direct effect induced CC enhancements are the prime

© University of Pretoria

UNIVERSITEIT VAN PRETORIA
UNIVERSITY OF PRETORIA
YUNIBESITHI YA PRETORIA

causes for the reduction of ST as well SSHF (Fig. 5a and b). Thus, the spatial correlation coefficients among ΔPBL (ΔSP) with that of NSUR-RF and ΔCC are quite reasonable (i.e., the magnitude of the correlation coefficients are within the range of 0.67 to 0.83). However, the sign of correlation coefficients of ΔPBL height and NSUR-RF (ΔCC) are correspondingly positive (negative); whereas, vice versa results are obtained in the case of ΔSP. As reported in different studies such as Yu et al. (2002), Miller et al. (2004b), Jacobson and Kaufman (2006), Jiang and Feingold (2006), Zhang (2008), the ST and SSHF reductions induce weakening of Convectively Driven Turbulence (CDT) and Surface Buoyancy Fluxes (SBF). As a result, a decline in ST and SSHF in turn, result in the reduction of PBL height plus the improvement in stability of the lower troposphere (e.g., Menon et al., 2002; Yu et al., 2002; Miller et al., 2004b). This stabilization, in conjunction with the dynamical feedbacks of aerosols, may lead to the SP enhancement (e.g., Jacobson and Kaufman, 2006; Zhang, 2008; Yu et al., 2002). Therefore, the aforementioned higher level of spatial correlation coefficients and their signs reflect the main causes which are primarily accountable for the reduction of PBL height and SP increase.

Aerosols' semi-direct influences on atmospheric thermodynamics and cloud cover consequently induce a change in surface wind fields (e.g., Menon et al., 2002; Miller et al. 2004b; Jacobson and Kaufman, 2006; Zhang, 2008). Accordingly, the aerosol-induced changes in surface wind fields [i.e., $\overrightarrow{\Delta W} = \Delta U + \Delta V$ - the respective differences in zonal (ΔU) and meridional (ΔV) wind components among AERO through CNT simulations as a vector arrow] are also shown in Fig. 7. The vector arrows which point to the east and north direction indicate the increase in zonal and meridional wind components, respectively. However, vector arrows which point towards the west and south directions indicate the contrary. Relatively higher changes in surface wind speed ($|\overrightarrow{\Delta W}|$ ~ up to 0.21 m/s) are predicted during extended summer seasons (NDJF through MA). Whereas, the amplitudes of surface wind speed changes ($|\overrightarrow{\Delta W}|$) within the course of the extended winter are weaker (by about 40%) than that of the extended summer season. This might be due to the advanced influences of aerosols on cloudiness during the wet seasons of extended summertime than that of the extended dry seasons (see section 3.3.2) (e.g., Jacobson and Kaufman, 2006).

During NDJF and MA, the reductions in meridional component (up to 0.18 m/s) are primarily located over the broader areas of the west and southwest parts of the country; whereas, the decrease (up to 0.1 m/s) in zonal wind are noted only in the west areas of the Northern Cape Province (see Fig. 7). Within the same seasons, in Limpopo and over the Highveld zones of South Africa both wind components exhibited an enhancement (which is up to 0.08 m/s for ΔU and 0.14 m/s for ΔV). In addition, over the south and southeast coastal areas, the improvement in zonal wind has also been noted. Even if our analysis shows that the magnitudes of ΔU and ΔV are relatively small during extended winter; however, their spatial converges are wider than that of NDJF and MA. During MJJ through ASO, over broader areas of Limpopo, North West, Northern Cape and southwest regions of South Africa; a reduction in zonal wind (up to 0.08 m/s) were found. Whereas, an increase in the zonal component (up to 0.1 m/s) appeared in the east and southeast areas of South Africa (i.e., Mpumalanga, KwaZulu-Natal and Eastern Cape). Moreover, during MJJ through ASO, over broader areas of the west and southwest parts of the country, the meridional component exhibited reductions (up to 0.09 m/s). However, over the central and wider areas of the northern parts of South Africa, enhancements in ΔV (up to 0.1 m/s) were found.

In general, by comparing the wind flowing directions of the CNT simulation (not shown) with that of $\overrightarrow{\Delta W}$ (Fig. 7), it has been noted that the aerosol dynamical feedbacks are playing a role in suppressing the northward surface airflow that predominantly flows through the Atlantic Ocean towards the western regions of South Africa. However, over the east, southeast and northern parts of South Africa; the bulk aerosol-induced regional circulation changes are found to strengthen the anti-clockwise surface air circulation. These all dynamical and other climatic effects of radiatively interactive aerosols, in turn, cause a positive or negative feedback on the aerosol loading itself (e.g., Marmer and Langmann, 2007; Perlwitz et al., 2001; Miller et al., 2004b; Yue et al., 2010b). Comparing the aerosol columnar mass distribution of AERO simulation with that of CNT (not shown), we found that the bulk aerosol burden in AERO is reduced by about ~ 12% relative to CNT. Especially, when comparing the individual aerosol columnar concentrations, we have noticed that relative to CNT the dust particle columnar burdens are decreased by about 11 % in AERO. Whereas, the change in mass distribution of aerosols that are donated from anthropogenic and biomass burning activities are quite small when they are compared with that of dust particles. Overall, the results found in this study are quite comparable with Tesfaye et al. (2013b), which studied, separately, the radiative and climatic influences of wind eroded desert dust particles, in South Africa using RegCM4. This has suggested that the direct and semi-direct effects of wind-eroded dust particles have a leading role in South Africa.

4 Summary and Conclusions

The present study examined the bulk (total) aerosols' direct and semi-direct effects, in South Africa. This study was conducted using Regional Climate Model version 4 (RegCM4) interactively coupled to chemistry/anthropogenic-desert dust aerosol schemes. Our simulation includes various externally mixed aerosol species that are attributed from both natural and anthropogenic activities. Two parallel simulations which encompass a period from 1997 to 2008 were conducted. All experimental setups of the two simulations were the same, except in the first one (CNT) aerosols are not radiatively interactive and in other (AERO) they are radiatively interactive. Comparing the two simulations, climate feedbacks associated with the radiative effects of aerosols were captured. The mean of the recent 11 years' results were analysed and discussed in terms of different seasons. The summary and the main conclusions drawn from this study are presented as follows:

- Owing to the differences in aerosol potential source regions and the anticyclonic air mass movement, the spatial distributions of aerosols in South Africa exhibit a unique feature. The contribution of individual aerosols to the total (bulk)aerosol optical depth (at 550nm) showed that over the west and southern areas of South Africa the wind-eroded desert dust particles are dominant. The maximum loads of secondary sulfate aerosols were situated in the Highveld parts of South Africa. Whereas, the higher loads of carbonaceous [Black Carbon (BC) and Organic Carbon (OC)] particles has been noted in the northern parts of

© University of Pretoria

Limpopo and over broader areas of Mpumalanga and Gauteng. Influenced by the anticyclonic air circulation, most of the above particles were distributed in the east and south-eastern parts of the country.

- The Short-Wave (SW) and Long-Wave (LW) surface radiative forcing of aerosols showed their maximum values (respectively up to -35 W/m^2 and 10 W/m^2) during spring and summer seasons. The SW absorption – primarily by BC plus partially by dust and OC particles – resulted in the enhancement of SW radiative heating (up to 26 W/m^2) within the atmospheric column. However, the dust particle LW radiative influences engender LW-radiative cooling within the atmosphere (~ up to -10 W/m^2).

- In all seasons, the highest direct radiative influences of aerosols were observed in areas of South Africa which are dominated by wind-eroded desert dust particles. Furthermore, due to the dominance of SW radiative influences of aerosols, the net surface and atmospheric radiative forcing of bulk aerosol, respectively, illustrate negative and positive values, which have similar spatio-seasonal variations as those of the aerosol SW radiative influences. Overall, the results reflect that the bulk aerosol radiative role in South Africa is reducing the net radiation absorbed by the surface by enhancing the net radiative heating within the atmosphere.

- Primarily, due to the radiative forcing of aerosols plus their semi-direct effects induced cloud cover (CC) enhancements - which reinforced the aerosol surface radiative cooling tendencies, the reductions in Surface Temperature (ST) and Surface Sensible Heat Flux (SSHF) were occurred. The highest values of ΔST (up to -1 K) and ΔSSHF (up to -24 W/m^2) were found during summer; whereas, the minimal ΔST and ΔSSHF in South Africa were observed during winter. In all seasons, the maximum changes in ST and SSHF were mainly located across the Northern Cape Province. Meanwhile, the intermediate and minimal values of ΔST and ΔSSHF were found in areas of South Africa that are bounded within the longitudinal range of 25°E to 33°E.

- The higher level of spatial correlation coefficients that were noted among ΔST (ΔSSHF) with that of ΔCC confirmed that, in addition to the aerosols' direct radiative influence, their semi-direct effect induced ΔCC also plays an important role in regulating the change in ST plus SSHF. This implies the necessity of considering, simultaneously, the direct as well as semi-direct effect of aerosols to get a better understanding of the overall role of aerosols in climate.

- Including the radiative feedbacks of all climatic components, the aerosols' effects on lower tropospheric (~ below 650hPa) columnar averaged Net Atmospheric radiative Heating Rate (NAHR) were computed. In different regions of South Africa, the bulk aerosol atmospheric radiative influences resulted in the enhancement of NAHR. Across the Northern Cape Province, the annual mean ΔNAHR illustrated its maximal values, which varied from ~ 0.25 to 0.7 K/day. Furthermore, over the Highveld zones of South Africa as well as in the coastal and northern parts of the country, the annual mean ΔNAHR shows reduced values (~ 0.08 to 0.25 K/day).

- The bulk aerosol-radiation-climate interactions induced low-level columnar integrated cloud cover (i.e., low-clouds which are formed below ~ 650 hPa) changes were also addressed. Over broader areas of South Africa, the presence of radiatively interactive aerosols predominantly induced enhancements of CC that were within a range of ~ 1 to 7%. In contrast, over the east and southeast coastal areas of South Africa minimal reductions in CC (~ -0.5 to -2.2 %) were also noted. Nevertheless, during all the seasons, the regional mean values of ΔCC showed that the bulk aerosol net influence in CC is positive (i.e., they were slightly enhancing the low-level regional CC).

- The seasonal variation in ΔCC indicates that the amplitudes of CC responses were not only dependent on the spatio-seasonal variations in aerosol radiation perturbations, but rather also reliant on seasonally variable cloud plus water vapor abundances.

- The present study also addressed the regional scale dynamical feedbacks of radiatively interactive aerosols. The results suggested that the ST and SSHF reductions, via promoting a weakening of convectively driven turbulence and surface buoyancy fluxes, they were inducing the Boundary Layer height (BL) reduction and Surface Pressure (SP) enhancement. The maximal ranges of ΔBL (~ -60 to -100 m) and ΔSP (+0.12 to +0.16 hPa) were found across the Northern Cape and the North West provinces. Intermediate values of ΔBL and ΔSP were predicted in broader areas of Limpopo as well as over the Highveld zones of South Africa; whereas, the coastal regions of South Africa displayed minimal changes in BL and SP.

- The presence of radiatively interactive aerosols induced - geographically and seasonally highly variable surface wind filed changes ($\overrightarrow{\Delta W}$). Comparing the wind directions of CNT simulation with that of $\overrightarrow{\Delta W}$, we noticed that the aerosol dynamical feedbacks slightly weakened the southerly waves which pass through Atlantic ocean and move towards the west regions of South Africa. Additionally, over the northern and coastal parts of the country the bulk aerosol-induced regional circulation changes were found to reinforce the anticyclone surface air circulation.

- Various studies in South Africa are more focused on anthropogenic and biomass burning aerosols (see Tesfaye et al., 2011 and references therein). Nevertheless, we would like to remark that, when we compare the results of the present contribution with studies reported elsewhere by the authors (Tesfaye et al., 2013b, 2013c and 2013d), it clearly indicates that the direct and semi-direct effects of wind-eroded dust particles have a leading role in South Africa. Therefore, the authors suggest that by designing different strategic approaches, which combine both observational and well-advanced modeling techniques; various climatic and ecological roles of wind-eroded dust particles need to be examined continuously in South Africa.

Acknowledgements

The authors are grateful to Addis Ababa University, Department of Physics, for providing computational facilities. For the

© University of Pretoria

UNIVERSITEIT VAN PRETORIA
UNIVERSITY OF PRETORIA
YUNIBESITHI YA PRETORIA

accessibility of RegCM model the authors are thankful to the International Centre for Theoretical Physics (ICTP). We are also indebted to Teresa Faleschini, Tamene Mekonnen, Fiona Tummon and Addisu Gezahegn, for their valuable assistances. This work was supported by African Laser Centre and NRF bi-lateral research grant (UID: 68688/65086), in addition to CSIR National Laser Centre.

References

Allen, R. J., and Sherwood, S. C. (2010). Aerosol-cloud semi-direct effect and land-sea temperature contrast in a GCM, Geophys. Res. Lett., 37, L07702, doi:10.1029/2010GL042759.

Andreae, M. O. and Gelencser, A. (2006).Black carbon or brown carbon? The nature of light-absorbing carbonaceous aerosols, Atmos. Chem. Phys., 6, 3131-3148, doi:10.5194/acp-6-3131-2006.

Andreae, M. O. and Merlet, P. (2001).Emission of trace gases and aerosols from biomass burning, Global Biogeochem. Cycles, 15, 955–966.

Boer, G.J. (1993). Climate change and the regulation of the surface moisture and energy budgets.ClimDyn 8:225–239, doi: 10.1007/BF00198617.

Cook, J. and Highwood, E. J. (2004). Climate response to tropospheric absorbing aerosols in an intermediate general-circulation model. Q.J.R. Meteorol. Soc., 130: 175–191. doi: 10.1256/qj.03.64.

Di Biagio, C. et al. (2012): Effect of surface albedo, water vapour, and atmospheric aerosols on the cloud-free shortwave radiative budget in the Arctic.ClimDyn (2012) 39:953–969, doi10.1007/s00382-011-1280-1.

Douville, H. et al. (2002). Sensitivity of the hydrological cycle to increasing amounts of greenhouse gases and aerosols. Climate Dynamics 20, 45–68.

Feingold, G. et al. (2005). On smoke suppression of clouds in Amazonia, Geophys. Res. Lett., 32, L02804, doi:10.1029/2004GL021369.

Forster, P. et al. (2007). Changes in Atmospheric Constituents and in Radiative Forcing. In: Climate Change 2007: The Physical Science Basis. Contribution of Working Group I to the Fourth Assessment Report of the Intergovernmental Panel on Climate Change [Solomon, S. et al. (eds.)]. Camb.Univ. Press, Camb., United Kingdom and New York, NY, USA.

Freiman, M. T., and Piketh, S. J. (2003). Air transport into and out of the industrial Highveld region of South Africa, J. Appl. Meteorol., 42, 994–1002, doi:10.1175/1520-0450(2003)042<0994:ATIAOO>2.0.CO2.

Fuzzi, S. et al. (2006). Critical assessment of the current state of scientific knowledge, terminology, and research needs concerning the role of organic aerosols in the atmosphere, climate, and global change. Atmos. Chem. Phys., 6, 2017-2038.

Giorgi, F. et al. (2012). RegCM4: model description and preliminary tests over multiple CORDEX domains. Clim Res 52:7–29.

Gu, Y. et al. (2006). Climatic effects of different aerosol types in China simulated by the University of California, Los Angeles atmospheric general circulation model. Journal of Geophysical Research 111: D15201. DOI: 10.1029/2005JD006312.

Haywood, J., and Boucher, O. (2000). Estimates of the direct and indirect radiative forcing due to tropospheric aerosols: A review, Rev. Geophys., 38(4), 513–543, doi:10.1029/1999RG000078.

Highwood, E.J. et al. (2003). Radiative properties and direct effect of Saharan dust measured by the C-130 aircraft during SHADE. 2. Terrestrial spectrum. J. Geophys. Res.,108,8578,doi:10.1029/2002JD002552.

Jacobson, M. Z. (2001). Global direct radiative forcing due to multicomponent anthropogenic and natural aerosols, J. Geophys. Res., 106(D2), 1551–1568, doi:10.1029/2000JD900514.

Jacobson, M. Z., and Kaufman, Y. J. (2006). Wind reduction by aerosol particles, Geophys. Res. Lett., 33, L24814, doi:10.1029/2006GL027838.

Jiang, H., and Feingold, G. (2006). Effect of aerosol on warm convective clouds: Aerosol-cloud-surface flux feedbacks in a new coupled large eddy model, J. Geophys. Res., 111, D01202, doi:10.1029/2005JD006138.

Johnson, B. T. et al. (2004). The semi-direct aerosol effect: Impact of absorbing aerosols on marine stratocumulus, Quat. J. Roy. Meteor.Soc., 130(599), 1407–1422, doi:10.1256/qj.03.61.

Koch, D., and Genio, A. D. (2010). Black carbon semi-direct effects on cloud cover: review and synthesis, Atmos. Chem. Phys., 10, 7685-7696, doi:10.5194/acp-10-7685-2010.

Lamarque, J.-F.et al. (2010). Historical (1850–2000) gridded anthropogenic and biomass burning emissions of reactive gases and aerosols: methodology and application, Atmos. Chem. Phys., 10, 7017–7039, doi:10.5194/acp-10-7017-2010.

Leibensperger, E.M. et al. (2012). Climatic effects of 1950-2050 changes in US anthropogenic aerosols - Part 2: Climate response. Atmos. Chem. Phys., 12, 3349-3362, doi:10.5194/acp-12-3349-2012.

Lesins, G. et al. (2002). A study of internal and external mixing scenarios and its effect on aerosol optical properties and direct radiative forcing. J. Geophys. Res, 107 (D10). 4094, doi: 10.1029/2001JD000973.

Liu, H.Q. et al. (2004). A modeling study of the effects of anomalous snow cover over the Tibetan Plateau upon the South Asian summer monsoon. Advances in Atmospheric Sciences, 21(6), 964-975.

Lohmann, U. and Feichter, J. (2001). Can the direct and semi-direct aerosol effect compete with the indirect effect on a global scale?,Geophys. Res. Lett., 28, 159–161.

Lohmann, U. et al. (2007). Cloud microphysics and aerosol indirect effects in the global climate model ECHAM5-HAM, Atmos. Chem. Phys., 7, 3425-3446, doi:10.5194/acp-7-3425-2007.

Mallet, M. et al. (2009).Impact of dust aerosols on the radiative budget, surface heat fluxes, heating rate profiles and convective activity over West Africa during March 2006. Atmos. Chem. Phys. 9:7143−7160.

Marmer, E. and Langmann, B. (2007). Aerosol modelling over Europe Part I: Inter-annual variability of aerosol distribution, J. Geophys. Res., 112, D23S15, doi:10.1029/2006JD008113.

Menon, S. et al. (2002).Climate effects of black carbon aerosols in China and India, Science, 297, 2250 – 2253.

Miller, R. L. et al. (2004a). Surface radiative forcing by soil dust aerosols and the hydrologic cycle. J Geophys Res 109:D04203. doi:10.1029/2003JD004085.

Miller, R. L. et al. (2004b). Feedback upon dust emission by dust radiative forcing through the planetary boundary layer, J. Geophys. Res., 109, D24209, doi:10.1029/2004JD004912.

Miller, R.L. and Tegen, I. (1998). Climate response to soil dust aerosol. J. Climate, 11, 3247-3267.

Pal, J. S. et al. (2000). Simulation of regional-scale water and energy budgets: Representation of subgrid cloud and precipitation processes within RegCM, J. Geophys. Res., 105(D24), 29579–29594, doi:10.1029/2000JD900415.

Penner, J. E. et al. (2001). Aerosols, their Direct and Indirect Effects, in: Climate Change 2001: The Scientific Basis, edited by: Houghton, J. T. et al. Report to IPCC from the Scientific Assessment Working Group (I), Camb. Univ. Press, 289–416.

Perlwitz, J. and Miller, R. L. (2010).Cloud cover increase with increasing aerosol absorptivity: A counterexample to the conventional semidirect aerosol effect, J. Geophys. Res., 115, D08203, doi:10.1029/2009JD012637.

Perlwitz, J. P. et al. (2001). Interactive soil dust aerosol model in the GISS GCM: 1. Sensitivity of the soil dust cycle to radiative properties of soil dust aerosols. J. Geophys. Res., 106, 18167-18192, doi:10.1029/2000JD900668.

Ramanathan, V. et al. (2001). Aerosol, climate, and hydrological cycle.Science 294, 2119-2124.

Ramanathan, V. et al. (2005). Atmospheric brown clouds: impact on South Asian climate and hydrologic cycle. ProcNatlAcadSci USA 102:5326–5333. doi:10.1073/pnas.0500656102.

Ramanathan, V., and Ramana, M. V. (2005).Persistent, widespread, and strongly absorbing haze over the Himalayan foothills and the Indo-Gangetic Plains. Pure Appl. Geophys., 162, 1609–1626, ,doi 10.1007/s00024-005-2685-8.

© University of Pretoria

UNIVERSITEIT VAN PRETORIA
UNIVERSITY OF PRETORIA
YUNIBESITHI YA PRETORIA

Ramanathan, V., Carmichael, G. (2008). Global and regional climate changes due to black carbon. Nat Geosci 1:221–227.

Reddy, M. S. et al. (2005a).Estimates of global multicomponent aerosol optical depth and direct radiative perturbation in the Laboratoire de MeteorologieDynamique general circulation model. J. Geophys. Res., 110, D10S16, doi: 10.1029/2004JD004757.

Reddy, M. S. et al. (2005b).Aerosol optical depths and direct radiative perturbations by species and source type.Geophys. Res. Lett., 32, L12803, doi: 12810.11029/12004GL021743.

Rosenfeld, D., and Woodley, W. (2001).Pollution and clouds, Phys. World, 14, 33 – 37.

Seinfeld, J. H. and Pandis, S.N. (2006). Atmospheric chemistry and physics: from air pollution to climate. Wiley. New York.

Shell, K. M., and Somerville, R. C. J. (2007).Direct radiative effect of mineral dust and volcanic aerosols in a simple aerosol climate model. J. Geophys. Res., 112, D03206, doi: 03210.01029/02006JD007198.

Slingo, A. et al. (2006). Observations of the impact of a major Saharan dust storm on the atmospheric radiation balance, Geophys. Res. Lett., 33, L24817, doi:10.1029/2006GL027869.

Solmon, F. et al. (2006). Development of a regional anthropogenic aerosol model for climate studies: Application and validation over a European/African domain. Tellus B, 58, 51-72.

Solmon, F. et al. (2008). Dust aerosol impact on regional precipitation over western Africa, mechanisms and sensitivity to absorption properties. Geophys. Res. Lett. 35(L24705). Doi:10.1029/2008GL035900.

Solmon, F. et al. (2012).Radiative and climatic effects of dust over West Africa, as simulated by a regional climate model, Clim. Res., 52, 97–113, doi:10.3354/cr01039.

Stanelle, T. et al. (2010).Feedback between dust particles and atmospheric processes over West Africa during dust episodes in March 2006 and June 2007.AtmosChemPhys 10: 10771−10788.

Tegen, I., and Lacis, A. A. (1996).Modeling of particle size distribution and its influence on the radiative properties of mineral dust aerosol. J. Geophys. Res., 101, 19237–19244.

Tesfaye, M. (2009).RetrivalOf Atmospheric Aerosol Optical And Microphysical Parameters From Ground Base Passive Remote Sensing Measurement Over Addis Ababa: M.Sc. Thesis. Addis Ababa University, Ethiopia.

Tesfaye, M. et al. (2011). Aerosol climatology over South Africa based on 10 years of Multiangle Imaging Spectroradiometer (MISR) data, J. Geophys. Res., 116, D20216, doi:10.1029/2011JD016023.

Tesfaye, M. et al. (2013a). Evaluation of Regional Climatic Model Simulated Aerosol Optical Properties over South Africa Using Ground-Based and Satellite Observations, ISRN Atmospheric Sciences, vol. 2013, Article ID 237483, 17 pages, 2013. doi:10.1155/2013/237483.

Tesfaye, M. et al. (2013b). “Mineral dust aerosol distributions, its direct and semi-direct effects over South Africa based on model simulation using regional climate model”, in review.

Tesfaye, M. et al. (2013c). “Simulation of anthropogenic aerosols mass distributions and their direct and semi-direct effects over South Africa using RegCM4”, in review.

Tesfaye, M. et al. (2013d). “Simulation of biomass burning aerosols mass distributions and their direct and semi-direct effects over South Africa using a regional climate model”, in review.

van der Werf, G. R. et al. (2010). Global fire emissions and the contribution of deforestation, savanna, forest, agricultural, and peat fires (1997–2009), Atmos. Chem. Phys., 10, 11707-11735, doi:10.5194/acp-10-11707-2010.

Wurzler, S. et al. (2000).Modification of mineral dust particles by cloud processing and subsequent effects on drop size distributions, J. Geophys. Res., 105(D4), 4501–4512, doi:10.1029/1999JD900980.

Yu, H. et al. (2002). Radiative effects of aerosols on the evolution of the atmospheric boundary layer, J. Geophys. Res., 107(D12), 4142, doi:10.1029/2001JD000754.

Yue, X. et al. (2010a).Direct climatic effect of dust aerosol in the NCAR Community Atmosphere Model Version 3 (CAM3). Adv. Atmos. Sci., 27(2), 230–242, doi:10.1007/s00376-009-8170-z.

Yue, X. et al. (2010b). Simulation of dust aerosol radiative feedback using the GMOD: 2. Dust-climate interactions, J. Geophys. Res., 115, D04201, doi:10.1029/2009JD012063.

Zakey, A. S. et al. (2006). Implementation and testing of a desert dust module in a regional climate model, Atmos. Chem. Phys., 6, 4687-4704, doi:10.5194/acp-6-4687-2006.

Zhang, Y. (2008). The Radiative Effect Of Aerosols From Biomass Burning On The Transition From Dry To Wet Season Over The Amazon As Tested By A Regional Climate Model: PhD thesis. Georgia Institute of Technology, United State.

© University of Pretoria

Chapter 8: Summary, conclusion and future perspectives

South Africa is bounded by the Atlantic and Indian Ocean in the south, which are the major sources of marine aerosols. Over the west, the arid areas of the Northern Cape, Namibia and Botswana are the major sources of desert dust particles in South Africa. Furthermore, South Africa is one of the most industrialized countries in Africa with a lot of mining and manufacturing industries plus large agricultural practices and thus are the major sources of anthropogenic and biomass burning aerosols. These multi-sources of aerosols/precursor gases and air mass transportations build a complex combination of atmospheric particulates in South Africa. Due to seasonally dependent natural/anthropogenic dynamics, as well as the seasonal variations of meteorological fields which have important influences on aerosol formation, atmospheric processes and properties - the load and climatic influences of aerosols in South Africa usually exhibit strong seasonal variations. Thus, the present thesis contribution initiated with the detailed examination of aerosol spatio-seasonal climatological characteristics in South Africa. The climatological study is performed based on 10 years data of aerosol extinction (τ_{ext}, at 558 nm) and absorption (τ_a, at 558 nm) optical depths that are delivered from Multi-angle Imaging SpectroRadiometer (MISR). Two additional optical properties of aerosols which are computed from MISR products [i.e., Angstrom exponent (α) in two different bands (visible and near-infrared) and its spectral curvature (α')] are also used to estimate the dominant size distribution modes. The background weather parameters such as relative humidity, rainfall and wind speed are used for interpreting the aerosol climatological characteristics.

Synchronized analysis of aerosol optical properties and local meteorological parameters demonstrate that the rainy season of summer followed by lower wind conditions of winter are the most unfavourable circumstances for aerosol generation and dispersion. As a result, the minimum load of aerosols in South Africa is found during the winter season. On the other hand, the dry winter season followed by the high wind conditions of spring are the most constructive situations for aerosol loading and dispersions. Therefore, the aerosol burden in South Africa (which is inferred from τ_{ext}) exhibits its maximum during the spring season. Furthermore based on the spatial distribution of aerosol burden level, South Africa was classified into three geographical regions (across the latitudes); which are the lower, central and upper parts - which respectively exhibit low, medium and high aerosol load levels. These classifications illustrate that the source mechanisms and transportation have a crucial influence in determining the aerosols distribution, even on a regional scale.

Simultaneous characterization of different aerosol optical properties and the back-ground weather parameters advance our understanding about the effects of regional meteorological conditions on the aerosol optical, microphysical properties and their dynamics. Such characterization which is related to other information is also important to estimate the primary regional source of aerosols:

> Wind driven marine aerosols and the air mass transfer from other regions of South Africa/neighbouring-countries are the major sources of airborne particles in the lower parts of South Africa (35°S to 31°S; 17.5°E to 30.5°E). The arid areas of the Northern Cape Province, Botswana and Namibia; industrial emissions primarily from the Highveld zones and the biomass burning activities in and around the eastern parts of South Africa are the main sources of aerosols in the central parts of South Africa (31°S to 27°S, 16.5°E to 33°E). Whereas, emissions from

© University of Pretoria

industrial/urban activities, biomass burning events, local agricultural practices, mining processes, air mass transport from other parts of South Africa and the neighbouring countries are the prevailing sources of aerosols over the upper part of South Africa (27°S to 22°S, 19.5°E to 32°E).

As stated in chapter 1, examining the climatic influences of aerosol particles based on their sources is crucial for various scientific understandings, for making different environmental plans, climate change mitigation and other issues. The results in chapter two (also different references therein); point-out that wind-eroded desert dust particles, emissions from industrial sectors, biomass burning events, local agricultural and mining practices are the main natural and anthropogenic activities which are responsible for the load of primary/secondary aerosol particles over large areas of South Africa. The marine aerosols such as sea-salt particles, dominate the coastal regions of South Africa during summer as well as different natural events/urban activities may also produce various types of aerosols which are quite important on a local scale. Nonetheless the spatio-temporal coverage of the marine aerosols and airborne particles from other events were dominated by particles which are produced from the aforementioned major sources. Therefore, this study focused on examining the radiative and climatic effects of aerosols that were attributed from the major sources.

In reality, air borne particles which are produced from various sources exist in the atmosphere as a mixture. Therefore to closely examine the complex interactions and feedbacks among aerosols from specific sources-radiation-climatic, interactively coupled aerosol-climate models are indispensable tools. Such studies are crucial to quantify separately the climatic signals of different aerosol types based on their sources. With regards to the resolution issue, for more explicit representation of spatio-temporarily highly variable atmospheric aerosol processes, aerosol modules which are interactively coupled with a high resolution regional scale model have a better precision than the global model. Therefore, this study - using the International Centre for Theoretical Physics (ICTP) Regional Climate Model (RegCM4) which is interactively coupled with anthropogenic/chemistry-desert dust schemes - thoroughly examined the distribution, direct and semi-direct effects of wind-eroded desert dust particles as well as different species of aerosols which were induced from anthropogenic and biomass burning sectors, in South Africa.

As is the practice, before employing the model for such purposes, its performance in simulating the optical properties of aerosols (OPA) ought to be examined. This, further than evaluating the model's OPA simulating performance - it is also important to point-out the model's deficiencies for future studies. The RegCM4 simulated AOD values (at Skukuza: 24°S, 31°E) were reasonable in terms of temporal variation; plus their magnitudes were within the standard deviation of AERONET and ± 25% of MISR observations. Over most areas of South Africa, the latitudinal variations of RegCM4 simulated AOD and SSA values were reasonable while they were compared with MISR retrieval. Nonetheless, there were some deficiencies, such as within the regions of 33.5°S to 27°S, the model tends to predict slightly higher values of AOD relative to MISR observations. This was predominantly caused by the dry bias in simulated precipitation that leads to the overestimation of dust and sulfate aerosol loads. In addition, within a latitudinal range of 25°S to 22°S (i.e., over Limpopo province), the model underestimated both AOD and SSA signals. It is primarily due to the RegCM4 shortcoming of co-operating the anthropogenic activities prompted dust loads, such as dust from agricultural and mining practices. Based on the results from chapter 2, this is considered as the main deficiency of RegCM4 in our region of interest (i.e., South Africa). The vertical profile of aerosol optical properties is vital in determining the semi-direct effects of airborne particles. RegCM4 also showed a good performance in capturing the main aerosol extinction profiles (particularly < 6 km), relative to LIDAR measurements.

© University of Pretoria

The desert dust particles which are primarily emitted from the arid regions of the Northern Cape Province, Namibia and Botswana, were concentrated over the western parts of South Africa. Due to the influence of anti-cyclonic air circulation: dust particles were usually dispersed towards the south-east and southern parts of the country; whereas, aerosols which are produced from different anthropogenic activities (primarily from the Highveld zones) and biomass burning events (primarily from the northern and eastern parts of the country) were distributed in the northern, central and eastern regions of South Africa.

Ambient meteorological conditions of summertime offered beneficial circumstances for the secondary sulfate aerosol formations. Therefore, the maximum column burden of anthropogenically induced sulfate aerosol was observed during this season. The most intense and large area covered biomass burning activities occurred during July to October (JASO). Open biomass burning emitted lower amounts of SO_2 plus the dry weather situation of JASO created inconvenient conditions for secondary sulfate aerosol formation. Due to these circumstances, the column burden and climate signal of sulfate aerosols that are resulted from open biomass burning activities were almost negligible when compared to the carbonaceous particles which were emitted from the same events.

Though emissions from anthropogenic activities are almost constant throughout the seasons, the dry meteorological conditions of austral winter reduced the removal of carbonaceous aerosols. Moreover, biomass burning activities which take place during the dry seasons are the main sources of carbonaceous aerosols. Due to these circumstances the carbonaceous aerosol load is higher during South Africa's dry seasons. Furthermore, following the surface wind speed seasonal variation, the minimal load in dust particles were found during winter and maximum during spring. Overall, the results confirmed that the dry season of South Africa are more favourable for the load, dispersion and long-term existence of absorbing aerosols, which is consistent with earlier MISR observations.

Generally, the aerosol radiative forcing showed similar spatio-seasonal patterns as that of the aerosol column loads. All species of aerosols lead to a reduction of net solar radiation at the surface (i.e., all aerosols caused negative Surface Radiative Forcing (SRF)). The maximal influence of SW-SRF for anthropogenically induced sulfate, BC and OC were respectively -12 W/m^2, -2 W/m^2 and -0.68 W/m^2; whereas, for biomass burning induced BC up to -0.7 W/m^2 and OC up to -0.65 W/m^2. The dust aerosols have capabilities of interacting with both SW and LW radiations as well as possess the ability of re-emitting thermal radiation. The maximum values of dust induced SRF in the SW and LW spectrum were -33 W/m^2 and 10 W/m^2, respectively. Due to the dominance of SW-SRF, the dust particles induce net (SW+LW) surface radiative cooling.

Sulfate aerosols reduce the net solar flux at the surface, by entirely scattering the solar radiation that enters the atmospheric column back to space; therefore, their ATM-RF is very minimal. Alternatively, the other species of aerosols caused net surface radiative cooling by enhancing net radiative heating within the atmospheric column (particularly via dust and BC aerosols). Overall, in all seasons, the highest net values of SW-SRF and ATM-RF were observed in areas of South Africa which were dominated by wind-eroded desert dust particles. Next to mineral dust, the total aerosols which are produced from anthropogenic activities exert significant radiative forcing in South Africa than that of biomass burning aerosols. The maximum value of total anthropogenic aerosol-RF is ~ 10 times (for SW-SRF) and ~ 2.5 times (for SW-ATM-RF) stronger than the total aerosols which are produced from local biomass burning activities.

© University of Pretoria

The interactions and feedbacks among aerosols, radiation, and climatic fields were jointly accountable for the changes in different meteorological parameters. The surface radiative cooling influence of aerosols plus their semi-direct effects induced CC changes and dynamical modifications were the primary physical processes which are responsible for the ΔST (ΔSSHF). Moreover, the results also suggested that the regional scale climatic feedbacks of aerosols which are produced from one sector - will impose important changes on atmospheric processes of different aerosols which are produced from other sectors. For example: the climatic feedbacks of radiatively interactive anthropogenic and biomass burning aerosols generated alterations in desert dust emission and burden level around the Northern Cape arid/semi-arid regions. This produced local atmospheric thermal structure adjustments and sequentially cloudiness alterations in areas which are away from the anthropogenic and biomass burning aerosol source regions. Therefore, during the presence of radiatively interactive anthropogenic and biomass burning aerosols, the northern, central and eastern areas of South Africa experienced ΔST and ΔSSHF which are respectively within the range of -0.03 K to -0.36 K and -0.5 to -6.3 W/m^2. Over the western areas of South Africa, the enclosure of different anthropogenic and biomass burning aerosols induced the ΔST and ΔSSHF which respectively varied from +0.03 K to +0.35 K and +0.5 to +4.8 W/m^2. Due to the dominance of dust aerosol radiative and semi-direct climatic influences, the maximum reductions in ST (up to -1.1 K) and SSHF (up to -24 W/m^2) were observed during the dust and bulk aerosol cases, across the Northern Cape Province. Furthermore, almost in all cases, the highest values of ΔST and ΔSSHF were found during the rainy season (summer) and the minimal during the dry season (winter). These seasonal phenomena were not only related with the aerosol load (or their net-SRF) seasonal variations; however they are influentially correlated with aerosols' semi-direct effects induced cloud cover changes. This implies that the change in cloudiness (depending on the sign and the level of ΔCC) by reinforcing or occasionally offsetting the aerosol surface radiative cooling tendencies - plays an important role in prompting the ΔST, ΔSSHF and other meteorological parameter anomalies.

The presence of radiatively interactive desert dust particles predominantly induced an enhancement on the lower tropospheric (~ below 650hPa) columnar averaged NAHR (maximum up to 1.2 K/day across the Northern Cape Province). Only over some constricted areas which were away from the dust source regions, the NAHR decreased (up to -0.4 K/day). This is primarily caused by the dust aerosol climatic feedbacks induced back-ground aerosol concentration changes. During the presence of different aerosol species which originated from anthropogenic and biomass burning activities, both the enhancement and reduction of NAHR were found. The presence of anthropogenically induced sulfate and OC aerosols induced radiative cooling across Mpumalanga, Limpopo, Free State and the Eastern Cape provinces. Whereas, around the Northern Cape Province and coastal areas of KwaZulu-Natal, the existence of these particles caused radiative heating. Both anthropogenic and biomass burning activities induced total aerosols (i.e., in case of SBO) and BC particles predominantly resulted in the enhancement of ΔNAHR which varied from +0.03 to +0.31 K/day. However, due to various reasons, such as radiatively interactive SBO (BC) aerosol climatic feedbacks induced back-ground aerosol concentration changes, over some narrow scattered areas radiative cooling were also found. Overall, attributed to the SW absorbing nature of BC, dust and OC particles, the bulk aerosols in South Africa predominantly induce the enhancement of NAHR. The highest values of increased NAHR, by the bulk aerosols, were located across the Northern Cape Province. The medium and lower values of bulk aerosol radiative heating influences were found over the Highveld zones of South Africa as well as in the coastal and northern parts of the country.

© University of Pretoria

The change in cloudiness is one of the important feedback mechanisms of the climate system in response to the radiative effects of aerosols. The vertical location of the aerosol layer with respect to clouds, the magnitude plus the sign of ΔNAHR, the underlying surface properties and aerosols stimulated dynamical state changes are quite important in determining the overall CC responses. When aerosols induce NAHR reduction, the atmospheric situations become more favourable for the formation of clouds. Therefore, in all cases (during the presence of dust and different species of aerosols which are produced from anthropogenic and biomass burning activities) where the ΔNAHR showed negative values, the columnar integrated low-level cloud cover exhibited an enhancement. When the inclusion of different aerosol species triggered the enhancement of NAHR - depending on various climatic features of the region considered and the magnitude NAHR increases - the CC response becomes more complex. During the dust and bulk aerosol cases, predominantly higher levels of NAHR enhancements were found. In such cases, the water vapour ascent and moisture convergence towards the upper regions of the lower-troposphere were enhanced. Attributed to these circumstances plus other dynamical aspects of the climate, in and around the dust and bulk aerosol major heating zones, the ΔCC showed increases.

On the other hand, the magnitude of NAHR enhancements, which are stimulated by different species of anthropogenic and biomass burning aerosols, were comparatively weaker than that of the dust and bulk aerosol cases. Thus, in these cases (during the presence of anthropogenic and biomass burning aerosols) the enhancement in NAHR leads to dual influences: over the wet and semi-wet parts of the country it resulted in the strengthening of CC (around the central, north and eastern regions of South Africa). While, around the arid region (especially over the Northern Cape Province) it reduced the CC. Overall, the amplitude of ΔCC is higher during the wet season (summer) than that of the dry winter season. This implies that changes in cloud cover are not only dependent on the seasonal variations of aerosol burden levels (their radiation perturbations); but are also highly dependent on seasonal variation of different climatic parameters such as the abundance of cloud and water vapour in the background atmosphere.

All the aforementioned changes which are attributed by radiatively interactive aerosols (i.e., changes on ST, the energy balances of surface-atmospheric system, cloudiness and other parameters) jointly induce a dynamical alteration in the lower parts of the troposphere. The aerosol direct and semi-direct effects mutually induce the change in ST and SSHF. These situations, by inducing changes in convectively driven turbulence and surface buoyancy flux sequentially, result in alterations in Boundary Layer height (ΔBL) plus the stabilization of the lower troposphere lapse rate [Surface Pressure (ΔSP)]. Therefore in all cases, in-line with the spatial patterns of ST (SSHF) reductions, the change in boundary layer height (ΔBL) and surface pressure (ΔSP), showed decreases and increases, respectively. Similarly, aligned with the spatial distributions of ST (SSHF) enhancements, the ΔBL and ΔSP showed increases and decreases, respectively. Higher values of ST (SSHF) reductions were found during the dust and bulk aerosol cases, across the Northern Cape Province. Therefore, the maximum values of BL reduction and SP enhancement were found across the arid areas of South Africa during these cases.

The presence of radiatively interactive aerosols induced - geographically and seasonally highly variable surface wind field changes ($\overrightarrow{\Delta W}$). The reductions of surface wind speed (particularly around dust source regions) may reinforce the stabilization of the lower troposphere lapse rate; therefore, it becomes another contributing factor for the enhancement in SP. In most cases, the dynamical feedbacks of different species of aerosols as well as the bulk aerosols caused regional circulation changes which primarily reinforce the anticyclone surface air circulation over the eastern and northern parts of the country. Furthermore, in most cases the dynamical feedbacks of aerosols in South Africa have a tendency to reduce the northward cold moist surface air that predominantly flows through the

© University of Pretoria

Atlantic Ocean towards the west regions of the country. Nevertheless, to give a detailed explanation on how aerosol semi-direct influences (i.e., changes in cloud cover, ST and SSHF) jointly induce regional circulation changes, further studies are required.

Overall this study advanced the understanding about the climatological characteristics of aerosols in South Africa as well as the direct and semi-direct effects of different species of aerosols which originated from various natural/anthropogenic activities in and around South Africa. However, due to the multiplicity of aerosol-climate interaction mechanisms this study needs to be taken as a first-degree assessment of aerosols-climate interaction in South Africa. Primary/secondary fine mode aerosols which resulted from anthropogenic activities are usually water soluble. Due to this they may have influential indirect as well as atmospheric chemistry effects. Thus, synchronizing both observational and high resolution model simulations - the indirect effects (aerosol-cloud interactions) and heterogeneous reactions of aerosols need to be examined carefully in future research. Such studies are important to render the overall aerosol radiative forcing uncertainties as well as to enhance our understanding of various climatic roles of aerosols (particularly aerosols' influence on hydrological cycle).

Regarding the direct radiative effects and semi-direct climatic influences of different aerosols in South Africa, the current study noticeably underscored that desert dust particles have a leading role amongst the different types of aerosols in South Africa. Perhaps, according to the results of this study the negative forcing by dust aerosols has a large potential to offset (or even around the Northern cape to surpass) the positive forcing of greenhouse gases. Moreover, as shown in IPCC (2001), including the indirect effects of aerosols will further reinforce their negative forcing. Thus to this end the author strongly suggests that wind-eroded dust particles need to be incorporated in climate change studies over South Africa. Further, by designing different integrated approaches, which strategically combine both observational and advanced modelling techniques; various climatic and ecological roles of wind-eroded dust particles need to be examined continuously in South Africa. Continuous observations are important for model evaluation (and in turn to improve the model representation of aerosol sources, atmospheric processes and properties), thus these practices should be encouraged.

Lastly, the author also would like to remark that the results of this study did not include dust particles which are produced through anthropogenic influences. However it is understandable that including anthropogenic dust will further intensify the role of dust in South Africa. Thus, progress is required in cooperating the production and atmospheric processes of anthropogenic dust on RegCM; which shall lead to one of our future research subject. The dominance of dust particle climatic signals perhaps requires some attention from the governmental or non-governmental environmental organizations which are working in and around South Africa: at least in terms of making some strategic plans on how to reduce the dust production and dispersions such as through mitigating aridity expansion via vegetation or other mechanisms.

© University of Pretoria

Contributions

PEER-REVIEWED JOURNAL PUBLICATIONS:

1) ***Tesfaye, M.***, *J. Botai, V. Sivakumar and G. Mengistu Tsidu (2013)*: Evaluation of Regional Climatic Model Simulated Aerosol Optical Properties over South Africa Using Ground-Based and Satellite Observations, *ISRN Atmospheric Sciences, vol. 2013, Article ID 237483, 17 pages, 2013. doi:10.1155/2013/237483. (Reproduced in chapter-3)*

2) ***Tesfaye, M.***, *V. Sivakumar, J. Botai, and G. Mengistu Tsidu (2011)*: Aerosol climatology over South Africa based on 10 years of Multiangle Imaging Spectroradiometer (MISR) data; *J. Geophys. Res., 116, D20216, doi:10.1029/2011JD016023. (Reproduced in chapter-2)*

3) *Sivakumar V,* ***Tesfaye M,*** *Alemu W, Sharma A, Bollig C and Mengistu G (2010):* Aerosol measurements over Southern Africa using LIDAR, Satellite and Sun Photometer World Scientific books, Advances in Geosciences, 16, Atmospheric Science, Chapter 23, 263-270, ISSN: 1680-7340& ISBN: 978-981-283-809-4.

4) *Sivakumar V,* ***Tesfaye M,*** *Alemu W, Moema D, Sharma A, Bollig C and Mengistu G (2009):* CSIR South Africa Mobile LIDAR – First scientific results : comparison with satellite, sun photometer and model simulations; South African J. of Science, 105, 449-455.

JOURNAL ARTICLES WHICH ARE UNDER SUBMISSION/REVIEWING PROCEDURE:

5) ***Tesfaye, M.***, *G. Mengistu Tsidu, J. Botai, and V. Sivakumar (2013):* Mineral dust aerosol distributions, its direct and semi-direct effects over South Africa based on regional climate model simulation, *J. Arid Environ., in review.*

6) ***Tesfaye, M.***, *V. Sivakumar, J. Botai, and G. Mengistu Tsidu (2013):* "Simulation of anthropogenic aerosols mass distributions and their direct and semi-direct effects over South Africa using RegCM4", *Int. J. Climatol., in review.*

7) ***Tesfaye, M.***, *J. Botai, V. Sivakumar and G. Mengistu Tsidu (2013):* "Simulation of biomass burning aerosols mass distributions and their direct and semi-direct effects over South Africa using a regional climate model", *J. Meteorol. Atmos. Phys., revised version submitted (this manuscript is to be accepted soon).*

8) ***Tesfaye, M.***, *J. Botai, V. Sivakumar and G. Mengistu Tsidu (2013):* "Simulation of bulk aerosol direct and semi-direct effects in South Africa using RegCM4", *J. Aerosol Air Qual Res., in review.*

PEER REVIEWED CONFERENCE PROCEEDING WITH ISBN:

9) ***Tesfaye, M.*** *G. Mengistu Tsidu, V. Sivakumar, J. Botai (2011):* Effective Single Scattering Albedo Estimation using Regional Climate Model Proc. 27th Annual conference of South African society for atmosphere science, ISBN 978-0-620 50849-0, Hartbeespoort, South Africa, 22-23 September 2011, Pg. 53-54.

10) ***Tesfaye.M****, V. Sivakumar, J. Botai and G. Mengistu (2010):* Latitudinal Variations of Aerosol Optical Parameters over South Africa Based on MISR Satellite Data *Proc.* 26th Annual conference of South African society for atmosphere science, *ISBN 978-0-620-47333-0, South Africa, 20-22 September 2010, Pg 103-104.*

11) *Sivakumar V, Bollig C, Sharma A and* ***Tesfaye M (****2010):* Development of 2-Channel (532 nm and 355 nm) Mobile LIDAR for Mapping Particulate Matter in the Atmosphere Proc. 26th Annual conference of South African society for atmosphere science, ISBN 978 0 620 47333 0, South Africa, 20-22 September 2010, Pg 103-104.

© University of Pretoria

12) ***Tesfaye M,*** *Sivakumar V, Mengistu G, Botai J, Sharma A, Bollig C and Rautenbach C.J.deW:*Atmospheric Aerosol load morphological classification and retrieved visibility based on LIDAR backscatter measurement Proc. of 25th International Laser Radar Conference, ISBN 978-5-94458-109-9, Saint Pietersburg (Russia), 487-490, 2010.

13) ***Tesfaye M****, Sivakumar V, Botai J, Moema D, Sharma A, Bollig C, Rautenbach H and Mengistu G.:*Retrieval of relative humidity from CSIR-NLC mobile LIDAR backscatter measurements Proc. 25th Annual conference of South African society for atmosphere science, ISBN 9780 620 44218 3, South Africa, 09-10 September 2009.

14) *Sivakumar V,* ***Tesfaye M****, Botai J, Moema D, Sharma A, Bollig C and Rautenbach H.*: CSIR NLC Mobile LIDAR for Atmosphere Remote Sensing Proc. of International Geoscience and Remote Sensing Symposium, ISBN 978-1-4244-3394-0, South Africa, 13-17 July 2009.

15) *Sivakumar V,* ***Tesfaye M,*** *Moema D, Sharma A and Bollig C*: CSIR NLC Mobile LIDAR – First Scientific Results Proc. of International Geoscience and Remote Sensing Symposium, ISBN 978-1-4244-3394-0, South Africa, 13-17 July 2009.

PRESENTATIONS:

16) Evaluation of regional climatic model simulated aerosol optical properties over South Africa using ground-based and satellite observations; International Conference on Regional Climate - CORDEX 2013; 4-7 November 2013 in Brussels, Belgium.

17) Simulation of seasonal distributions, direct and semi-direct effects of mineral dust aerosols over South Africa; International Conference on Regional Climate - CORDEX 2013; 4-7 November 2013 in Brussels, Belgium.

18) Simulation of sulphate, carbonaceous and total anthropogenic aerosol seasonal distributions, direct and semi-direct effects over South Africa using-RegCM4; International Conference on Regional Climate - CORDEX 2013; 4-7 November 2013 in Brussels, Belgium.

19) Effective Single Scattering Albedo Estimation using Regional Climate Model; the 27th Annual conference of South African society for atmosphere science, Hartbeespoort, South Africa, 22-23 September 2011.

20) The interactions of air pollution with global chemical and climate change “Changing Chemistry in a Changing Climate: Human and Natural Impacts over southern Africa – C4-SAR”, Midrand, South Africa, (31 May – 3 June 2011).

21) The 10th Scopex Astronomy and Telescope Expo: "Light detection and Ranging (LIDAR) – An atmospheric probe" by Melaku Yigiletu of the National Laser Centre; Johannesburg, War Museum (May 7, 2011).

22) 4th African Laser Centre Student Workshop, Zevenwacht Wine Estate, Stellenbosch, Western Cape, South Africa (9 – 13 November, 2011).

23) 3rd African Laser Centre Student Workshop, Zevenwacht Wine Estate, Stellenbosch, Western Cape, South Africa (23 – 26 September, 2010).

24) Atmospheric Aerosol load morphological classification and retrieved visibility based on lidar backscatter measurement; *25th International Laser Radar Conference, Saint Pietersburg, Russia 2010.*

25) Retrieval of relative humidity from CSIR-NLC mobile LIDAR backscatter measurements, *25th Annual conference of South African society for atmosphere science, South Africa, 09-10 September 2009.*

26) 2nd African Laser Centre Student Workshop, Kariega Game Reserve, South Africa, (2 – 5 July, 2009).

© University of Pretoria